Instituto Tecnológico de Costa Rica
Escuela de Ingeniería en Construcción

Seismic performance of SMA-Reinforced ECC pier system of the Salitral Bridge

Proyecto final de graduación para optar por el grado de
Licenciatura en Ingeniería en Construcción

Jose Ignacio Matthews Garro

Cartago, Mayo 2019.

**CONSTANCIA DE DEFENSA PÚBLICA DE
PROYECTO DE GRADUACIÓN**

Proyecto de Graduación defendido públicamente ante el Tribunal Evaluador, integrado por los profesores Ing. Gustavo Rojas Moya, Ing. Adrián Chaverri Coto, Ing. Hugo Navarro Serrano, Ing. Ángel Navarro Mora, como requisito parcial para optar por el grado de Licenciatura en Ingeniería en Construcción, del Instituto Tecnológico de Costa Rica.
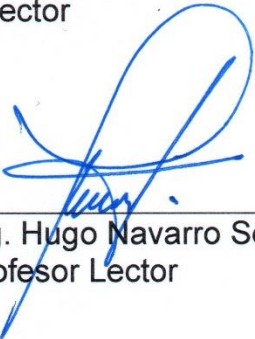
_____
Ing. Gustavo Rojas Moya.
Director

_____
Ing. Adrián Chaverri Coto.
Profesor Guía

_____
Ing. Hugo Navarro Serrano.
Profesor Lector

_____
Ing. Ángel Navarro Mora.
Profesor Lector

Seismic performance of SMA-Reinforced ECC pier system of the Salitral Bridge

Abstract

Resumen

The emerging smart materials change the paradigm of design from the no-collapse stage to no-damage after extreme loading and immediate use. The superelastic Nitinol shape memory alloys (SMA) is an emergent material that remembers its original shape after plastic strain, combining the Nickel and Titanium in an alloy. The Engineering Cementitious Concrete (ECC) is a bendable concrete with a ductile behavior compared to regular concrete, allow high tensile stresses and produce recoverable micro-cracks in it. Using the Superelastic SMA (SE-SMA) and ECC combined in the main rotation zones of the piers can eliminate the plastic hinges in the structure after extreme loading.

The initial cost of the use of SMA-ECC in the piers of the bridge is 5% more of the initial value that using ordinary RC (Clines, 2017). However, it is considered the cost of the retrofit and maintenance of the structure the value of the SMA-ECC represents unique advantages.

The recovery capacity of the SMA-ECC frame system of the Salitral bridge increased to an average of 90% with lateral load induced. The statistical analysis showed that there are significant differences in the recovery capacity using SMA and ECC combined, but not each one separately.

Los emergentes materiales inteligentes cambian el paradigma de diseño de la etapa de no-colapso a no-daño después de cargas extremas y uso inmediato. La aleación Nitinol con memoria de forma súper-elásticas (SMA) es un material emergente que recuerda su forma original después de deformado inmediatamente que es descargado, combinando el Níquel y el Titanio en una aleación. El "Compuesto Cementicio Ingenieril" (ECC) es un concreto flexible con un comportamiento dúctil comparado al concreto ordinario, permite altos esfuerzos en tensión y produce microgrietas en él. Usando el Súper-elástico SMA (SE-SMA) y ECC combinados en las zonas de rotación principales puede ser eliminadas las rótulas plásticas en la estructura después de cargas extremas.

El costo inicial del uso del SMA-ECC en las pilas de un puente es 5% más del costo inicial que usando ordinario RC (Clines, 2017). Pero si se considera el costo de rehabilitación y mantenimiento de la estructura el SMA-ECC representa grandes ventajas.

La capacidad de recuperación del sistema de marcos SMA-ECC es incrementado en un 90% inducido con carga lateral. El análisis estadístico mostró que existen diferencias significativas usando SMA y ECC juntos, pero no cada uno por separado.

Seismic performance of SMA-Reinforced ECC pier system of the Salitral Bridge

JOSE IGNACIO MATTHEWS GARRO

Proyecto final de graduación para optar por el grado de Licenciatura en Ingeniería en Construcción

Febrero del 2019

INSTITUTO TECNOLÓGICO DE COSTA RICA
ESCUELA DE INGENIERÍA EN CONSTRUCCIÓN

Content

List of Symbols

t	Time
β_{eq}	Equivalent Viscous Damping
f_y	Yielding stress of steel
f_{ySMA}	Yielding stress of SMA
d_b	Diameter of the bar
$f'c$	Compressive strength of hydraulic concrete in cylinders of 30 cm of height and 15 cm of diameter at 28 days of made.
M	Moment resultant
me	Milli strain
E	Elasticity Modulus
ECC	Engineering Cementitious Concrete
E_D	Energy dissipated
lp	Plastic Hinge Length
E_{so}	Elastic energy dissipated
M_s	Martensite start temperature
M_f	Martensite finish temperature
RVC	Recovery capacity
R_s	R phase start temperature
R_f	R phase finish temperature
$\ddot{u}$	Acceleration
$\dot{u}$	Velocity
u	Displacements
$\ddot{u}_g$	Ground Acceleration
Φ	Modes Matrix of the system
A_g	Area of the cross-section
A_s	Austenite start temperature
A_f	Austenite finish temperature
ρs	Transverse reinforcement ratio
ρl	Longitudinal reinforcement ratio
z	Distance from the critical section to the point of contra-flexure

Preface

The structural columns in the structures are one of the essential elements in an structural system due to its capacity to transmit loads to the foundation and dissipate energy. In the case of the bridges, the piers represent these characteristics and are designed to maintain the safety of the civilians and the integrity of the superstructure under optimum conditions.

Under extreme loadings, as earthquakes the piers of the bridge usually take more contribution of base shear and the ground accelerations to protect the superstructure combined with isolators or dampers. The extreme induced loads to the piers usually conduce to plastic deformation, large cracks and loss in the structural integrity. Therefore, if the structure survives to the earthquake, will be necessary retrofit, repairs or even demolish of elements due to the damage received. These repairs or retrofits are usually expensive and complicated also interrupt the transit in the operational use of the surface of the bridge. High costs also can be achieved by the use of heavy machinery, specialized personnel and design of the most beneficial solution.

Costa Rica is one of the highest seismic countries around the world due to the several tectonic plates of subduction, thus vulnerability of the structures is increased and therefore the considerations in the design of the structural elements. Also, tropical storms, complicated topography, and slide of slopes cause severe damages to the Costa Rican infrastructure every year.

The use of emergent smart materials has improved the structural engineering to create new methods of design, considering in the configuration its capability to auto-repair and auto-centering of the structural elements.

The use of these smart materials leads the home university to the vanguard of the structural researches across the World. The implementation of materials like shape memory alloys and Engineering Cementitious Concrete is starting to be seen in the studies for structural researches. At this time there is only one small bridge in Seattle that used SMA as reinforcement rebars and ECC as concrete — demonstrating the feasibility of the researches and the progress made on site projects.

The researches in the structural area using new smart materials as SMA and ECC together on the piers of Costa Rican bridges bring significant benefits. The magnitude on the researches made by the faculty of Construction Engineering and the Instituto Tecnológico de Costa Rica giving academic relevance of the studies made. Also brings benefits to the country and Ministry in charge of the projects. Due in Costa Rica, the structural maintenance of constructed bridges is the minimum by the government then seismic dampers or dissipator are usually useless. The philosophy of design with new materials is not only achieving the no-collapse phase after strong earthquakes but also avoiding damages in the structures and making it self-repairing. A decreasing of the costs of structural maintenance or retrofit almost to zero and giving a better solution to the retrofit of bridges in rural zones where heavy machinery is tough to get and bridges with a high level of importance or with high vehicular transit.

This research has the primary objective to identify the benefit of the use of smart materials like SMA as reinforcement rebars on ECC in the plastic hinge zone compared to conventional reinforced concrete piers and asses its performance under seismic events, push-over and reverse cyclic analysis. It is using as a base the Salitral Bridge in Orotina, Costa Rica. Due to its relevance to the economy of the country, the cost of the project, critical connection to airports, maritime ports, hospitals and dense flux of vehicles.

I want to give thanks first to God and the Virgen María to achieve this Graduation Project research. Also, to the incredible help of Dr. Dan Palermo and grateful for giving me the opportunity

of doing the Research[1] under his supervision and attending courses at York University[2]. To the MSc. Michael Soto-Rojas for the help and advices given, to my Mother Eugenie Garro-Díaz, my grandmother Eliette Díaz-Ramirez, grandparent Álvaro Garro-Marlay for the backing and unconditional support of Mónica Hidalgo-Ramírez, Guadalupe Gómez-Rojas, Emmanuel Cubillo-Hernandez, and Mark Jones-Sánchez. I also thank the help and support given by Ricardo Quesada from Edunámica[3] and Sonia Astúa[4] from ITCR[5] it was a wonderful experience.

Extended Summary

This thesis is a research based on the benefits of smart materials in the piers of bridges to prevent not only the collapse but severe damages after extreme loading.

The study is part of the Graduation Project at Bachelor at the Technological Institute of Costa Rica, Costa Rica, under the supervision of Dr. Dan Palermo at York University, Canada. As collaboration to the problematics on the infrastructure of the home country (Costa Rica). The research was focused on the Costa Rican feasibility, identifying the leading causes of structural damages in the bridges of the country, earthquake engineering and the capacity of investment on infrastructure by the Government.

As part of the objectives are to identify the current causes of failures on the bridges of Costa Rica. Identification of the benefits of shape memory alloys in concrete structures and civil structures. Identification of smart materials as engineered cementitious concrete to improve the response to extreme loading of structural elements and the identification of an essential bridge in Costa Rica to assess the improvement and performance using smart materials. Modeling of the pier system reinforced with smart materials under extreme loading. Assess the pier system of the bridge comparing it using regular RC versus improved materials.

The title and objectives describe by itself the relevance of the research and the importance to the country, decreasing the maintenance and retrofit costs significantly to the Government. The Construction Engineering faculty, the Home university, and the inviting international university get relevant benefits by applying knowledge and studies on main problems of the structural area all around the world using smart materials at the vanguard of the structural technology, based on the finite element analysis and seismic performance.

The literature review exhibit that the whole territory of Costa Rica is immersed in the seismic zone known as the Ring of Fire where are the subduction zones of the main tectonic plates in the world and is usual that occur most significant earthquakes. Therefore, Costa Rica is one of the most seismic countries in the world, plus the entropy in the topography, frequent raining, and tropical storms add instability to the foundations, slide of the slopes and flashing floods that causes high constant damages to the infrastructure.
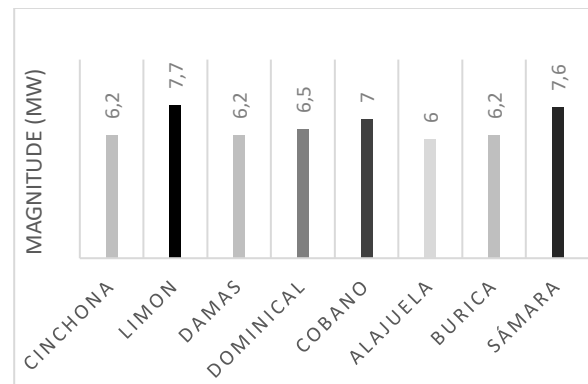

Figure 1. Most relevant earthquakes in Costa Rica since 1991.

As mentioned, most of the damages of the bridges in Costa Rica are not due to the magnitude of a seismic event. In recent times the worst earthquakes damages were provoked by the Limón Earthquake in 1991 and the Cinchona Earthquake in 2010. As seen in the first figure, the Cinchona one is far from the highest magnitude events in the country. The main reason of the damages was due to the instability of the infrastructure, the slide of slopes and topography of the zone.

The bridge over the Salitral river in Costa Rica is one of the most important in case of emergency, also to the economy and present dense flux of vehicles, is a national highway, also due to the investment made, it is essential to get to the airports, maritime ports, tourism, and hospitals. This bridge was designed in 1994 and constructed in 2000, at this time was not ready the LRFD philosophy of design for the bridges on AASHTO.

The piers of the bridge have 36,0 meters height with a hollowed squared cross-section.

This bridge is in a category cataloged as alarming by the inspection "Lanamme" funded by the Government and the University of Costa Rica. The actual state of the cracks or different damages in the piers of the bridge is unknown due to the difficulty to access it.

Figure 2. Actual footage of the Salitral bridge, in the national route number 27.
Source: (Vargas-Alas, Villalobos-Vega, Gooden-Morales, & Castillo-Barahona, 2017)

Most of the structural devices applied in the bridge are useless due to the low maintenance since constructed and some structural elements of concrete present significant cracks and some of the steel damages in corrosion and bending.
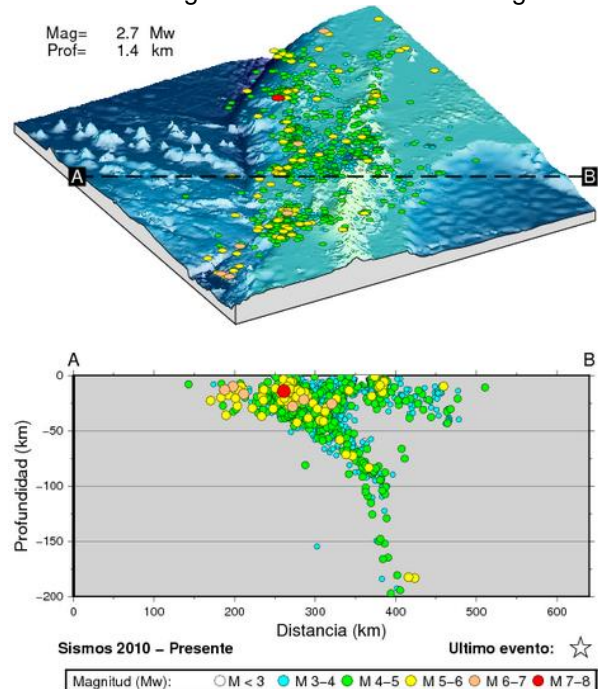

Figure 3. Cross-profile to the subduction zone of Costa Rica.
Source: (Universidad de Costa Rica, 2018)

A simulation made by the Laboratory of Earthquak Engineering of Costa Rica, an earthquake on the downtown of San José will create a propagation wave that will acquire direct impact in the zone where the bridge is located. As seen in figure 3 this zone is where more of the seismic events occur in the country with multiple consecutive events.

The use of Shape Memory Alloys (SMA) has achieved great relevance in the structural area of the civil engineering due to its capability to remember the original shape after plastically deformed. SMA can improve the response of a structure under extreme loading and the recovering capacity decrease the cost of retrofit or repair. There are two main types of shape memory alloys, the martensitic shape memory alloy that can be plastically deformed up to 6-8% and the residual deformation can be recovered applying heat to the element. The other type is the superelastic SMA (the one used in this research) where the element is instantly recovered once is unload (superelasticity).
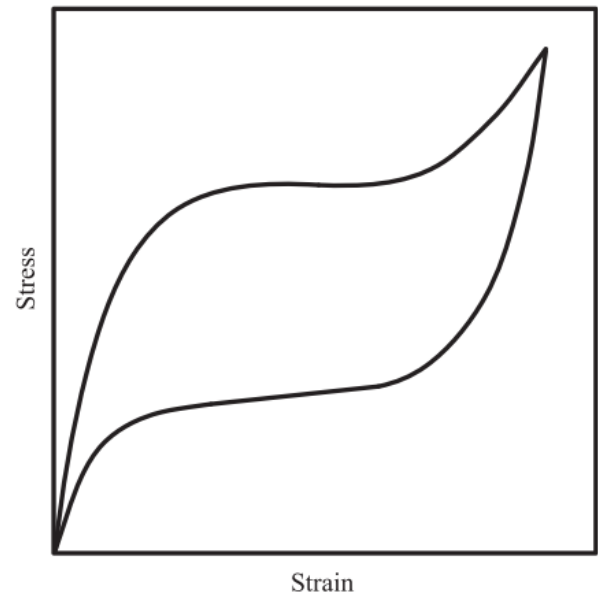
Figure 4. Classic superelastic SMA stress-strain response.
Source: (Abdulridha, Palermo, Foo, & Vecchio, 2013)
Behavior and modeling of superelastic shape memory alloy reinforced concrete beams.

Figure 4 shows the typical stress-strain curve of superelastic SMA, where once the peak load is achieved can be recovered to the point of origin. The alloy used in the research is based on Nickel and Titanium, this composition is called Nitinol and is the most common SMA in the structural

researches. The Shape memory alloys have been used in several types of structural uses, for example as isolators, dampers, braces, reinforcement, and others. The reinforcement of concrete structures using SMA present remarkable results in the recovery once unload the element. The use of this material creates larger located cracks in the concrete and can be recovered. SMA bars are smooth therefore it is necessary to use mechanic couplers between this and the steel reinforcement rebars. Each SMA bar cost 90 times more than a steel reinforcement bar. Therefore the use of SMA in all the structure is economically unfeasible; thus it is only used in the plastic hinge zone of the system.

The use of the SMA in the concrete structures require a special concrete to contrast the located larger cracks created in the plastic hinge. The use of Engineering Cementitious Concrete (ECC) is relevant in this side; this is a bendable concrete made with fly ash, fibers and superplasticizer that has large tensile strain capacity and produce an own remarkable characteristic that is the creation of micro-cracks in it regardless of the reinforcement around 50 μm.
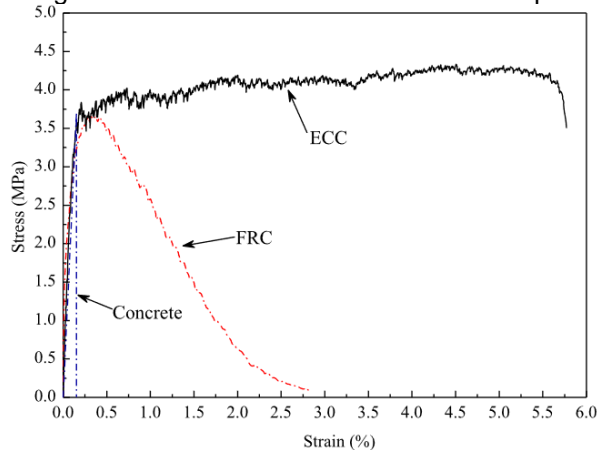

Figure 5. Tensile stress-strain curves of strain-hardening ECC, tension-softening FRC, and quasi-brittle concrete.
Source:(X. Li, Li, & Song, 2015)

The ECC behaves differently than concrete, and fiber reinforced concrete (FRC) as seen in the previous figure. The micro-cracks are completely recoverable and with the combined use of the SMA can decrease significantly the damage produced in the plastic hinges and recover the structure at considerable strain and rotation.

To model the bridge in the software was divided into two essentials models, depending on the axis of the earthquake-induced. In the software

used to apply the non-linear static and reverse cyclic analysis, the axis of the lateral load changes the model. Due to the software work in 2-D if the lateral load is in the Y-axis as shown in figure 6 the columns of the frame behave as individual piers. However, if the load is in the X-axis, the system behaves as a frame and the coupling beams acquire high relevance to the analysis. Therefore, the Model 1 is the one referring to the Y lateral load and Model 2 to the lateral load in the X-axis.

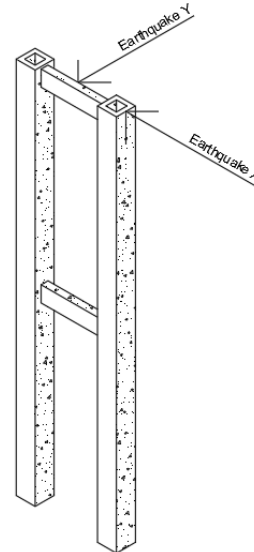Figure 6. Principal axials of the earthquake and lateral loads induced to the Bridge.

The seismic analysis was made tridimensional with a static, modal and time-history analysis each one in the X and Y-axis previously defined.
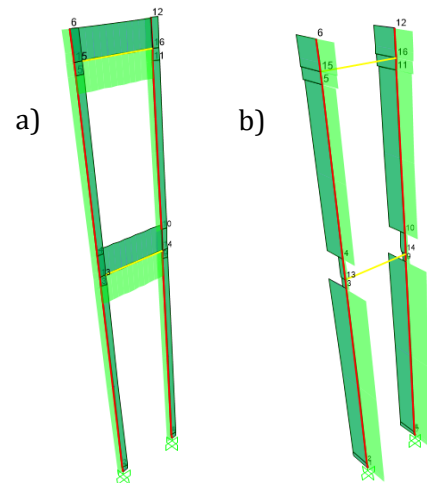

Figure 7. Time-History response of the Limón Earthquake, (Costa Rica, 1991) of the pier system a) Envelope response Shear in X-axis b) Envelope response of Shear in the Y-axis ground acceleration.

As ground acceleration was induced the Limón and Sámara earthquakes, (in 1991 and 2012) the strongest events with registered data on the country. The maximum shear of the system was around 176 kN on the piers.
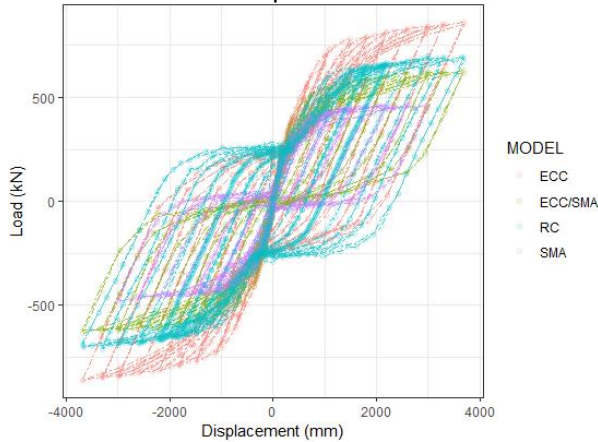

Figure 8. Reverse cyclic response of the Model 1.

With the reverse cyclic response of the models was calculated the recovery capacity, lateral load capacity, energy dissipation and viscous damping per each drift load. The recovery capacity of the models using ECC and SMA separately, but a remarkable recovery occurred when the SMA and ECC were used together, achieving an average recovery capacity of 90%.
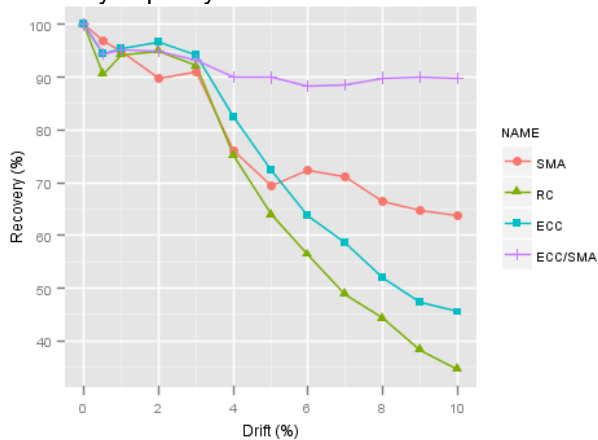

Figure 9. Recovery capacity versus lateral drift of the reverse cyclic loading in the first Model.

In the pushover analysis, the response using ECC presented a large capacity of drift to high lateral load, compared to the models using ordinary concrete. Therefore, the peak load and peak displacement were incredibly high compared to the original response, giving significant changes with the use of ECC. The use of SMA decreases the lateral load capacity due to the elastic modulus of the material.
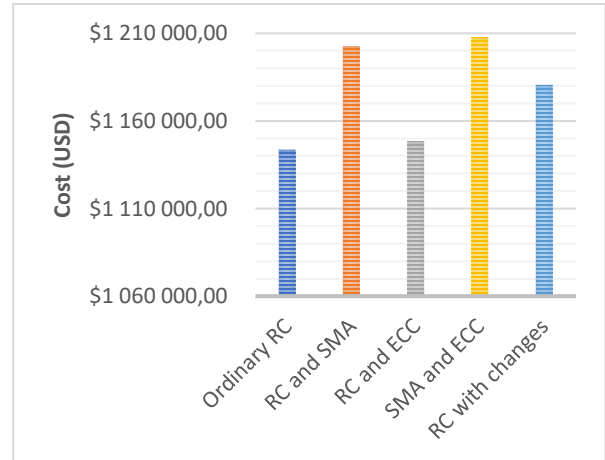
Figure 10. Comparison of the cost of both Frames using SMA and ECC in the Salitral Bridge.

The cost of use SMA and ECC together is 5% more compared to the reinforced concrete frame system of the Salitral Bridge. This higher initial cost is an investment considering the savings in maintenance, retrofits or demolishing.
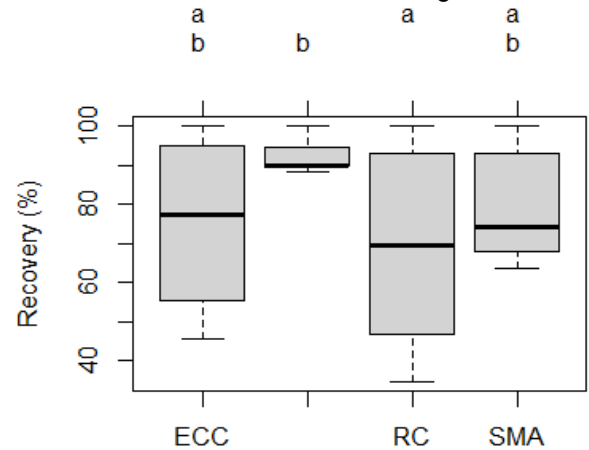
Figure 11. Anova test to identify significant statistical differences in the models.

There was made four different statistical analysis to identify if there were significant differences between the use of SMA and ECC compared to RC due to the increment on the cost. It was discovered that there are significant differences in the response using just SMA and ECC together but not separately. Therefore, the relevance in this research of the combined use of both materials in the piers of Bridges with extreme lateral load induced.

Introduction

Some of the recent seismic events around the world have demonstrated that the national seismic codes have focused-on preservation of the life of the civilians. In cases where a significant earthquake enters the infrastructure, it is acceptable to have some damage under extreme loadings and then it will be necessary to retrofit the affected structures, due to the tolerance on lateral strain and deformations. This behavior was shown in the earthquakes like the Sámara Earthquake of 2012, 2010 in Chile and 1991 in Limón, Costa Rica. It is causing expensive costs in the repair, retrofit, demolishing and reconstruction of the damaged infrastructure.

The structural area in engineering usually trends to design accepting structural damage in the structures and preventing the collapse of these, to providing safety to the users and civilians, as specified in international Codes as FEMA.

The use of new smart materials can provide extra safety in the structural elements, preventing the collapse but also eliminating severe damage and the repairs, retrofits and demolishing after extreme loadings as earthquakes and removing the plastic hinges in the structures or self-repairing after applied loads, behaving as elastic elements. The use of shape memory alloys as reinforcement rebars on concrete show exceptional characteristics under extreme loading, as re-centering, self-repair and memory of the shape after plastic deformation. One of the most used shape memory alloys (SMA) is Nitinol, based on an alloy of Nickel with Titanium and depending on the percentage of each material used will be derived from two different SMAs. The SMA that can deform plastically and apply heat to the element, this will remember its shape and come back to its original position is called Shape Memory Effect. Then, the other type of SMA that recovers its original shape instantly without applying heat is called Super-elastic SMA. The use of superelastic SMA as reinforcement rebars produce located cracks in the structural elements that can be auto-recovered once the component is unloaded without residual strain.

The smart material called Engineering Cementitious Concrete (ECC), also known as bendable concrete that contrary to the ordinary concrete presents a ductile behavior. The use of this concrete produce micro-cracks in it at high tensile stresses compared to ordinary concrete, these micro-cracks can be recovered automatically once the element is unloading. The use of Shape Memory Alloys and Engineering Cementitious Concrete provides high flexibility to the structures with high levels of recovery with minimum or null loss of strain. Therefore, the investment in costs to the structures will be almost zero once the extreme loading is induced, bringing great results in the cost-benefit ratio.

The columns represent one of the most critical elements in the structures, is one of the main elements to transmit loads from the top or upper floors and to the foundations, usually receives considerable axial and lateral load simultaneously and is one of the most critical parts in the dissipation of energy and contribution of stiffness to the structure. In the bridges, the piers represent the same behavior of columns in the structures. Usually between the piers and the superstructure of the bridge is use the dampers or/and energy dissipators. Therefore the piers receive great participation of the whole extreme load. Usually, this means the creation of plastic hinges in the piers or considerable opening in the cracks transforming into a loss of structural capability. This behavior is why it is essential to assess the use of these new materials in the piers of the bridges and bring full safety to the system.

Consequently, this research assessed the performance of SMAs and ECC piers of the bridge under extreme loading compared to conventional concrete piers. As a relevant parameter, it is based on a previously designed bridge with vital importance in Costa Rica and assessed the performance. The bridge used to generate the models was the Salitral Bridge, located in Orotina,

Alajuela, Costa Rica. This bridge makes an essential point of transit to the economy and tourism of Costa Rica, also conduce to airports, and marine ports and is located in one of the most important highways in Costa Rica. With a height of 36 meters, it was designed in 1994 and constructed in 2000.

The models were made with the finite element analysis (FEM) mainly used with the software VecTor2, created in the University of Toronto, Canada. The software is capable of recreating the pattern of cracks and openings of the cracks produced in the structures under different loading analysis, can predict the flattening in the concrete and plastic deformation of the steel. Also, permit the use of smart materials in the structures as shape memory alloys and fibers reinforced concrete.

As a part of the objectives of the research is to identify the optimal kind, quantity, and location of the SMAs in the structure of the models to create a response with better performance than regular reinforced concrete structure. Also, identify the kind, quantity, and location of the ECC used in the construction to decrease the damage in plastic hinges. Then, design the model of the piers of the bridge using the finite element analysis and the previously identified parameters of the smart materials. Moreover, compare the performance of the use of the smart materials to the already designed bridge under seismic, monotonic and reverse cyclic loadings.

Most of the researches about shape memory alloys are in medical purposes, some of the structural investigations are using SMA by applying heat to the elements as the researches made in the University of Illinois by the Dr. Bassem Andrawes. One of the most similar analysis compared to this project is the research "Energy-dissipating and self-repairing SMA-ECC composite material system" (X. Li, Li, & Song, 2015) in which is evaluated the performance of SMA-ECC structures and compared to reinforced concrete structures. The research uses a generic bridge with a single pier in the middle, different from the behavior of this research in which the response depends on the axis studied and can become modeled as a frame system. Also, the height and magnitude of the bridges differ significantly. As a part of the conclusions was identified that the use ECC that provides micro-cracks and the capacity of recovery of the located cracks in the shape memory alloys produces significant improvement once the elements are unloaded but dissipate less energy compared to the reinforced concrete elements due to its hysteretic response.

Another important research is "Study on seismic behavior of an elevated concrete tank with the frame-shaped base using SMA damper" (Khosravi et al., 2017) where one of the most relevant points of study for this project is the different response of the structure depending on where the shape memory alloys were located. Where was discovered that not necessarily due to more amount of shape memory alloy will generate a more improved response but will be economically unfeasible, with few amounts of smart materials can be achieved considerable improvements in the structure.

Therefore, on this research to achieve economic feasibility is one of the most relevant parameters thus the shape memory alloys must be just in the plastic hinges and more vulnerable zone due to its expensive cost besides the considerable height of the frame. Only the construction of the piers of the bridge with ordinary reinforced concrete overpass $1 million in 2018. As saw, there is no necessity to have a high amount of shape memory alloys to improve the response.

Background

After seismic events often, the structures suffer a different type of damages for various circumstances, usually, the type of damages depends directly on the behavior of the earthquake-induced to the structure. It is essential to clarify this explanation; that the soil can change the behavior and amplify the magnitude of damages, depending on the depth, type of soil, distance, duration, and frequency. This means after a seismic event people can describe it in different ways, depending on where they were located when the event occurred.

One of the most critical damages in columns of concrete structures after extreme loadings are the cracks. Have a cracks controls are one of the essential parts in the maintenance of the element and integrity of it. As (Y. Li et al., 2018) mention:

> *Cracking is one of the main nonlinear characteristics of reinforced concrete (RC) structures. Once tiny cracks are created, they may expand and lead to accelerated corrosion of steel bars, which reduce structural reliability and durability. Moreover, the large cracks exceed the limit may cause structural failure. Therefore, the durability and carrying capacity of structures can be effectively improved by controlling the development of cracks.*

There can be cracks for several effects, like base shear on columns, diagonal stress, axial force, fatigue and stress in some parts of the column induced by a flexural moment. Therefore, this research has studied the use of new materials of concrete that can resist stress and present a ductile behavior.

Is important to understand the behavior of the earthquakes has produced different affectations on the infrastructure. Not because the event magnitude of one earthquake is quantitatively stronger than another means this will have more damage to the structures on the affected zone.

Costa Rica is a crucial case of study because it is one of the highest seismically countries in the world, with numerous actives volcanoes and a lot of tectonic failures of subduction. Plus, the low investment in infrastructure and researches of structural design or retrofit and null maintenance in constructed structures.
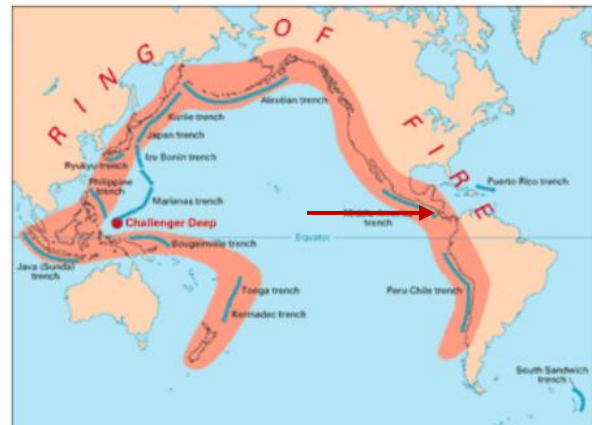
Figure 12. Ring of Fire of earthquakes in the World.
Source: (Pantazopoulou, 2018a)

As seen in the first figure the whole Costa Rican territory is contained in the region known as Ring of Fire where the significant earthquakes occur and are rounded by close tectonic plates in the Pacific side. These plates are due to the subduction of tectonic plates in the world, these types of seismic events produce the earthquakes with higher magnitude events on earth.

In the history of Costa Rica has been numerous earthquakes of significant magnitude, an event in recent times several earthquakes have occurred causing significant costs in the economy of the country, relocation of communities, affected people and dead or missing people, causing the loss of the investment of whole families. In **Figure 13** it can be observed the event magnitude of representative seismic events since 1991.

Figure 13. Representative event magnitude of different Earthquakes in Costa Rica since 1991.
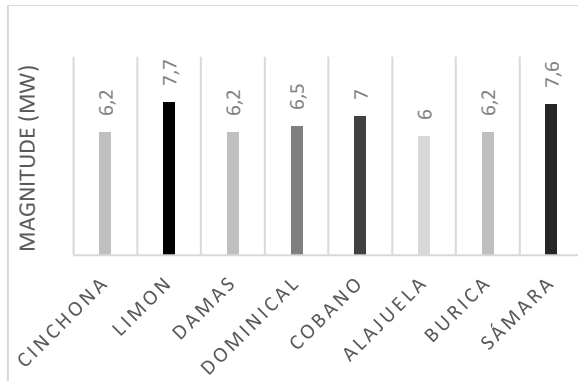Software used: Microsoft Excel.[6]

However, this figure cannot represent the behavior of the earthquakes; it is essential to know the performance of the ground accelerations of these, the amplitude, duration, and other variables. **Figure 14** can be observed the dispersion of the ground acceleration of each seismic event with the data from the Seismologically Web of Costa Rica (RSN). In **Figure 14** there is a boxplot representing the quartiles of the points and the mean of these. All the means are in the same position what indicates all have a normal behavior in statistical analysis as expected. Which is a very good first parameter in the study of data, to check the information can be related just if the behavior of the data is statistically normal. Otherwise, the seismic events cannot be compared.
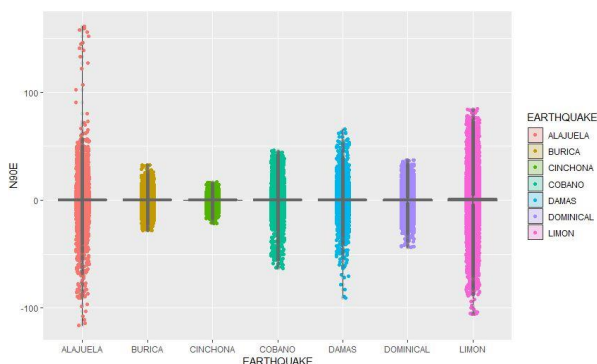

Figure 14. Boxplot of the representative seismic events in Costa Rica, x-axis.
Software used: RStudio.[7]

In the Alajuela's Earthquake, the points of ground acceleration are higher in the magnitude of acceleration and more disperse points than the rest. The Cinchona's Earthquake can be observed a very good aggrupation of the points and all the points are grouped in mainly around the fourth part of the highest and minimum marks of the rest. This does not represent the Alajuela's Earthquake was more intense than the Cinchona's one; it can be viewed in **Figure 13**. Also, does not describe the Alajuela's Earthquake that had more damages in the structures than the rest.

To achieve a better interpretation of the behavior of the seismic events that have occurred in Costa Rica is essential to plot the tendency of the points of the accelerations in function of the time. In this way can be observed the real behavior of the seismic events.

Figure 15 represents the real behavior of some seismic events during the time in Costa Rica. This behavior is in the "*X*" axis, the dataset has the performance of each earthquake in the "x", "y", and "z-axis", this is important to consider because the behavior of the earthquake change depending on the axis taken, in a way to resume the information.
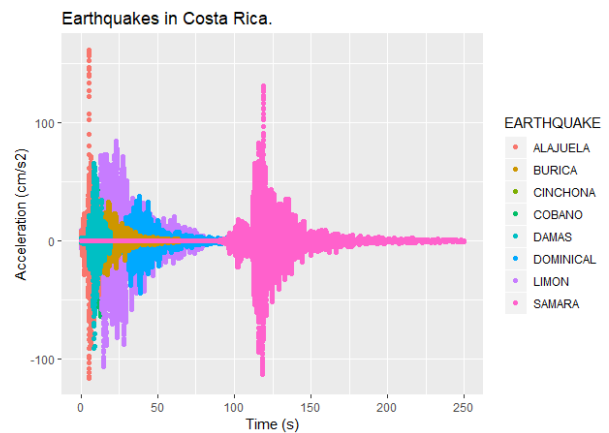
Figure 15. The behavior of the acceleration in function of the time of representative seismic events in Costa Rica since 1991.
Software used: RStudio.[8]

In **Figure 15** just represent the x-axis of every represented earthquake. As shown in the figure the Samara's Earthquake has the highest point of acceleration and the Alajuela's one at the minimum

---

[6] Data from Laboratory of Seismic Engineering, UCR, Costa Rica in X-Axis.

[7] Data from Data from Laboratory of Seismic Engineering, UCR, Costa Rica. Created in RStudio.

[8] Data from Data from Laboratory of Seismic Engineering, UCR, Costa Rica. Created in RStudio.

point. The mean and the median must coincide closely because of the normal behavior is shown in **Figure 14**, this mean of ground acceleration must represent a median magnitude of the event. Is essential to distinguish the behavior of the events during the time, for example, the earthquake of Damas had an ephemeral behavior and low ground accelerations, in another way the earthquake of Samara shows a prolonged event during the time and high accelerations this could lead the structural elements induced by this a failure for fatigue.

As known one of the most certain parameters in the earthquakes is the magnitude of the event. In Costa Rica the highest magnitude recorded was the earthquake of Limón in 1991 with a magnitude of 7,7 Mw.

Figure 16. Consequences of 1991 Earthquake in Limon, Costa Rica.
Source: (Telenoticias, 2018)

This seismic event was traumatically to the whole population of Costa Rica. The seismic event had significant costs and damages in the infrastructure of a missed territory in Costa Rica. Limon is a province that adjoins with the Caribbean Sea; this made liquefaction on most of the soil of the structures due to the high phreatic level of the soil and the sand of the ground. Also, was frequent that people did not follow the Seismic Code of Costa Rica. Usually people used water of the sea as reactive for the cement, this provoked the reinforcement rebars embedded in the concrete were completely rusted or disappeared, the structural elements lost the ductile behavior of the reinforcement designs required for the Seismic Code and the ACI[9] and converted to fragile

components, making the majority fail quickly and unexpected during the earthquake.

Figure 17. Damages in Bridges after the Earthquake of Limon in 1991, Limón, Costa Rica.
Source: (Telenoticias, 2018)

As mentioned, one of the significant parameters is the magnitude of the event, but not always shows the reality of the total damages caused. For example, the site of construction, the site response motion can be amplified by soil conditions and the attenuation of the seismic waves.

An example of this was shown in the earthquake of Cinchona in Costa Rica had a magnitude of 6,2 Mw on 2009, with a depth of 6,0 km and in soil type S-2 (Hard)[10] provoked 25 people die, 17 people disappeared, damages in the hydro-electrical projects of Toro II and Cariblanco. As is explained in the earthquake report (Alvarado et al., 2009) there were 14 affected bridges with a cost of ₡ 1 617 391 200 ($ 2 862 639 USD approx. on august 2018) In which in the report mention that one of the three replaced bridges were superseded on three occasions because it was affected by natural conditions in less than one month. There was a new bridge that had a length of 60 meters preventing that the bases stayed away from the center of the river. Then, just nine months after of the colocation of a "provisional" bridge, this was lost. As mentioned in the final report of the risk management of Costa Rica (Brenes, 2010) the whole seismic event cost USD 546.239.341,17 in 2009.

Furthermore, the earthquake of Samara in Costa Rica with a Magnitude of 7,6 Mw in a soil type S-2 (Hard) with a depth of 14,2 km on 2012, provoked volcanic seismicity and activation of tectonic failures. As Dr. Lepolt Linkimer Abarca mentioned in (Blanco, 2012) that in Costa Rica earthquakes occurs frequently, one proof of this is since 1821 have been 51 earthquakes. This

---

[9] American Concrete Institute, Unite States A.

[10] Agency Lab. Ing. Sismica, INII-UCR, Costa Rica

earthquake was felt in all the country and even in some places of Nicaragua, Panamá, El Salvador and Guatemala. The Government of Costa Rica assessed the costs were around ₡ 22.360-millions (around USD 39.575.221 in 2012) and 240 people in temporary hostels.

Figure 18. The slope of the affected zone after Cinchona's Earthquake in Costa Rica in 2009.
Source: (Díaz, 2015).

This shows that usually more significant magnitude of an earthquake will generate bigger damages in the structures and the socio-economical part of the affected regions. However, this, as shown, is not a rule. The losses in the infrastructures by an earthquake depend not only by its magnitude, but there are also other variables like depth, duration, distance from the hypocenter, direction, and type of the failure, soil supporting the structures.

There are several aspects to consider for the evaluation of susceptibility of disasters in case of an earthquake, for example, the risk of the slide of slopes is a major problem in Costa Rica because of the topography, for instance in the earthquake of Chinchona shown in **Figure 18**. Also, is important to consider the type of soil near to the structures because during an earthquake can generate liquefaction and after this provoke a flashing flood. This has always been the main problem to the bridges and its piers, foundations and structural behavior.

The slide of high slopes is usual in Costa Rica due to the topography filled with valleys, mountains, mountains range and multiple actives volcanoes in the most populated zone of the country.

Figure 19. Damages in the Bridges of Costa Rica as a consequence of NATE Storm, Universidad de Costa Rica.
Source: (Muñoz-Barrantes, 2017)

Another natural event that brings direct consequences to the civil structures in Costa Rica and is one of the most often affectations to the country is the storms. The tropical storms produce damages in the slopes in high mountains and scour the foundations of structures and affectations in the pier of the bridges.

The water level of the river can be as high as the pavement surface of the bridge in some cases, putting vulnerable the whole structure. The water level rises that high due to the vast accumulation of water in the mountains and the ambiance, the whole big trees fall and get stuck in the pier system of the bridge, sometimes miscellaneous structures. This provokes a high hydraulic jump in the river that magnifies the water level — also producing a subcritical flux of water before the bridge and supercritical after this. Also, more material and garbage still accumulating in the

pier system that could induce premature failure or unexpected damages in the design.

Figure 20 shows the affected bridges in the Nate storm in 2017. By color is shown the level damage in the bridges where sky-blue is none and red is high damage. As seen in the national routes of Costa Rica are all over the road. As seen a high storm produce significant damages in the infrastructure and bridges of the Country. The National Route marked as "RN" number 27 is the route where the Salitral Bridge is located what refers to possible altercations made to the piers system.
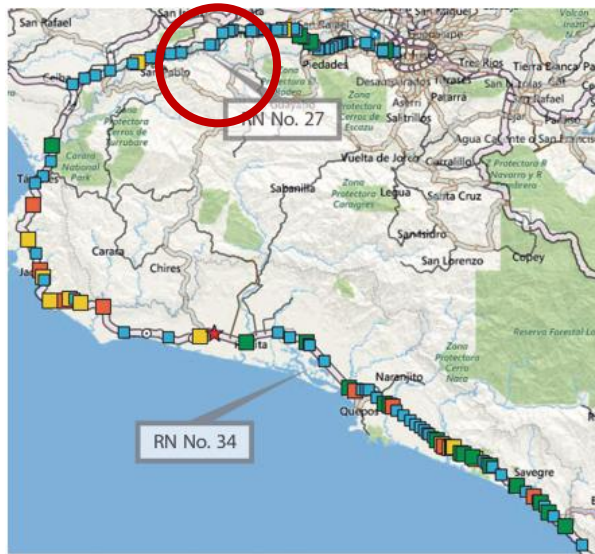

Figure 20. Spatial affectations of the damages caused by the Nate Storm, Costa Rica 2017.
Source: (Muñoz-Barrantes, 2017)

Figure 21 shows the level of damage that can be achieved under a tropical storm in Costa Rica. The complete fallen of a bridge over a river. The magnitude of the water and the flashing floods can be as elevated to disappear entire structures as seen in Costa Rica and Panamá several times. This figure shows the damage produced by the Nate Storm in 2017, taken in the report of damages by the national inspection entity of bridges Lanamme.

Figure 21. Truss of the Bridge over the Pacuare River in National Route N° 243 that collapse as a consequence of the Tropical Storm Nate, Costa Rica 2017.
Source: (Muñoz-Barrantes, 2017)

In the presentation about the resilience in the structures under the climate change, as explained by (Delgado-Pitti, Corrales-Poveda, Rojas-Morales, & Naranjo-Castillo, 2018) in the risk report of United Nations, Costa Rica is the number five in the top 15 reported most exposed countries to natural threats and in risk is number eight. These positions are taken without considering climate change in the frequency of natural events from 2012 to 2016. Countries like Japan and Netherland are top in the side of the threats but not in the risk positions due to work done in the vulnerability of the structures decrease the risk significantly. This is directly proportional to the direct and indirect costs of the Government, reconstructing and retrofitting the infrastructure more often.

Salitral Bridge

The Salitral bridge is located in the highway Jose María Castro Madriz, national route #27, located on the 48 kilometer of this. The columns or piers of this bridge will be used in this research as an example of the comparison between the behavior of a constructed the bridge with ordinary concrete and steel as a reinforcement. The model of the same columns using smart materials and engineered cementitious concrete will recreate the model of the improved pier system.

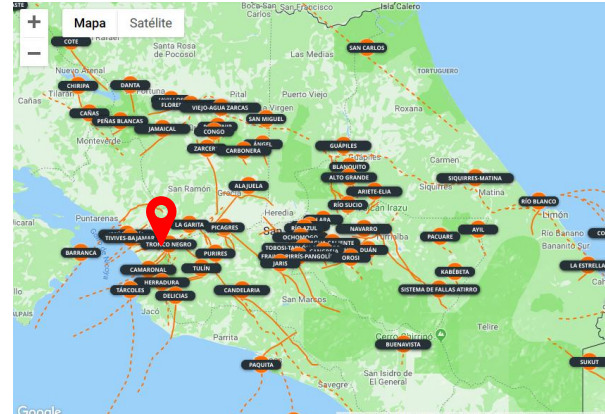Figure 22. Location of Salitral Bridge, Costa Rica.
Source: Google Maps.

Due to there are several types of research using and studying generic columns or piers of the bridge, even testing in real scale piers of bridges. For example in the University of Illinois, the U.S.A. by the Dr. Bassem Andrawes, but in Costa Rica the use and information of these smart materials in the columns or structural elements is almost null. There are researches about the use of other smart materials but used as energy dissipators (ED), dampers or utilized in the retrofits.

Most of these ED are used to protect the superstructure of the Bridges and is usual to locate this in between the piers and the superstructure, as shown in **Figure 36**, otherwise if these ED were found in the base of the columns could make the structure unstable, but this generates the columns receive almost all the extreme loads directly, which provokes plastic hinges in the elements and cracks and continuing maintenance is necessary. It is essential to make researches that help Costa Rica due to the low maintenance investment in the bridges, helping and researching about problems that can contribute to the infrastructure and economy of Costa Rica will always bring benefits to the population.

Figure 23 present the multiple local tectonic failures in the zone close to the location of the Salitral Bridge. Most of these failures are in the Route number 27 and in the downtown of San José, where a simulation of the high magnitude seismic event in this zone will create a magnification of the event on the Salitral bridge.

Figure 23. Local failures close to the Salitral Bridge.
Source: (Universidad de Costa Rica, Rica, & Instituto Costarricense de Electricidad, 2018)

Taking a designed and constructed a bridge in Costa Rica, in a highway that is important or necessary to the economy of the country will help to the objective of the research that goes beyond the structural engineering. The use of smart materials in piers could help in to reduce the time of retrofit or maintenance and expected the life of the structures. This can be useful in highly transited roads or very far areas in rural cities where the transportation of machinery and professionals could be difficult.

Figure 24. Salitral Bridge from above.
Source: (Vargas-Alas et al., 2017)

The Salitral Bridge's superstructure is based in two steel sections beams supported on two frames of reinforced concrete with four mobile restrains, with a tread surface of a concrete made as a rigid pavement in the bridge, with a length of 160,0 m. It was designed in 1994 and constructed in 2000, is located in Orotina, Alajuela with a live load of HS20-44 and based on the AASHTO 1992 15 Ed,

based on the last measure in 2016 the average diary transit is of 20686 vehicles[11].

Figure 25. View of the piers of the Salitral Bridge, Costa Rica.
Source: (eBridge, 2018)

The columns have a height of 36 meters, from the ground to the superstructure. Has a foundation based on stilt and based on the "Lineament of Design of seismic-resistant of Bridges of Costa Rica" is in a seismic zone III shown in **Figure 26** which corresponds to the second highest seismic zone, but is very near to the most upper seismic region of Costa Rica.
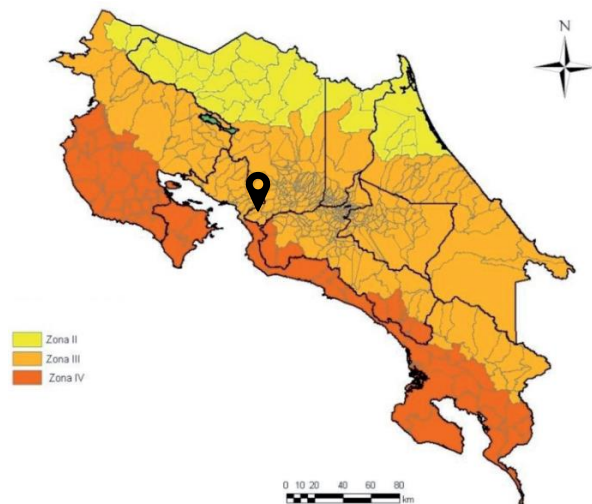

Figure 26. Seismic Threat zones in Costa Rica.
Source: (Colegio Federado de Ingenieros y Arquitectos de Costa Rica, 2012) "Lineamientos para el Diseño sismorresistente de puentes".

As shown in **Figure 28** this bridge is between several active failures that can potentially generate an earthquake with a magnitude of 6,5 Mw or

more; this is necessary to be considered as near failures.

Figure 23 represents some of the local failures in Costa Rica around the position of the Salitral Bridge. As seen in the figure several close failures remark the seismic vulnerability of the bridge. Therefore, the probability of significant earthquakes during the life expectancy of the bridge.

As specified by the Dr. Mariano Protti, an expert in earthquakes in OVSICORI[12], (Telenoticias, 2018) there are potential of a significant earthquake in the south part of Costa Rica (location of the Salitral Bridge), this earthquake could achieve a magnitude around 7,2 Mw or 7,4 Mw
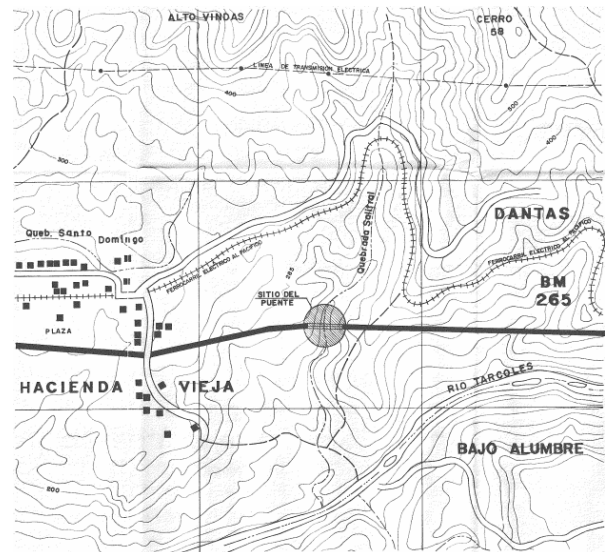
Figure 27. Location of the Bridge in the Original Blueprints (Hacienda Vieja, Orotina, Alajuela, Costa Rica).
Source: (eBridge, 2018)

The Salitral Bridge was designed by Ph.D. Miguel Cruz, one of the most recognized engineers in Costa Rica and was part of the persons in charge of the creation of the "Seismic Code of Costa Rica", the "Alignment of Bridge Design in Costa Rica", and professor of Graduate and Undergraduate at the program of Civil Engineering and Structural Degree at the University of Costa Rica. This is the primary reason to expect an exquisite structural design of the bridge and not supposed to have a lot of plastic deformation or unexpected failures, proving the behavior and performance of the piers

---

[11] Source: Lanamme, University of Costa Rica.

[12] Vulcanological and Seismological Observatory of Costa Rica.

a remarkable bridge under extreme loadings and compare it to the use of new technologies in the materials of structural engineering. The bridge was designed with the "Standard Specification for Highway Bridges A.A.S.H.T.O 15 Edition 1992", "Interim Specification 1993", Live loads: HS-20-44, seismic load: acceleration = 0,35G. The construction was designed by "Specifications for the Construction of roads and bridges" (Costa Rica) CR-77.
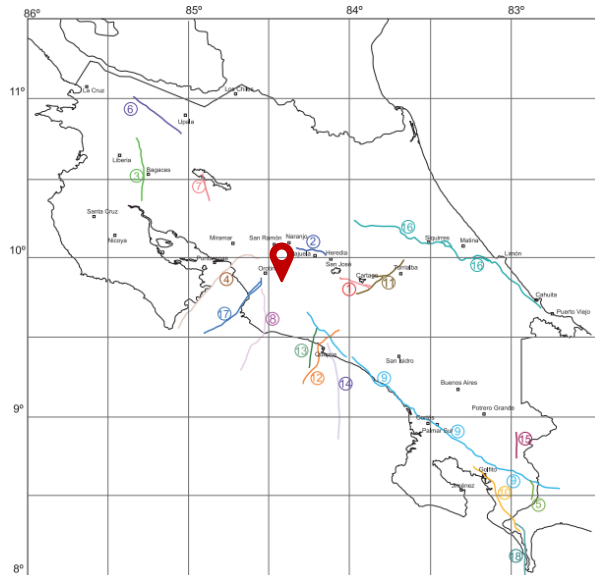

Figure 28. Active failures with a potential Earthquake of 6,5 Mw or more in Costa Rica.
Source: (Colegio Federado de Ingenieros y Arquitectos de Costa Rica, 2012) "Lineamientos para el Diseño sismorresistente de puentes".

Also is mentioned in the "Lineamientos para el Diseño sismorresistente de Puentes." (Colegio Federado de Ingenieros y Arquitectos de Costa Rica, 2012) this is a bridge with an operational importance factor of 1,25, the highest level of importance in this lineament due to it's a bridge that is required after an earthquake and is fundamental to the economic activity of the region and the country, is in strategic routes to harbor, the two main airports of Costa Rica and borders and with a higher investment of USD 10,000.00 in 2012. This is also important in the selection of this bridge, as a part of the research and comparison with new materials.
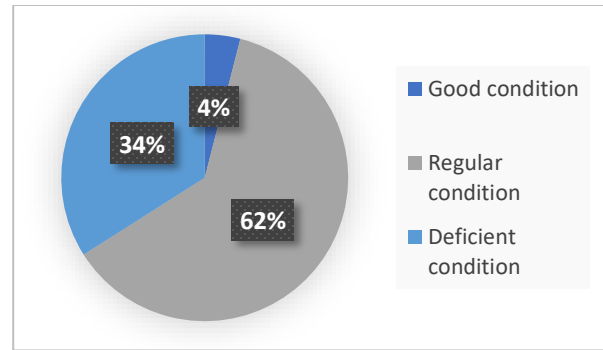

Figure 29. The necessity of Attention of the structures.
Source: (Umaña-Venegas, 2018)[13]

In November of 2018 was released the remarkable information showed by the experts of the eBridge program in Costa Rica. In the interview made to the experts as shown in **Figure 29** just the 4% of the bridges in Costa Rica (National highways without considering "Redes cantonales" bridges) are in good condition, also was exposed in the forum that will be necessary $ 1.500 million (USD) retrofits the bridges in deficient conditions. The exhibitor Eng. Giannina Ortiz from the I.T.C.R.[14] exposed the importance of investment in modern technologies of the Bridges to prevent the severe damage. Also, was mentioned by Eng. María Ramírez-González in charge of the Department of Bridges in the M.O.P.T.[15] the importance of applying funds to the maintenance of bridges in Costa Rica and there are 10% of the studied bridges are in a critical stage, and 25% require retrofit actions.

The actual state of the Salitral Bridge is cataloged as alarming by Lanamme[16], the entity on the charge to review the condition of the bridges with the eBridge program. The report remarks the severe damages in the structure of this bridge located in the national route #27. Most of the main worries are in the surface and the pavement of the superstructure, but there is also evidence of reduction of structural capacity in the inspection and lack of information about some structural elements indispensable to create a criterion of the structural capacity.

---

[13] The figure was made with Microsoft Office. The values were taken from Umaña-Venegas (2018).
[14] Instituto Tecnológico de Costa Rica.

[15] Ministry of Public Works and Transportation, Costa Rica.
[16] Universidad de Costa Rica, Costa Rica.

Figure 30. State of the shock-transmitters of the Bridge on bastions with dust, moisture, and trash inside the cover. Source: (Vargas-Alas et al., 2017)

Figure 31 shows the footage of the actual stage of the shock-transmitters of the bastions, used to decrease the seismic impact under extreme loading in the bridge. There is evidence of dust, moisture, and trash inside the elements that contain these transmitters. Also, as indicated in the figure there is a missing element related with the oil flow, this could lead to a reduction in the capacity response to ground accelerations or null seismic advantage. The Lanamme concluded that these shock-transmitters had not received timely maintenance.

Figure 31. Detachment of the paint and corrosion protection system, PTFE pot bearing, support south of Bastion 1. Source: (Vargas-Alas et al., 2017)

Also, as seen in **Figure 31** a detachment of the protection system in the inferior face of the metalic plates and there is rust in the screw of the joint. It was recommended to make a detailed inspection of the PTFE pot bearing to assess the durability

and structural capability and conserve the protection of the system.

Figure 32. Cracks in the bastions of the Salitral Bridge. Source: (Vargas-Alas et al., 2017)

Also, was evident the cracks in the bastions of the bridge that could lead to a reduction in the structural capacity. The cracks are in about 0,50 mm with a separation of 1500 mm; there are large cracks in the horizontal and vertical axis. There is a detachment of concrete in the corners of the and exposure of the reinforcement.

As part of the alarming conclusion of the report, the main recommendations are

- Evaluate the live load capacity of the bridge using the LRFD methodology described in the AASHTO Assessment of Bridges 2011.
- Make an immediate intervention in the structural slab of the bridge.
- Assess the condition of durability and structural capacity in the restraint in the piers of the Bridge.
- Assess the condition of durability and structural capacity in the PTGE pot bearing and shock-transmitters and include a guide of inspection.
- Constant review in the cracks of the bastion and retrofit of these.
- Put the missing screws in support of the restrains.

It is remarkable to describe that there was not found reports or inspections where was reviewed the frames or piers of the bridge, even when these are the main structural system to maintain the integrity of the system. Due to the severe slope in the topography represents the difficulty in accessing at the bottom and top of the piers. Therefore, there are no reports of these, and there

are not proves of cracks, or other structural damages in these or the restrains at the top. This information is not only relevant to the development of the research but also the security of the transit, civilians and public investment.
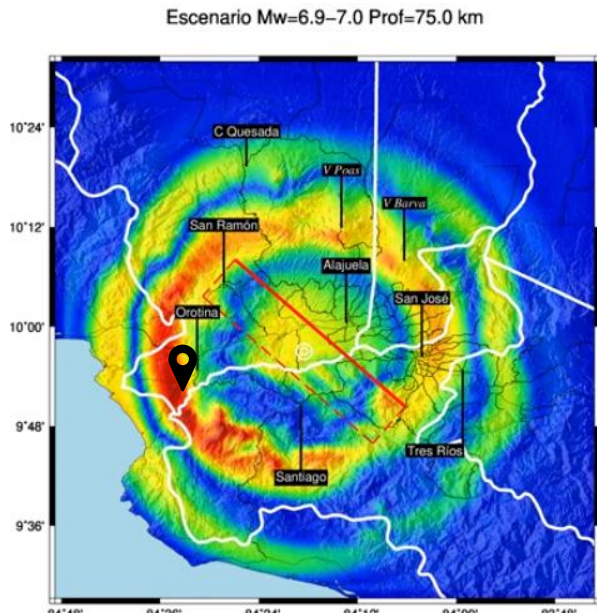

Figure 33. Simulation of an Earthquake in the Central Valley of Costa Rica (Downtown).
Source: (Universidad de Costa Rica, 2018)

The laboratory of Seismic Engineering, part of the University of Costa Rica, made a simulation of an earthquake with a magnitude between 6,9 Mw and 7,0 Mw and depth of 75,0 km. The simulation was located in the urban part of the country with a higher density of infrastructure and people. In this area is usually to have seismic activity with significant magnitude.

As seen high magnitude event will create big propagation waves that will impact directly to the location of the Salitral Bridge in Orotina, Costa Rica. The waves will have a higher increment in this zone. Therefore, the importance of assesses the behavior of this Bridge is relevant to the investment of the Country.
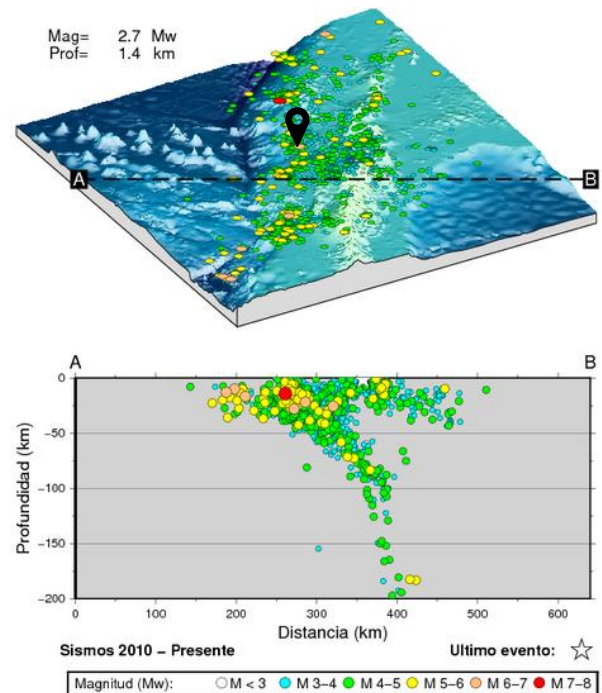

Figure 34. Cross-profile to the subduction zone of Costa Rica.
Source: (Universidad de Costa Rica, 2018)

Figure 34 shows the seismic event since 2010 in Costa Rica, in the upper part of the figure is the location of the events, as seen the bridge is located in a high seismicity zone where many earthquakes with a magnitude between 5,0 Mw and 6,0 Mw has occurred and is close to one between 7,0 Mw and 8,0 Mw as the red point indicate it. The highest part of the topography in the figure corresponds to the territory of Costa Rica in Land. The bottom of the figure represents the depth of the events occurred; it is evident that most of the higher earthquakes have been in the zone between -50,0 km and the surface, which indicate the high seismicity of the country. This figure also puts in evidence the structure in the study has a high vulnerability to seismic events during its service life.

Bridge Piers

The piers of a bridge are the connection between the substructure or foundations and the superstructure. The primary purpose of this is to transmit the charges (live and dead) of the superstructure to the foundations and to the ground. This means the primary goal of the piers in

the bridge is to support the applied axial loads, but in case of extreme loading is applied to the bridge the piers will have the main point of importance in the behavior of this.

Under extreme loading as earthquakes, tsunamis, high wind, crashes the piers of the bridge will have applied moments or flexo-compression and shear, this could be implemented for the base shear of an earthquake.

As mentioned in (Moon, Roh, & Cimellaro, 2015) the damping or energy dissipation capacity of bridge columns is critical because of it is directly related to the design spectrum and affects the seismic performance of whole bridge systems. This is one crucial reason why the piers of the bridge should have the capability of energy dissipation.

In the piers of RC is essential to have a regular control of the width of the cracks, this is directly related to the structural behavior of the bridge. The cracks are generated in the part of the element submitted to tensile strain, due to the low resistance to deformation of the concrete, it produces fragile cracks in the column, and the steel of reinforcement is the one that makes ductile the element supporting the loads in part in tension. Therefore, the importance to use improved materials as the implementation of reducer of cracks in the concrete, the use of fibers in the concrete adds great resistance to tensile strain and produces a ductile behavior.

In structural terms, it exists two different kinds of structural columns, the short columns, and the long column. The first one is a robust column, with a significant length-cross-section ratio, compared to the other kind; this kind of columns have a fragile behavior, and the failure is abrupt. Otherwise, the long columns the usual failure mode is by buckling, these could sag before structural failure occurs. The separation between these two kinds of columns changes depending on the seismic codes.

One of the principals causes of damages in the bridges of Costa Rica are the events known as flashing floods this consists in a massive amount of cumulative water from the mountain that descends at high speed bringing with it strong fallen trees and big rocks, hitting the piers of the bridge and affecting this directly or the foundation of this. In **Figure 35,** it can be observing the damage provoked for this kind of event in the bridges of Costa Rica.

Figure 35. Affectation of the foundation of the pier of the Bridge "La Alegria" caused by the effects of the river, Turrialba, Costa Rica (2015).
Source: Vías y puentes colapsaron a causa de temporal. Extra Newspaper.

In this **Figure 35** during the event commented the water level of the river reached the superstructure of the bridge, applying in this way constant horizontal push to the pier, this is an important parameter to consider in the design of this kind of elements or the retrofit of this. Today, the pier of the bridge still with the same state of the damaged foundation. This exemplified the low investment of maintenance and renovation of structural elements and infrastructure in Costa Rica.

Another structural problem caused by the low maintenance of infrastructure is the null control of the width of the cracks in RC elements or the condition of the paint or corrosion in steel elements. The visits are sporadic with low technology to give an accurate judgment. Also, there are near very active volcanoes that produce acid rain what provokes the metallic elements to get corroded faster. Therefore, is essential to have new technologies like the SMA as reinforcement or dampers, engineered cementitious concrete and other new materials in the bridges, to reduce the cracked elements, self-rehabilitation, re-centering of items, the high resistance of corrosion and low costs of maintenance.

Figure 36. Bridge Cañas-Liberia Highway, Costa Rica.

As shown in **Figure 36** the use of seismic dampers is frequently used in Costa Rica and around the world. These dampers are usually put in between the connection of the piers of the bridge and the beams. This produce that the base shear, fatigue, and push caused by an earthquake enters to the columns and dissipate in the dampers and the super-structure of the bridge have negligible earthquake loads. Therefore, the columns receive almost all the seismic loads provoking severe damages in these. The cracking is one of the most critical parameters to consider in retrofit after seismic events, technologies as SMA and ECC combined could help to decrease these, therefore, the costs of maintenance.

Plastic Hinge

One of the most important parts to consider on the design, inspection, and retrofit of structural elements in a bridge is the creation of plastic hinges in RC elements. Hinges are zones in the structures where plastic deformation occurs with higher intensity compared to the rest of the structural elements, for example, in RC sections in the hinges the concrete is cracked, and the steel yielded. This was provoked for cyclic loads or extreme induced loads. The plastic hinge is defined as an inelastic deformation in structural elements, as beams and columns. This deformation usually cannot be recovered and is produced by a load beyond the yield point of the ductile material. The creation of plastic hinges breeds fragile elements and susceptible to failure if the loads still increasing. Hinges are usually formed at the start and end of the beams and columns. Some of the common plastic hinges are flexural hinges, shear hinges, and axial hinges

As mentioned in (Yu-Chen & Nguyen, 2014) when a ductile RC member is subjected to severe earthquake loadings, its end regions typically show severe damage, forming plastic hinges.

To achieve accurate results in a nonlinear static analysis requires adequate modeling of the plastic hinges generated in the structures, this is why it is essential to know the possible points of

the creation of plastic hinges. "Modeling of connection stiffness for FR moment frames shall not be required except for joints that are intentionally reinforced to force the formation of plastic hinges within the beam span, remote from the column face. For such joints, rigid elements shall be used between the column and the beam to represent the effective span of the beam". (FEMA 356, 2000).

In the research (López López, Tomás Espín, & Sánchez Olivares, 2017) it was studied different kinds of Plastic hinges, for example, the proposed in the FEMA-356[17] and two other modeled by empirical experiments. As shown in **Figure 37** it can be observed the behavior of the curves of plasticization of the Piers.
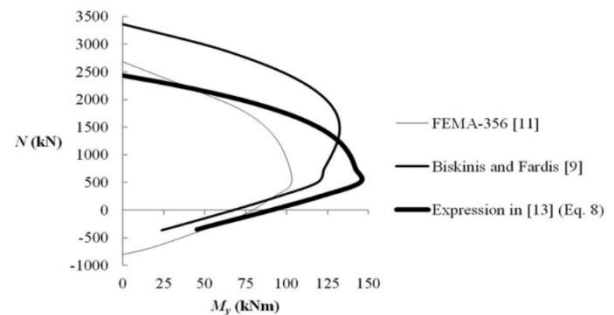

Figure 37. Plasticization of Piers under different Plastic hinge models.
Source: (López López et al., 2017) "Influencia del tipo de rótula plástica en el análisis no lineal de estructuras de hormigón armado"

As shown the FEMA-356 presents more conservative behavior compared to the models proposed by Biskinis and Fardis, and the adjusted models of these authors. As conclusion of studying the influence of the kind of plastic hinge on the nonlinear analysis of RC structures, Antonio López and Gregorio Sánchez concluded that the adjusted models presented more resistance and capacity of deformation, these models had more base-shear and control displacements, but the results of spectral accelerations are higher and take more forces to the structure. Also, that the proposed plastic hinge models help to contrast with the models included on the normative, these usually are more conservative. This contrast is more pronounced the higher the height of the structure and the value of the acceleration of the ground, as

---

[17] Federal Emergency Management Agency (U.S.A. Government).

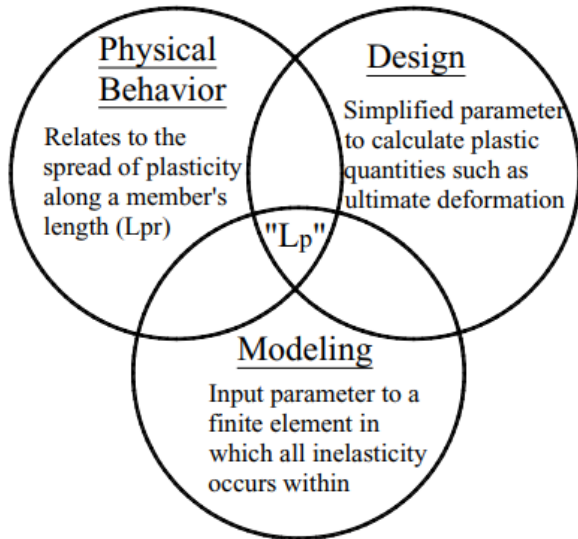well as when considering the modal lateral load pattern in the analysis.

Figure 38. Meanings of the Plastic Hinge Length, Lp. Source: (Fedak, 2012)

In the hinge rotation at a certain point of the structure at the yield point can be calculated as

$$\theta_y = \left(\frac{M_y}{E_c I}\right) l_p$$

Equation 1

Where the M_y is the yield moment capacity of the shear wall or segment, the E_c is the concrete Modulus, I the member moment of inertia and l_p the assumed plastic hinge length. In which the analytical models the value of l_p shall be set as equal to 0,5 times the flexural depth of the element, but less than one story height for shear walls and less than 50% of the element length for segments.

Shape Memory Alloys

The Shape Memory Alloys (SMA) is one kind of innovative materials called smart materials, in which these materials can change the properties under specific circumstances. There are different kind of Shape Memory Alloys, one of the most used is the Nickel-Titanium alloy known as NiTi or Nitinol.

As mention in (Mihálcz, 2001) the Shape Memory Effect (SME) was discovered by A. Olander in 1932, he found the pseudo-elastic behavior of the alloy made of Au-Cd (Gold and Cadmium) trying to make an innovative fusion for the submarines with corrosion resistance. In 1938 the composite based on Cu-Zn was observed the appearance and disappearance of the Martensite phase in function of the variable temperature. Then, the most used alloy was discovered in the early of 1960s at the U.S. Naval Ordnance Laboratory, this alloy is also known as Nitinol derived the name from this discovery, "Nickel-Titanium Naval Ordnance Laboratory".

The NiTi alloy has two specific phases; these two phases are directly depending on the temperature. This material is called smart because of the tendency to change the shape depending on the heat applied. Other aspects continue to be the same as the volume, weight, and density. At lower temperatures, the NiTi phase is called Martensite and at Higher temperatures in the Austenite phase.

As also mentioned in (Mihálcz, 2001) "The composition and metallurgical treatments have dramatic impacts on the above transition temperatures. From practical applications, NiTi can have three different forms: martensite, stress-induced martensite (superelastic), and austenite". The martensite form is ductile it can be easily deformed, otherwise when does the austenite from the material is hard like the Titanium.

The behavior of Nitinol directly dependent of the temperature and the change of the two phases previously mentioned is called thermoelastic martensitic transformation, this is just the transformation crystal structures at the atomic scale, at macro-scale, this is recovering of the original shape of the element. "While most metals can be deformed by slip or dislocation, NiTi responds to stress by simply changing the orientation of its crystals structure through the movement of twin boundaries." (Mihálcz, 2001).

This transformation of phases will not always occur if a NiTi specimen is applied axial force beyond the maximum strain will be deformed permanently without the Shape Memory Effect (SME).

One of the most critical aspects in the NiTi SMAs is the super-elasticity, it refers to the capacity of the alloy to return to its original shape upon unloading after a substantial deformation. This is the transition of Martensite to austenite to its stable structure. It can be strained several times without being plastically deformed.
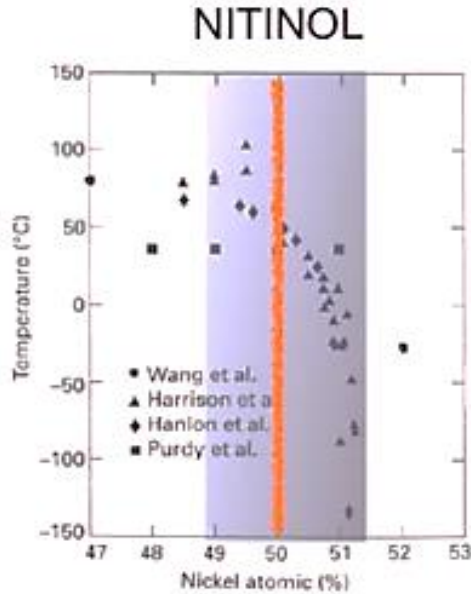
Figure 39. The composition of the Nitinol alloy.
Source:(Stoeckel, 2011)

In the atomic composition of the material **Figure 39**, as seen, it represents the quantity of each composite to create the alloy. The range of the transformation temperature of the alloy is around 100°C to -100°C, concluded by the researches made. The percentage of Nickel used in the Nitinol alloy can be useful and work from an engineering perspective from 49% to 51% (Stoeckel, 2011), represented as a gray column in the figure. One relevant aspect to consider is that adding or subtracting 1% or less have significant implications in the transformation temperature of the material, usually in more than two orders of magnitude.

However, the most remarkable point in the figure is the difference of having more Nickel or Titanium in the composition, due to its relevance in the behavior of the element.

If the Nitinol alloy has less the 50% of Nickel in the composition the behavior of the material it is the SME or how it is called the Martensite SMA, where if the material is plastically deformed it will not be recover by itself at ambiance temperature. The alloy will need heat to be induced above the transformation temperature to remember its original shape. Then, the change in the behavior depends in the atomic composition of the alloy in function of the quantity of Nickel. The main change is represented with an orange line in the figure at 50%. If the percentage of Nickel is more than 50% the transformation temperatures decrease drastically and more of the compositions

presented at 30°C or less. Which it means that composition of the alloy behaves different, in this case, the SMA present the characteristic called Superelasticity, therefore the alloy is Superelastic SMA. Thus, minimum changes in the atomic composition of the alloy represent remarkable changes at the macro behavior of the elements, varying from Martensite SMA or Superelastic SMA and the range of the quantity of each composite should be similar to produce effective SMAs.
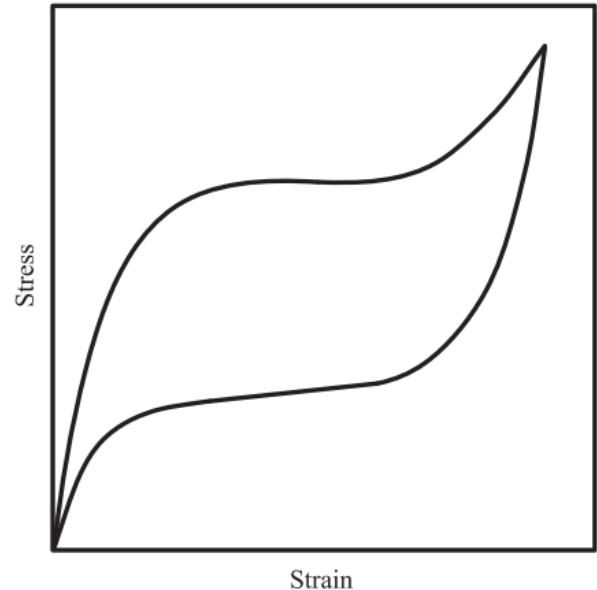
Figure 40. Classic superelastic SMA stress-strain response.
Source: (Abdulridha et al., 2013) Behavior and modeling of superelastic shape memory alloy reinforced concrete beams.

In the superior curve of **Figure 40,** it can be seen that there is the material of SMA in the Martensite phase, once is in the maximum point start to decrease and go back to its initial point (with some negligible loss of recovery) in an Austenite phase. This behavior is in function directly of the temperature that is induced to the element.

Figure 41. The generic stress-strain response of an SMA above temperature A_f.

Source: (Khosravi, Ghaderi, Atashi, & Mousavi, 2017) "Study on seismic behavior of a concrete elevated tank with the frame-shaped base using SMA damper."
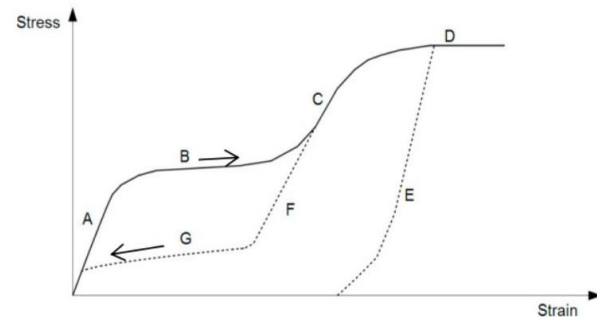
"About 8% strain can be recovered by unloading and heating. Strain above the limiting value will remain as a permanent plastic. Service stresses must be safely below the yield strength of the material, and in cyclic loads, the service stress must be kept below fatigue limit". (Mihálcz, 2001)
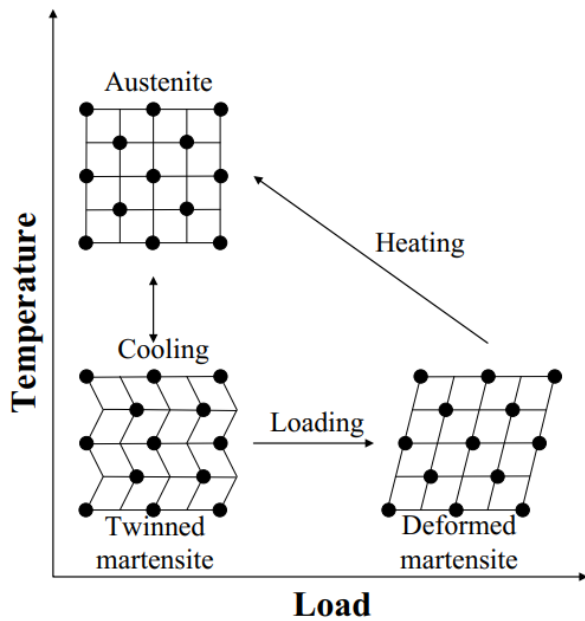

Figure 42. Representation of the transformation of the Martensite and Austenite phases depending on the temperature and deformation.
Source: "Performance of Superelastic Shape Memory Alloy Reinforced Concrete Elements Subjected to Monotonic and Cyclic Loading" (Abdulridha, 2013)

The martensite phase consists of the stage the alloy of NiTi has at low temperatures or after high stress induced. Has a parallelogram structure of 24 crystals and the type of face-center cubic (FCC) usually seen in the steel by the rapid cooling of the Austenite, this is transformed to Austenite until the lower temperature is reached M_f. Martensite is stress-induced if loaded at a temperature above A_f if the stress is released this becomes unstable, resulting in the superelastic effect.

Once start heating the element this reaches the temperature of transformation M_s in which the phase changes to Austenite, stable at higher temperatures and low stresses. In this phase, the structure is Body-Center Cubic (BCC). The rapid transformation between these two phases when the element is load and unload or

when it changes the temperature the behavior of smart material. The atomic structure of the Titanium is BCC with a packaging factor of 0,68 and presents allotropy; otherwise, the atomic structure of the Nickel is an FCC with a packaging factor of 0,74, this is an element promoter of the Austenite, give more resistance to high and cryogenic temperatures. However, offer more strength to corrosion and more ductility; the alloy of NiTi conduces the variety of structures depending on the heat applied, due to the thermo-elastic nature of SMAs an increase in temperatures act as a decrease in stress

Table 1. Selected Mechanical properties of the NiTi		
Parameter	Austenite	Martensite
Ultimate tensile strength (MPa)	800-1500	103-1100
Tensile yield strength (MPa)	100-800	50-300
Modulus of elasticity (GPa)	70-110	21-69
Elongation at failure (%)	1-20	Up to 60

Fuente: (Mihálcz, 2001) "Fundamental characteristics and design method for nickel-titanium shape memory alloy."

SMAs present six unique characteristics: Shape Memory Effect (SME), one-way memory, SME two-way memory, Superelasticity, damping hysteresis, minimal fatigue and absence of corrosion as mentioned by (Abdulridha, 2013)
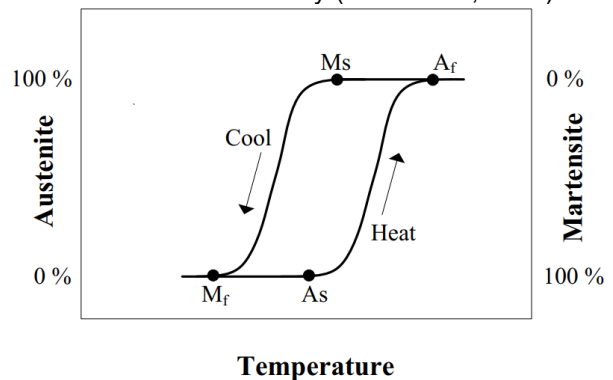

Figure 43. Temperature Hysteresis.
Source: "Performance of Superelastic Shape Memory Alloy Reinforced Concrete Elements Subjected to Monotonic and Cyclic Loading" (Abdulridha, 2013)

In **Figure 43** is presented a representation of the behavior of SMA consisting in a temperature cycle, as shown at lower temperatures the SMA is in

starting the Austenite phase (A_s) when heat is applied, and the element start warming and can be hotter than the point of the finish of the Austenite (A_f). Then the element starts cooling a begin the transformation of the microstructure to the twinned martensite, continuing to the Martensite phase (M_s) until it is completely cold to achieve the 100% of the Martensite phase (M_f), completing like this the cycle of temperature that represents the SMAs. This cycle does not represent any stresses applied is essential to say the figure represents only changes made by the temperature on the SMA.
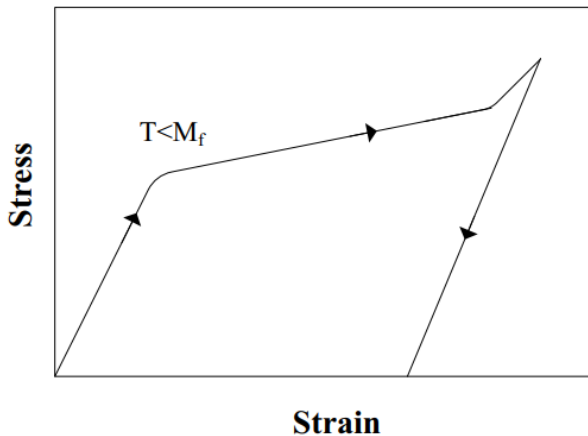

Figure 44. Martensite Stress-Strain Relationship
Source: "Performance of Superelastic Shape Memory Alloy Reinforced Concrete Elements Subjected to Monotonic and Cyclic Loading" (Abdulridha, 2013)

When the temperature is under the M_f, the SMA is in the Martensite phase and can be easily deformed as shown in **Figure 44** and at this moment the SMA Martensite is like ordinary steel with a residual deformation.

In the transition stage between M_s and M_f as shown in the figure **Figure 43** the alloy is in both phases at the same time, Martensitic and Austenitic phase as can be seen in the **Figure 45** thanks to the Austenite, when temperature is more than the M_f but less than A_s there is a reduction of residual deformations relative to when the temperature is below M_f.
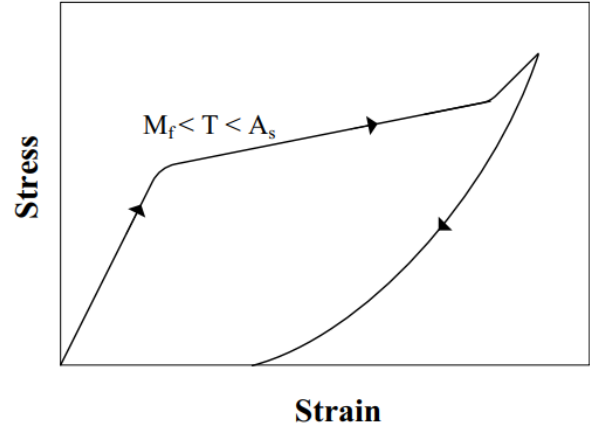

Figure 45. Transition Stage Stress-Strain Relationship
Source: "Performance of Superelastic Shape Memory Alloy Reinforced Concrete Elements Subjected to Monotonic and Cyclic Loading" (Abdulridha, 2013)

Then, if the temperature continues increasing and overpasses the A_f point, the response is altered as shown in **Figure 46**. Moreover, it can show that when the SMA is on entirely in the Austenite phase can be achieved full recovery of residual deformations. One of the main characteristics is the Superelasticity of the SMA that can pass from Martensite to Austenite and vice versa, only with loads and not depending on the temperature, SMA can recover from strains up to 10% and still fully recovering the deformation. Depending if the SMA was cold worked or heat treated the material will have shape memory or Superelasticity.
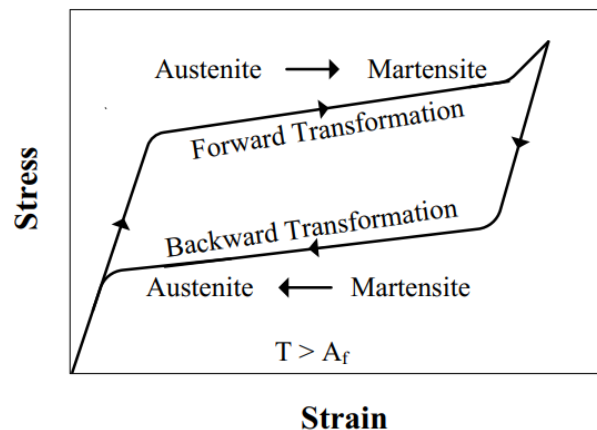

Figure 46. Austenite Stress-Strain Relationship.
Source: "Performance of Superelastic Shape Memory Alloy Reinforced Concrete Elements Subjected to Monotonic and Cyclic Loading" (Abdulridha, 2013)

When the use of the Superelasticity is required the SMA element needs to mold the piece in the

required shape. This is important to have in mind because it is limiting from the constructive point of view. The fabrication of the shear and confinement reinforcement in the concrete elements are usually with several shapes, unlike the longitudinal reinforcement bars. This will be a deficiency in the use of SMA as reinforcement. Nowadays in the construction industry can exist the pre-construction sub-area using Building Information Modelling (BIM) and other aspects to previsualize the consecutive phases of construction, but usually, there will always be red-line blueprints and changes in situ, these changes will represent severe costs in the new fabrication of original shapes of the SMAs.

Due to the SME the SMA has the capability to recover the original shape, passing from Martensite to Austenite this is called one-way memory, but the material can be "trained" to "remember" two different configurations, by deforming the SMA in the Martensitic phase and heating it into the Austenite phase, where it regains to its original size prior to deformation.

characteristics of the use of SMA in concrete or as a damper are the extensive plastic deformation, large capacity to absorb energy, ability to re-center and conserve the integrity of the structure. Also, the use of SMA extends the lifetime of the structures and can be included in existing structures.

As shown in **Figure 48** there is a graphic resume of the shape memory alloys, where presents the difference between the two stages of the alloy depending on the temperature. As explained the behavior of this material depends directly on the temperature regardless if this is an super-elastic SMA or Shape Memory SMA. Both type of SMA present a martensite and austenite stage but differs on the range of temperature. The martensite stage is seen at lower temperatures and high stresses, otherwise the austenite stage at high temperatures and low stresses. The main change of the behavior is consequence of the atomic structure of the material due to this does not dislocate when is plastic deformed but change from austenite to martensite.
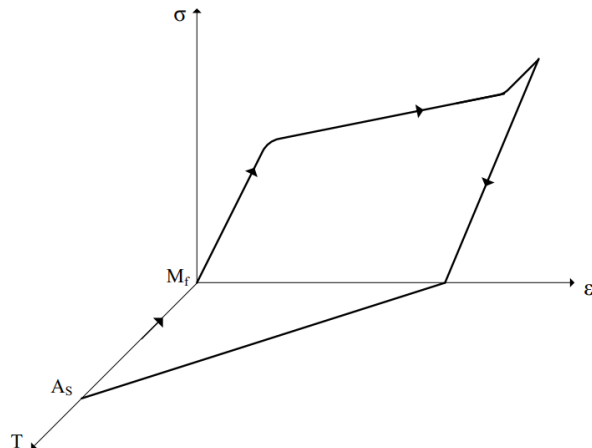

Figure 47. Stress-Strain Temperature Curve for SME
Source: "Performance of Superelastic Shape Memory Alloy Reinforced Concrete Elements Subjected to Monotonic and Cyclic Loading" (Abdulridha, 2013)

Since these dates of 1960s with the researches about these smart materials start to increase dramatically and search for the use of this particularly. The SMA has been used in diverse applications, for example in aero-spatial engineering, mechanical engineering, glasses, toys, cellphone antennas (old cellphones), golf clubs and one of the primary uses is in Medical applications, there are many types of research about SMAs in this topic. Some of the essential
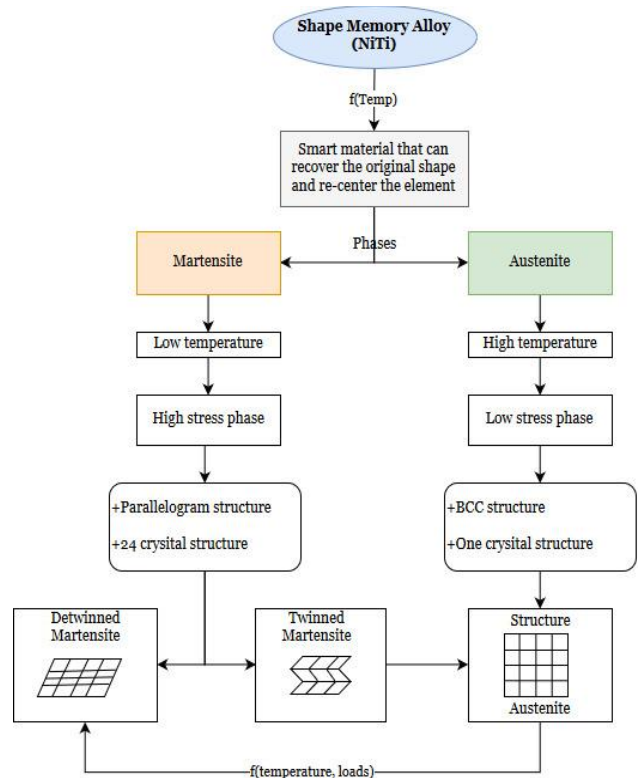

Figure 48. SMA detail of the structure material.
Software used: Draw.io

Recently, are increasing the cases of researches in the civil engineering, specifically in the structural department. There are researches about the behavior of SMAs under axial forces, stress, fatigue, strain. Also, several structural uses like in wires inside of beams, braces, energy dissipaters, re-centering devices in bridges, in water tanks, connections in structural steel, as reinforcement in the concrete.

For example in the Research Article "Nonlinear Analysis for the Crack Control of SMA Smart Concrete Beam Based on Bidirectional B-Spline QR Method" (Y. Li et al., 2018) studied the crack control of RC beams reinforced with SMA wires. The study with bidirectional B-spline QR method (BB-SQRM), this presents the discretization with a set of spline nodes in a two-way plane model. The structural displacements were proposed with a linear combination of cubic B-spline interpolation functions, and the elastoplastic stiffness equation of the beams was derived with an explicit method for the constitutive law of concrete. The results of the model were compared with ANSYS models this uses a Finite Element Method (FEM), the results between the method and the software were very close and that the depth-span ratio of RC beams, pre-strain, and eccentricity of SMA wires have a significant influence on the control performances of beam cracks.

Also, the research article "Performance of Seismic restrainer with SMA Springs for Sliding isolation of single-layer spherical lattice shells" (Zhuang & Wang, 2016) put under different seismic excitations a single-layer of the spherical shell to see the seismic response using sliding isolator. This isolation is based on flat steel-Teflon sliding isolators and superelastic SMA spring restrainers. One of the important points of study in the research is large-scale superelastic NiTi helical spring studied through a cyclic experimental test. There is a complex model modeling the isolation by a bilinear force-displacement hysteresis model; a based on the mechanical behavior of the SMA was made a multilinear model, and hysteresis model and the shell was modeled with Finite Element Method. "The study shows that the seismic response of the controlled lattice shell can be effectively reduced by using isolation and control devices. Furthermore, the seismic response of the isolation system such as peak displacement and residual displacement can be effectively controlled by using the developed SMA spring restrainers".

(Zhuang & Wang, 2016). Also, was found that the residual displacements of the isolation are almost zero, demonstrating the re-centering capability and large deformation property of SMA and can be used to eliminate permanent deformation in isolators and to protect the structure under extreme loadings.

The "study on the seismic behavior of a concrete elevated tank with the frame-shaped base using SMA damper" (Khosravi et al., 2017) as the SMAs are not sufficiently economical to be used in structures, designers found a combined usage of these materials along with the steel to have high efficiency. This research is about an elevated tank with a volume of 1500 m^3 and frame-shaped base of 37,5 m. The tank is on a frame-shaped base with eight columns with a cross-section of 1,2 m x 1,2 m on a seventh floor (with a moment frame system) and a height of 37,5 m above the foundation.

As seen in **Figure 49** there were different models of the position of the dissipaters with SMA in the elevated tanks to be compared. El-Centro Earthquake data was used to simulate the behavior of the container with the accelerations. Many types of research use El-Centro Earthquake as an example of a representative earthquake in the structure; this seismic event was an Earthquake with a magnitude of 6,90 Mw in California, United States.
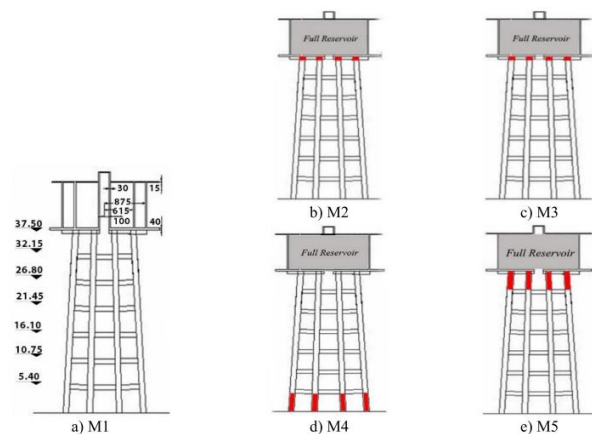

Figure 49. Modeling of the elevated tanks of the research. Source: (Khosravi et al., 2017) "Study on seismic behavior of a concrete elevated tank with frame-shaped base using SMA damper."

The red elements in this figure represent the use and position of SMA in the frames. The model M1 does not have SMA; the M2 had a single-string of SMA damper, M3 had a double-string of SMA

damper in the upper section, M4 had SMA in the first-floor rebar and M5 on the seventh-floor rebar of the tank. As part of the conclusions the M2 model presented 30% less displacement than a tank M1 without SMA, the M3 had a 5% improvement of reduction of movement compared to M2. M2 and M3 presented more substantial ductility than M4 and M5, which is mainly due to the placing of the SMA at the base. Therefore the use of these dampers is suggested in high seismic areas.

Moreover, M4 and M5 are not economically viable to be used in a real design. This research gives a fundamental lesson, the use of dampers or energy dissipaters are expensive, and not because there is more SMA means there will be more reduction of the displacements and high consumption of these can make a construction project in real life no viable due to the high costs. This is why the importance of the optimize the quantity and location of dampers, dissipaters, and use of SMA in the models analyze see deep the behavior under extreme loadings.

In the research of the paper "Nonlinear dynamics of SMA-fiber-reinforced composite beams subjected to a primary/secondary-resonance excitation" (Asadi, Bodaghi, Shakeri, & Aghdam, 2014) was studied nonlinear free vibration and the primary/secondary resonance analyses of SMA fiber reinforced hybrid composite beams with symmetric and asymmetric lay-up.
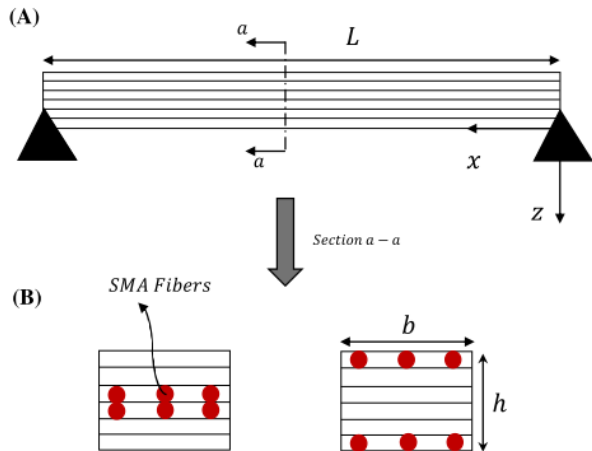

Figure 50. Schematic of the hybrid laminated composite beam. Beams studied in the research.
Source: (Asadi et al., 2014). "Nonlinear dynamics of SMA-fiber-reinforced composite beams subjected to a primary/secondary-resonance excitation."

To simulate the behavior of the SMA materials and calculate the recovery stress was used the simplified Brinson constitutive model and cosine phase transformation kinetics. To predict the action of the smart laminated beam was used the Euler-Bernoulli beam theory and nonlinear von-Kármán strain field.
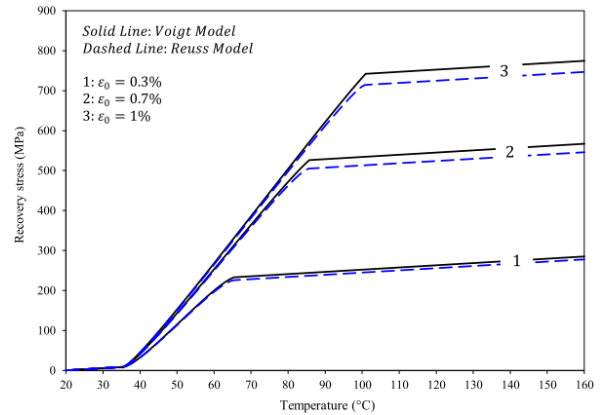
Figure 51. SMA recovery stress versus the temperature with different pre-strains.
Source: (Asadi et al., 2014). "Nonlinear dynamics of SMA-fiber-reinforced composite beams subjected to a primary/secondary-resonance excitation."

The results showed "geometrical and physical parameters such as the SMA volume fraction, the amount of pre-strain in the SMA fiber, the orientation of composite fiber, vibration amplitude and temperature are important factors affecting the free vibration characteristic in the pre/post-buckled region and primary and secondary resonance." (Asadi et al., 2014).
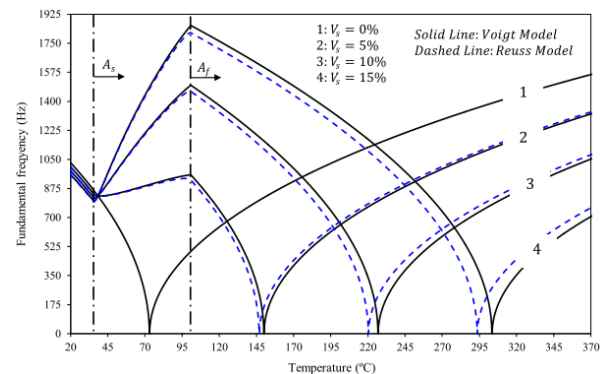
Figure 52. Variation of the fundamental frequency in the pre/post-buckled regions for $\varepsilon_0 = 1$ %.
Source: (Asadi et al., 2014). "Nonlinear dynamics of SMA-fiber-reinforced composite beams subjected to a primary/secondary-resonance excitation."

In the research about "An Experimental Study on the Structural Behaviors of HIRC Beams using Nickel-Titanium SMA wires" (Jo & Min, 2017) was

studied a comparison between ordinary RC beams and Highly intelligent reinforced concrete (HIRC) beams. The main achievements in the research were to determine the behavior of the HIRC elements, load-temperature deflection curve, ductility-effective depth, recovery, cracks patterns, and failure mode. There were different beams tested, for example, Reinforced concrete (ordinary), Beams with SMA wires, Garnet additive and Nylon fibers called HIRCGN, another with SMA wires, Garnet additive and Polypropylene fibers called HIRCGP, other beam used was the one with SMA wires, Fly-ash additive and Nylon Fibers called HIRCFN and the last beam had SMA wires Fly-ash additive and Polypropylene fibers
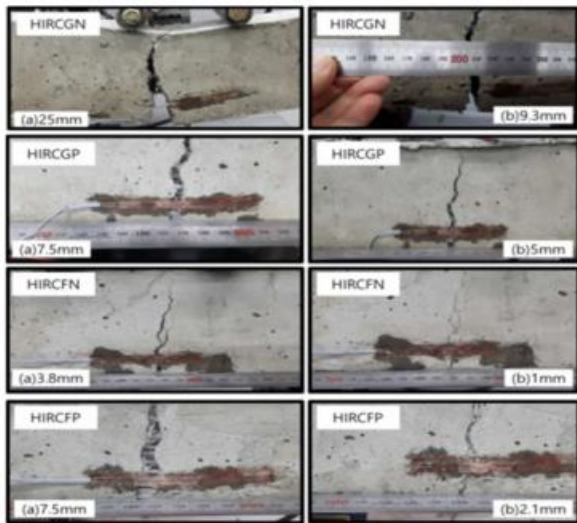

Figure 53. Crack pattern of specimens: (a) Before activation of SMA (b) After activation of SMA.
Source: (Jo & Min, 2017) "An Experimental Study on the Structural Behaviors of HIRC Beams Using Nickel-Titanium SMA Wires"

The results of the research indicated that a good recovery rate in the HIRC beams could be obtained when heat is added to the SMA wires and could be potentially used for structural self-rehabilitation capability and deformation monitoring. The RCB showed fragile behavior compared to the flexibility showed by the HIRC beams in which the high stiffness was maintained until the beam yielded despite the crack occurrence. Majority of the HIRC beams showed compressive fractures rather than sudden fractures, in the conclusions these results were attributed to the deep beam shape, this had a shear span-to-effective depth ratio in the range of-2.5. Although large crack width and deformation

occurred in the tension part of the beams these were capable of maintaining the loads, then once the elements were unloading and applied heat to these nearly restored the residual crack width and deformation, the most effective were the HIRCGN and the HIRCFP.

In the paper about the "Seismic performance of Segmental Rocking columns connected with NiTi Martensitic SMA Bars" (Moon et al., 2015) is research of segmental blocks of columns post-tensioned with 36,5 mm martensitic SMA bars as energy dissipators bars. The research used two types of SMA bars to compare the differences. This is a way too important to have a reference in the design and the models of the main research. It was used Martensitic NiTi SMA bars and NiTi superelastic bars, the main difference between these is that the first ones recovers the shape until heat is applied to the element and the superelastic bars re-center their original shape instantly.

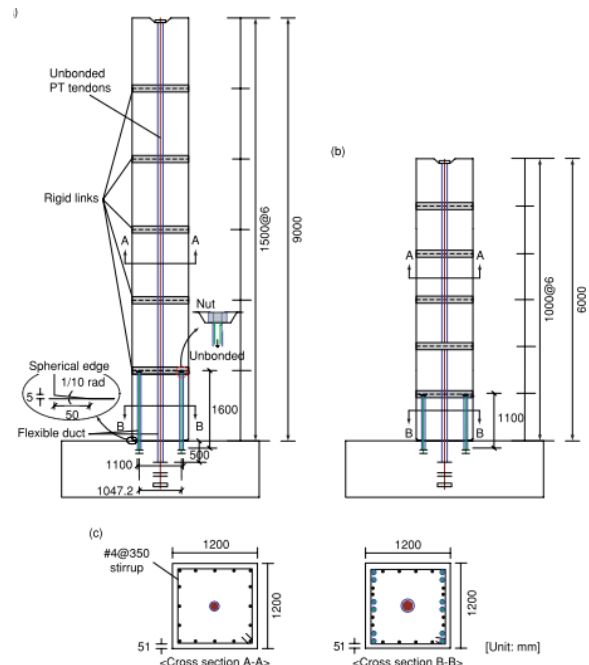Figure 54. Segmental column specimens: (a) aspect ratio of 7.5 (Roh et al. 2012); (b) aspect ratio of 5.0; and (c) tendon, rebar and SMA bar arrangements for sections A-A and B-B
The table aspect ratio of 7.5 (Roh et al. 2012); (b) aspect ratio of 5.0; and (c) tendon, rebar and SMA bar arrangements for sections A-A and B-B
Source: (Moon et al., 2015) "Seismic Performance of Segmental Rocking Columns Connected with NiTi Martensitic SMA Bars."

As a part of the conclusions, applying 50% post-tensioned force increase the lateral resistance but decrease the energy dissipation, around 1%. Therefore it was concluded that the post-tensioned force considered does not affect the seismic performance of the columns. The equivalent viscous damping ratio of Martensitic SMA bars obtained 10,5%-12,5%. The superelastic bars used as an energy dissipater the damping ratio shows 5%-7%, almost half compared to the Martensitic. Moreover, the post-tensioned force level and column aspect ratio have a little effect on their damping capacity. Therefore the selection of the SMA type is the most useful parameter to decide the seismic performance of the columns.

The study of "Behavior and modeling of hybrid SMA-steel reinforced concrete slender shear wall" (Palermo & Abdulridha, 2017) as explained the plastic hinges are designed to be controlled by flexural yielding while preventing non-ductile modes of failure. Although the primary performance objective may be achieved, the damage and permanent deformations could prevent a structure from being serviceable after a seismic event and, besides, prohibit post-earthquake repairs. SMAs can dissipate energy through hysteretic damping and provide strength and displacement capacities comparable to conventional deformed reinforcement but also has high fatigue and corrosion resistance. Furthermore, the superelastic properties of SMAs are dependent on the temperature, and the lower elastic modulus (approximately 60 GPa) relative to steel reinforcement (200 GPa) results in greater displacements under service loads.

The paper investigates the performance of a concrete shear wall reinforced with superelastic SMA in the plastic hinge area; the SMA was only used as the principal longitudinal reinforcement in the boundary zones, while the longitudinal reinforcement in the web region consists of deformed steel reinforcement under cycling loading. The choice of SMA bar size was designed based on readily available bar size, and boundary zone of the steel reinforced wall, it was used couplers to connect the bars of steel to NiTi. Six additional sharp end bolts were distributed in two rows at each coupler, with this modification, the SMA bar sustained its full-strength capacity and strains in the range of 10%, as seen in the **Figure 55**.

Figure 55. The modified coupler of the Research.
Source: "Behaviour and modeling of hybrid SMA-steel reinforced concrete slender shear wall" (Palermo & Abdulridha, 2017)

The NiTi sample was in compliance with ASTM F2516-07, the modulus of elasticity of the SMA bar was approximately 38 GPa, while the steel bar experienced a 205 GPa modulus. The SMA bar demonstrated a rounded response before yielding. Therefore, the yield point was based on 0,2% offset, resulting in approximate stress of 380 MPa. During the last loading cycle, the SMA bar strained to 8,4% and had remarkable residual recovery.
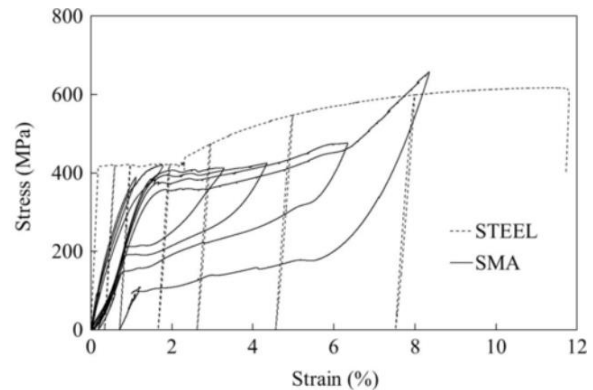
Figure 56. The cyclic stress-strain response in the reinforcement.
Source: "Behaviour and modeling of hybrid SMA-steel reinforced concrete slender shear wall" (Palermo & Abdulridha, 2017)

A critical part to remark is that the SMA bar failed earlier than expected at the couplers, the SMA bars presented a 91% strain recovery capacity. Otherwise, the steel presented a strain recovery of 6%. In **Figure 56** is shown a remarkable comparison between the ductile steel and the Superelastic SMA, under cyclic loads as shown. As it can be seen the behavior of the SMA recovers almost all the strain after cycling loads. Otherwise the steel is under the plastic range what it means, once the element is unloaded the strain cannot be recovered. Then is essential to use if possible SMA

in the plastic location of elements, making the element can recover its structural capability once is unload.

In the cracking characteristics, during the first load stage, both shear walls experienced flexural cracks near to its bases, corresponding to a lateral load of approximately 48kN and displacement of 2,4 mm (0,1% drift). At the end of the second stage of the load it was evident diagonal shear cracks. The residual crack widths demonstrated the capacity of the SMA wall to recover displacements, the recovery of the crack width and crack opening recovery capacity for the SMA wall was 88% throughout testing, with steel was only 24%. In the load-displacement response the steel reinforced wall yield at 9,4 mm (0,39% drift) corresponding to 116 kN of load, while the SMA wall yielded at 26,4 mm (1,1% drift) of displacement corresponding to 112 kN of load, the peak average load sustained by the wall with steel was 156 kN corresponding to 76 mm, for the SMA wall was 133 kN corresponding 72 mm.
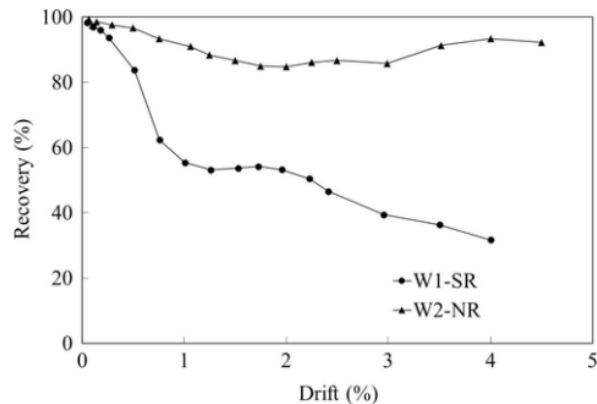

Figure 57. Displacement Recovery Capacity-Lateral Drift Responses.
Source: "Behaviour and modeling of hybrid SMA-steel reinforced concrete slender shear wall" (Palermo & Abdulridha, 2017)

As shown, the recovery of strain and re-centering on the W2-NR wall (with SMA) was remarkable compared to the W1-SR with only ductile reinforcement. The steel in the W2-NR yielded before the SMA bars, due to this the wall had a minimum of 85% of recovery capability up to 3% drift. Which demonstrates the SMA bars have the capacity to recover large displacements while other reinforcement bars are yielding. At the point of rupture of the steel the SMA wall presented more capacity of recovery acting at 93% up to 4% drift, staying by itself and without the plastic

deformation of the steel reinforcement. The recovery capacity of self-centering systems is intended to permit post-earthquake repairs.

In the dissipation of energy, the wall with SMA dissipated 7750Nm of energy, that corresponds to a 60% of the energy dissipated by the wall W1-SR.

Figure 58 shows the stress-strain response of the research based on super-elastic Nitinol bars changing the temperature. As seen the recovery capacity decrease when the temperature is increased.
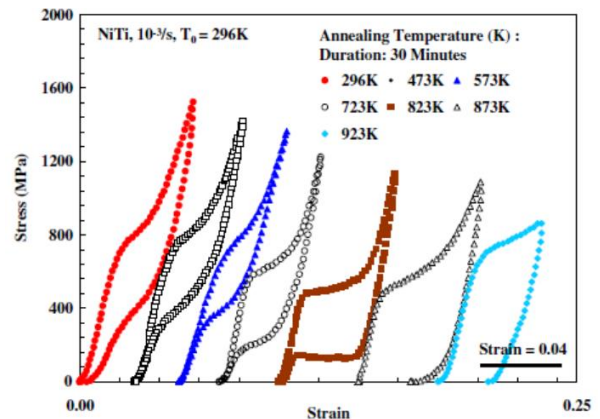
Figure 58. Stress-Strain Curves for Different Annealing Temperatures (Nemat-Naser and Guo 2006). "Superelastic and cyclic response of NiTi SMA at various strain rates and temperatures."

Also, the company FIP Industriale, known for its structural products, as dampers and isolators are investigating and already are products using Superelastic SMA as axial restraint to take advantage of the superelasticity of the SMA in the austenitic state, as shown in **Figure 60**.
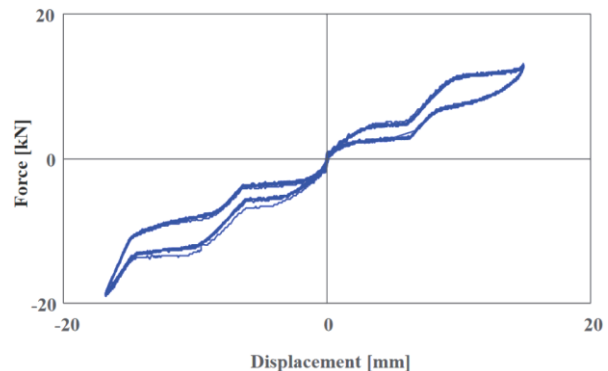
Figure 59. Experimental force vs. displacement curve of a SMAD.
Source: (FIP, 2016)

Figure 59 represents the hysteretic response of the SMAD under experimental cyclic loading; it was remarked in the product information the strong re-centering capacity of these devices.

Figure 60. SMADs as installed in the Basilica of San Francesco in Assisi, Italy. Source: (FIP, 2016)

The devices used are shown in this previous figure, where the SMAD seems to be located as dovel in the slab of the Basilica. As seen even when the SMA are an emerging technology in the construction industry there is a substantial research under this material and used in as several mechanisms, reinforcement, dissipator, retrofit and wires in tension. Therefore, the importance of study in the vanguard of the technology in the structural area in a country with high seismicity as Costa Rica, and possible solutions to the low maintenance in the structures.

Engineering Cementitious Concrete

This material was first developed by Dr. Victor C. Li in the University of Michigan in the Faculty of Civil and Environmental Engineering. He developed the Engineering Cementitious Concrete (ECC) as part of the researches on high tensile concrete with fibers. Nowadays there are several types of ECC, but usually this material present 300 times more deformation capacity, more than two times flexural strength, and higher compressive strength.
ECC is a type of ultra ductile fiber reinforced cementitious composites developed for applications in massive material usage, cost-sensitive construction industry (V. C. Li, 2003). This technology was helped by the active participation of many organizations internationally. This material presents 500 times larger strain capacity compared to ordinary concrete or fiber reinforced concrete (FRC), around 5% of strain. Can be cast as self-compacting casting, extruded or sprayed.

The cost-benefit ratio presents a higher initial cost than concrete; the long term benefits are sufficient to drive it to the construction industry.
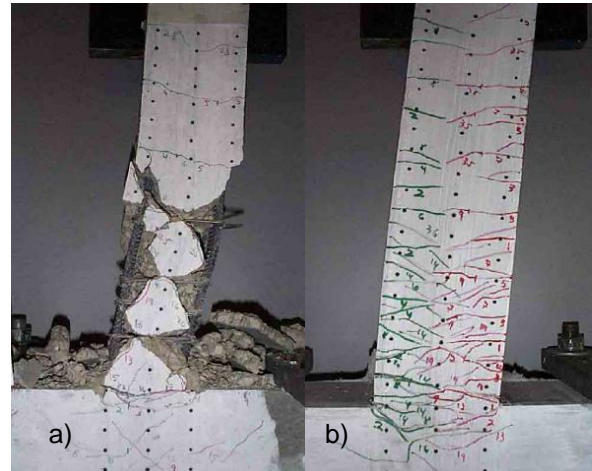
Figure 61. Damage behavior of (a) R/C and (b) R/ECC without stirrups, shown at 10% drift. Even at this high drift level, no spalling of the ECC was observed. In contrast, the R/C column lost the concrete cover after bond splitting, and spalling occurred.
Source: (V. C. Li, 2003)

Figure 61 shows the performance of columns using ordinary concrete and ECC columns without shear reinforcement. A reverse cyclic loading showed that the use of ECC in structural elements without shear reinforcement produced more dissipation of energy and drift capacity that reinforced concrete as conclusion may need less or no conventional steel shear reinforcements. Also, it was showed that the integrity of the column could be better maintained replacing the ECC for stirrups.

A uniaxial tensile test confirmed that large deformation (1,3% strain) could be imposed without causing any cracks. Compared to high strength concrete, ECC revealed significant improvement in flexural performance regarding ductility, load-carrying capacity, shear resistance, and damage control.

ECC differ from other types of high-performance fiber-reinforced cementitious

materials (HPFRCC) in that the microstructures are optimized using micromechanical models to achieve high ductility, with crack widths limited below 100 μm (Hosseini & Gencturk, 2015).

Figure 62. Compatible deformation between ECC and steel reinforcement (right) showing microcracking in ECC with load transmitted via bridging fibers. In contrast, the brittle fracture of concrete in normal R/C (left) causes unloading of concrete, resulting in high interfacial shear and bond breakage.
Source: (V. C. Li, 2003)

Four different ECC mixtures, which were designed for full-scale applications, with different cost and material sustainability indices (MSI) were investigated.

The mixture designated as M45 is the most commonly used ECC design. HFA mixture was considered for being greener than the other ECC mixtures due to its high fly ash content. PPF mixture uses a low-cost fiber, and it is considerably more economical than the other ECC mixtures. Finally, SF mixture includes very thin particles only, and it is considered as a trial mixture to investigate potential improvements in tensile properties (Hosseini & Gencturk, 2015).

In the research made by Hosseini & Genturk (2015) was calculated the cost and Material Sustainability Indices (MSI) in function of ordinary concrete as the primary variable. The cost of each mixture was estimated based on the unit costs of the constituents (for large purchases) which were obtained from the leading suppliers of the materials in North America. The cost of each ECC mixture is given relative to the cost of concrete. The costs associated with the preparation of the mixtures were not included in the calculations as they might vary depending on the project and other factors such as the cost of electricity.

The ECC mixtures can be up to 3,3 times more expensive than conventional concrete, and the main contributor to the cost is the existence of the fibers. Therefore, PPF is the less costly compared to other ECC types.

The ECC was designable for achieving targeted structural performance levels, sustainable concerning social, economic and environmental dimensions; self-healing when damaged and functional to meet requirements beyond structural capacity.

"Engineered Cementitious Composite (ECC) is an exclusive type of cement mixed with a unique composition of low volume fibers and different composites to impart high flexibility, high tensile strength besides the ability to repair. Conventional concrete and fiber reinforced concrete has brittle nature and hence crack easily under environmental and mechanical loads affecting the durability of structures." (Kewalramani, Mohamed, & Syed, 2017).

As explained previously, the creation of plastic hinges in the structures is harmful to the safety of the these. It causes permanent damage to the elements, structural capacity and could eventually collapse the structure. In RC structures one of the main reasons for the creation of plastic hinges are the cracks produced. A cracked zone in an element represents a region of potential plastic deformation in which the damages cannot be recovered in Ordinary RC (ORC) (Portland cement and steel bars).

The use of use of ECC reduces the formation of plastic hinges dramatically, because of its unique capacity to enduring tensile forces. The purpose of ECC makes more flexible elements compared to ORC structures; this does not mean the structure will have more lateral displacements but can achieve more movements without several damages.

Table 1. Mixture constituents, sustainability indices and relative costs, and mechanical properties of considered micro concrete and ECC mixtures (mixture proportions are in terms of weight and fiber content is 2% by volume for all mixtures PVA: polyvinyl alcohol, PP: polypropylene).

		ECC Mixtures			
	Concrete	HFA	M45	PPF	SF
Mix constituents					
Cement	1	1	1	1	1
Fly ash	0	2	1,2	2	0
Silica fume	0	0	0	0	0,1
Sand	3,25	0,8	0,8	0,8	0
Water	0,65	0,57	0,55	0,65	28
High-range water reducer	0	0,01	0,01	0,013	0,006
Cellulose	0	0,00112	0,00112	0,00112	0,005
Fiber	-	PVA	PVA	PP	PVA
Sustainability indices and cost					
Total energy (MJ/L)	2,46	5,39	5,96	4,51	10,95
Water used (L/L)	0,4	0,93	1	0,93	1,07
Solid waste (kg/L)	0,2	−0,76	−0,46	−0,73	0,33
CO_2 (g/L)	373,28	532,98	623,5	511,85	1431,29
Unit cost (1/L)	1,00	2,53	2,60	1,55	3,29
Mechanical properties					
Compressive strength (MPa)	37,5	58,6	55,2	54,5	56,2
Strain at compressive strength (%)	0,3	0,3	0,3	0,3	0,3
Cracking strength (MPa)	2,9	1,75	1,5	1	1
Tensile strength (MPa)	2,9	3,25	2,5	1,75	1,75
Strain at tensile strength (%)	0,0091	2	1,75	1,75	1,75
Ultimate tensile strain (%)	0,0091	4,5	4,25	4	4
Young modulus (MPa)	17500	25000	25000	25000	25000

Source: (Hosseini & Gencturk, 2015)

The use of ECC in Costa Rica, and especially in the bridge specified for this research is expected to have better performance than regular concrete in structural behavior improving the ductility of the RC elements, but also gaining in other characteristic.

For example in the research "Engineered cementitious composites for modern civil engineering structures in hot arid coastal climatic condition" by (Kewalramani et al., 2017) explained the behavior of ECC in hot and coastal conditions improving the capabilities of the concrete, the location of the used Bridge of Salitral have these two parameters took in the research.

As explained ECC is designed to produce strong a ductile material that can be used when the fiber RC may not be appropriate. For example, brittleness of concrete increases with an increase in compressive strength, putting a limit in high strength concrete. The use of ECC develops highly flexible cementitious materials for structural and infrastructural applications, having characteristics of high strength concrete beside increased tensile strain capability compared to standard fiber

reinforced concrete. The ECC is high-performance fiber reinforced cementitious composites designed to resist large magnitudes of tensile and shear forces.
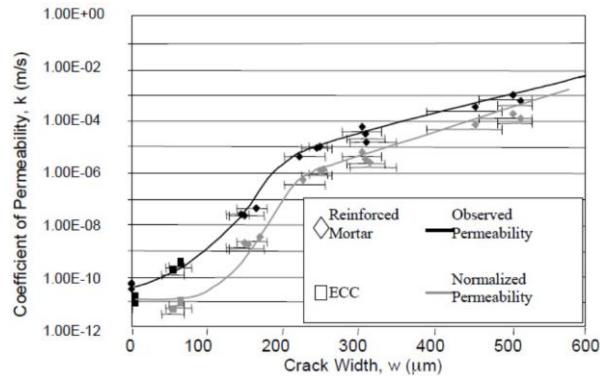

Figure 63. The coefficient of permeability vs. crack width for ECC and reinforced mortar
Source: (Kewalramani et al., 2017)

As shown in **Figure 63** the use of ECC reduces the width of the cracks, the quantity and reduces permeability which decreases the possibility of corrosion of the steel, usually vulnerable in coastal zones.

In the research "Energy-dissipating and self-repairing SMA-ECC composite material system" (X. Li et al., 2015) explained how due to the deformation incompatibility between brittle concrete and ductile steel, the energy dissipation capacity of steel might not be fully engaged during extreme loading. Moreover, the use of more reinforcement in the critical regions will lead to construction difficulties and reduce RC component ductility due to the less yielding of steel rebars. Also, the whole structure may survive an earthquake the severe damage to concrete, and large drift is inevitable, leading to significant repair and retrofitting efforts and costs.

Table 2. The mix design and compressive strength investigated								
Specimen	Water	Cement	Sand	Fly ash	Superplasticizer	Fiber coarse aggregate		Average compressive strength
	(kg/m^3)	(kg/m^3)	(kg/m^3)	(kg/m^3)	(kg/m^3)	vol (%)	(kg/m^3)	(MPa)
ECC	307	227	556	999	2,6	1,8	-	36,5
Concrete	207	370	721	-	-	-	1142	44,4

Source: (X. Li et al., 2015)

As explained, the use of ECC materials unlike the standard fiber reinforced cementitious (FRC) elements, features a pseudo-strain-hardening behavior under tension with tensile strain capacity hundreds of times that RC or FRC.
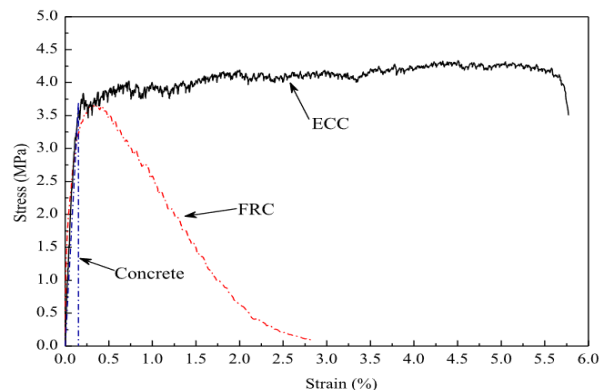

Figure 64. Tensile stress-strain curves of strain-hardening ECC, tension-softening FRC, and quasi-brittle concrete.
Source:(X. Li et al., 2015)

The use of ECC is produce more ductile behavior compared to FRC even when both use the same type and amount of fibers. The design of the ECC gives extra strain and permits large tensile stress.

ECC can be tailored to dissipate energy upon straining while preventing large cracks and fractures, therefore the plastic hinges in the structures. By eliminating the typical fracture modes such as bond splitting, spalling, and large cracks under large applied deformation, the ECC can protect the SMA from a hostile environment (X. Li et al., 2015).In the research was developed a novel SMA-ECC composite with ultra-ductile ECC with a design of 5,5-6,6% of strain and microcrack width below 40 µm. The high flexibility of ECC also ensures the structural integrity of SMA-ECC by eliminating the typical fracture failure modes like bond splitting, spalling, and large cracks under large applied deformation.
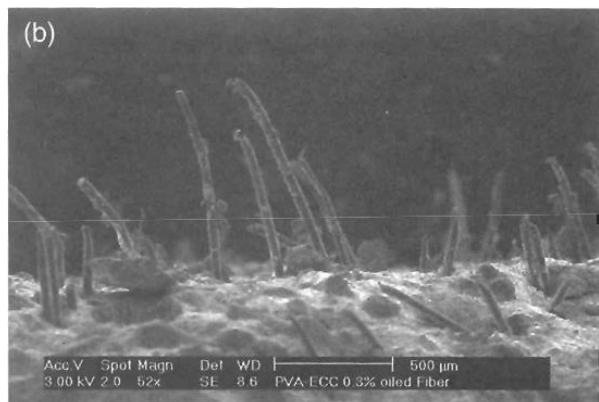
Figure 65. Protruded fibers at fracture surface: PVA-ECC (0,3% oiled REC fiber, Vf = 2%, w/c = 0,45 and s/c = 0,6. Source:(V. C. Li, Wang, & Wu, 2001)

In **Figure 66** is shown the performance of the beams of RC-SMA and ECC-SMA before, during and after monotonic loading. These remarkable figures show the difference between the cracks after unloading. The importance of using new structural materials like SMA can bring significant benefits but if also use another material like ECC makes the structure entirely ductile and eliminate cracks and plastic hinges after extreme loading and creating the structural elements in the elastic zone.

The use of SMA on RC structures creates large located cracks on the concrete, this behavior is presented when regular concrete was used. Otherwise, the use of ECC on the structures generates multiple micro-cracks on the concrete, this behavior is independent of the reinforcement of the structure (SMA or steel), even without reinforcement the micro-cracks will be produced. Therefore, this is a unique characteristic of the material.

This is why the ECC is used on the zones (plastic hinges) where is also used SMA, to provide extra safety to the structure and prevent the large located cracks produced by the SMA. This also will generate that the structure dissipate energy by plastic deformation, creating that the plastic hinge stay under elastic deformation.
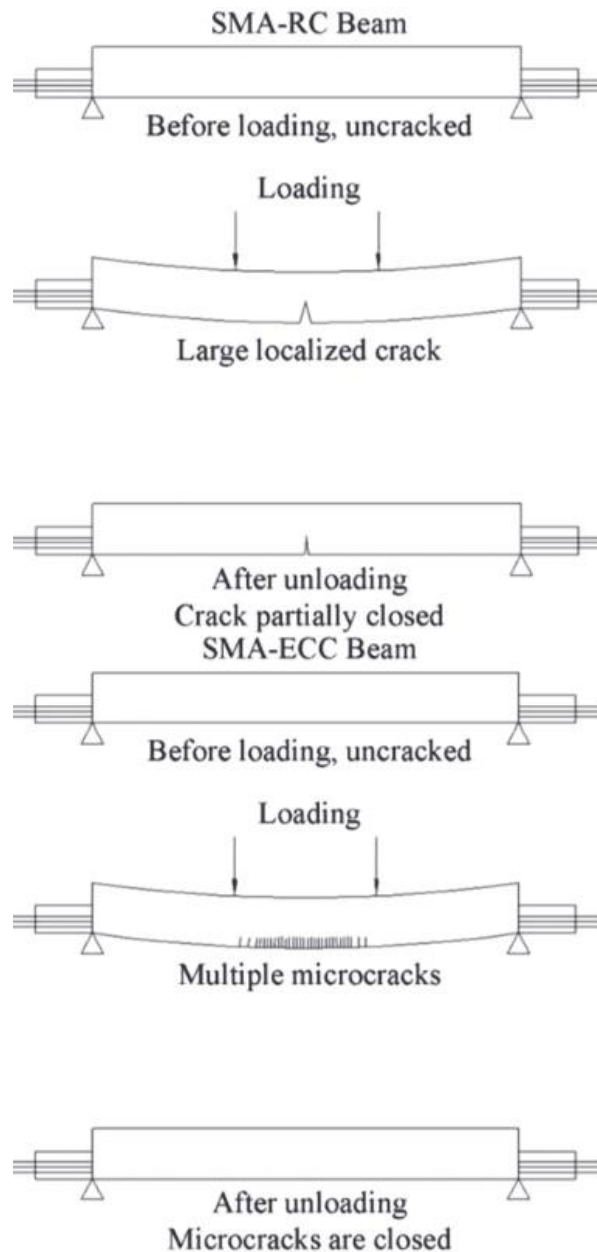

Figure 66. SMA-ECC beams behavior. Source:(X. Li et al., 2015)

In **Figure 67** is seen the curve of the stress-strain element using ECC and the micro-cracks produced. These cracks are complete recoverable once the element is unloading, due to its small dimensions and the ductile behavior of the ECC material.
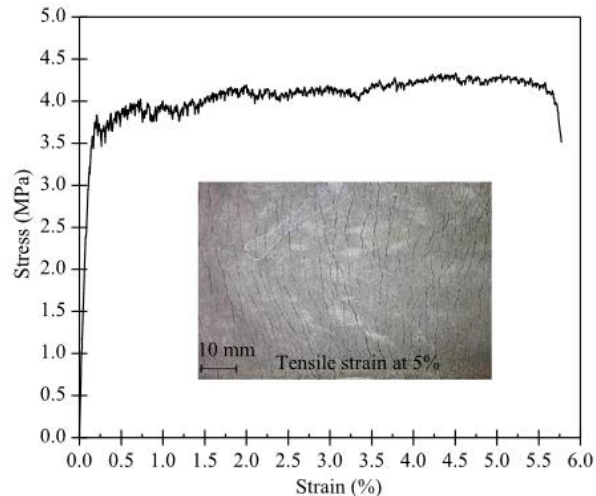
Figure 67. Tensile stress-strain response and distributed multiple microcracking of ECC. Source:(X. Li et al., 2015)

As a part of the conclusions in the research, was shown that the ECC-SMA beams presented extraordinary energy dissipation capacity, minimal residual deformation, and full self-recovery capability. The self-recentering factor of the SMA-RC beams was similar to the SMA-ECC beams; the main differences were in the crack pattern, the ECC-SMA produced micro-cracks meanwhile the SMA-RC produced located cracks not fully self-recoverable.
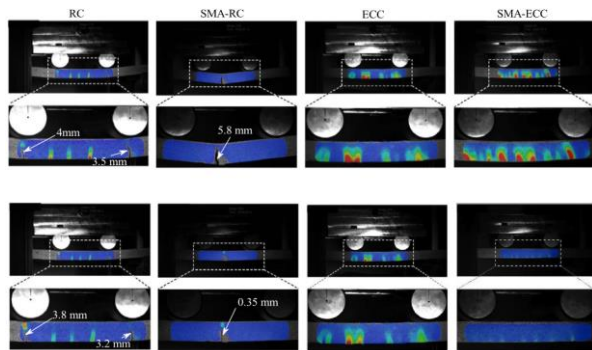

Figure 68. Experimental results of the beams studied after the 7th cycle.
Source:(X. Li et al., 2015)

As explained in the report provided by Dr. Saiidi "A Study of Concrete Bridge columns using innovative materials subjected to cyclic loading" (O'Brien, Saiid, & Sadrossadat-Zdeh, 2007) the most usual fibers are Polyvinyl Alcohol fibers (PVA) or the high modulus polyethylene fibers (PE), the average crack width is 50 μm while the ordinary concrete have crack around 0,2 mm. One of the most critical parameters in the ECC is that can achieve ultimate

tensile strain around 3% to 5%, almost 500 times larger than conventional concrete or Fiber Reinforced Concrete (FRC), this is attributed to the strain-hardening behavior. The spacing of the micro-cracks in the ECC is around 0,5 mm to 5 mm without considering the reinforcement in it, therefore is a property of the material.

As seen on **Figure 69** the ECC does not have rocks as aggregate, just present sand as maximum size of the aggregate. Most of the bigger particles on the ECC are the fibers, sand and the concrete particles.

Figure 69. ECC used in the construction of the Pier of the Bridge unique in the World reinforced with SMA, Seattle Nevada.
Source: (Clines, 2017).

The bendable concrete used in the construction of the Shape memory pier in Seattle also used ECC as a part of the smart materials in the plastic hinge calculated.

As a part of the feasibility of the research, is presented in **Figure 70** the construction of the first pier of the bridge designed using SMA and ECC in the plastic Hinge. As presented in "*The Seattle Times*" this is the first bridge in the world with a new type of column that flexes during the earthquake and then snaps back to its original shape. The bridge was designed based on the researches made by the Dr. Saiid Saiidi, a professor at the University of Nevada, Reno; he invested more than 30 years looking for the new technologies in the bridges to be earthquake-resistant.

The use of SMA as seen on this figure is over all the plastic hinge length, replacing all the steel bars of the pier in this zone. On this report of the Salitral Bridge was simulated this method and also replacing just the most critical steel rebars of the plastic hinge length.

Figure 70. Construction of the Pier using Superelastic SMA and ECC as structural elements in the Plastic Hinge, Seattle, U.S.A. Source: (Clines, 2017).

The research was funded by $ 400 000 from Federal Highway Administration. As the engineer in charge of the construction explained, the vision of the design is not only based on not-collapse but no-damage after a strong earthquake and achieve immediate use for emergency vehicles.

Pushover Analysis

The Pushover is a non-linear static analysis method, in which the structures are taken under gravitational load and a lateral load pattern. This lateral load increase in a monotonic way until obtaining an objective lateral displacement. At the end of the model it can be reached a "Pushover curve," this is lateral load versus lateral displacement, this is used to estimate the real global flexibility of the analyzed structure. Also, it can be reached by the estimated mechanism, load level and deformation that produces the collapse of the building.

When the frames are analyzed, it must be considered the non-linearity of the material in a discrete location where occurs the plastic rotation, as explained in the FEMA-356. One of the main limitations is that this analysis can only show one mode of oscillation if this is not representative cannot work with a valid review. Also, the Pushover analysis is static analysis, and it does not capture torsional effects, in non-regular structures, this is another deficiency in this analysis.

As shown in **Figure 71**, there are some critical points in the curve to consider, these points in the curve are the used in the design of the model and the user in the Seismic Codes. These points are called performance level

- **Operational**
  - *Fully Functional*: At this point, the structure is completely safe and does not have significant structural and non-structural damage.
- **Immediate Occupancy**
  - *Operational*: With non-significant damage, the structure can be used, but some retrofit maybe will be needed.
- **Life Safety**
  - *Life Safe:* There are significant structural damage and reduction of stiffness. Occupancy may be prevented until retrofit.
- **Collapse Prevention.**
  - *Near Collapse:* Main structural and non-structural damage, some falling debris hazards may occur.
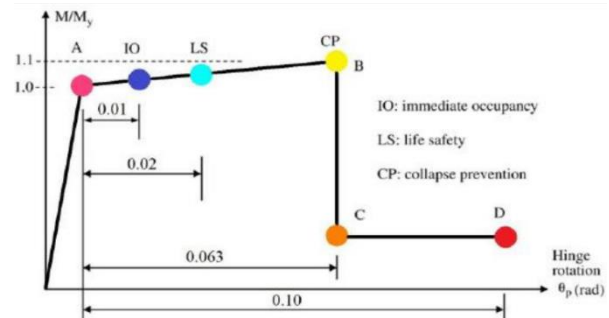

Figure 71. Example of the behavior of plastic hinge under a Pushover analysis.
Source: (Villalobos, 2018)

Some of the conventional Pushover analysis methods are the Capacity Spectrum Method (CSM), Improved Capacity spectrum Method

(ICSM), N2 method, Displacement Coefficient Method (DCM) and Modal Push Over Analysis (MPA). One of the essential uses of the Pushover analysis is to compare the base shear of the dynamic analysis to compare it to the response on the capacity curve as shown in **Figure 72**.
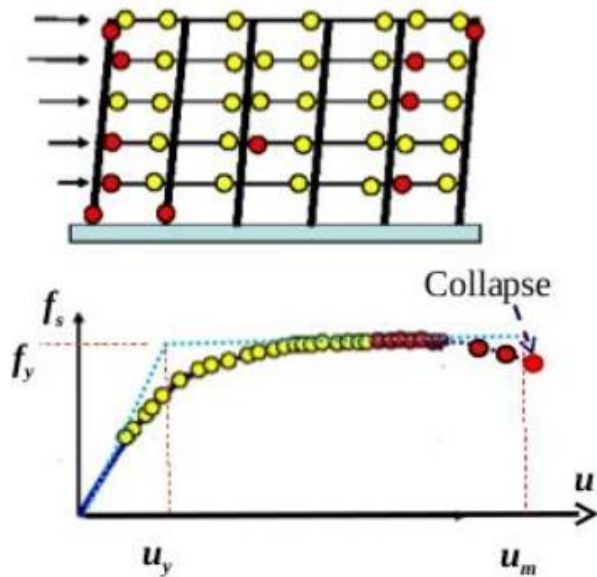

Figure 72. Example of Pushover analysis curve.
Source: (Villalobos, 2018)

The non-linear static analysis produces a static lateral load into the structure per each level. Each stage conserves the non-linear response of the structure. It can be induced the final loads of

collapse and the most affected elements of the structure.

In the thesis "Evaluation of Plastic Hinge Models and Inelastic analysis tools for the Performance-Based Seismic design of RC Bridge Columns" (Fedak, 2012) is shown the behavior of the plastic hinges and response of the structure under different Models presented. The plastic hinges presented are used explicitly for RC columns of bridges. In this was also presented as the review in the literature the usually acceptable drift depending on the damage of the structure.

Table 2. General Example of Performance-Based Design		
Damage State	**Performance Level**	**Limit State**
None	Fully operational, immediate occupancy	drift < 0.2%
Repairable	Operational, damage control, moderate	drift < 0.5%
Irreparable	Life safe, near collapse	drift < 1.5%
Severe	Hazard reduced	drift < 2.5%
Replacement	Collapse	drift > 2.5%

Source: (Fedak, 2012).

Background Studies

As a part of the background of the graduation project, this section refers to a background made in York University and the University of Toronto, also some researches made by the group of structural engineering in Lassonde school of engineering at York University, Toronto, Canada. To produce a separation of the papers and information recollected, these researches are based on similar investigations by undergraduate and graduate students with similar interests and objectives under the supervision of Dr. Dan Palermo.

Researches

Some of the researches made under the guidance of the previously mentioned professor, Dr. Dan Palermo, will be presented here, to have similar projects, studies, and thesis and achieve a more specific and relevant background.

The primary research made under the supervision of Dr. Dan Palermo is the thesis of Dr. Alaa Abdulridha to achieve the title of Doctor in Philosophy in Civil Engineering in the University of Ottawa "Performance of Superelastic Shape Memory Alloy Reinforced Concrete Elements Subjected to Monotonic and Cyclic Loading" in this was tested and modeled structural beams and shear walls under monotonic and cycling loading. The use of SMA was not in all the longitudinal reinforcement of the elements, due that as seen is expensive the purpose of this material. Therefore, was used superelastic SMA with a diameter of 9,50 mm and a length of 300 mm for the shear walls and 600 mm in the RC beams, and for the overlap between the SMA and the steel was used couplers, these can be seen **Figure 73**.
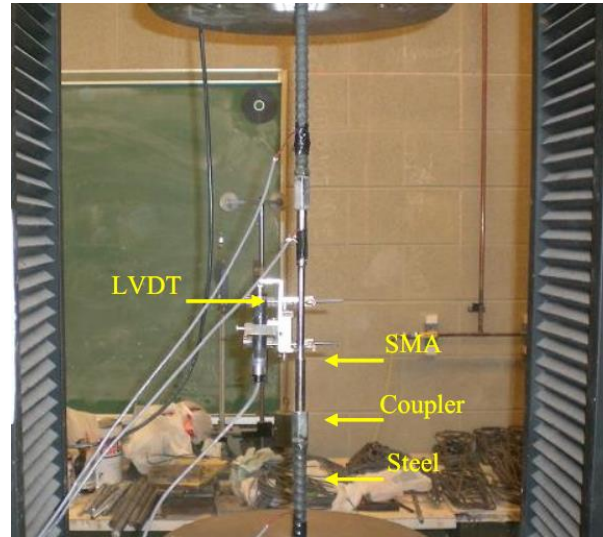
Figure 73. Mechanical SMA-Stell couplers used.
Source: "Performance of Superelastic Shape Memory Alloy Reinforced Concrete Elements Subjected to Monotonic and Cyclic Loading" (Abdulridha, 2013)

In **Figure 74** is shown one of the types of loading used in the tested beams and the model, the reverse cycling loading.

Figure 74. Reverse Cyclic Loading Sequence for Beam Tests
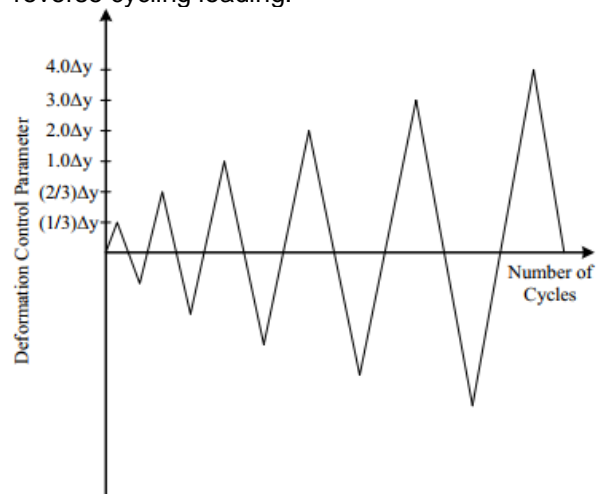Source: "Performance of Superelastic Shape Memory Alloy Reinforced Concrete Elements Subjected to Monotonic and Cyclic Loading" (Abdulridha, 2013)

The Monotonic loading (Pushover) and this reverse cycling loading will be applied in this research, due to the quantity of essential data that can be achieved under the hysteretic response, therefore the plastic and elastic deformation, energy dissipation and other. One crucial parameter to observe in this **Figure 74** is the gradual increment of the cycles in the ordinate axis, changing the maximum displacement per cycle in 0,33, 0,66, 1, 2, 3 and four times the yield displacement of the structure in function of the abscissa axis. This increment will create a hysteretic curve.

Figure 75. Comparison between the cracked pier and the analytical Model with concentrated axial.
Source: Soto-Rojas, M. (2016)

In the researches made by Michael Soto-Rojas under the supervision of Dr. Dan Palermo (Soto-Rojas, 2016; Soto-Rojas & Palermo, 2018) of the retrofit of one pier in the bridge over the "Grande de Tarcoles" river it was used the software Vector2 to model and simulate the initial state of the bridge, the cracked pier and repaired using Fiber Reinforced Polymer Sheets (CFRP). **Figure 75** shows the accuracy of the models using this software, not just in the response of the structure but in the crack-pattern observed in the inspections.

In the article "Cyclic loading testing of repaired SMA and steel reinforced concrete shear walls" (Cortés-Puentes, Zaidi, Palermo, & Dragomirescu, 2018) it was used the SMA as reinforcement in the concrete to retrofit shear walls under cyclic loading. In this research was studied the recovery of the walls and the dissipated energy.

The recovery capacity of the elements was calculated from the ratio of the difference between the peak displacement and the residual displacement for each drift level for the positive direction of loading.
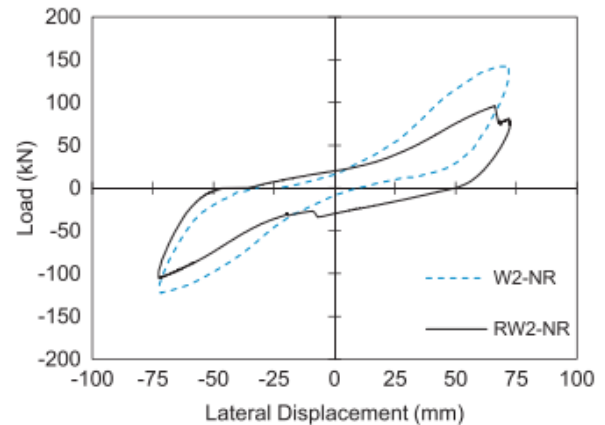

Figure 76. Hysteretic responses at peak displacement of 72mm.
Source: (Cortés-Puentes, Zaidi, Palermo, & Dragomirescu, 2018)

This approximation will be used in this research to calculate the recovery capacity of the piers of Salitral's bridge. To achieve the dissipated energy of the structure under a cyclic testing can be calculated obtaining the area under the curve, **Figure 76** used the curve of 72 mm due to the relevance in the analysis, which corresponds to the peak lateral load experienced by walls.

VecTor2 Software

Vector is a free use software suite of computer programs dedicated to nonlinear FEM of RC (NLFEARC). Vector2 is a program for the analysis of two-dimensional reinforced concrete membrane structure subjected to quasi-static and dynamic load conditions. VecTor2 uses a smeared, rotating-crack formulation for RC based on the Modified "Compression Field Theory" and the "Disturbed Stress Field Model" (Vecchio, Wong, & Trommels, 2013). The program's solution algorithm is based on a secant stiffness formulation using a total-load iterative procedure, giving it numerically robust and stable performance with good convergence characteristics.

Incorporated into the program's analysis algorithms are second-order effects such as compression softening due to transverse cracking, tension stiffening, shear slip along crack surfaces, and other mechanisms important in accurately representing the behavior of cracked reinforced concrete structures. Recent enhancements include provisions for the consideration of

nonlinear expansion and confinement, cyclic loading, effects of slip distortion on element compatibility relations, a bond slip of rebars, and application to the analysis of repaired or rehabilitated structures. A wide range of model behavior models is available for representing each of the various constitutive responses and mechanisms considered.

The plans were developed in the University of Toronto, to achieve more accurate assessments of structural performance as strength, post-peak behavior, failure mode, deflections and cracking. The FEM method allows to address the composite nature of RC material, changing material properties due to progressive cracking, challenging geometries and loadings-complexities which might thwart conventional analysis techniques. As a part of the input to use in a Vector2 model are mesh topology, material selection, boundary conditions, load representation, and computational efficiency.

VecTor2 use the FEM for the analysis of two-dimensional RC membrane structures to predict the load-deformation response of a variety of RC structures exhibiting well-distributed cracking when subject to short monotonic cyclic and reverse loading. (Vecchio et al., 2013).

The theoretical bases of Vector2 are the "Modified Compression Field Theory" (MCFT) and the "Disturbed Stress Field Model" for predicting the response of RC elements subject to in-plane normal and shear stresses. Models cracked concrete as an orthotropic material with smeared, rotating cracks. The program utilizes an incremental total load, iterative secant stiffness algorithm to produce an efficient and robust nonlinear solution.

This software uses the constitutive relationships of MCFT, then developments have incorporated alternative consecutive models for a variety of second-order effects including compression softening, tension stiffening and tension splitting. "Capabilities of the VecTor2 have been augmented to model concrete expansion and confinement, cyclic loading and hysteretic response, construction and loading chronology for repair applications, bond slip, crack shear slip deformations, reinforcement dowel action, reinforcement buckling, and crack allocation processes". (Vecchio et al., 2013).

The mesh used in the software is of low-powered elements as an advantage of computational efficiency and numerical stability.

There are three-node constant strain triangle, a four-node plane stress rectangular element and a four-node quadrilateral element for modeling concrete with smeared reinforcement and two-node truss-bar for discrete reinforcement.

MCFT

The "Modified Compression Field Model" is an analytical model for predicting the load-deformation response of reinforced concrete membrane elements subjected to shear and normal stresses, as shown in **Figure 77**.
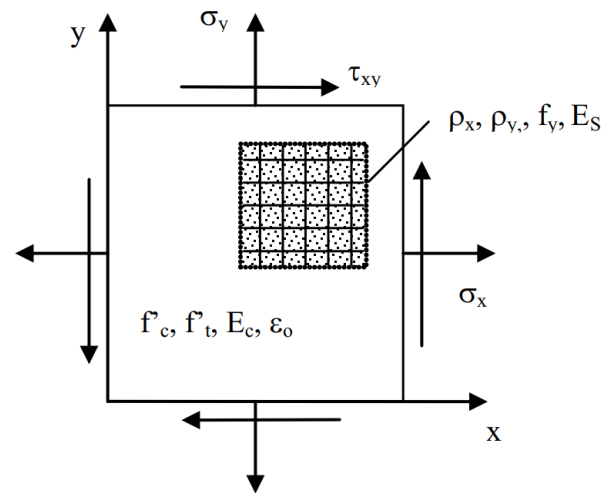

Figure 77. Reinforced concrete membrane element subject to in-plane stresses
(Vecchio et al., 2013) "Vector2 & FormWorks user's manual."

The model considers cracked concrete as an orthotropic material using a smeared rotating crack approach. Cracked concrete is treated as a robust continuum with cracks distributed over the membrane element, as opposed to a solid interrupted by discrete physical discontinuities. The smeared cracks feely reorient, remaining coaxial with the changing direction of the principal concrete compressive stress field.

The theory is comprised of three sets of relationships: compatibility relationships for concrete and its common reinforcement strains, equilibrium relationships and constitutive relationships for cracked concrete and reinforcement. These constitutive relationships for the cracked concrete result from tests of reinforced concrete panels using a purpose-built Panel Element Tester at the University of Toronto. Then,

the models include realistic constitutive models for concrete based on experimentally observed phenomena, in which the cracks are smeared, and the relationships are formulated regarding average stresses and strains, a critical aspect of the MCFT is the consideration of local strain and strain conditions at cracks. There are some assumptions that are considered in the model for example:

- Uniformly distributed reinforcement
- Uniformly distributed and rotating cracks
- Consistently applied shear and normal stress
- Unique stress state for each strain state, without consideration of strain history
- Strain and stresses are average over distances including several cracks
- Orientations of principal strain and the direction of principal stress are the same.
- The perfect bond between reinforcement and concrete
- Independent constitutive relationships for concrete and reinforcement
- Negligible shear stresses in reinforcement.

As one of the advantages of Vector2 over another software, is that is specified to be used in RC elements, this makes the predictions and simulation more accurate
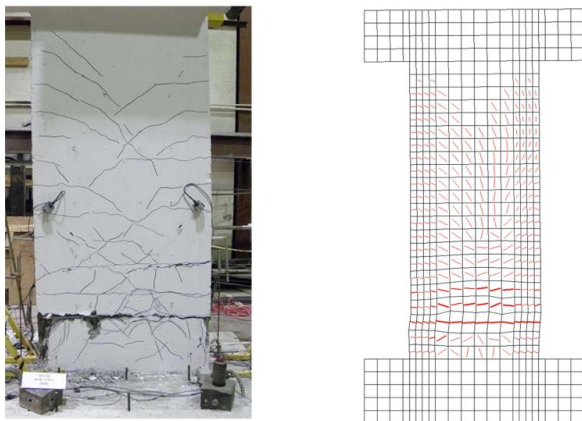

Figure 78. Example of cracks under experimental tests and the predicted by the Model with Vector2.
Source:

Figure 78 shows a hybrid of SMA-steel reinforced slender Shear Wall, obtained in the Vector2 course.

Modeling of the SMA

One of the main purposes of use of the Vector2 as the software of analysis of the results, besides is a software specifically designed to model RC structures and elements under tests for FEM, the software has the advantage that has incorporated different types of SMA that can be used in the models.

Other software does not have the SMA as a part of the default materials, in which can be possible to create a new material and gives the characteristics of the SMA to this; but due to the complex superelasticity and shape memory alloy behavior of the Austenitic and Martensitic SMA, will be different to give an hysteretic performance that the SMA has. Then, as was explained and illustrated many remarkable types of research used the software Vector2 to simulate the performance of the structural elements with SMA and ECC incorporated, obtaining accurate results compared to the tests made. This software has three different types of default SMA materials to be used.

Shape Memory Alloy 1.

The first type of SMA has an idealized behavior with no strain offsets, it has a flag-shaped hysteresis, as shown in **Figure 79.**
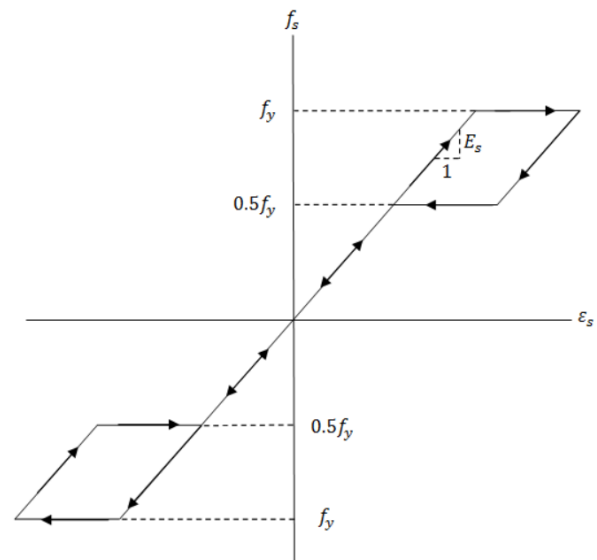

Figure 79. Stress-strain response of SMA 1.
Source: "Vector2 & Formworks user's manual" (Vecchio et al., 2013)

Shape Memory Alloy 2.

Developed in the University of Ottawa, the SMA incorporated hardening as well as small strain offsets, as shown in **Figure 80**.
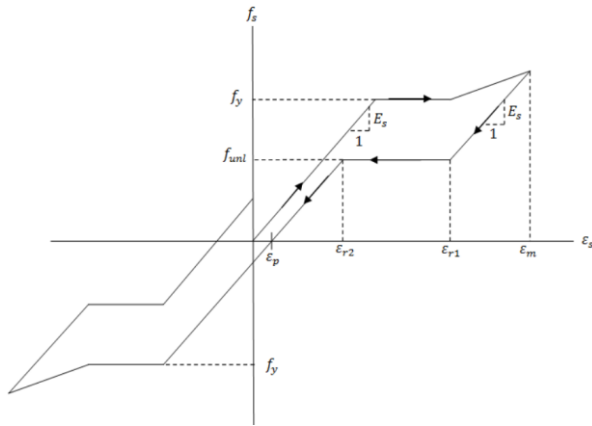

Figure 80. Stress-strain response of SMA 1.

Load Data Group

There are different types of loads scenarios that can be achieved using Vector2, under different load patterns and load cases will be different responses of the structure modeled.

Static Analysis with Vector 2.

The static analysis is a set of loads that are proportionally increased or decreased by a standard load factor. For instance, lateral loads defined in one load case may be monotonically increased, while gravity loads defined in another load case remain constant, for example in a Pushover analysis. **Figure 81** shows the loading protocol of the non-linear static analysis input on the VecTor2 software.
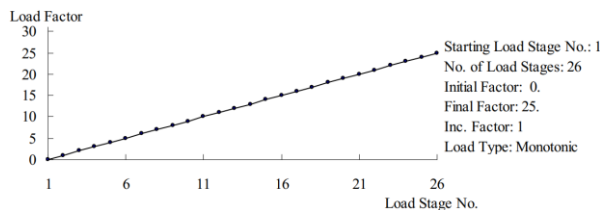
Figure 81. Monotonic type loading.
Source: "Vector2 & Formworks user's manual" (Vecchio et al., 2013)

The cyclic loading protocol is shown on **Figure 82**, using three repetitions per each loop.
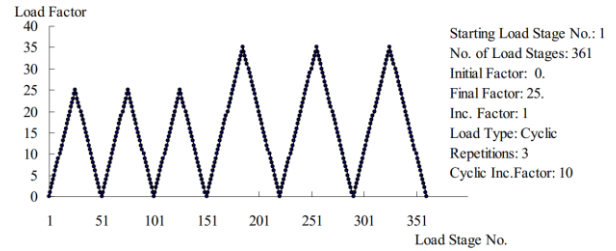
Figure 82. Cyclic type loading.
Source: "Vector2 & Formworks user's manual" (Vecchio et al., 2013)Source: "Vector2 & Formworks user's manual" (Vecchio et al., 2013)

The reverse cyclic loading is presented on **Figure 83** with three repetitions per loop, recovering per each stage.
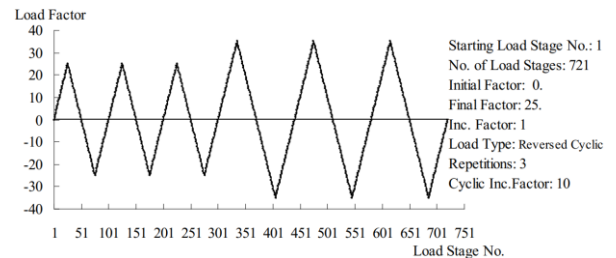
Figure 83. Reversed cycling type loading.
Source: "Vector2 & Formworks user's manual" (Vecchio et al., 2013)

The default steel behavior is presented on **Figure 84** of the software VecTor2.
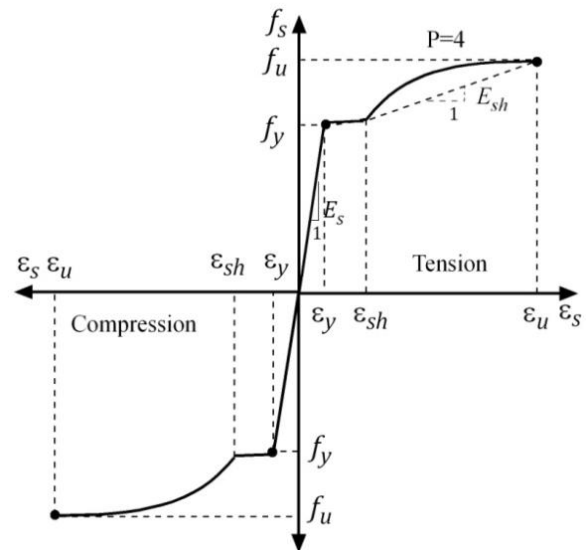
Figure 84. Ductile reinforcement stress-strain response.
Source: (Vecchio et al., 2013)

Figure 84 represents the behavior the response of the ductile steel reinforcement in the VecTor2 software. As seen in the figure, the steel can achieve a response, yield point and ultimate strain for compressive strengthening. There are different types of materials can be used in the FEM as reinforcement, there is a type of material called "Tension Only Reinforcement" in which the response under compressive force is always zero. This is important to consider in the model, to identify differences in the performance of the structure using reinforcement as the ductile reinforcement and with tension only. The material with "Tension only" can be usually used in FEM to represent fabric-type FRP reinforcement that has no resistance in compression.

Methodology

The use of the Salitral Bridge as base, as already explained can be useful to the country, the institution, and this research. **Figure 85** shows a part of the original Blueprints of the designed Bridge; these blueprints were made by hand and then scanned as a JPEG format, therefore the low resolution of this figure and inconsistencies in the dimensions of the Bridge.

In total are four piers of the bridge, but it was put in pairs, and these pairs were also joined by two coupling beams, one beam in the top of the pair of the piers and the other almost in the middle of these. It can be seen the difference in the shear reinforcement; there are five different phases and transitions for each pier, in which the minimum separation is 10,0 cm and the maximum 30,0 cm, between each stirrup. It is not that easy to see the difference of the longitudinal reinforcement steel, in the bottom of the piers the reinforcement bars are #11 in the corners and #10 in the middle, at the top is #8 in the edges and #7 in the middle, making a soft transition of the longitudinal reinforcement during each phase, previously mentioned.

As the piers are joined, to make a new system of analysis, creating a frame system. To model, the bridge is necessary to understand the behavior of the bridge under certain conditions. If the earthquakes are induced parallel to the ways of the superstructure, the piers behave as separated columns. However, if the earthquakes are induced perpendicularly to the surface of the bridge, the act is a frame. Therefore, it is necessary to create and model two different study cases in this bridge and then analyze the performance of the bridges.
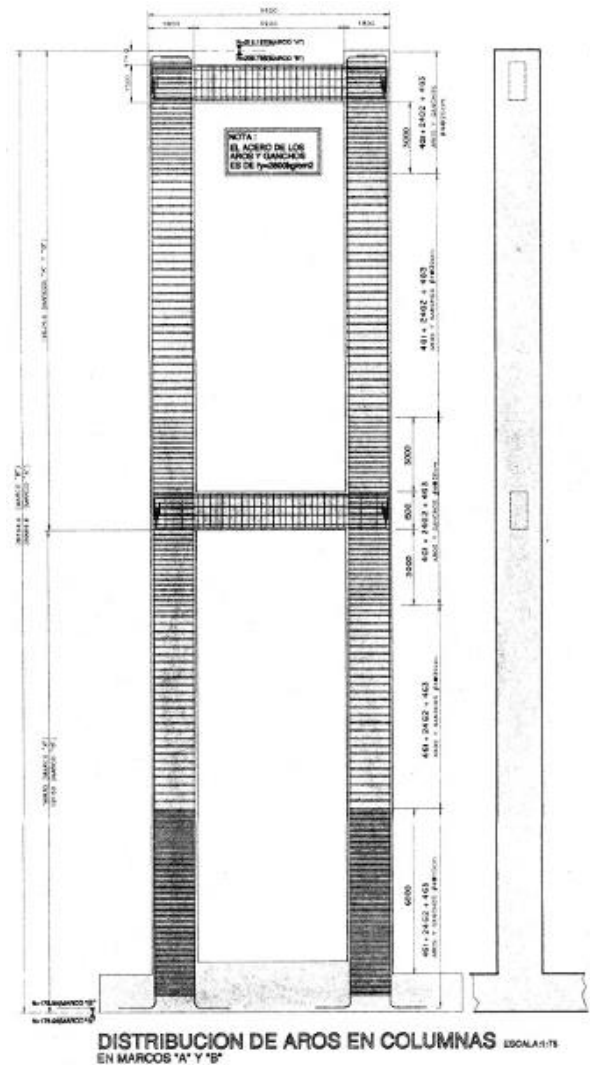

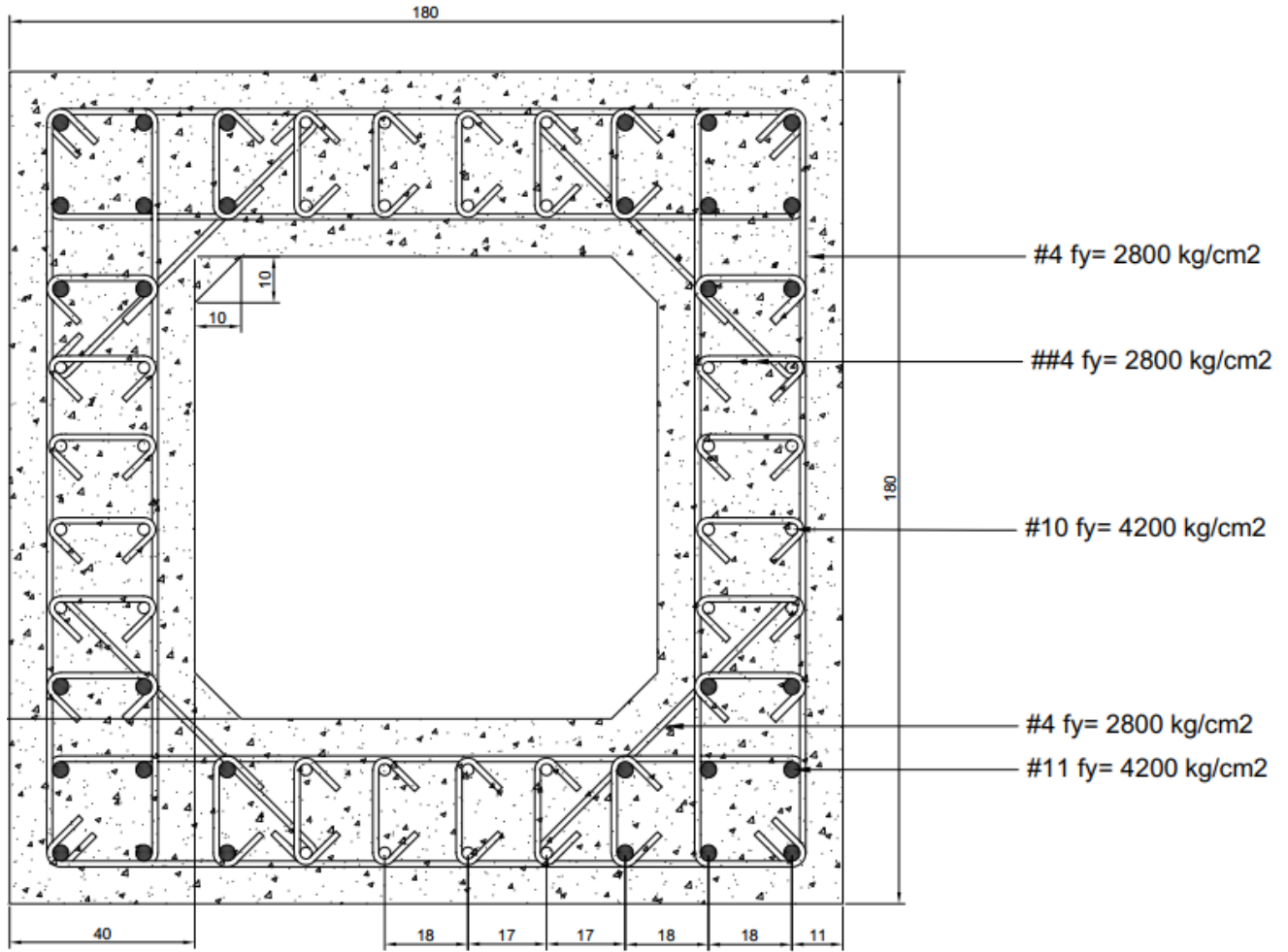Figure 85. Blueprints of Salitral Bridge.
Source: eBridge

Figure 86. Typical cross section of the piers of Salitral Bridge, cm units.
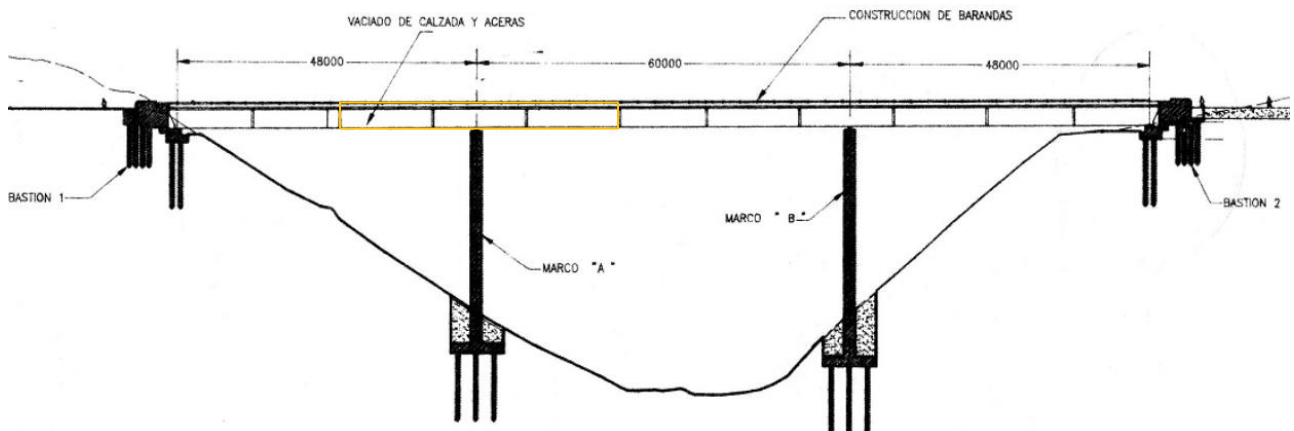Software used: AutoCAD.

Figure 87. The original figure of the section of the bridge.

Figure 86 represents the typical cross-section of the piers of the bridge, this part, in particular, is at the bottom of this. As seen, it is a hollowed squared column in the center, with dimensions of 180,0 cm of width and borders of 40,0 cm. The figure was made by the author of the research due to the low resolution of the original blueprints. The longitudinal reinforcement and the shear reinforcement have different points of yielding as appreciated; the first one has a fy= 4200 kg/cm^2 and the second a fy of 2800 kg/cm^2, respectively.

There are three different kinds of stirrups on the piers, as shown in **Figure 86.** It can be seen the length of the hooks designed and the angle, there are four G1, 24 G2 and four G3 in each cross-section of the Pier. The compressive strength of the concrete is 280 kg/cm^2 without any other particular aggregate and a supposed aggregate with a nominal size of 12 mm. The shear reinforcement was modeled as smeared in the concrete. The longitudinal reinforcement stayed as truss bars, and following the transitional details shown on the blueprints.

The software Vector2 cannot model elements with a hollow in the center as the piers of this bridge, as can be seen in **Figure 86**. It was designed an equivalent cross-section to approach accurate results on the software, it was created a new section or a compound section, as this way can be modeled a model very similar behavior to the real structure.

The software uses a membrane in two dimensions X-Z and use the thickness of the elements as third dimension. Therefore, the cross-section of the pier changes as the seen in the seen in **Figure 95**. This shape acquires the figure of a T-beam, represented in red as a line is the plane "zero" of the models. When the thickness of each region is put, it moves half out of the plane and another part inside the plane, creating like this a tridimensional solid that can be assigned with the properties and characteristics of the material.

As a second step, once is defined the cross-section and the optimum model to use, is setting the materials, this particular step is another variant if is compared to other structural software as SAP2000, Etabs, Safe, Robot and others. Vector2 discriminate the materials not just for the mechanical, thermic, capability and resistance characteristics but also with the dimensions of the elements, it is necessary to input the thickness from each material. Therefore, if one element has only one real material for example concrete with a

compressive strength of 210 kg/cm^2 but different widths in the element, will be necessary to create different materials for each different thickness in the element with the same compressive strength.

The behavior of the piers depends directly on the axis of the seismic events, depending on which axis is the earthquake, the piers will behave as individual elements or as a whole system of the frames. As can be seen in **Figure 88** if the earthquake enters to the structure in the Y-axis the columns can achieve individual displacements, otherwise, if the seismic event is induced to the system in the X-axis, the beams work transmitting the forces and displacements, and the behavior is as a frame system. Then it is necessary to make to different models searching an accurate result; the Model 1 will be the one representing the individual pier of the bridge and the earthquake in the Y-axis. Therefore the Model called 2 is the whole system with the loading of earthquake in the X-axis.
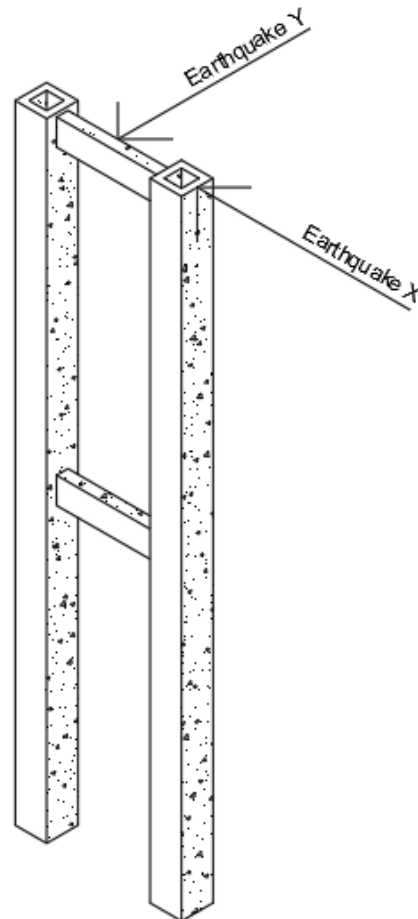
Figure 88. Diagram of the axis of the Seismic events. Software used: AutoCAD.

Another critical point to show, seen in the Salitral bridge is that the piers have a hollowed cross section as in **Figure 86**, but not during all the length of the element, there is section in the piers where the column is a complete massive element and does not have hollows, this differentiation is shown in **Figure 89**.
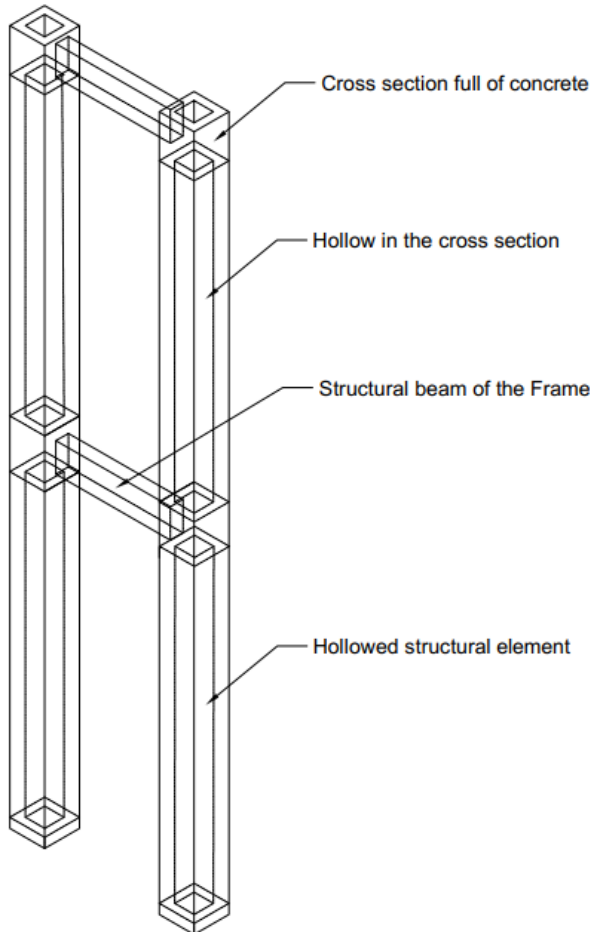
Figure 89. Diagram of holes in the cross-sections of the structure.
Software used: AutoCAD.

This difference between the cross-section of the element is one important parameter to show, in the places where the cross section is full, it works as a way of connection between the beam-column intersection, the connection between the restrains of the bridge and the top of the column and with the foundation. The cross sections filled start and finish 50,0 cm above or under the intersection and/or connection of each element.

ELEVACION LATERAL DE PLACAS INFERIOR Y SUPERIOR ESCALA 1:50
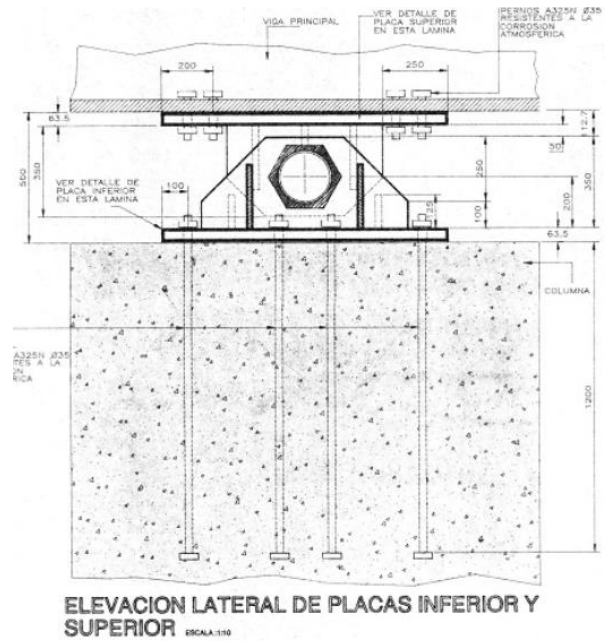
Figure 90. Restrain in the top of the Pier, "Y axis."
Source: eBridge.

In this figure is shown the pinned restraint used in the top of the piers of the bridge. As shown are made of steel and use steel in the plates, with rebars and cap screws to join it to the structure. This restrains in this axis transmit the axial load to the structure but does not transmit the shear or flexural moment, therefore, the system behaves as a single degree of freedom system (SDOF).
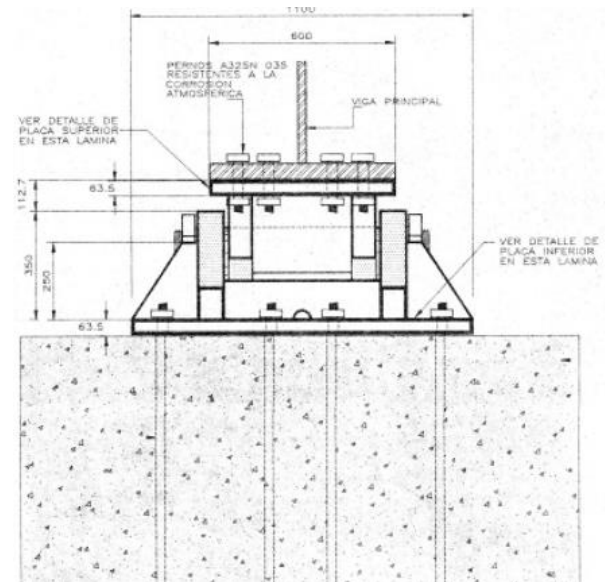
Figure 91. Restrain in the top of the Pier, "X-axis."
Source: eBridge.

Axial load

One of the crucial parameters to consider in the models made is the axial load applied. As the actual research, an already designed and constructed bridge, the tributary weight, live loads, wind loads, and earthquakes loads can be calculated and induced to the model. However, most of the researches, all the studied papers used an axial load ratio expressed as the percentage of load over the column's nominal crushing capacity. Therefore, the question is which axial load use? As a part of the models of SMA-ECC and RC was achieved models using a different percentage of axial load. Also, the loads used to design the bridge are unknown and as expressed on the reports and inspections it is necessary to make a research on the actual loads of the bridge to actual seismic and bridge codes. Due to the design of the bridge was made the ASD philosophy of design and not the LRFD, as previously explained.

One of the essential comparisons of models is between the models using the real axial load of the bridge, and another model using a number mean of the variations in the references. There was used model using 15% of the axial load and the actual load of the bridge, then will be decided based on the response what model will be the base to add SMA and ECC in the next models.

The numerical model of the length of the plastic hinge is designed for circular piers of columns. Thus a squared hollowed pier will be challenging to find an adjusted equation can be useful in the research.

Due to the significant displacements that were achieved at the beginning of the models, it was proceeded to calculate the maximum load of the slender columns. To verify if the pier does not actually fail but the displacement is so significant that the element is useless. Therefore, the calculation is:

$$Pcr = \frac{\pi^2 * EImin}{(KL)^2}$$

Equation 2

This calculation brings as result that to achieve the maximum load of Euler is necessary a force in the top equal to 37453,39 kN. The same parameter was calculated using the software SAP2000 v20; the results show this load is equal to 37360,84 kN,

giving an error of 0,24%. Using K equals to 2,0 dues to its cantilever behavior; the length, Inertia, elasticity modulus, and pi are known constants or information known.

The total weight of the bridge is 1 956 503,78 kg including tread surfaces, supports, and structural steel.

$$Wdist = \frac{1\,956\,504,78\,kg}{10,32\,m * 156,00\,m} = 1215.28\frac{kg}{m^2}$$

Equation 3

$$Wdist = 1,21\frac{ton}{m^2} * 54,0\,m * 10,32\,m \approx 677,07\,ton$$

Equation 4

Using the width and the whole length of the surface is obtained a 1,22 ton/m². Then, using the tributary shown in **Figure 87,** length and width of the frame is obtained 677,077 ton per each frame. Divided by two now is reached 338 538 kg per each pier of the bridge.

To calculate the percentage of the axial load was used in the next equation:

$$Axial\,load\,\% = \frac{P}{f'c \cdot Ag} * 100\%$$

Equation 5

Where *P* is the axial load induced to the pier, *f'c* is the compressive strength and *Ag* is the area of the cross-section of the element in the analysis.

This percentage is used to calculate the ratio of the axial load induced to the piers of the bridge. It can be estimated the percentage of the load with the axial load of the superstructure of the bridge and also using different rates, representing several stages, load-pattern or load combinations of the loads.

It was used **Table 3** to identify the mean and standard deviation of the nominal axial load used on most of the researches using piers of bridges. It was identified that 12,37% is the mean, therefore, in this research will be used 15,0%.

Table 3. Axial loads used in different researches of piers of bridges.							
Reference	Unit	Length (in)	L/D	P/f'cAg (%)	ρl	ρeff	S/db
Davey 1975	No. 2	68,9	3,5	12,07	0,0271	0,0461	3,53
Munro et al. 1976	No. 1	107,5	5,5	0,34	0,0271	0,0948	1,85
Ng et al. 1978	No. 3	36,6	3,7	33,95	0,023	0,2173	0,83
Ang et al. 1981	No. 1	63	4	20,81	0,0256	0,0881	2,5
Stone et al. 1986	Model N6	59,1	6	10,49	0,0196	0,1283	2,07
Stone et al. 1989	Full Scale Flexure	359,8	6	6,85	0,02	0,0826	2,07
Watson & Park 1989	No. 10	63	4	52,76	0,0192	0,0743	5,25
Kowalsky et al. 1996	FL1	143,9	8	29,65	0,0362	0,1176	4,79
Kowalsky et al. 1996	FL2	143,9	8	27,13	0,0362	0,0724	3,21
Kowalsky et al. 1996	FL3	143,9	8	28,11	0,0362	0,1115	4,79
Kunnath et al. 1997	A2	54	4,5	9,44	0,0204	0,1439	2
Kunnath et al. 1997	A3	54	4,5	9,44	0,0204	0,1439	2
Kunnath et al. 1997	A4	54	4,5	8,56	0,0204	0,1176	2
Kunnath et al. 1997	A5	54	4,5	8,56	0,0204	0,1176	2
Kunnath et al. 1997	A7	54	4,5	9,26	0,0204	0,1272	2
Kunnath et al. 1997	A8	54	4,5	9,26	0,0204	0,1272	2
Kunnath et al. 1997	A9	54	4,5	9,35	0,0204	0,1284	2
Kunnath et al. 1997	A10	54	4,5	10,14	0,0204	0,1546	2
Kunnath et al. 1997	A11	54	4,5	10,14	0,0204	0,1546	2
Kunnath et al. 1997	A12	54	4,5	10,14	0,0204	0,1546	2
Hose et al. 1997	SRPH1	144,1	6	14,82	0,0266	0,0965	2,56
Henry 1998	415p	96	4	12,04	0,0149	0,0857	2
Henry 1998	415s	96	4	6,02	0,0149	0,0428	4
Lehman et al. 1998	407	96	4	7,22	0,0075	0,1028	2
Lehman et al. 1998	415	96	4	7,22	0,0149	0,1028	2
Lehman et al. 1998	430	96	4	7,22	0,0302	0,1028	2
Lehman et al. 1998	815	192	8	7,22	0,0149	0,1028	2
Lehman et al. 1998	1015	240	10	7,22	0,0149	0,1028	2

Calderone et al. 2000	828	192	8	9,06	0,0273	0,113	1,33
Calderone et al. 2000	1028	240	10	9,06	0,0273	0,113	1,33
Kowalsky & Moyer 2001	1	96	5,3	4,31	0,0207	0,1427	4,01
Kowalsky & Moyer 2001	2	96	5,3	4,12	0,0207	0,1365	4,01
Kowalsky & Moyer 2001	3	96	5,3	4,44	0,0208	0,1478	4
Kowalsky & Moyer 2001	4	96	5,3	4,16	0,0208	0,1385	4
Statistics	**Mean**	105,9	5,4	12,37	0,0221	0,1157	2,59
	Stand. Dev.	69,8	1,8	10,54	0,0063	0,0339	1,11
	Coef. Var.	0,7	0,3	0,85	0,2873	0,2931	0,43
	Minimum	36,6	3,5	0,34	0,0075	0,0428	0,83
	Maximum	359,8	10	52,76	0,0362	0,2173	5,25

Source: (Fedak, 2012).

Plastic Hinges Length

There are numerous models of prediction to calculate the length of the plastic hinge in RC piers of the bridges, as concluded and tested by Fedak (2012) there are not accurate models, it was compared several ways to calculate it. The most used by the researches is the Priestly (1996), but it is not as accurate as the model presented by Berry et al. (2008) under monotonic, cyclic and reverse cyclic load. Therefore, the model is the length calculated with minor error:

$$Lp = 0,0375L + 0,01fy\frac{db}{\sqrt{f'c}} \qquad (psi)$$

Equation 6

Where *db* is the diameter of the longitudinal bars and *L* is the length of the structural element. This calculation is based on RC piers of bridges; therefore, it can be calculated and use that length to identify the length of SE-SMA necessary. However, there is recent research that estimates length of the plastic hinge in RC-SMA columns of bridges. This equation represents a calibrated model due to its relevance to the project and materials used.

$$\frac{Lp}{d} = 1.05 + \left(0,25\frac{P}{f'c*Ag}\right) + \left(0,08\frac{L}{d}\right)$$
$$+(0,0002fy_{SMA}) - (0,16\rho_l) - (0,019f'_c)$$
$$- (0,24\rho_s)$$

Equation 7

Where *d* is the diameter of the pier in mm, *P* the axial load, *Ag* the area of the cross-section, ρ_l the longitudinal reinforcement ratio and ρ_s the transverse reinforcement ratio and *L* the length of the Pier. This numerical model was proposed by (Billah & Shahria Alam, 2016) in the Research "Plastic hinge length of shape memory alloy (SMA) reinforced concrete bridge pier." The model was calibrated using a different type of SMA, for example was used NiTi, FeNCATB, and CuAlMn, where the fy of SMA represents the phase in austenite to martensite starting stress. However, this equation is limited by a particular condition, which are:

1. $0,05 \leq \frac{P}{f'c*Ag} \leq 0,2$
2. $0,8 \leq \rho_l \leq 3,0$
3. $200\ MPa \leq fy_{SMA} \leq 750\ MPa$
4. $30\ MPa \leq f'c \leq 75\ MPa$
5. $3 \leq L/d \leq 15$

These parameters are not all applied in the model of Salitral bridge, for example, the case that is designed for circular piers and the hollowed squared pier of the Costa Rican bridge. Due to the relevance of the model and the research calculating length of the plastic hinge using SMA in RC bridges is remarkable to calculate the length and compared it.

In the research made by Dr. Saiidi (Nakashoji & Saiidi, 2014) the length of the plastic hinge in columns with SMA and ECC is derived from the Paulay & Priestly equation, adding more parameters to the database and modifying the factors it was achieved:

$$L = 0,04L + 0,25d_bf_y \geq 0,33d_bf_y$$

Equation 8

Where *L* (in) is the length of the column and d_b (in) the diameter of the longitudinal bars and *fy* the yield stress of the steel on kilo pound squared inch (ksi) units, this equation is one of the models with minor error compared to experimental test and Finite element models. If the equation is not used in the units previously showed the solution gives an inaccurate result.

The Salitral Bridge pier structure is basically a big frame system, where the frame only works in one axis of the load. Therefore, it is important to calculate the length of plastic hinges in the beams of the frame due to it are critical elements in the structural capability. A research about the plastic hinges in flexural beams made by the Department of Building and Construction of Hong Kong, China (Zhao, Wu, Leung, & Lam, 2011) exhibit several models presented by different authors, one of the most recent and applied in beams is the expression made by Paulay and Priestly (1992) where the length of plastic hinge in the beams is:

$$l_p = 0,08z + 0,022d_bf_y$$

Equation 9

This equation also works for plastic hinge lengths of columns. Where *z* is the distance from the critical section to the point of contra-flexure, d_b and f_y are parameters previously explained. In the

journal in the ACI[18] (Panagiotakos & Fardis, 2001) was developed models of the plastic hinge length in beams, this was:

For cyclic loading

$$L_{pl,cy} = 0,12L_s + 0,014a_{sl}d_bf_y$$

Equation 10

For monotonic:

$$L_{pl,mon} = 1,5L_{pl,cy} = 0,18L_s + 0,021a_{sl}d_bf_y$$

Equation 11

Where L_s is the shear span of member (=M/V), then a_{sl} is a coefficient for slip equal to 1 if there is slippage of the longitudinal bars from the anchorage beyond the section maximum moment, or 0 if there is not, this expressed the effect of pullout of longitudinal bars from anchorage zone beyond section of maximum moment and f_y shall be used in MPa. These expressions as the best-fitted models in a linear function under 875 tests.

      In the calculations of the plastic hinges, will be used the ones presented in the thesis "Evaluation of Plastic Hinge Models and Inelastic analysis tools for Performance-Based Seismic design of RC Bridge Columns" (Fedak, 2012). Due to the relevance in this project, the research focus in specifically in reinforced concrete bridge columns that are typical in the majority of highway bridge columns in seismic zones. These types of structures commonly show higher than expected damage after high-intensity earthquakes. Bridge codes typically dictates that all inelastic action occurs in the bridge columns where damage is easily inspected and repaired while the bridge superstructure is to remain elastic.
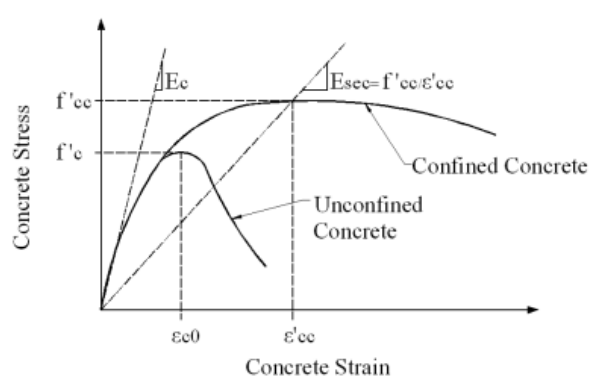

Figure 92. Confined versus Unconfined Concrete (Adapted from Priestley et al. 1996). Source: (Fedak, 2012).

---

[18] ACI Structural Journey

One of the critical parameters to consider in the models and the calculations of the plastic hinges is that the compressive strength of the concrete is increased by the reinforcement increasing the f'c due to the confinement concrete. In the response of the models should be considered the confinement of the concrete and the increase on f'c but sometimes can achieve higher values. based on **Figure 92** should be analyzed the behavior and reconsider debugging of the Models if necessary. The software VecTor2 consider this effect by itself and it can be identified in the response presented on Augustus but must be analyzed by the user.

Recovery Capacity

The recovery capacity of the structure under cyclic loading is an important parameter to consider when is used materials as the SMA and the ECC due to its capability of re-center after unloading or plastic deformation in the whole system as previously explained. As explained by (Cortés-Puentes et al., 2018) the recovery capacity in reverse cyclic testing can be obtained from the ratio of the difference between the peak displacement and the residual displacement for each drift level for the positive direction of loading, also, previously explained in the background. Therefore, if we have a hysteretic curve as the response of the reverse cyclic analysis

$$RVC = \frac{pd - rd}{pd} * 100\%$$

Equation 12

Where *RVC* is the recovery capacity of the structure and *pd* is the peak displacement in the positive side. Measured since the displacement is equal to zero and *rd* is the residual displacement of the response in each cycle, this is the magnitude of the length where the loop is coming down from the positive peak displacement to the intersection with the displacement-axis, in which this loop is making the transition to the negative peak displacement.

Energy Dissipation

The dissipation of energy (E_D) in a system can be calculated by numerical and arithmetical approximations, but this will be a result of some suppositions or inferences of the structure. Therefore the value may not as accurate as required. **Equation 13** represents one of these ways to calculate the Energy dissipated

$$E_D = \pi \eta k \rho^2 = 2\pi \eta E_{so}$$

Equation 13

However, this equation presents variable sometimes difficult to achieve. In the present research is not that difficult due to the frame system of the piers can be considered as a SDOF. However, this is not the most used way of calculating the energy dissipated by the system. An accurate value of the E_D is to calculate the area under the curve in a reverse cyclic analysis; this equivalent area is represented in **Figure 93**.
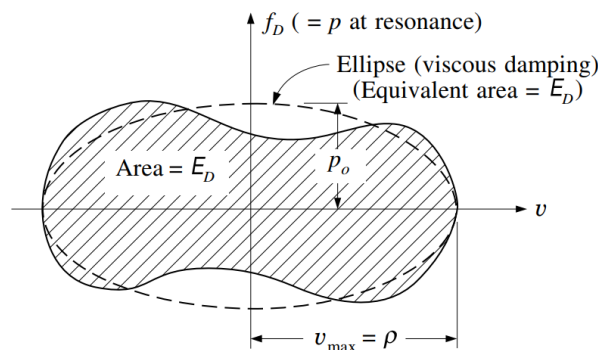

Figure 93. Actual and equivalent damping energy per cycle.
Source: (Clough & Penzien, 2010)

This figure, shows the equivalent area for an ellipse with viscous damping, as explained by (Clough & Penzien, 2010) if the shape of the applied-force/displacement diagram is from nonlinear viscous damping form can also be obtained as the linear viscous damping presented in **Figure 93**. Dr. Saiidi (Cruz Noguez & Saiidi, 2013; Nakashoji & Saiidi, 2014; O'Brien et al., 2007) researching about the advantages of the use of SMA and ECC together in piers of bridges submitted the element to reverse cyclic loading and the hysteretic response of the analysis also was used to calculate the energy dissipation in the element.

Viscous Damping

The equivalent viscous damping can be calculated in the system as explained by (Cortés-Puentes et al., 2018) during a reverse cyclic loading. The viscous damping is directly proportional to energy dissipated and is a ratio between the E_D and elastic energy dissipated (E_{So}) and a constant, as shown

$$\beta_{eq} = \frac{1}{4\pi} \frac{E_D}{E_{So}}$$

Equation 14

Where E_D is the parameter previously discussed, and E_{So} is the elastic energy dissipated obtained in the hysteretic curve of the reverse cyclic analysis, also can be calculated as the area under the geometrical figure made by the initial point, the peak lateral load and the peak displacement of each loop.
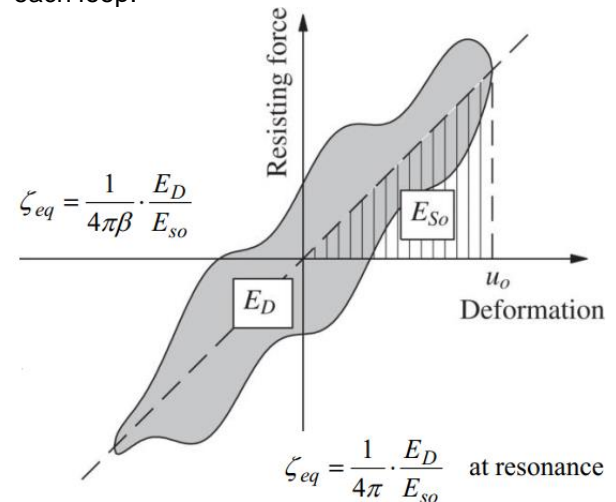
Figure 94. Equivalent energy dissipation for a Single degree of freedom system at resonance.
Source: (Pantazopoulou, 2018b)

Figure 94 shows the equivalent energy dissipation of a Single Degree of Freedom System (SDOF), where the E_{So} can be calculated with the area of the representation of the figure, where does not consider entirely the shape of the hysteretic curve. This approximation can be inferred to the frame system of the piers; this was used in researches using also shear walls with SMA. Also, it can be calculated for each step of cyclic loading.

Methodology of the FEM

There was used two different types of basic models, depending on the direction of the earthquake. If the seismic event enters the structure in the Y-axis as shown in **Figure 88**, the model behaves as a simple pier in the cantilever. However, if the extreme loading enters from the X-axis, the model acts like a complete frame system. Therefore, was used these two different basic models, the Model 1 is representing the Y-axis earthquake and the Model 2 in the X-axis. From these two models are derived another sub-model changing the characteristics of the materials, the load analysis, the loads, materials, restrains and others. The software Vector2 has a limiting in the model of FEMs, due can only permit 6000 total elements, therefore defining an accurate design of the mesh is necessary, plus with a structure as big as the piers of the Salitral bridge.

Then, it is necessary to design the mesh of each region in the model; it can be rectangular, quadrilateral and triangular. More elements mean more proper behavior and precision of the model based on FEM, but one limited in the use of Vector2 is that can be only used 6000 elements as a total, this means for a 36 meters pier the elements should be optimized. One way to do it is to put more elements where more cracks can be achieved; this is possible to be created in the plastic hinges of the piers, usually made in the top and bottom of the columns. However, as a first parameter, every element of each region of the mesh should have the same dimensions and height-width ratio, then see the behavior of the element, crack patterns, displacements, and performance, in the most affected zones should be used a finest mesh to achieve better and more accurate results.

The Model 1 uses typically rectangular elements with a size of 200 mm of width and 200 mm of height with a maximum aspect ratio of 2.5 or 3 to achieve the more accurate precision in the model without overpass the 6000 total elements and avoid triangular elements due to its less accuracy. For the Model 2 was used rectangular elements with a size of 400 mm x 400 mm with a maximum aspect ratio of 4, because using a

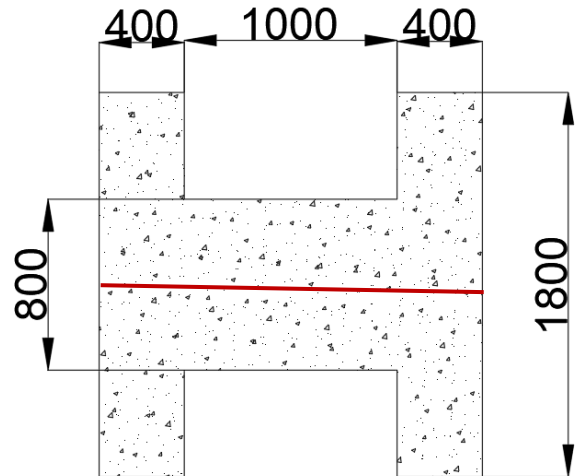smaller proportion of the mesh pass the 6000 elements.

Figure 95. Transformation of the cross-section of the Model, Saltrital Bridge, units in millimeters.
Software used: AutoCAD.

For the longitudinal bars was used truss bars to achieve better detail in the results of the response, for the Model 1 of RC was used 12 different types of reinforcement to represent the transition of the nominal numbers of the bars during all its length. For Model 2 was used 14 types of reinforcement because of the steel in the beams of the frame.

For the shear reinforcement was used as smeared reinforcement at 0° and out of the plane smeared. Therefore, it was necessary to create different materials in the model, depending on the thickness of the cross-section and in the smeared reinforcement. In Model 1 was used eight different materials to represent this and in the Model 2 was used nine different materials because of the beams of the structure.

The structure presents the use of piles as a foundation; therefore, the model represents the set-in model, restraining the displacements, moments and loads in the X and Y axis.

There are necessary calculations to approach the FEM effectively, aside from the estimate to introduce as input to the model.

For example, in the Software Vector2 one of the first steps to make the model it is necessary to put the number of load stages, it means the number of iterations. Therefore, the number of points in the curves achieved, this procedure changes depending on the type of applied load. The number of load stages is defined as:

$$No.\,Stages = \begin{cases} \dfrac{LFf - LFi}{LS\,inc} + 1 & monotonic\ loading \\[2mm] 2(R*S)\left(\dfrac{LFf - LFi}{LS\,inc}\right) + \left(\dfrac{R*Cinc}{LSinc}\right)[S(S-1)] + 1 & cyclic\ loading \\[2mm] 4(R*S)\left(\dfrac{LFf - LFi}{LS\,inc}\right) + \left(\dfrac{R*Cinc}{LSinc}\right)[S(S-1)] + 1 & reverse\ cyclic\ loading \end{cases}$$

Equation 15.

In which the *LFi* is the initial load factor, the *LFf* is the final Load factor, *LSinc* is the load factor increment for each load stage, *R* is the number of repetitions, *S* is the number of Sets of full repetitions, and *Cinc* is the cyclic load factor increment.

There are other parameters that the software uses as accurate approximations of the material if these parameters are impossible to find in the blueprints. This is an example of what happened in this research due the plans are old and made by hand there is not much information about the parameters of the materials. Therefore, will be used the equations used in the software to use it as input. The tensile strength of the RC structure is presented as:

$$f't = 0,33\sqrt{f'c} \quad [MPa]$$

Equation 16

Then, the initial Tangent Modulus is:

$$Ec = 5500\sqrt{f'c} \quad [MPa]$$

Equation 17

Also, the compressive strength of the concrete, is the cylinder strain at f'c, the software uses this as:

$$\varepsilon_o = 1.8 + 0.0075 * f'c[MPa] \quad [millistrain]$$

Equation 18

To calculate the smeared reinforcement in the concrete is as shown in the next equation.

$$rho = \frac{As}{b * separation} * 100\%$$

Equation 19

In which, the r_{ho} represents the reinforcement ratio, As the area of reinforcement perpendicular to the cross-section, *b* the width of the cross section analyzed, and the separation means the length between stirrups in the shear reinforcement. This formula is only for smeared reinforcement in the reinforcement used for shear. The longitudinal reinforcement was used as truss bars in this research, to identify the failures modes of the elements more accurately but can also be used as smeared reinforcement if the user requested.

Representation of the Models

Figure 96 presents the comparison between Model 2 and the original constructive blueprints of the bridge. The model represents on different colors the type of materials used depending on the separation of the shear reinforcement and in the borders, there is also a difference because of the differentiation in the thickness of the piers. Also, the longitudinal bars change its colors depending on the nominal number of the bar and in the number of bars going out of the plane. It was used 5981 elements for the design of the mesh in Model 2, using only RC materials, the number of elements increases depending on the use of SMA as truss bars.
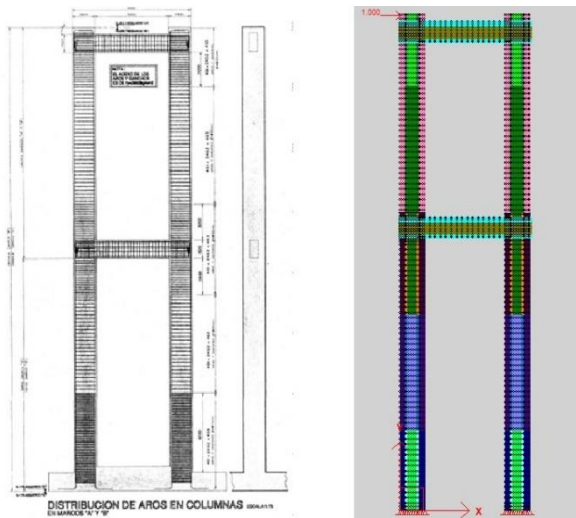
Figure 96. Representation of the Model versus the Constructive blueprints, Model 2 FormWorks.

On **Figure 97** is explained graphically the representation of the finite element models. The models differ depending in which axis is studied. It can change from a single pier to a frame system, if the lateral load is induced on the Y or in the X-axis.

The use of SMA on the plastic hinge length differ significantly depending on the amount of the SMA bars on the cross-section.

Figure 97. Diagram of the Models used and its nomenclature. Software used: Draw.io

Modeling of the SMA

Table 4. Characteristics of the SMA

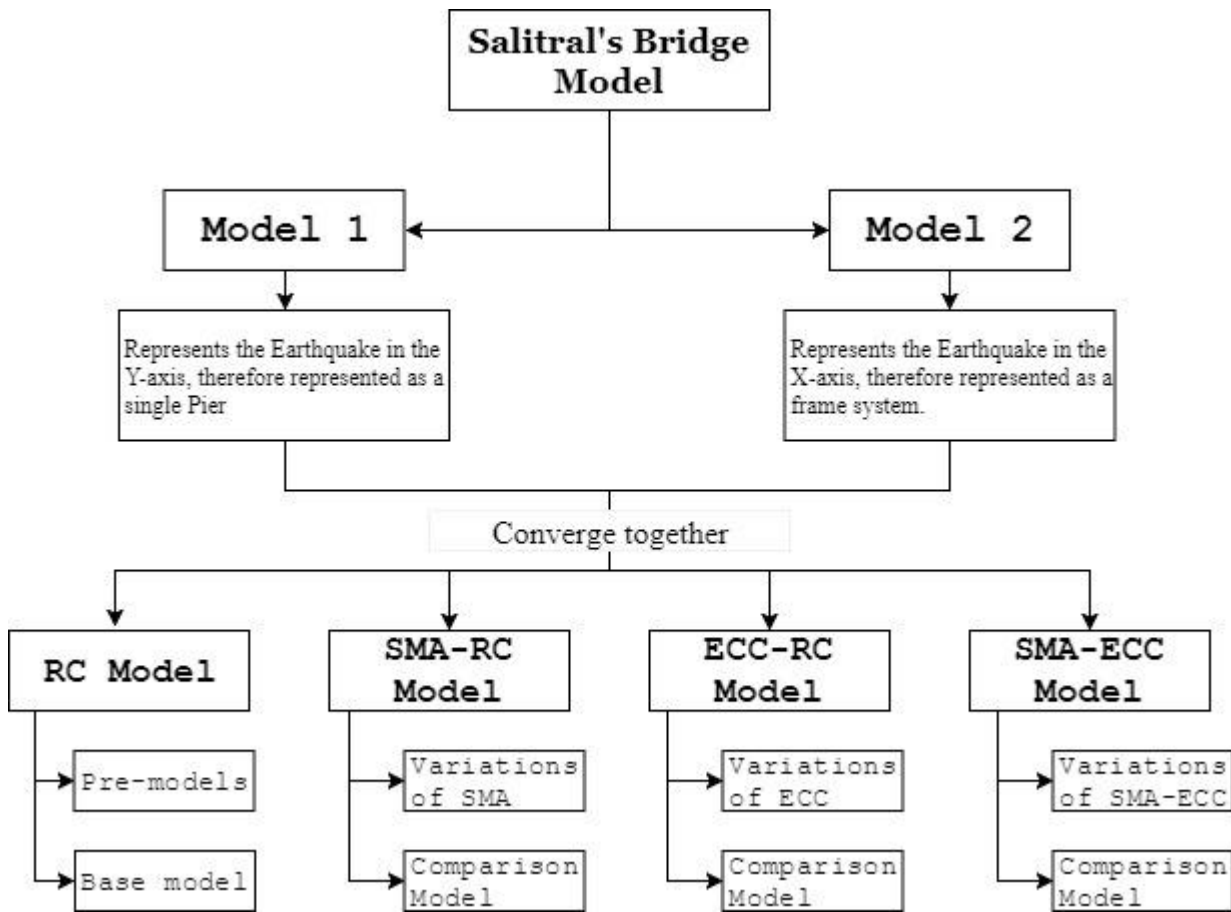| Parameter	Value	Units
SMA	SE-SMA NiTi	
Composition	56% Nickel-44% Titanium	
Fy	380	MPa
Fu	900	MPa
Temperature	Ambiance	
E	60000	MPa
εs	6,0	%
Plastic Strain	6-8	%

Software used: Microsoft Word.

The SE-SMA use as a coupler, conventional mechanical coupler made of steel. These have a fy equal to 690 MPa and fu of 795 MPa; these characteristics were used in the Models as truss bars with the usual length.

Table 5. Properties of NiTi provided by SAES

Physical Properties	Density	6,5 g/cm^3
	Melting Point	1310 °C
	Modulus of Elasticity	41-75 x10^3 MPa
	Electrical Resistivity	32 $\mu_o$hm-cm
	Coefficient of Thermal Expansion	11x10^{-6} °C
Mechanical Properties	Yield Strength (min.)	379 MPa
	Ultimate Tensile Strength	1068 MPa
	Total Elongation(min.)	10%
	Permanent Set After 6% Strain	0,10%
	Transformation Temperature A$_f$	(-30)-10°C
Chemical Composition	Nickel	55.8 wt.%
	Titanium	Balance
	Iron (max.)	0.05 wt.%
	Carbon (max.)	0.02 wt.%

Source: (Abdulridha, 2013).

Table 5 shows the physical, mechanical and chemical characteristics of the Nitinol SMA of the research made by Dr. Abdulridha in 2013 as a part of the doctoral thesis under the supervision of Dr. Dan Palermo. These properties are the technical information provided by SAES, the provider of the Shape Memory Alloys bars dealers to use it in the experimental tests. Based on this information was provided the **Table 4** simulate the experiments under Finite element method, also in Vector2.

Modeling of the ECC

The bond between the reinforcing bars and concrete is a critical feature to represent the prototype behavior (Hosseini & Gencturk, 2015).

There is a compatible deformation between ECC and reinforcement, ECC with steel reinforcement, both steel and ECC can be considered as elastic-plastic material capable of sustaining deformation up to several percent strain. As a result, the two materials remain compatible in deformation implies that there is no shear lag between the steel and the ECC, resulting in a shallow level of shear stress at their interface (V. C. Li, 2003).

As a result of low interfacial stress between steel and ECC, the bond is not as critical as in RC; the stress can be transmitted via bridging the fibers directly through the ECC, even after micro-cracking.

After concrete cracks in an RC element, the concrete unloads elastically near the crack site, while the steel takes over the additional load shed by the concrete. This leads to incompatible deformation and high interface shear stress responsible for the commonly observed failure modes such as bond splitting and/or spalling of the concrete cover. The compatible deformation between ECC and reinforcement has been experimentally confirmed (Fischer and Li 2002a) as explained by Victor C. Li (2003).

Constitutive models of ECC have been constructed and implemented into FEM codes for prediction of structural behavior. They should be useful for exploring the selective use of ECC in critical elements of a structural system, without excessive demands on expensive experimentation.

The software VecTor2 does not have a constitutive model to represent the behavior of the ECC. Therefore, it was necessary to determine some specific parameters and indicate these to the software and apply a similar behavior of the

system. First, it was necessary to introduce the points manually in the curve of "Tension softening"; the points were introduced based on the experimental result of the ECC tensile stress-strain curve of Victor Li (2003). Then the mechanical characteristics of the material were based on the ECC HFA (Hosseini & Gencturk, 2015) due to the high compressive and tensile stress capacity, categorized as of one of the greenest ECC and lower cost compared to other ECC; the comparison is shown in **Table 1**.

The amount of fiber was selected as 2% based on (Hosseini & Gencturk, 2015; V. C. Li, 2003; Uttamraj, Ashwanth, & Rafeeq, 2016). Then, parameters as fiber length, diameter, tensile strength, and bond strength were indicated to the software based on (Anwar, Hattori, Ogala, Ashraf, & Mandula, 2009) and based on the PVA fibers technical information of the material (Buddy Rhodes, 2019). The diameter of the PVA fiber is used as 0,03 mm and 8,0 mm of length with 1400 MPa of tensile strength (V. C. Li et al., 2001) and the bond strength was used the default value by the software (used in Polypropylene deformed Fiber reinforcement as default values) but in reality are poly-vinyl-alcohol (PVA) fibers, as researched these present highest bond strength than polypropylene fibers (Horikoshi T, Ogawa A, Saito T, 2006).

Pushover Analysis

The models were analyzed under a Pushover analysis with the software Vector2, defining the configuration under **Equation 15** with a monotonic load applied. Usually in the models were used an initial factor of zero, a final factor of 10000 and increments of 100. The final factor was chosen because of the failure was achieved usually in the factor around 8000 and 9000, then the incremental factor was selected to produce an optimum time in the computational analysis. For some models, the additional factor was reduced to 25 or 10 to produce more accurate response curves, due to the previously defined points was generated a lot of noise in the curves.

The push used in the models had a magnitude of 1,0, increasing the load to generate a displacement equivalent to 1,0 millimeters per each stage, creating a response curve of the applied loads versus the movements obtained.
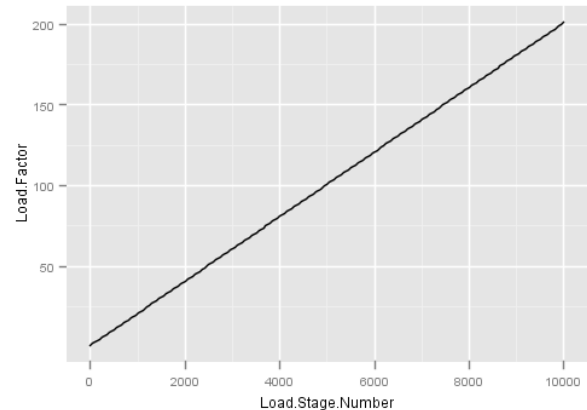

Figure 98. Loading Protocol of the Non-linear static analysis in Vector2, Load stage equal to 10 000 and load factor of 201. Software used: Deducer.

The lateral load of the Pushover was located on the top-left node of the piers. This lateral load pushes the structure from the equilibrium state to the right until it collapses or present a structural failure.

Reverse Cyclic Analysis

The reverse cyclic loading of the models was based not in the yield point of the system, as usual; it was made based on different drift points of the structure due to its large yield displacements the loops in the reverse cyclic will achieve distant peak displacements.

Said this it was derived the points of failure of the structure based on the Pushover results, where the ultimate displacement at failure usually occur around the 10% of drift with 15% of the axial load.

Then, the loading protocol was proposed to increase in one-unit percent per each cycle except the first one. As previously said the reverse cyclic analysis consists of a lateral push and pull of one top element in the structure with an absolute magnitude to achieve a given lateral displacement. Therefore, the displacements are proposed then are known parameters but the lateral loads to achieve that displacement is based on different responses of the structure taking the response of the previous cycle as the cracked system, compression of the concrete, slip of the bars and others. Therefore the lateral loads are not previously known parameters. This could increase or decrease depending on the response of the structure.
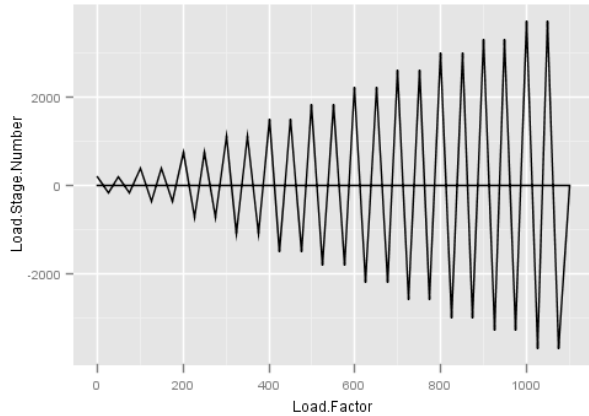
Figure 99. Reverse cyclic protocol of loading used in both models.
Software used: Deducer.

As seen the loading protocol start in 0,5% of lateral drift, the second stage is 1,0% of lateral drift, and then the loading protocol is expecting to add one percent of lateral drift more in each cycle until the 10% of drift or the failure in the system is achieved.

Figure 99 shows the loading protocol of the reverse cyclic analysis, as seen each circuit must laps or cycles until continue with the next lateral drift. The two repetitions per stage were designed based on the computational development of the structure due to if the reverse cyclic analysis is made with three repetitions as usual in the software the models will take too long to complete inaccurate time.

The reverse cyclic analysis is one of the most important studies that can be used in the FEM due to its relevance to calculate different parameters of the system. Based on this will be calculated the dissipated energy of the system, the recovery capacity, the plastic hinge length, viscous damping, and lateral cyclic loading. With this information can be plotted per each cycle versus the drift and be compared the solution of the relevance of the smart materials added.

Seismic Analysis

The Seismic analysis of the Model was designed using the structural software SAP2000 v20. In this was used a tridimensional model to represent the frame of the piers of the bridge. It was made with concrete columns, and beams using the default materials of the software with a hollowed cross-section in the zoned required and filled in the zone where the blueprints indicated, for the columns

was used the reinforced of the concrete just in the RC model to be checked by the software.

It was made three different seismic analysis, it was made a static analysis to review the accurate signs of the loads and to compare it with the dynamic response, also was made a modal analysis based on the "Seismic Code of Costa Rica" using the dynamic spectral factors that comes with the software. Using seismic zone of 3, a Soil type III and the importance of the structure as "A", the most critical kind of structure to preserve after extreme loading, the reason of the use of these parameters as input in the software for the modal analysis was discussed and explained in the background of the research.
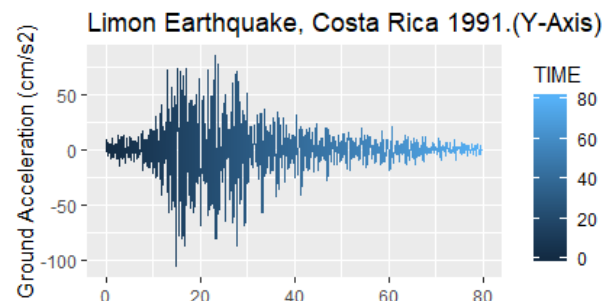

Figure 100. Ground acceleration Limon Earthquake, Costa Rica 1991 N90E. Software used: RStudio.

For the Time-History analysis was induced to the structure the Earthquake of Limón, Costa Rica occurred in 1991. As explained, this is one of the most remarkable seismic events in Costa Rica and where the information of ground acceleration is available. **Figure 17** shows the magnitude of damage that this earthquake provoked to important bridges in the Caribbean side of Costa Rica. These bridges were also designed without considering the LRFD philosophy of design in the structures as the Salitral bridge. The model was made presented to vary during the time, but the results in the research will be presented as an envelope of the maximum and minimum shear and flexural moments in the elements. Also, was induced to the structure the Samara's earthquake that occurred in Costa Rica on 2012, this is the second most significant earthquake in the history of Costa Rica with an available record of ground accelerations during the event.

The Response-Spectrum Analysis (RSA) is a linear-dynamic statistical analysis method which measures the contribution from each natural mode of vibration to indicate the likely maximum seismic response of a substantially elastic

structure. The response-spectrum analysis provides insight into dynamic behavior by measuring pseudo-spectral acceleration, velocity, or displacement as a function of the structural period for a given time history and level of damping. It is practical to envelop the response spectra such that a smooth curve represents the peak response for each realization of the structural period.

The response-spectrum analysis is useful for design decision-making because it relates structural type-selection to dynamic performance. Structures of shorter period experience greater acceleration, whereas those of more extended period experience greater displacement. Structural performance objectives should be taken into account during preliminary design and response-spectrum analysis (Kalny & Napier, 2014).

Statistical Analysis

As part of the seismic, pushover and reverse cyclic analysis made it can be compared with a statistical analysis the responses of these. The statistical analysis can compare different models and declare if there exist significant differences between the modes in an objective way. This can provide a quantitative result of the grade of difference between the models.

This is important due to the use of SMA and ECC increase the cost of the structure it is essential to know if the improvement in the results is significantly based on an objective result and not in a subjective answer of yes or no. The statistical analysis compares data groups of the models that are statistically normalized.

To validate if there are significant differences is necessary to apply more than one test due to if just one is applied this could incur in mistakes. This analysis was made in "R" a code language; this is a free solution of open code to analyze data supported by a large community of active researchers all around the world (Hidalgo-Ramirez, 2018; Kabacoff, 2015).

It is used the test of the hypothesis that allows accept or refuse approach. The test of the hypothesis is made of a null hypothesis (this correspond to the affirmation trying to test) and an alternative hypothesis (the false option of the null hypothesis). In this work was based on a 5% level of significance, it means there are 5% of probability

of an incorrect result (Millones, Barreno, Vasquez, & Castillo, n.d.).

After the test are applied the p-values must be compared to verify if the null hypothesis is accepted or rejected. This applied to the p-value is more the significance value the null hypothesis can be accepted.

T-student Test

Identify if exist statistically significant differences between two mean of the database. It is used the hypothesis of "two tails" it means takes a null hypothesis that there are no significant differences between the two means.

The formula interface is only applicable to the 2-sample tests. Performs one and two sample t-tests on vectors of data (RStudio Team, 2018).

A two-sample t-test allows us to test whether the means of two independent groups. H_0 (null hypothesis): The true probability of success is not equal to what was proposed. H_1 (alternative hypothesis): The true probability of success is not equal to what was proposed. If (p-value > 0.05) the null hypothesis cannot be rejected.

Therefore, if the p-value is greater than 0.05 means that there are no significant differences between the two populations, in the other case are significant in the statistical difference of the data.

Correlation Pearson Test

The test of correlation says how much related are the data compared to each other. Then, infers if any linear model (statistical models) that can be adjusted.

Test for association between paired samples, using one of Pearson's product moment correlation coefficient, Kendall's tau or Spearman's rho.

The correlation coefficient of Pearson will have a value between -1,0 and 1,0. If the coefficient is equal to zero means that the parameters compared are not independent. Also, takes as a null hypothesis that there is no relation between the data.

The test puts each parameter in a two-dimensional plot, one in each axis, giving the correlation of the populations based on the slope

of the trend. The confidence level of the correlation depends on the designer or the client; it is recommended to use a correlation value equal to or higher than 0,95. This means the correlation of the 95% between the populations to induce that there are no significant differences between the individual parameters.

ANOVA Test

This (generic) function returns an object of class Anova. These objects represent analysis-of-variance and analysis-of-deviance tables. When given a single argument it produces a table which tests whether the model terms are significant (RStudio Team, 2018). The comparison between two or more models will only be valid if they are fitted to the same dataset.

The test is like the t-student test due to the comparison method is the mean of the database. This method also uses as the null hypothesis that there is no relation between the data. This Anova test plots a graphical result of the significance of the difference between two or more models simultaneously.

The plot given consist in a series of boxplots (one per each parameter compared) and in these can be compared the normality and the difference of the means and quartiles. Then, in the top of the plot are some letters (a, b, c, …). The boxplot that shares letters between them mean that there are no significant statistical differences

in these. However, if a model does not share letters with other means significance in the differences. Due to this, it can be possible that some parameters (boxplots) present differences with some models but not with others, this depend on the quantity of letter it has.

This is also a significant advantage of this test compared to another statistical R test, giving a visual representation of the values and comparison of different models at the same time.

Shapiro-Wilk Normality Test

This test is used to determine if there are a parametric behavior of the data compared. It is applied to the deviation of the data. The test has a null hypothesis that the data has a normal distribution. All the previous test has the same assumption; therefore, data must be normalized before compared with these tests.

This test is applied to the standard deviation of two independent variables. Therefore it is necessary to calculate the standard deviation of the populations between them, before applying the Shapiro-Wilk test.

Then, the Shapiro test is applied to the deviation and if the p-value given by R is more than 0.05 means that there are no significant differences between the proposed models. Otherwise, there are significant statistical differences

Results

As explained in the methodology there will be two different types of models, depending on the direction of the applied load, simulating the trends of the earthquake or extreme loadings. From there, will be derived from different models for each one, changing the monotonic load, cyclic load, reverse cyclic load, materials, reinforcement, parameters, pressures, the capacity of the materials.

To recreate the FEM the more accurate possibly, it was modeled several models under different conditions, changes the loads, the characteristics of the materials, type of analysis and others.

In these results are only presented the one discussed on the analysis of results, some results are relevant but not consider on the conclusions, therefore, these are presented on the annexes.

Model 1

When in this research is talking about the *MODEL 1* or *MOD 1* is referred when the earthquake or the extreme loading is in the Y-axis, as seen in **Figure 88**, therefore the model will be represented as one pier due the null restrain in the top or another part of this. The restraint in this axis behaves as a pin, therefore it acts as a cantilever column. The type of pinned restrain in the top of the building, transmit the only axial load from the superstructure to the pier but does not transmit shear or Moment.

The models will present abbreviation on the names, for example in the MOD1-P-RC, the first part means the name of the model (Model 1). The second means the type of analysis, if it is *"P"* means Pushover analysis if else is a *"RC"* the Reverse Cyclic Analysis. Then, the last part identifies the material, where *RC* is reinforced concrete, *SMA* is SMA and *ECC* is ECC.

RC Models

These results are the responses of the models made in different software using the reinforced concrete single pier model due to the direction the induced load. The reinforced concrete models are modeled based on the original blueprints of the piers from 1994.

Pushover Responses

It was made a non-linear static analysis of the bridge using different nominal axial loads also, was used the dead load of the superstructure as base model. The Pushover analysis was made on VecTor2, in this the lateral drift is increased gradually as specified by the user meanwhile the lateral load is increased automatically by the software to produce the drift requested.

The lateral load was located at the top-left corner node of the piers and was pushing laterally the structure to the right until it collapses.

Debugging Pre-models

In order to debug the first responses obtained of the models was changed different input parameters and constitutive models. It was also changed the axial load applied to the piers to identify the behavior of the responses. It was changed the rupture deformation and rupture point of the reinforcement. Also, was made some models using the steel plate showed on the blueprints with infinite stiffness in order to assess only the RC structure.

It was identified that there was created simultaneously two different plastic hinges in the piers, therefore was changed the shear and longitudinal reinforcement to propose changes in the design of SMA.
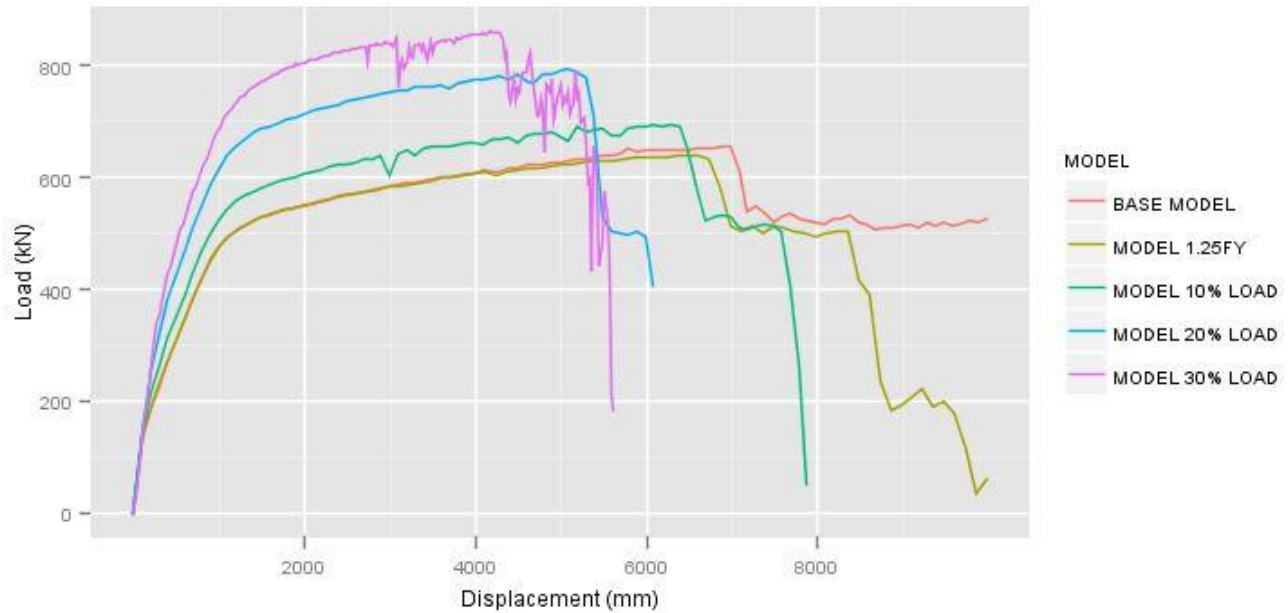
Figure 101. Comparison of the resume of the pre-models Push-overs made.   Software used: Deducer.

Pre-models refers to the fact that was modeled the FEM of RC as the original blueprints indicated, without any modification of SMA or ECC incorporated to the models. To compare the significant differences between the models changing different initial parameters. The initial models were made on FormWorks with the settings shown in the details of the blueprints. It was used ε_u=150 milistrain for longitudinal and shear reinforcement and fu=1,5fy. Then, was proposed other models using ε_u= 100 milistrain and the fu=1,25fy. Also, was made models using a steel plate on the top of the columns with a dimension of 180x180 cm and other using 110x110 cm as shown in the details of the supports. Then, the axial load of the Pier was incremented gradually from 5% (dead load of the superstructure) until achieving a 30%, the usual design load for piers and used in the literature review.

This is shown on **Figure 102**, the curves of each pre-model are completely presented as the response showed on VecTor2. Therefore, the last load and displacement are not defined, this represent the structural failure of the structure due to it is relevant to the pre-models identify the behavior of the structure once the peak load is achieved. Consequently, the whole curve is presented

Based on the models using different axial load, was made a plot with the peak lateral loads

and lateral peak displacements. The points on the figure vary depending the axial load. As the axial load increase the size of the bubble is increased. This plot was made to identify if there exist a linearity depending of the axial load on the piers, this is shown on **Figure 102**.
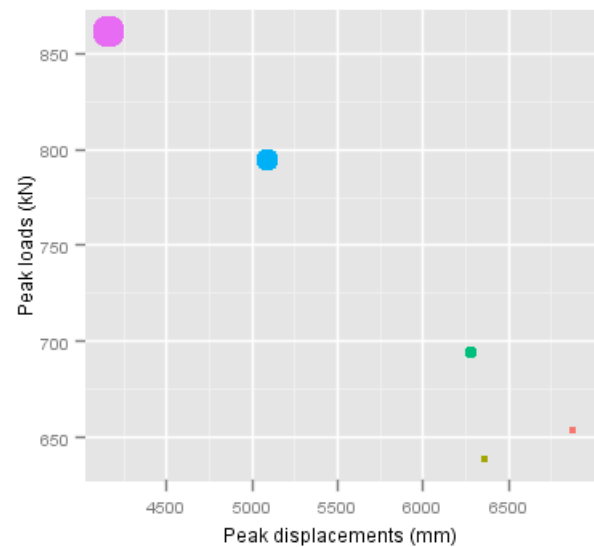

Figure 102. Peak load versus peak displacements in pre-models Model 1. Software used: Deducer.

On **Figure 103** is presented as tabular results and output of the structure, the loads and displacements of the responses using different axial load on the pushover analysis.

Presented by colors is shown the results of the peak displacements, due to the peak lateral displacements is the most relevant parameter of the response. This was used to debug the models and use a base model to compare it with the SMA-RC, ECC-RC and SMA-ECC.

The results shown in green are the optimum results to be used as base model. Otherwise, the results close to red (orange and yellow) represents the models with the need of debug on the models. Putting red as a critic result and green as good acceptable result.

On this figure Δy means the yield point of the structure, $\Delta peak$ the peak lateral load and Δu the ultimate lateral load received. These are partial results therefore the peak load and the ultimate load are the highest and last load received by the structure until it collapses. The yield point was achieved using an approximation of 0,75 of the peak lateral loads.

The name of the Models are abbreviations of the information analyzed. For example, in MOD1-P-RC the first part (MOD1) means the number of the model, in this case is Model 1. The second part "P" means that was made a Pushover analysis. The last part means the material used where RC represent the reinforced concrete.

Model	Δy	$\Delta peak$	Δu	Load_y	Load_peak	Load_ult
MOD1-P-RC	1328,31	6877,53	7974,50	513,10	654,40	523,52
MOD1-P-RC plate on top 110x110	1328,30	6977,20	7974,42	513,00	655,00	524,00
MOD1-P-RC plate on top 180x180	1328,33	7475,71	7974,46	508,50	664,10	531,28
MOD1-P-RC (fu=1,25fy, er=100) 110x110	1328,33	6379,34	7975,77	513,20	639,50	511,60
MOD1-P-RC (fu=1,25 er=100)	1328,31	6977,40	7981,28	513,10	645,90	516,72
MOD1-P-RC fu=1,25fy, er=100 smeared er=100	1328,31	6354,38	7976,28	508,90	638,70	510,96
MOD1-RC fu=1,25fy, er=100 smeared er=100 PL 110x110	1328,30	6379,30	7976,28	513,10	644,30	510,96
MOD1-P-RC (10% Load)	1195,54	6279,94	6455,44	543,50	694,30	555,44
MOD1-P-RC (20% Load)	1195,60	5084,08	4865,07	639,40	794,40	635,52
MOD1-P-RC (30% Load)	1162,40	4161,99	4487,27	724,40	861,10	688,88
MOD1-P-RC without cha(30% Load)	1162,40	4161,99	4487,27	724,40	861,10	688,88

Figure 103. Table with the primary response of the pre-models Model 1.[19]
Software used: Microsoft Excel.

Figure 103 shows the detail of the models made; these models were plotted as shown in **Figure 101**. Apparently can be observed that is not the same quantity of models, because some models had the same response results as shown in the previous table. Therefore, was decided to print the remarkable achievements of the pre-models and avoid have noise in the figures and achieve better analysis

Once the base model is identified, then the need of debugging is necessary due to the large displacements obtained. There was used a yellow line to represent the difference on the behavior of the models, this is shown on **Figure 104**. This yellow line is located at the yield point of the responses to identify a change of the behavior before and after of this point.
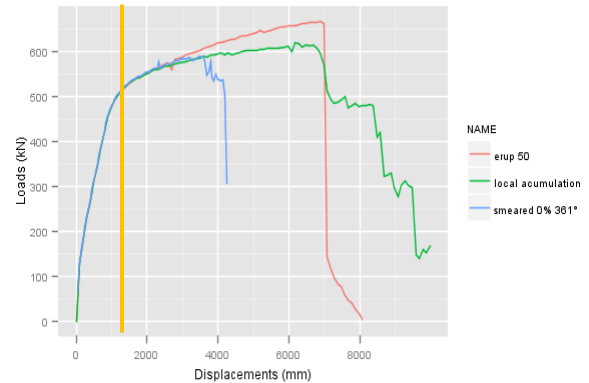

Figure 104. Push-over of pre-models RC in the Model1.
Software used: Deducer

Trying to decrease the large lateral displacements obtained was made other pre-models. It was changed the rupture deformation of the models

---

[19] Units of Δ (displacements) are in mm and the lateral loads are in kN.

(erup), also was used the hysteretic response of the reinforcement model from the Bauschinger Effect (Seckin) to the Seckin Model with local accumulation, due to this consider drastically the cracks produced on the concrete and its
.

implications on the reinforcement. Also was used 0% of smeared reinforcement (shear reinforcement) in the out of the plane axis (361°). This was made in order to debug the model and present acceptable deformation of the piers.
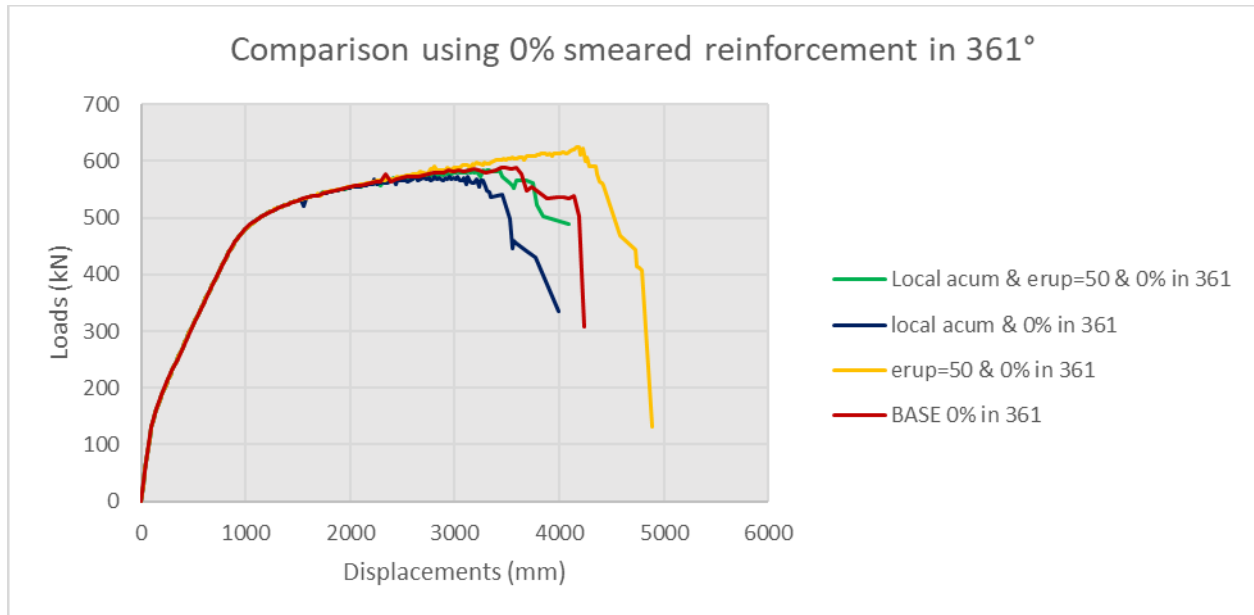

Figure 105. Last modification of the pre-models, Model 1 Pushover analysis.   Software used: Microsoft Excel.
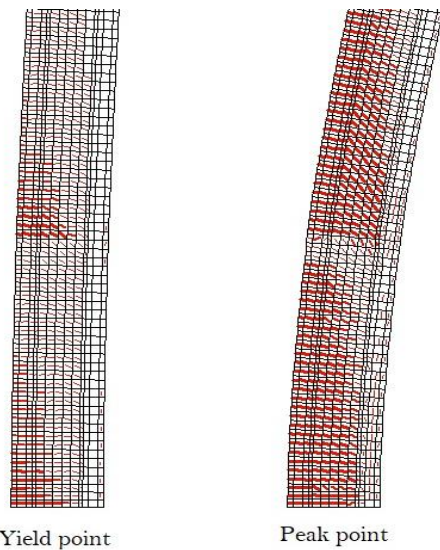

Figure 106. The crack pattern in MOD1, set magnification of 1. Software used: Augustus.

On **Figure 106** is presented a problem identified on the models that two different plastic hinges on RC models created at the same time. This figure

shows the crack pattern, width and deformed shape on the base of the piers.

It was seemed that there was produced two different plastic hinges on the RC models. On the base of the piers also, on the zone where is a variation of longitudinal and shear reinforcement (up to 6,0 meters).

Figure 107 shows the crack width of the models and its location. On this figure present in detail the width of the cracks showed on the previous figure. Separating by colors the variation of the crack widths. Here is represented just the critical zone of the piers, the rest of the structure does not present crack, therefore is in color blue.

Figure 107 shows in detail the width of the cracks in the critical zone of the piers at the peak load. The rest of the structure that is not presented on the figure does not have cracks therefore it is in color blue.
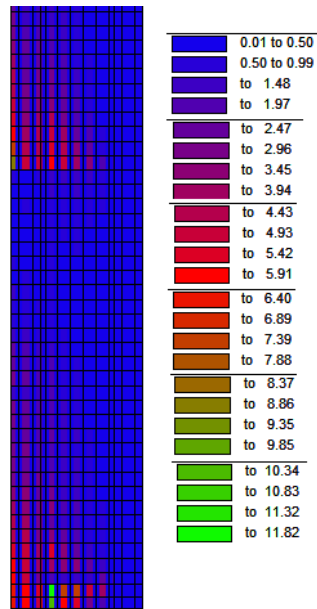
Figure 107. Crack width Pushover MOD1-P-RC, units in mm. Software used: Augustus.

On **Figure 108** is presented the solutions made to contrast the behavior of the two simultaneous plastic hinges on the piers.

The capacity curve of the **Figure 108** is presented on **Figure 109**. Using changes on the longitudinal and shear reinforcement.

In order to identify the main problem of the creation of two simultaneous plastic hinges was made three different models changing the shear reinforcement, the longitudinal reinforcement and other one changing both. Where on **Figure 109** "*sep*" means that was changed the separation of the stirrups and "*truss bars*" the longitudinal reinforcement.
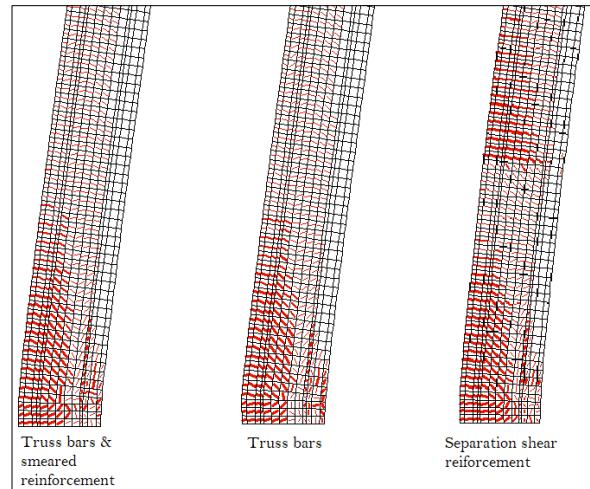

Figure 108. Crack pattern in the MOD1-RC Pushover analysis, changing the longitudinal and shear reinforcement. Software used: Augustus
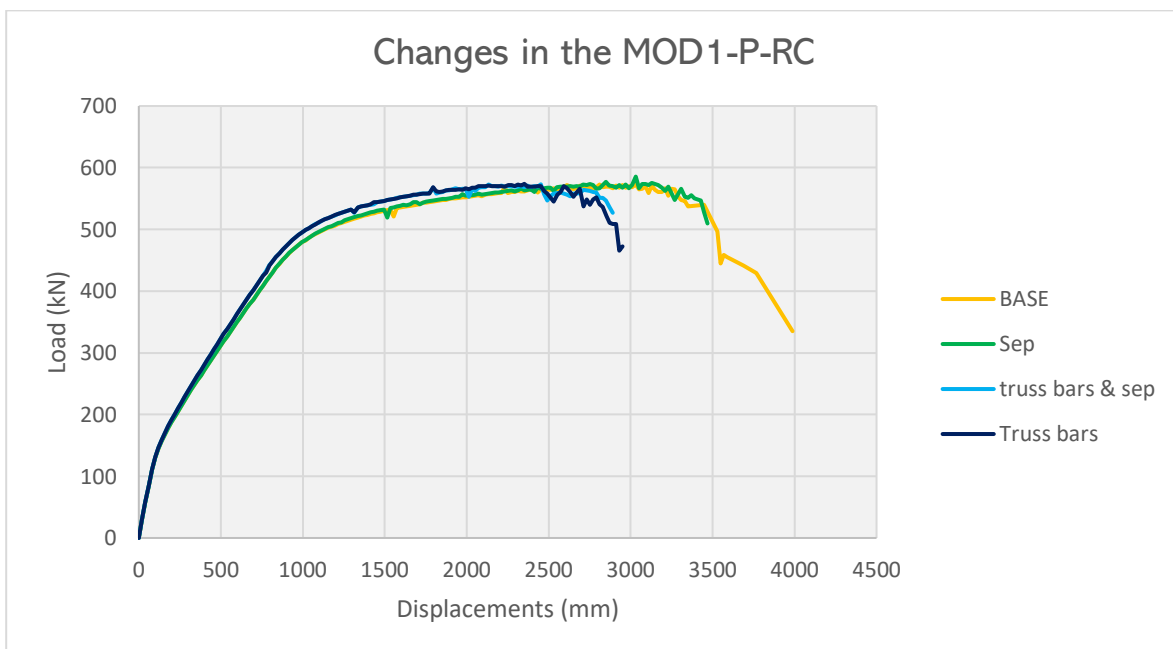

Figure 109. The response of the MOD1-P-RC changing the longitudinal and shear reinforcement.   Software used: Microsoft Excel.

SEISMIC PERFORMANCE OF SMA-REINFORCED ECC PIER SYSTEM OF THE SALITRAL BRIDGE

Definitive Model

Once the pre-models are debugged the definitive parameters of the RC model is defined. Therefore, it can be proceeded to make the definitive Pushover analysis. Based on this is made the reverse cyclic analysis and with changes on the plastic hinge the SMA and ECC models.

The definitive model was made using 15% of nominal axial load as explained on the methodology. It was the "Seckin (with local accumulation)" model on the reinforcement on VecTor2, then it was used 0% on the smeared reinforcement on the out of the plane axis (361°) and the overlap indicated on the original blueprints to produce just one plastic hinge.
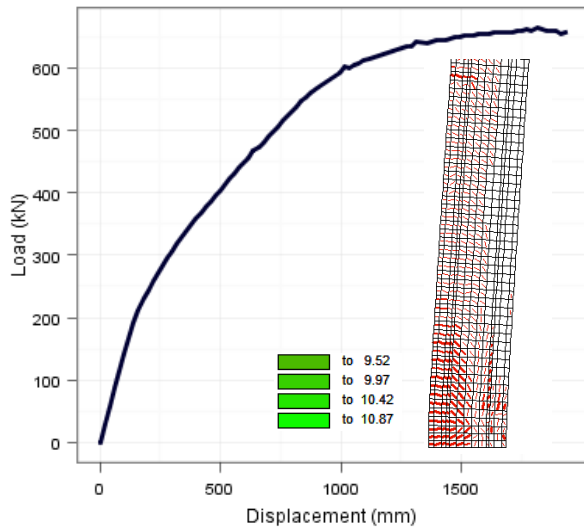

Figure 110. Definitive Pushover response of the Model 1 using 15% of nominal axial load, Crack width on green (units in mm).

On **Table 6** is presented the points obtained in the response of the definitive Pushover. The yield point was obtained based on the secant stiffness intersection method at 75% of the peak load. The peak load corresponds to the highest lateral load achieved and the peak displacement is the displacement that intersect the curve at the peak load. The ultimate point in this table correspond at the last load and displacement obtained in the response due to this point correspond the collapse of the structure.

The ductility was obtained based on the ratio of the ultimate displacement divided by the yield displacement of the structure. The drift corresponds to the peak displacement divided by the whole height of the piers of the bridge.

Table 6. Points of the importance of the response MOD1-P-RC.

Parameter	Displacement (mm)	Load (kN)
Yield point	929,89	572,10
Peak point	1813,89	663,80
Ultimate point	2113,42	419,10
Ductility	2,27	
Drift	0,05	

Reverse Cyclic Response

On **Figure 111** is presented the reverse cyclic response of the Model 1 using just RC with 15% of nominal axial load. The reverse cyclic analysis was made based on the definitive model of the Pushover analysis using the same input parameters. The lateral load of the push was located in the same position of the Pushover. On the reverse cyclic analysis, the lateral load does not only push the structure but also pull, this is why on the elements of the grid where was located the lateral load was used infinite stiffness material.
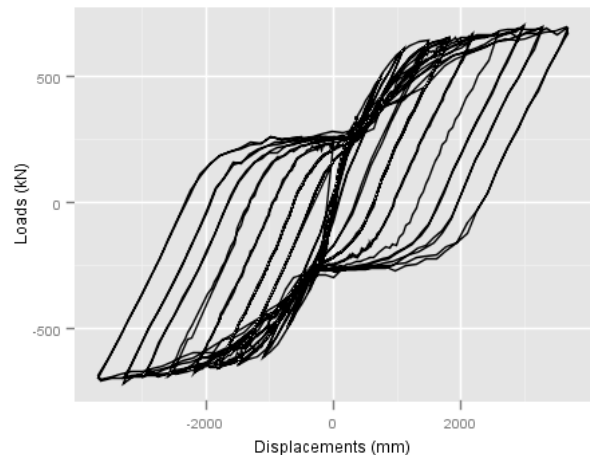

Figure 111. Reverse cyclic analysis, Model 1 RC with 15% of the axial load applied.
Software used: Deducer.

This **Figure 112** represents the differences of the responses of the reverse cyclic analysis using just the dead load (DL) of the superstructure and 15% of the nominal axial load. The black line represents the X-axis to identify better the intersection point of the reverse cyclic responses.
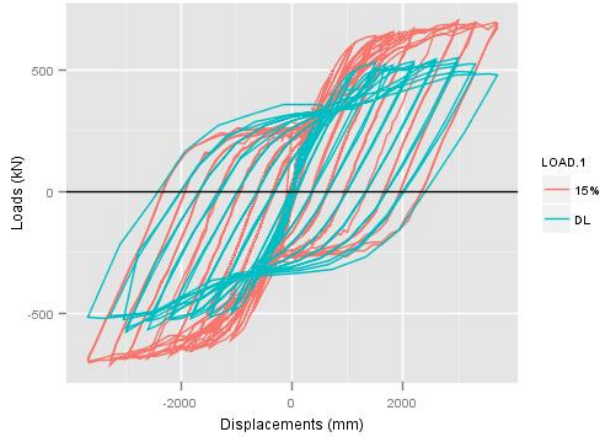
Figure 112. Comparison of the response of MOD1-RC-RC under reverse cyclic analysis, using 15% of the axial load and the Dead Load of the superstructure.
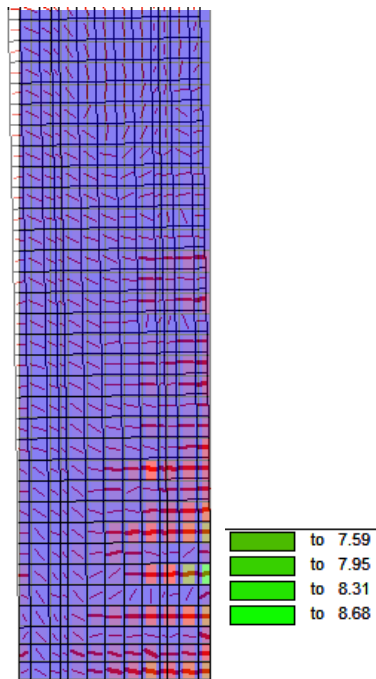Software used: Deducer.

Figure 113. Crack width of the reverse cyclic response on RC, units in mm.

Elastic Response

It was made a three-dimensional model using the software SAP2000 v20. It was assessed the structure to identify the most critical elements and compared them with analysis made with VecTor2. This is presented on **Figure 114.**

The software VecTor2 works on a two-dimensional plane therefore the supposition made that the Model 1 behaves as a single pier system cannot be corroborated, therefore another analysis on a different software is recommended. A three-dimensional model can predict the behavior of the structure and assess its performance. Confirming if the suppositions made on the methodology was true or behaves differently.
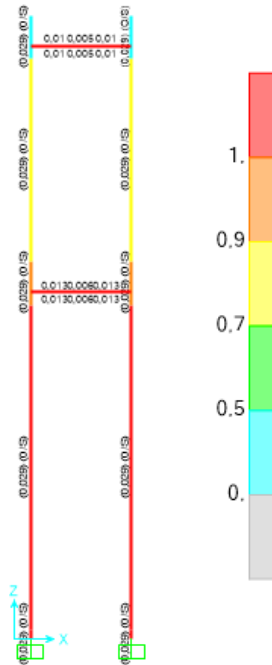

Figure 114. Check of the frame in the Model ACI 318-14.
Software used: SAP2000 v20.

One of the most relevant parameters on the structural engineering is to identify the shear a flexural moment diagram. Because these represent the most affected elements, the magnitude of the internal forces and distribution of forces.

The shear diagram of the three-dimensional model is presented on the next figures. The **Figure 115** represent the shear diagram on the Y-axis and **Figure 116** on the X-axis. Then, **Figure 117** shows the flexural moment diagram on the Y-axis and **Figure 118** on the X-axis.

These results verify the suppositions imposed on the background and methodology proposing the piers behaves as single piers on the Y-axis and as a frame on the X-axis.
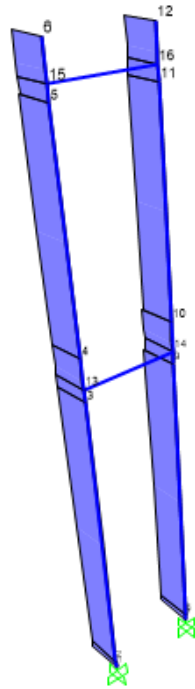
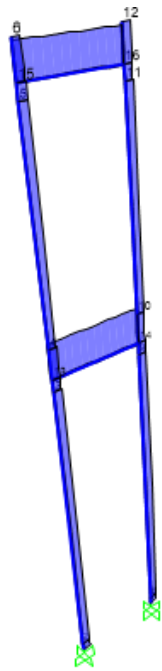Figure 115. Shear V3 Diagram, Earthquake in Y-axis.
Software used: SAP2000 v20.

Figure 116. Shear V2 Diagram, Earthquake in X-axis.
Software used: SAP2000 v20.

Table 7 shows the results of the Modal analysis made with the parameters of the site, based on the

Seismic Code of Costa Rica (2010). It was induced the loads in the Y and X-axis as previously defined in the methodology. This three-dimensional model can confirm the suppositions made to model on the software VecTor2. As explained in the background the Salitral Bridge is located on Orotina, Alajuela, Costa Rica on a Seismic Zone II. The axial load of used on this model was 15%, the same used on the Pushover and reverse cyclic analysis.

The results shown are only the most critic of the response, this are usually the one used to design the dimensions of the elements.

Table 7. Maximum Shear per element[20].				
Structural Element	*Analysis*	*Direction*	*Shear*	*Units*
Pier	Modal	Y-axis	35,192	kN
Pier	Modal	X-axis	93,711	kN
Beams	Modal	Y-axis	0,000	kN
Beams	Modal	X-axis	368,458	kN
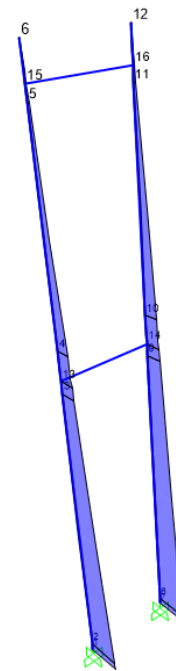
Figure 117. Moment 2-2 Diagram, Earthquake in the Y-axis.
Software used: SAP2000 v20.

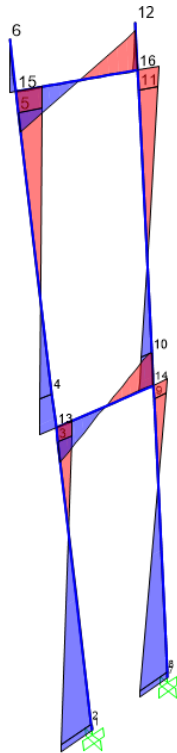
[20] Using the Software SAP2000 v20.

Figure 118. Moment 3-3 Diagram, Earthquake in the X-axis. Software used: SAP2000 v20.
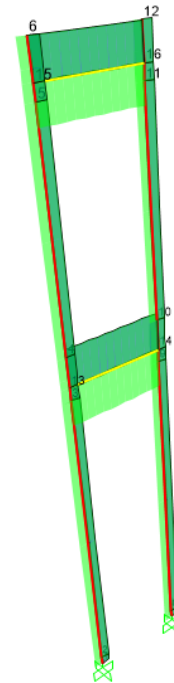

Figure 119. Time-History response X-axis, Shear Envelope Limón Earthquake 1991 Costa Rica N00E (Base Shear 176,703 kN).
Software used: SAP2000 v20.

Using the Limon and Samara earthquake record was made a time-history analysis. The internal forces of the frame vary depending on the time. On each second the shear and flexural moments diagram is different, therefore it was made an envelope response to represent the maximum and minimum shear and moments. These plots are presented on **Figure 119** and **Figure 120**.

These earthquakes are the highest magnitude events recorded on the history of Costa Rica, therefore the most relevant events in this research. The dataset used was taken from the stations "Cipet en Alajuela" and "Edificio del INS" from the Laboratory of Earthquake Engineering in Costa Rica, due to the facility to obtain it online.

As explained on the background these are the most critic earthquakes on magnitude event, but not on damages. The Cinchona's Earthquake was one of the most critic earthquakes seemed from the economic and social part, but it was because of the topography, soil type and slide of slopes in the foundations. Therefore, was not that relevant in the time-history analysis made with SAP2000.
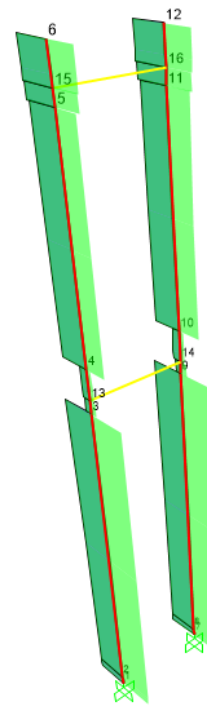

Figure 120. Time-History response Y-axis, Shear Envelope Limón Earthquake 1991 Costa Rica N90E (Base Shear 107,341 kN).
Software used: SAP2000 v20.

SEISMIC PERFORMANCE OF SMA-REINFORCED ECC PIER SYSTEM OF THE SALITRAL BRIDGE

SMA-RC Models

In the models where the SMA was used on the plastic hinge and ductile reinforcement on the rest of the structure with ordinary concrete was called as MOD1-P-SMA. This model represents the response of the structure with ordinary reinforced concrete, and a nominal axial load of 15% and have continuity on the bars from the bottom to the second stage of material. Due to the original model was created two different plastic hinges simultaneous, the incorporation of SMA will be increased and will be necessary to put it in two different locations or use a large length of SMA. Both hypotheses are unviable due to the high cost of SMA and are not recommended to have two different plastic hinges in the same pier to prevent high rotation of the structure.

The use of SMA on the structural engineering is relatively new therefore there is not already a basic design of this. The length of the bars of SMA is the length calculated of the plastic hinge. Based on different researches was calculated the plastic hinge length of the piers, as seen in **Table 8**.

Table 8. Length of Plastic Hinge.		
Research	**Material**	**Lp (m)**
Billah & Shahria Alam (2016)	SMA	1,29
Fedak (2012)	RC	1,69
O'Brien M, Saiidi MS, Zadeh MS (2007)	SMA	1,79
Nakashoji B, Saiidi MS. (2014)	SMA-ECC	1,79

Based on **Table 8** was defined that the length of the SMA bars will be 1,80 m. Starting from the base up to 1,80 m of height.

The SMA bars as previously explained there is not already a defined design, therefore the diameter of the bars is the same of the steel rebars previously designed but with the nominal length used by the sellers. This is why the SMA bars have a diameter of 35,0 mm replacing the #11 bars on the borders of the piers as seen on **Figure 121**. The rebars #10 still been used with steel, the red points of the figure are the location of the SMA bars. The connection of the SMA bars with the steel rebars are with mechanical connectors, these were also modeled on VecTor2.
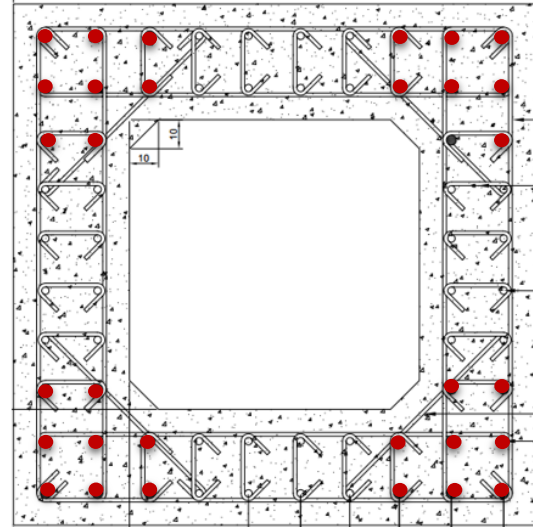
Figure 121. Location of the SMA used in the Model, SMA bars presented in red on the cross-section of the pier.
Software used: AutoCAD Autodesk.

Pushover Response

The lateral load of the Pushover was on the same spot of the RC Pushover. The model represents basically the same input parameters except by the use of SMA bars and mechanical connectors on the borders of the plastic hinge previously calculated.

Figure 122 represents the non-linear static analysis response of the model using SMA and steel on the plastic hinge length.

Figure 122. Non-linear static analysis of Model 1, the comparison between using RC and SMA in the plastic hinge with 15% of the axial load applied.
Software used: Deducer.

The crack pattern and orientation of the cracks is presented **Figure 123** due to the pushover analysis induced to the structure and then, **Figure 124** the crack width of the piers due to the monotonic load applied.

Figure 123. MOD1-P-SMA, Crack pattern and displacements set magnification = 1,0.
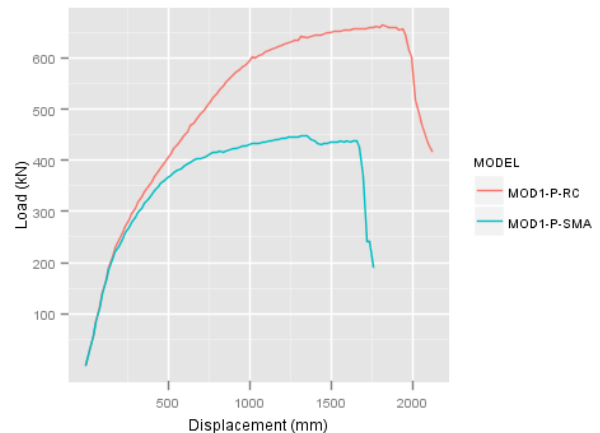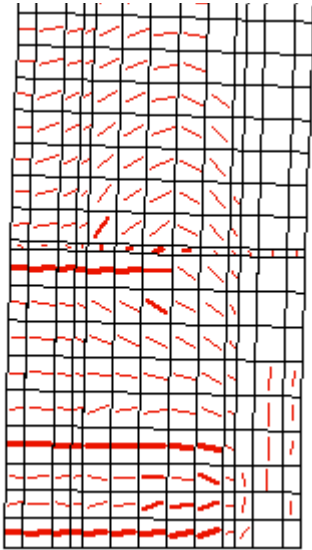Software used: Augustus.
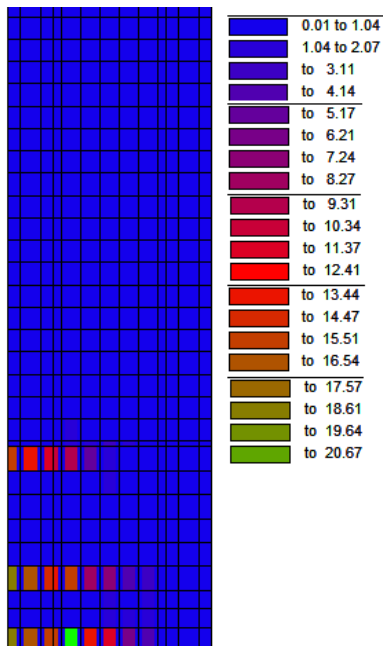
Figure 124. Crack spacing MOD1-P-SMA, units in mm.
Software used: Augustus

Table 9. Points of importance of the response MOD1-P-SMA.

Parameter	Displacement (mm)	Load (kN)
Yield point	531,42	370,30
Peak point	1355,73	447,20
Ultimate point	1754,98	190,80
Ductility	3,30	
Drift	0,04	

The points of the **table 9** were calculated as explained on the description of **Table 6**.
A correlation test was made to identify if there are differences on the displacements of the SMA and RC responses, this is shown on **Figure 125**. As method of correlation is presented the equation and the value of R.
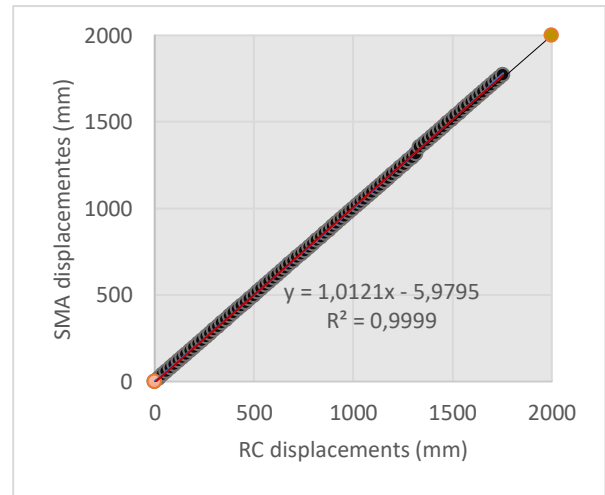
Figure 125. Correlation of SMA displacements versus RC displacements of the Model 1 using 15% of axial load in the Pushover.
Software used: Microsoft Excel.

Reverse Cyclic Response

The reverse cyclic response of the model using SMA is presented on **Figure 126** and then, on **Figure 127** is presented the comparison of the hysteretic curve between the SMA-RC and RC response using 15% of axial load and the loops presented until 10% of lateral drift. On **Figure 128** is presented the crack pattern of the reverse cyclic and on **Figure 129** its width.
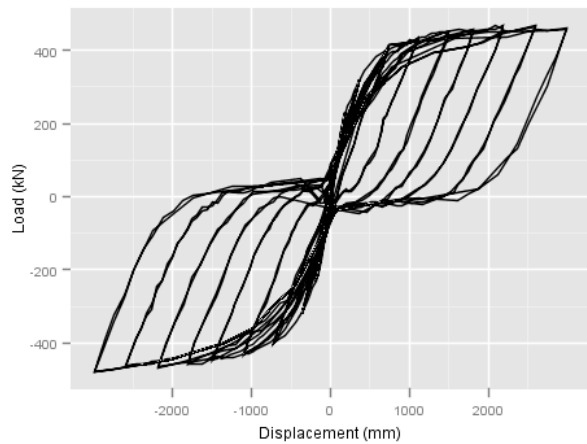
Figure 126. The response of the reverse cyclic loading of the MOD1-RC-SMA with 15% of the axial load.
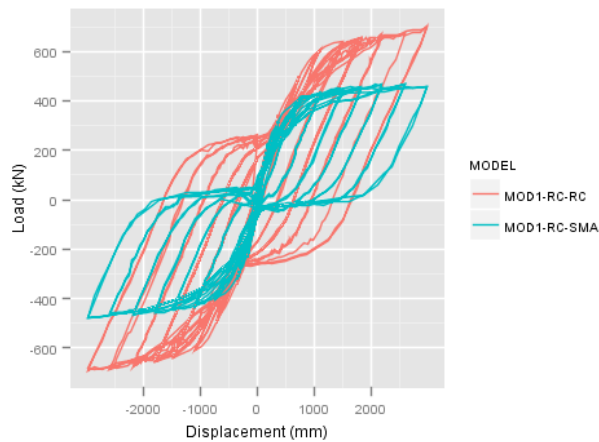
Figure 127. Reverse cyclic analysis of MOD1-RC-SMA compared to MOD1-RC-RC, with 15% of the Axial load. Software used: Deducer.
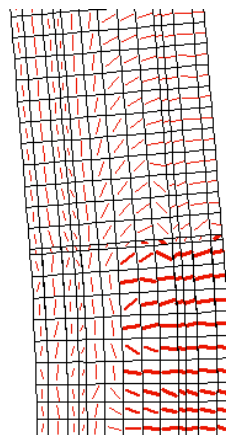
Figure 128. Crack direction and displacements combined in the Reverse cyclic analysis at 10% of strain, set magnification of 1,00.
Software used: Augustus.
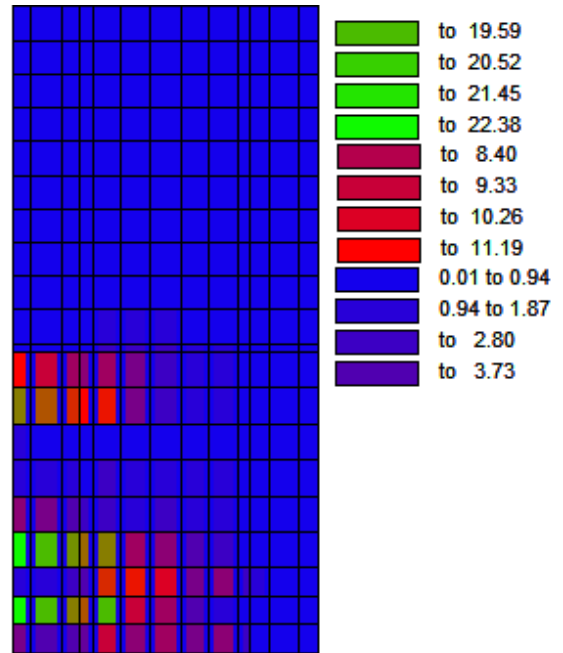
Figure 129. Crack width of the Reverse cyclic loading in MOD1-RC-SMA at 8% of strain, units in mm.
Software used: Augustus.

Figure 130 present the difference of the variation on cracks depending on the lateral drift stage. The cracks do not change its length or width but increase the quantity of these.
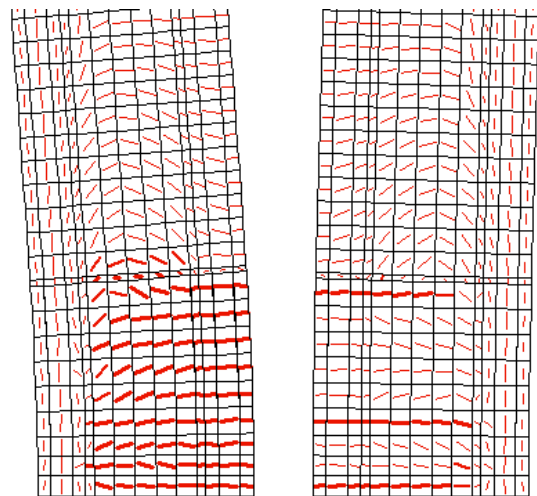
Figure 130. The crack pattern of the reverse cyclic analysis at 9% (left) and 4% of drift (right) of the MOD1-RC-SMA.
Software used: Augustus.

Sub-models with differences on the quantity of SMA

To identify if the proposal of location and quantity of SMA bars is the finest option was made different pre-models or sub-models. In these was changed the length of the SMA bars in the plastic hinge. In other comparison was used the SMA bars in all the cross-section of plastic hinge with the previously defined length.

In these sub-models was tested diverse reverse cyclic analysis to identify different parameters as the energy dissipated and lateral load capacity.

Then, it was made different models changing the plastic hinge length based on the literature review, to identify if there exist significant differences, this is shown on **Figure 131**.
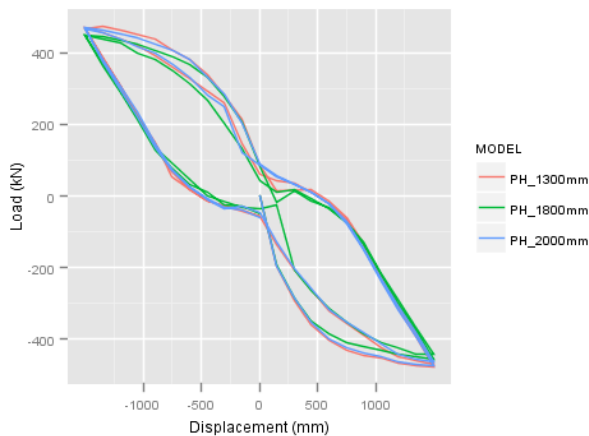
Figure 131. Change in the length of the SMA in the reverse cyclic analysis in the MOD1-RC-SMA at 4% of drift.

One of the most relevant models of this research was using SMA rebars in all the cross-section on the plastic hinge length and not just on the borders. This was the most used method on the literature review.

It was made a non-linear static and reverse cyclic analysis; these figures show the comparison between the use of SMA on the borders and SMA on all cross-section of the plastic hinge length. This will identify if there exist significant differences between the proposed model and the model recommended on the literature review.
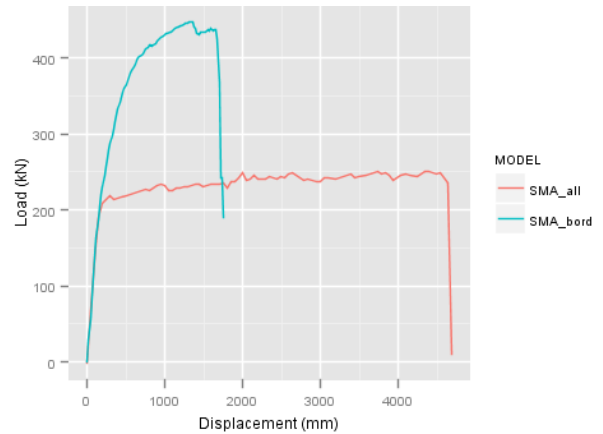
Figure 132. Comparison between using SMA in the main longitudinal bars presented in red before versus using SMA in all the longitudinal bars of the plastic hinge length.
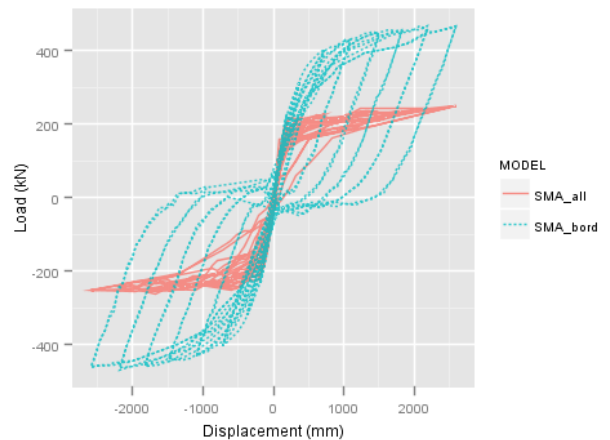
Figure 133. Comparison between the reverse cyclic analysis using SMA in the red indicated points versus in al the longitudinal bars of the plastic hinge.
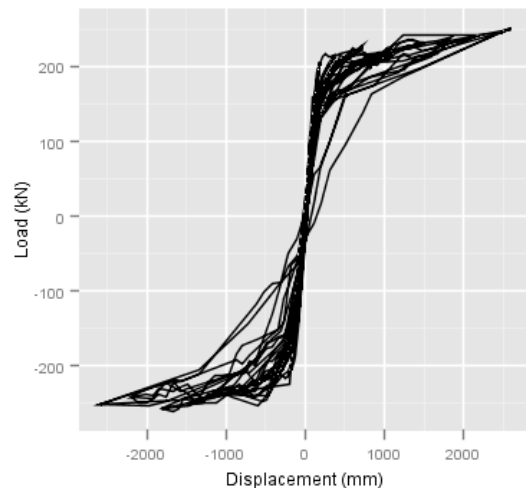
Figure 134. Reverse cyclic analysis of the MOD1-RC-SMA using the SMA in all the length of the plastic hinge.
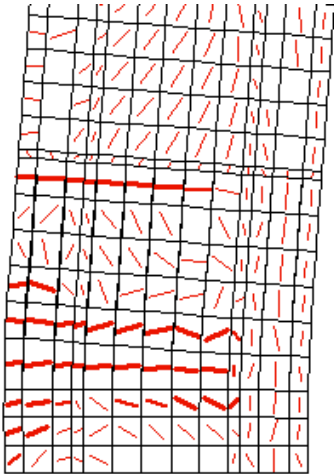
Figure 135. Crack directions of the reverse cyclic analysis using SMA in all the plastic hinge at 8% of drift. Software used: Augustus.
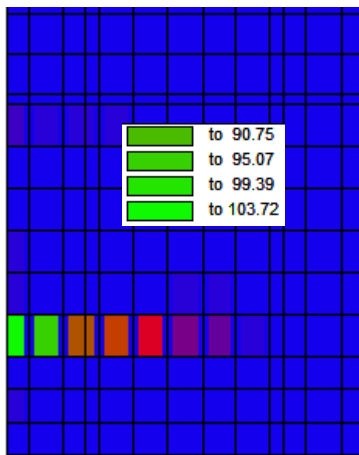
Figure 136. Crack width of the MOD1-RC-SMA using SMA in all the plastic hinge zone, units in mm. Software used: Augustus.

As part of the identification if there are significant differences on the quantity of the SMA used on the cross-section of the plastic hinge length of the piers was made different plots, where was presented the lateral load capacity, energy dissipated and recovery capacity versus each drift stage.
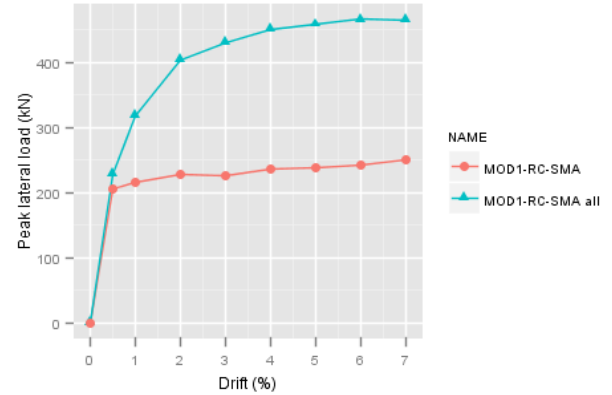
Figure 137. Peak lateral load versus lateral drift using SMA in the indicated zone and all the plastic hinge length. Software used: Deducer.
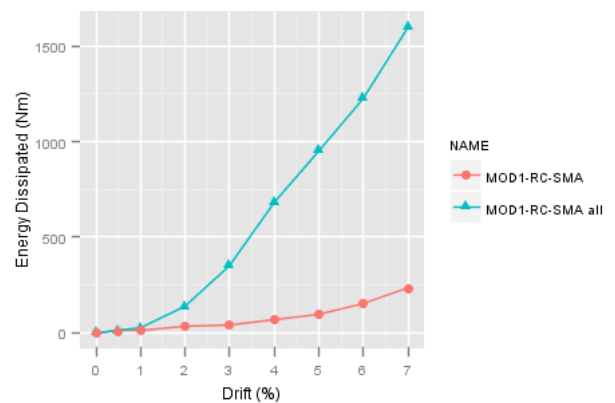
Figure 138. Energy dissipated versus lateral drift using SMA in the indicated zone and all the plastic hinge length. Software used: Deducer.
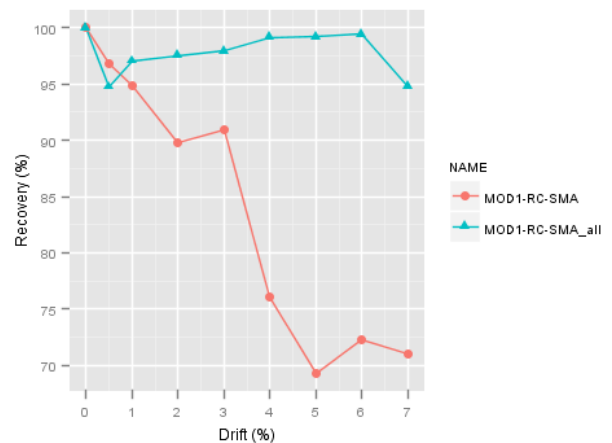
Figure 139. Recovery versus lateral drift using SMA in the indicated zone and in all the plastic hinge length. Software used: Deducer.

ECC-RC Models

The response here presented is using ECC just in the plastic hinge length calculated previously. These models present steel as reinforcement, ordinary concrete in the structure and ECC just in the plastic hinge length with PVA fibers.

The models are simulating the use of HFA-ECC on the plastic hinge due to this is the type that present the highest cracking, tension and compression forces. Also, is one of the greenest and cheapest compared to other types of ECC.

Pushover Response

The Pushover was made in the same way the previous non-linear static analysis made with a lateral load on the top-left corner node of the pier, pushing the structure to the right until it collapses.

It was also used a 15% of nominal axial load on the pier, it was used as base the definitive model of RC changing just the material of the plastic hinge to ECC reinforced with steel.

Figure 141. Displacements and crack directions combined of the Pushover analysis of MOD1-P-ECC.
Software used: Augustus

Figure 140. Non-linear static response of the ECC Model 1 with 15% of the axial load (ECC just used in the plastic hinge length).
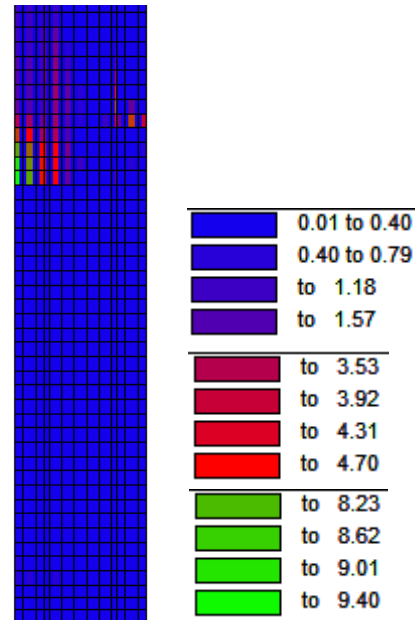
Figure 142. Crack width of the Pushover response using ECC in the plastic hinge, units in mm.
Software used: Augustus.
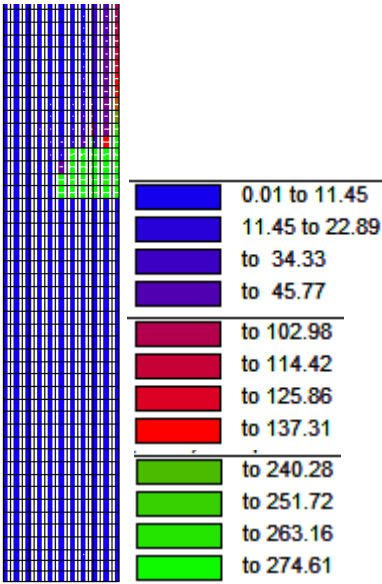
Figure 143. Stress in the steel reinforcement of the model due to lateral non-linear push, units in MPa.
Software used: Augustus.

Reverse Cyclic Response

Using the same model of the Pushover using ECC on the plastic hinge was made a new model but now making a reverse cyclic analysis up to 10% of lateral drift. Proposing the same number of cycles used on the RC and SMA models. The reverse cyclic response is shown on **Figure 144**, using 15% of axial load on the piers.
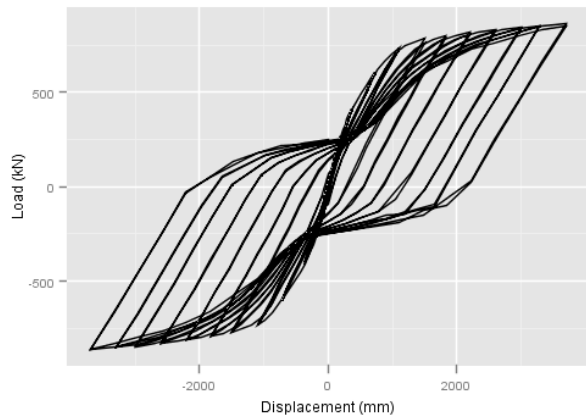
Figure 144. The hysteretic response of the reverse cyclic analysis on the first model using ECC on the plastic hinge length.
Software used: Augustus.

Figure 145. Crack pattern and displacement of the reverse cyclic Mod1-RC-ECC.
Software used: Augustus.
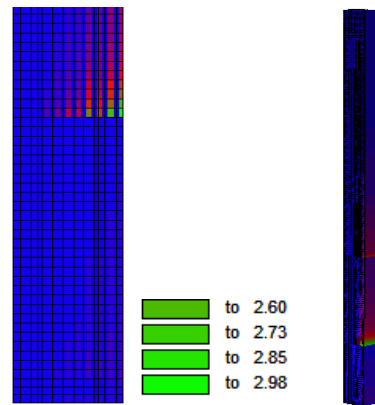
Figure 146. Crack width of the Mod1-RC-ECC, units in mm.
Software used: Augustus.
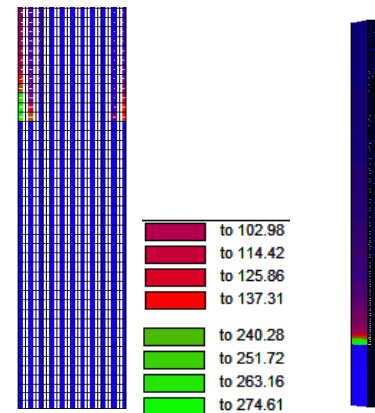
Figure 147. Stress on the reinforcement bars, units in MPa.
Software used: Augustus.

SMA-ECC Models

These responses show the results of the first Model with the lateral load in the Y-axis, all using 15% of the axial load. The use of the SMA and ECC is only in the length of the plastic hinge. The SMA used is the Nitinol alloy and the ECC simulated by the finite element model is HFA with PVA fibers.

Pushover Response

On **Figure 148** is presented the non-linear static response of the pier using SMA and ECC combined in the plastic hinge length of the element. Also, is presented the capacity curves of the previous models using just SMA, ECC and RC to identify differences between the responses.
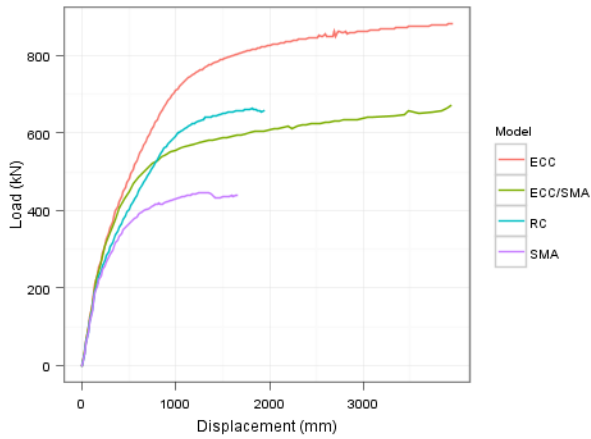
Figure 148. Non-linear static response of the ECC-SMA model with 15% of axial load compared to the rest of the proposed models.
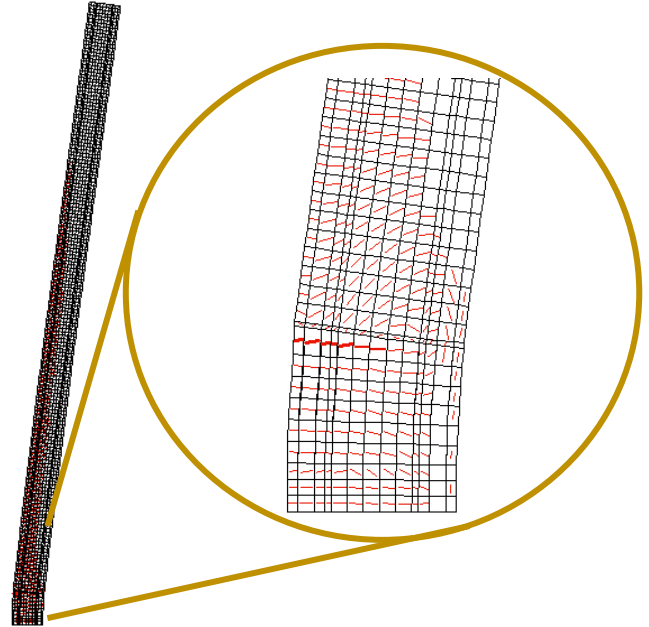
Figure 149. Displacements and crack directions of the Pushover response using SMA-ECC.
Software used: Augustus.
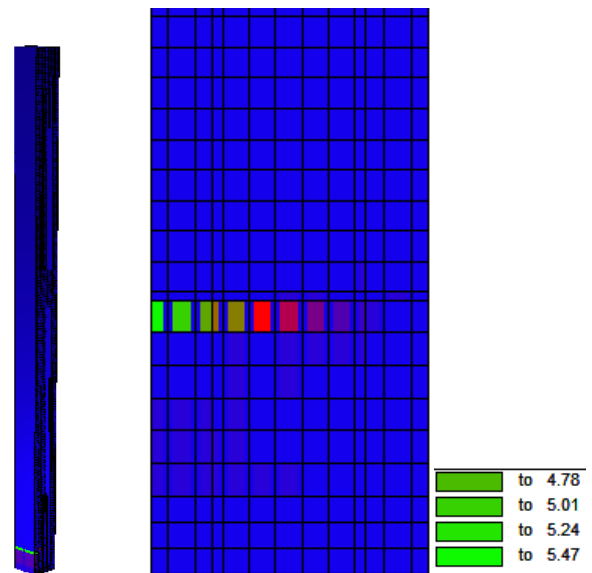
Figure 150. Crack width of the ECC-SMA model, units in mm.
Software used: Augustus.
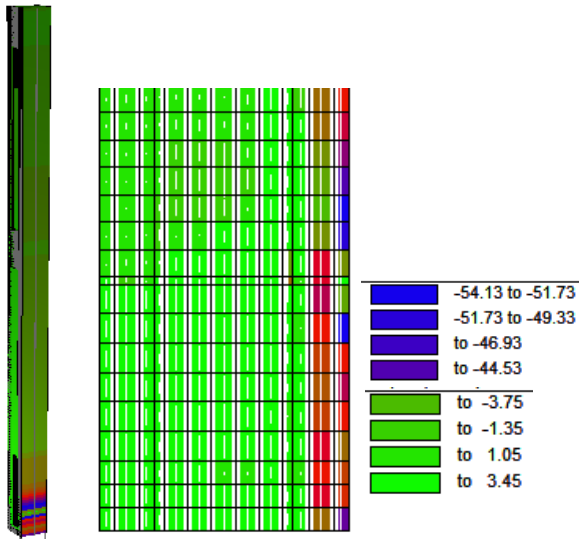
Figure 151. Stress in the concrete due to the Pushover in the critical area, units in MPa.

Software used: Augustus.

Figure 152. The stress of the steel in the critical zone of the model, units in MPa.

Software used: Augustus.

Reverse Cyclic Response

Figure 153. The hysteretic response of the SMA/ECC Mod1 reverse cyclic at 10% of lateral drift.

Software used: Deducer (JGR).
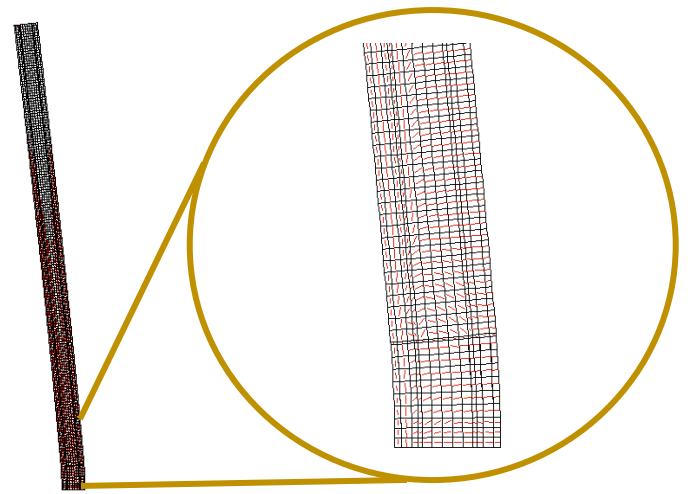
Figure 154. Crack pattern and displacement of Mod1-RC-SMA/ECC.

Software used: Augustus.
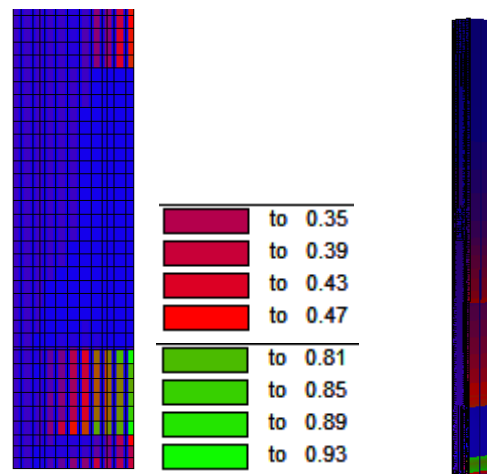
Figure 155. Crack width of the system, units in mm.

Software used: Augustus.
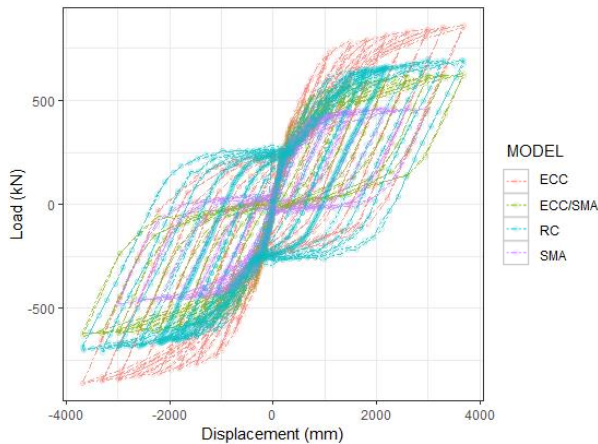
Figure 156. The combined hysteretic response of the piers under Reverse cyclic loading.
Software used: Deducer (JGR).

As presented on the results using SMA on all the cross-section of the plastic hinge, it was made the comparison of different parameters as peak lateral load, recovery capacity, energy dissipation and equivalent viscous damping versus each lateral drift stage. The next four figures present these relevant curves to identify the trending and behavior of the response and identify if there exist significant differences due to the use of SMA and ECC together or by itself on the pier system.

In some models the structure presented a premature failure on the system or produced a significant noise on the FEM therefore the behavior of the system was extrapolated with the most adjusted equation to predict the missing values.
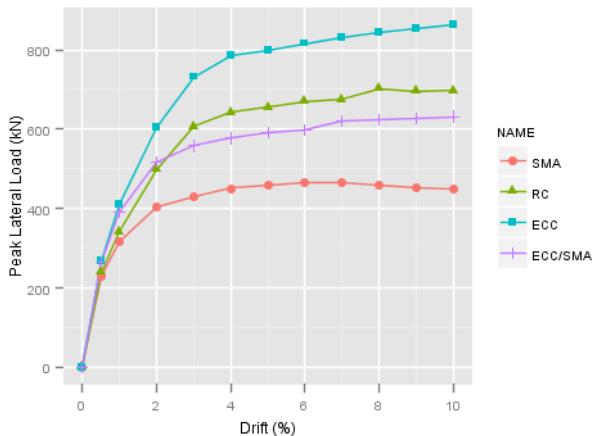
Figure 157. Lateral load versus drift of the reverse cyclic loading.
Software used: Deducer (JGR).
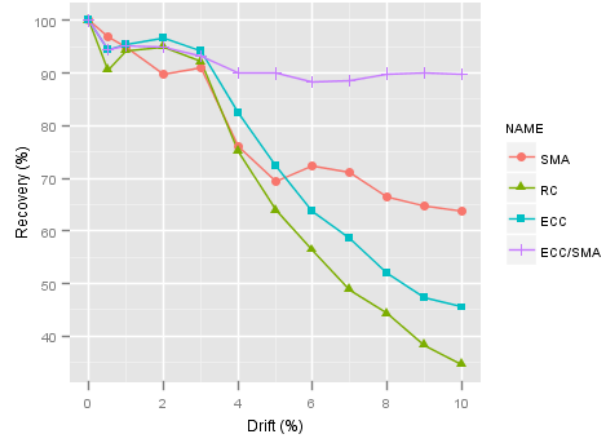
Figure 158. Recovery capacity versus drift of the reverse cyclic loading.
Software used: Deducer (JGR).
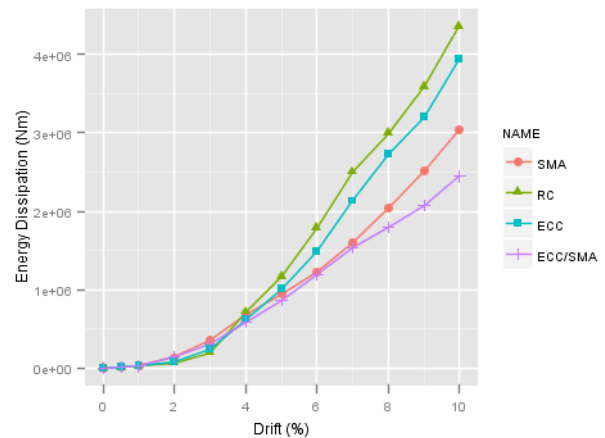
Figure 159. Energy dissipation versus drift of the reverse cyclic loading.
Software used: Deducer (JGR).
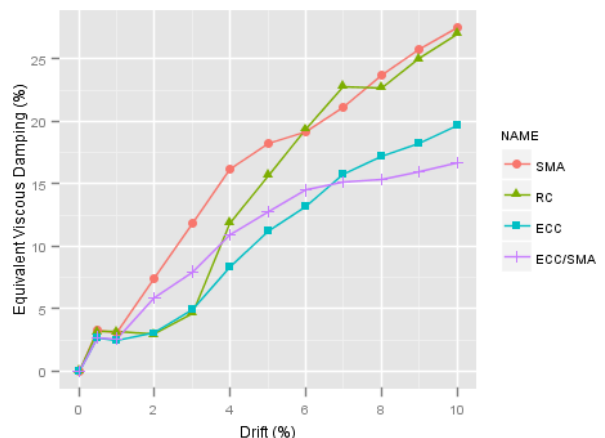
Figure 160. Equivalent viscous damping versus drift of the reverse cyclic loading.
Software used: Deducer (JGR).

Statistical Analysis

As previously mentioned, it was made an statistical analysis to produce an objective response to the identification of significant differences on the models using the smart materials and the methods proposed.

As explained on the Methodology it is recommended to use more than just one statistical test to identify significant differences. The Pearson, T-student and Shapiro test can compare just two variables at the same time; therefore, it was compared the SMA, ECC and SMA/ECC models to the RC model and assessed its improvement. The ANOVA test is capable to compare several variables at the same time and produce a graphic response of the results.

The statistical analysis was made on the most relevant parameter of the research. This is the recovery capacity due to this research looks for the auto re-centering capacity of the piers after strong earthquakes using smart materials. Therefore, this result is the most relevant result to conclude the feasibility of the research

Table 10. Statistical tests results.			
Compared to RC	Correlation Pearson test	T-test	Shapiro test
	(Corr. Confidence)	(p-value)	(p-value)
SMA	0,9547127	0,223400	0,10700
ECC	0,9980430	0,544500	0,16110
SMA/ECC	0,8280368	0,008829	0,05444

Software used: Microsoft Word.
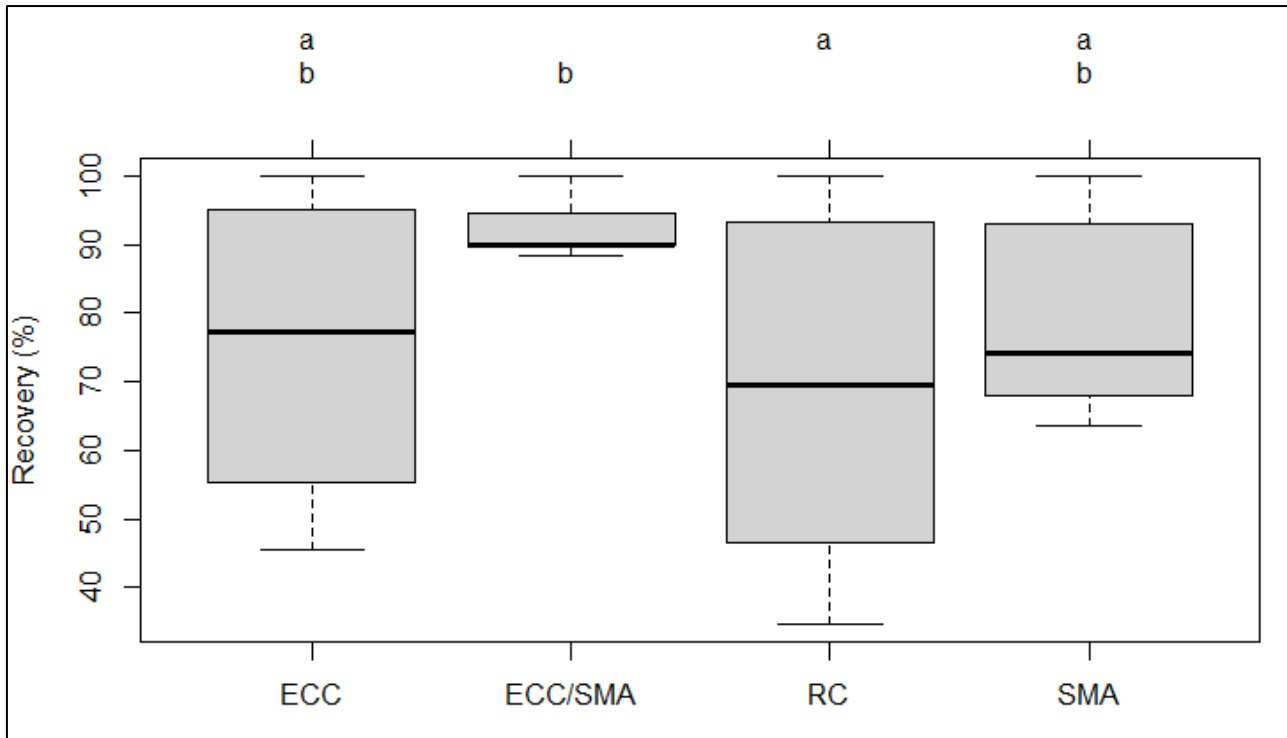
Figure 161. Anova test is comparing the recovery capacity of the models.
Software used: RStudio.

Model 2

These results are the responses of the structure as is presented in real life, as a frame system, formed by two parallel piers and a beam in the middle and another one in the top of the piers, the two beams are presented as coupling beams in the structure. The models are presented by the load of the piers in the X-axis as presented in **Figure 88.** Therefore, this model is also important to analyze and

SEISMIC PERFORMANCE OF SMA-REINFORCED ECC PIER SYSTEM OF THE SALITRAL BRIDGE

understand the behavior of the beams due to are directly related to the structural capability of the system.

RC Models

Pushover Response

The non-linear static response is produced now on the top of the left pier with a monotonic lateral load pushing to the right. It was used reinforced concrete in all the structure simulating the actual state of the constructed piers.
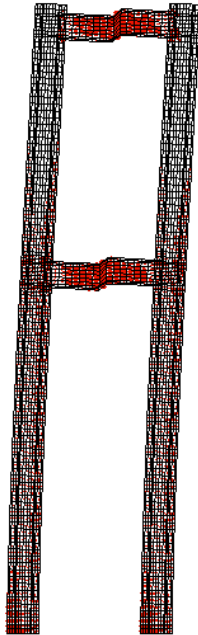
Figure 162. Model 2, crack pattern and displacements combined, cantilever, set magnification used of 5,0 Pushover. Software used: Augustus.

This figure represents the response of the Model 2 to the monotonic load applied in the top left corner, with restrains in the top in the Y-axis to simulate the first restraint with a set magnification of 3,0 in Augustus and the initial load of the Bridge.

Debugging sub-models

In order to debug the modes as first parameter, as previously made and explained with the first model (Y-axis). It is relevant to produce the debug of the

model plot the responses of both models to compare the behavior and identify differences.
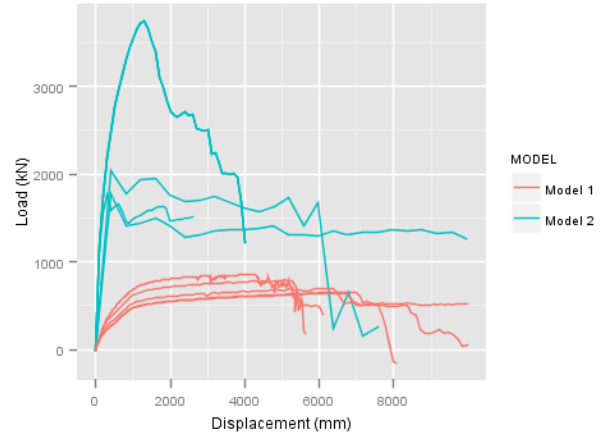
Figure 163. Comparison between Model 1 and Model 2, pre-models of RC. Pushover analysis.
Software used: Deducer.

This **Figure 163** represents a comparison between the behavior of the two Models with different start parameters. This figure is a combination of **Figure 101** and **Figure 165**. It is essential to create this figure for a better appreciation of the magnitude of the two Models, due separately the statistics are not easy to show the magnitude differences.
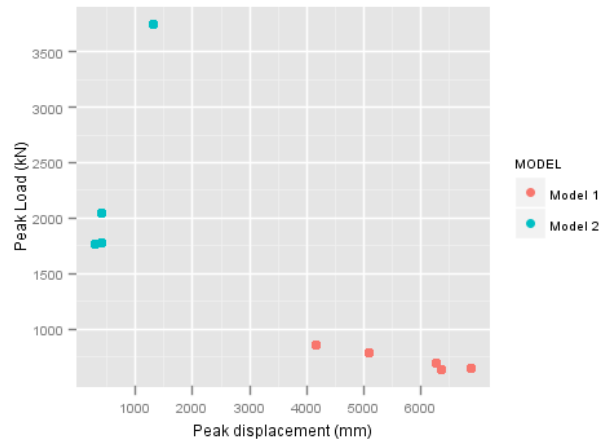
Figure 164. Peak load versus peak displacements, the comparison between the pre-Models, Model 1 and Model 2.
Software used: Deducer.

In this **Figure 164** are represented the two models, in the points of the Model 2 there are four points but can be only seen four, due there are three points in the same coordinate "X" and "Y." Therefore, the point in the top of the graph is three different points converging in one.

Different to the first model in this model the behavior of the structure with a lateral load induced is restrained by the beams. Also was uncertain the behavior of the structure with different connection methods. This is why on **Figure 165** is presented the behavior of the frame system restraining in the Y and X-axis simulating a pinned system and on cantilever as made with the first model, in order to debug the models.
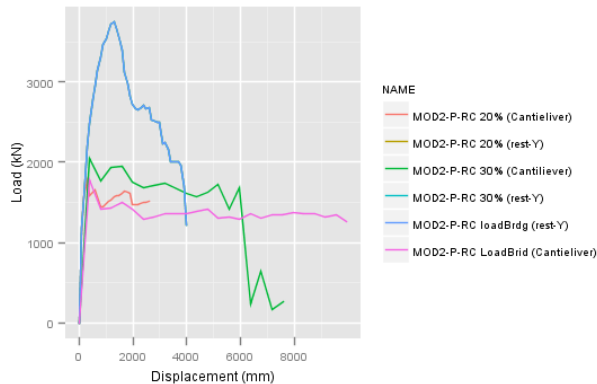
Figure 165. Load versus displacements, pre-Model 2. Push-over analysis
Software used: Deducer.

In this figure are represented six models, but can be only seen four, because the ones with restraining in the Y-axis have the same behavior. Therefore, there are three curves over the same points.

Definitive Model

Once the model is debugged the definitive Model 2 is found and represents the base of the consequent model to change the material on the plastic hinge.

Now the critical zone of the frame is the middle of the coupling beams. Therefore, in order to improve the behavior of the structure will be relevant the improvement of the cross-section of the beams.
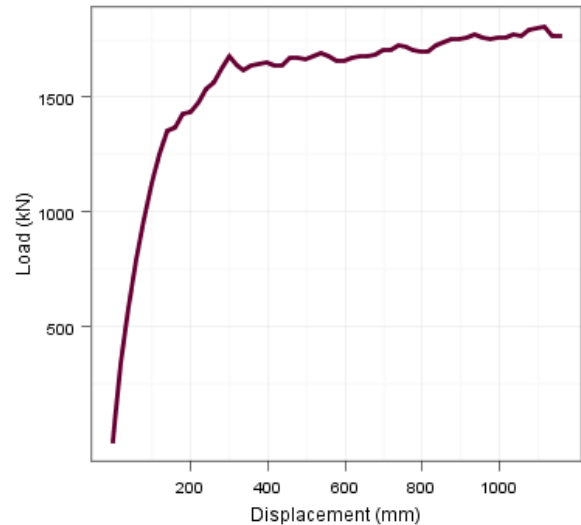
Figure 166. Definitive Pushover response of MOD2-P-RC using 15% of the axial load.

Figure 167 shows the in detail the crack width of the critical zone. Making a differentiation by colors as is usual on the FEM. The deformed shape of the structure and the cracked frame is presented on **Figure 162**.

Then, the response of the software shows the cracked and uncracked zones of the structure in a binary way. The base of the piers are cracked as shown on **Figure 168** but the crack width are not significant to be consider as critic. Therefore, changing the direction of the lateral load from Y to X the critical zone of the structure also changes. Confirming also, the behavior seen on the elastic analysis that as seen on **Figure 116** the highest shear is on the beams. Therefore, the three-dimensional model and the model on VecTor2 confirm the behavior.
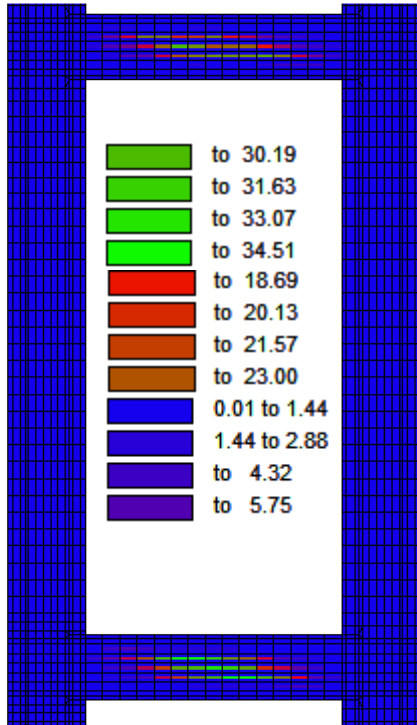
Figure 167. Crack width, MOD2-P-RC at peak load.
Software used: Augustus
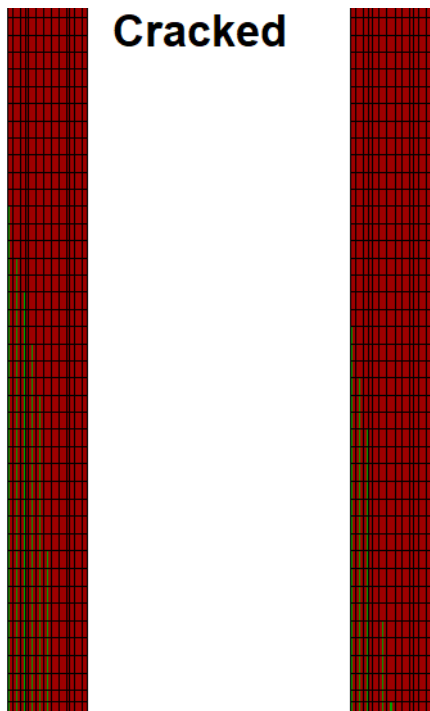
Figure 168. Cracked elements in MOD2-P-RC at peak load.
Software used: Augustus.

Reverse Cyclic Response

To produce an optimum FEA with the reverse cyclic loading of the second model it was necessary to use infinite rigid elements (elements of the mesh from the FEM) where the lateral load was located. Due to when the lateral load pulled to the left side the tensile strength of the concrete was not capable to hold the stresses and produced an undefinition of the stiffness matrix. It was used as previously the nominal axial load was 15% to make consequent the previous models.
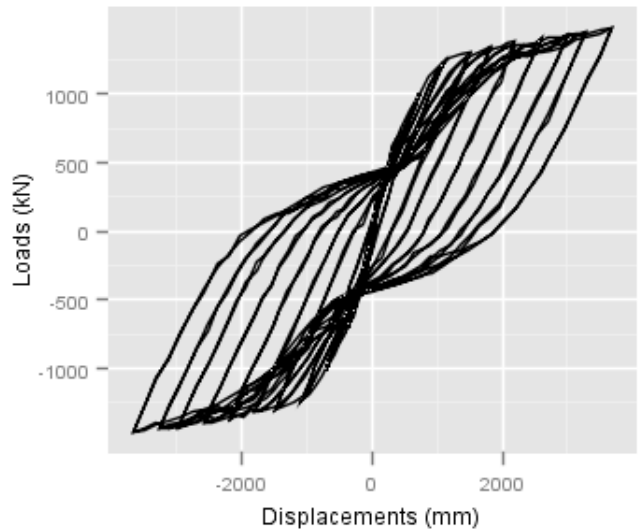
Figure 169. Reverse cyclic response of MOD2-RC-RC with 15% of axial load in each pier, during ten cycles.
Software used: Deducer
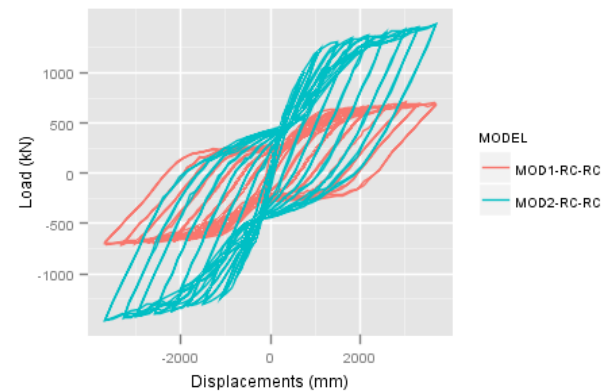
Figure 170. Comparison of the responses of MOD1-RC-RC and MOD2-RC-RC under reverse cyclic.
Software used: Deducer

Crack Angle θ

	to 67.42
	to 74.91
	to 82.41
	to 89.91
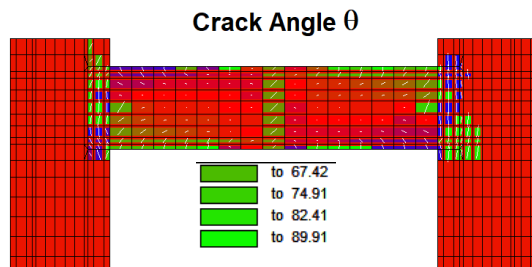
Figure 171. Crack angle in the Model
Software used: Augustus.

Crack Width w_{cr}

	to 665.43
	to 697.12
	to 728.81
	to 760.49
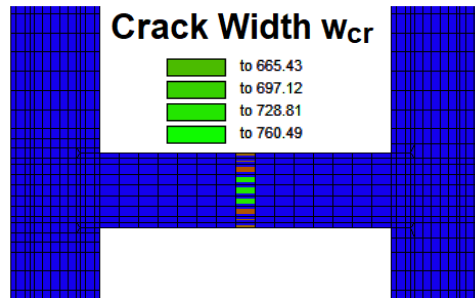
Figure 172. Crack width of MOD2-RC-RC in the critical point, units in mm.
Software used: Augustus.
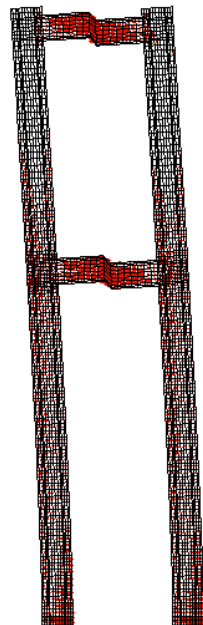
Figure 173. Displacements and crack directions combined view set magnification equal to 1,0.

To identify just the behavior of the piers on the second model was made a model using infinite rigid beams as seen on **Figure 174**. In this the critic zone now will not be on the middle of the beams.
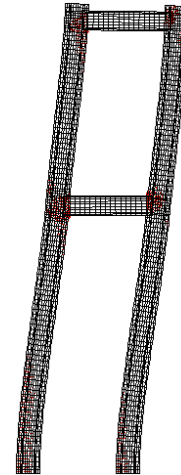
Figure 174. Reverse cyclic of MOD2-RC-RC with 15% of axial load, using the beams as infinite stiff in the Model.
Software used: Augustus

SMA-RC Models

As a part of the reinforced concrete models in the MOD2 as explained in the Methodology, it is necessary to consider the behavior of the beams in the system due to the relevance in the structural analysis. The frame system of the Piers in the Salitral Bridge has relevance in the X-axis earthquake, therefore to re-center the structure it is necessary to calculate the plastic hinge length in the beams and apply SMA and ECC in this region.

Table 11. Plastic hinge length on the beams		
Reference	**Analysis**	**Length (m)**
(Zhao et al., 2011)	Monotonic	0,323
(Panagiotakos & Fardis, 2001)	Monotonic	0,904
(Panagiotakos & Fardis, 2001)	Reverse cyclic	1,357

Software used: Microsoft Word.

This plastic hinges length was used using a_{sl} equal to 1,0 and taking L_s equal to z in **Equation 9**, **Equation 10** and
Equation 11. If a_{sl} is equal to 0 the plastic hinge length with monotonic load is 0,355 m, and the reverse cyclic length will be equal to 0,533 m.

These results show the response of the structure analyzed with different methods. This

second model is based on the same plastic hinge length in the piers as the Model 1 on the columns of the frame, just in the red points. The use of SMA in the beams to improve the recovery was used in the plastic hinge length calculated in **Table 11**. It was decided to use 100 cm as the plastic hinge length in the beams due to the plastic hinge length observed in the response of the RC Model.
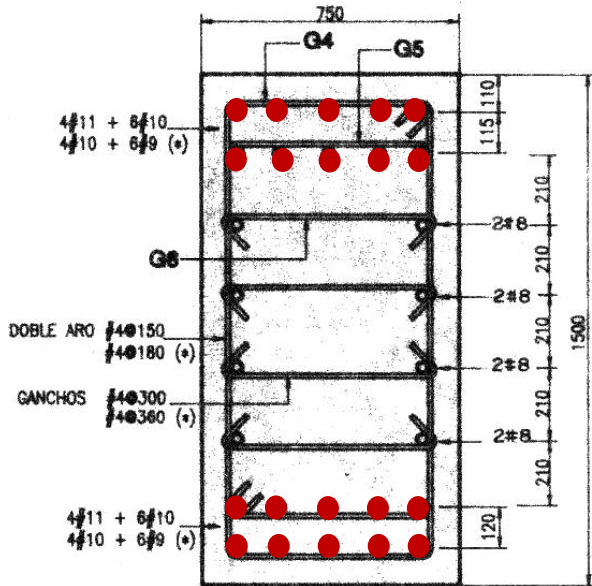
Figure 175. Location of the SMA in the cross-section of the beam in the Model 2, red points represents SMA bars used in the plastic hinge length.
Software used: Microsoft Word.

Pushover Response

On **Figure 176** is presented the non-linear static response of the model using SMA on the borders of the plastic hinge and concrete in all the structure. The lateral load was located at the same position of the previous Pushover made and explained with the same nominal axial load of 15%.
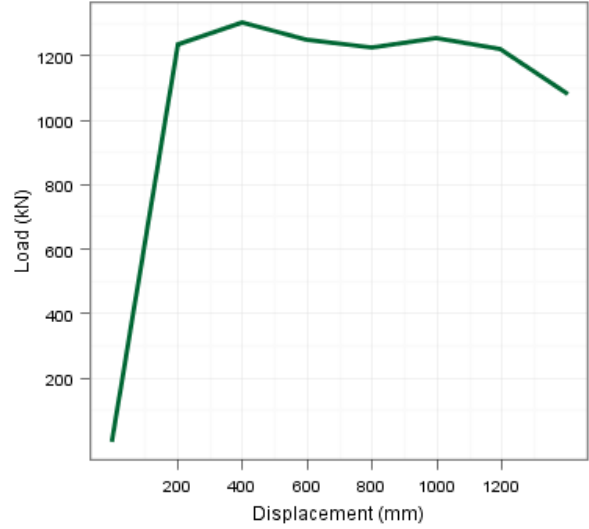
Figure 176. Non-linear static response of the second Model using SMA in the plastic hinges and using 15% of the axial load.
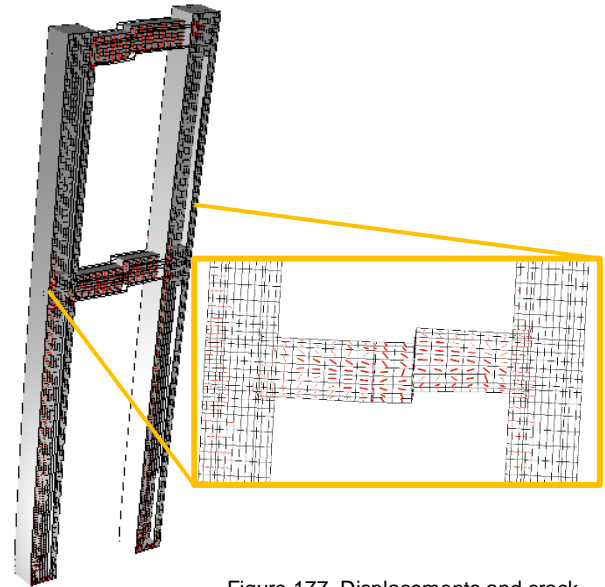
Figure 177. Displacements and crack directions of the Pushover analysis using SMA at the failure point.
Software used: Augustus.
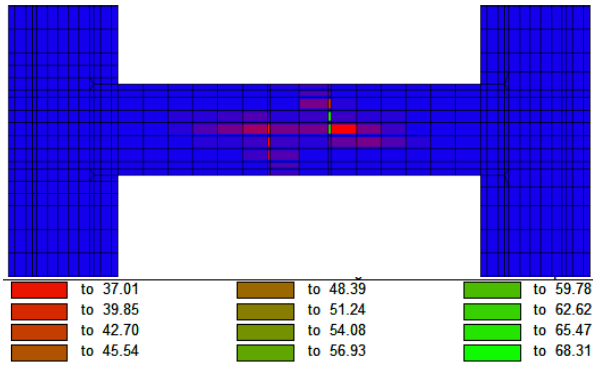
Figure 178. Crack width of the Pushover in the peak load of the Pushover curve showed in Figure 176, units in mm. Software used: Augustus.

On **Figure 179** is presented where are located the most critical zone of the reinforcement bars, as expected this are located on the plastic hinges calculated and verifies the proposed location of these.
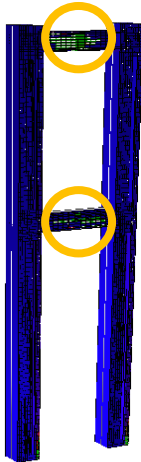
Figure 179. The stress of the steel and SMA in the model. Software used: Augustus.

Reverse Cyclic Response

As made with the RC reverse cyclic model, on the SMA reverse cyclic models it was used infinite elements of the mesh where the lateral load was located to produce a convergence on the stiffness matrix of the structure.
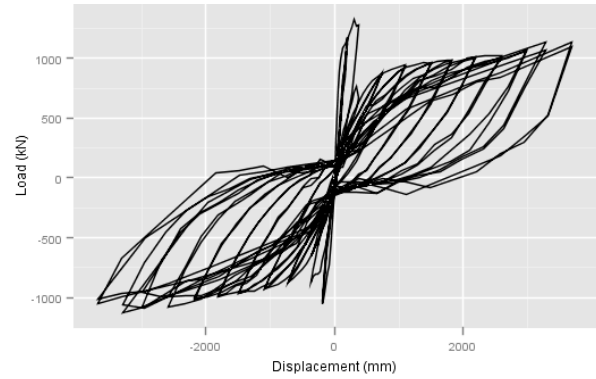
Figure 180. The response of the MOD2-RC-SMA in the reverse cyclic loading with 15% of the axial load and SMA in the beams and columns of the frame. Software used: Deducer JGR.
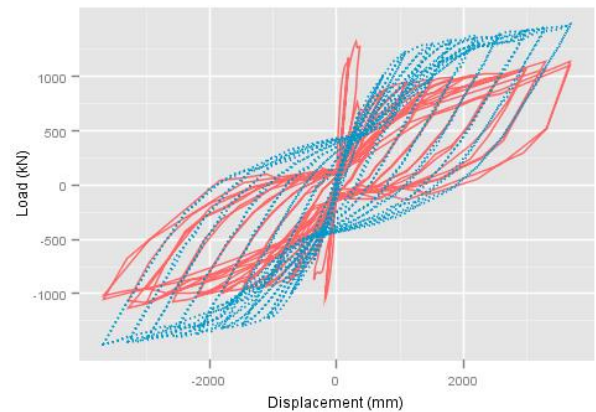
Figure 181. Reverse cyclic response of the Model 2 using just RC (blue line) and SMA (pink) comparison.
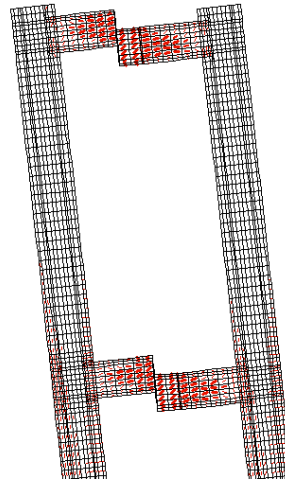
Figure 182. Displacement and crack direction response of the second model with SMA.SMA-RC Models at 10% of drift. Software used: Augustus.
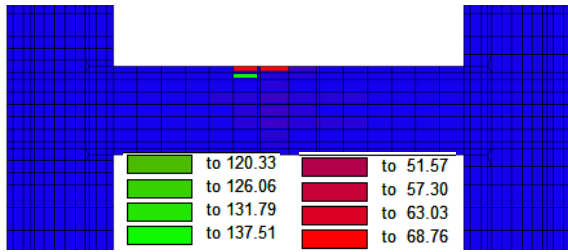
Figure 183. Crack width (in mm) of the MOD2-RC-SMA using SMA in the most critical zone at 10% of drift.
Software used: Augustus.

ECC-RC Models

Pushover Response

The use of ECC on the plastic hinges of the system produced a significant different behavior of the cracks and response of the structure. This can be seen on **Figure 184**.
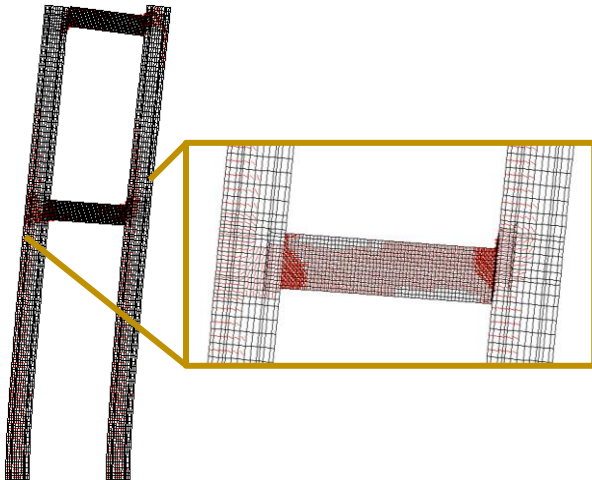
Figure 184. Displacements and crack directions of the non-linear static analysis.
Software used: Augustus.
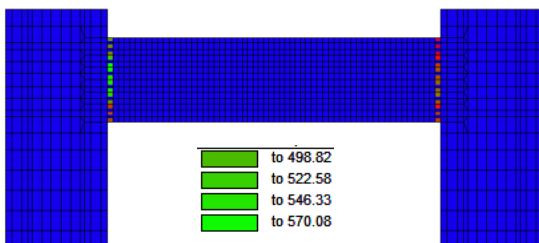
Figure 185. Crack width of the pushover, units in mm.
Software used: Augustus.

Figure 186. Stress in the reinforcement bars of the pushover, units in MPa.
Software used: Augustus.

SMA-ECC Models

The use of SMA and ECC combined produced a behavior closer to the one presented by the ECC model and not to the SMA one. The crack pattern, width and location of plastic hinges in basically the same produced on the ECC response.

The use of SMA and ECC combined are only in the plastic hinge of the structure, on the rest of the structure is used regular concrete and steel reinforcement bars. The shear reinforcement bars were used of steel in all the structure and there are not shear reinforcement made of SMA.

Pushover Response

On **Figure 187** is presented all the capacity curves of the non-linear static analysis made on the X-axis of the frame. This was made to produce an easier comparison between the response of the models. **Figure 188** shows the crack pattern of the pushover response and the width of the cracks are the same as the **Figure 185**.

SEISMIC PERFORMANCE OF SMA-REINFORCED ECC PIER SYSTEM OF THE SALITRAL BRIDGE
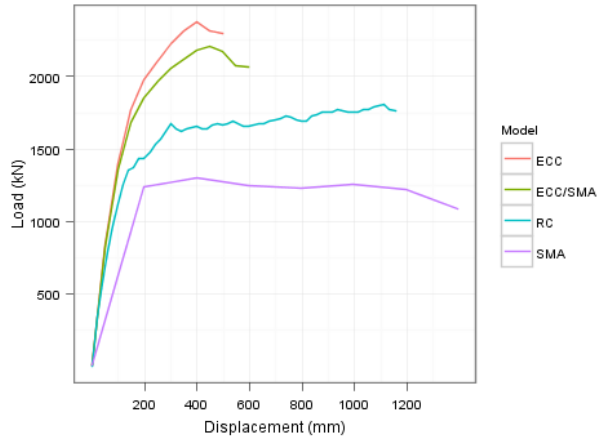
Figure 187. Comparison of the Pushover responses of the Model 2.

that the premature failure of the structure using ECC at 2% of lateral drift achieved more than two times the lateral load capacity on the structure. This means that adding ECC to the structure on the plastic hinge during a reverse cyclic loading is required almost 2,5 times lateral load compared to the use reinforced concrete regardless the use of SMA or steel as reinforcement bars.
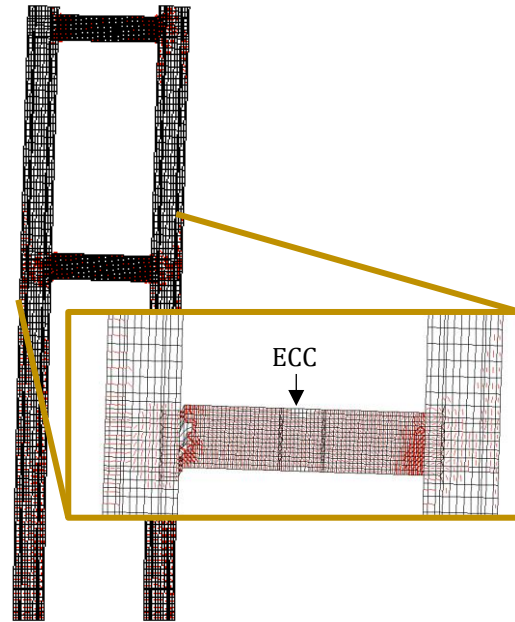
Figure 189. Crack pattern and displacements of the SMA/ECC response on the pushover analysis.
Software used: Augustus.

Figure 188. Crack pattern and displacements of the Pushover using SMA/ECC.
Software used: Augustus.

Reverse Cyclic Response

The reverse cyclic response of the structure using ECC on the system produced a premature failure and was not possible to achieve a lateral drift of 10%. **Figure 189** shows the behavior of the structure under reverse cyclic loading, this is basically the same produced on the pushover analysis.

Then, **Figure 190** present the reverse cyclic response of the frame using RC, SMA, ECC and SMA/ECC together. This was made to identify

Figure 190. Reverse cyclic response of the frame system using different materials.
Software used: Deducer (JGR)

Costs of the Project

It was calculated the cost of the two frames (*Frame A* and *Frame B*)[21] of the Salitral Bridge using different materials. The costs were calculated in detail taking just the price of the materials due to the cost of the workers and machinery is the same and does not require specialized workers. Also, the cost of the scaffolding, formworks, concrete trucks and other required components will be the same. Therefore, the cost will not present difference on the relative cost and does not present significant relevance in the objectives of the research.
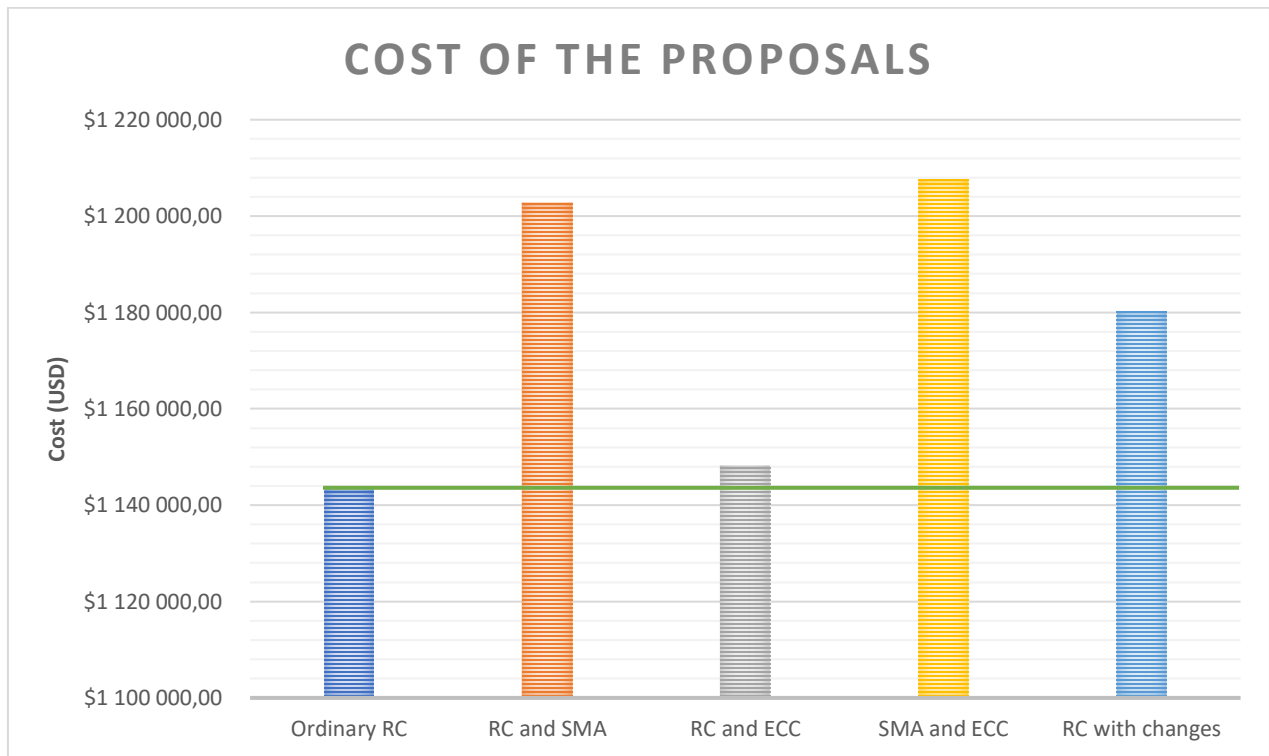
Figure 191. Cost of the Pier system of the Salitral Bridge in Costa Rica using the proposed quantity of materials in the results. Software used: Microsoft Excel.

Table 12. Comparison of costs using smart materials			
Model	**Total Cost**	**Difference**	**Relative cost**
Ordinary RC	$ 1 143 250,63	$ -	0,000%
RC and SMA	$ 1 202 695,87	$ 59 445,24	4,943%
RC and ECC	$ 1 148 115,81	$ 4 865,18	0,424%
SMA and ECC	$ 1 207 561,05	$ 64 310,42	5,326%
RC with changes	$ 1 180 243,99	$ 36 993,36	3,134%

Software used: Microsoft Excel.

---

[21] As seen on Figure 87.

Comparison between the Pushover and the Base Shear

On the assess the seismic performance of the piers was used the most critic base shear obtained on the dynamic analysis made.

The most critical condition was presented on the time-history analysis as previously explained. The highest base shear was achieved using the Limón earthquake record. It was induced the earthquake record on the X and Y-axis of the structure.

With the base shear obtained on the X and Y-axis was intersected the pushover responses of each model (Model 1 and Model 2) with the corresponding axis. Then, was obtained the displacement achieved on the top of the structure due to the Limón earthquake simulation.

In this way can be calculated the operational capacity of the structure under a strong earthquake event and can be used the parameters presented on the FEMA to identify the level of damage.

It was necessary to apply a personalized scale of the plot, due to the base shear was to low compare to the capacity curves obtained in the pushover responses. Therefore, as seen on **Figure 192** and **Figure 193** the scale is not linear.
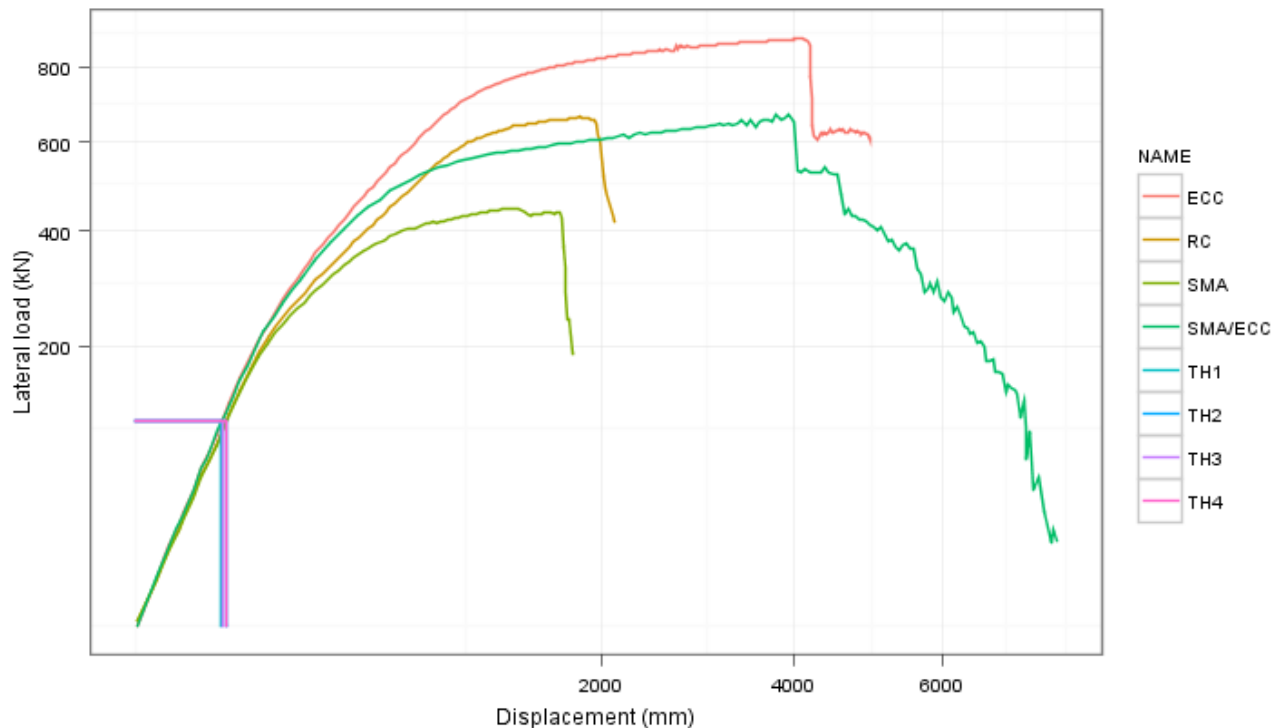
Figure 192. Seismic performance of the pushover with the Time history response envelope of the Limon earthquake on the Y-axis. Software used: Deducer (JGR).
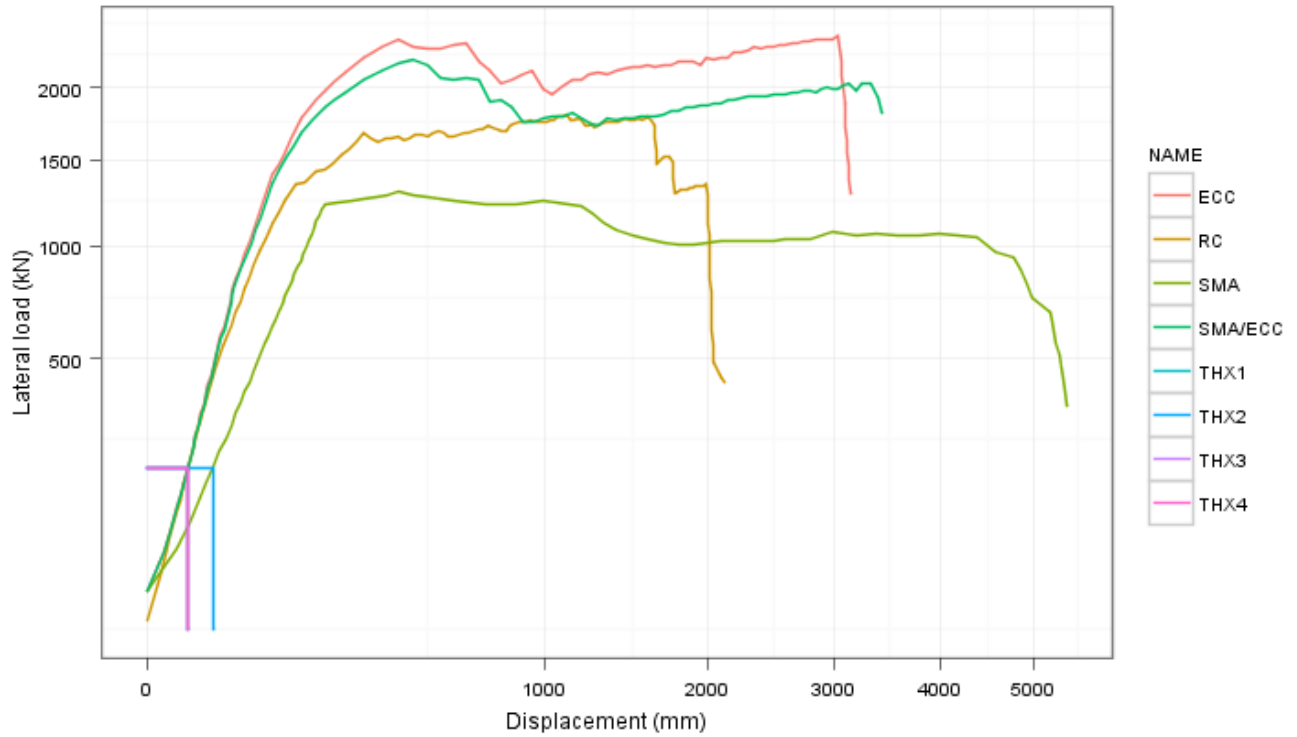
Figure 193. Seismic performance of the pushover with the Time history response envelope of the Limon earthquake on the Y-axis. Software used: Deducer (JGR).

SEISMIC PERFORMANCE OF SMA-REINFORCED ECC PIER SYSTEM OF THE SALITRAL BRIDGE

Results Analysis

In order to debug the RC models and sub-models, there was used different parameters and characteristics of the materials and analysis to achieve an acceptable response. To these models varying the initial parameters are called pre-models, referring to the optimum model to compare with SMA-RC, ECC-RC, and SMA-ECC models and use it as a base model.

Then, as explained in the results there are two main models called Model1 and Model 2 and represented as MOD1 and MOD2. In which the model one refers to the Y-axis earthquake in **Figure 88** and as explained is described as a single column or pier and the Model 2 represents the quake in the other axis. Therefore, the contribution of the beams is relevant accordingly the system behaves as a frame. From here, there are sub-models of the model one and two representing the different parameters in the Models as the sub-models made of RC, SMA-RC, SMA-ECC, and SMA-ECC. However, there are also pre-models debugging the RC base model. These hierarchies are represented in **Figure 97.**

Having said this **Figure 101** represented the full data of the response of the models called pre-models of the Model 1. It was changed the characteristics of the material, for example, using $f_u= 1,5f_y$ and $\varepsilon_u=150$ milli-strain as default by the software and $f_u= 1,25f_y$ and $\varepsilon_u=100$ milli-strain as recommended in the literature. These changes were used in the models using the axial load of the superstructure of the bridge (around 5%). Also, these variations were applied to models using a percentage of the axial load of 10%, 20%, and 30% to see the behavior of the Piers under different axial loads.

Therefore in **Figure 101** should be at least eight different curves of response. Indeed there are but can be only seen five. Because using the dead load of the bridge there are two different responses depending on the characteristics of the materials, but with the increments of load made the response of the structure is the same independent of the f_u

and ε_u of the reinforcement steel, due this the curve of response is only one and is represented as the change of the load.

In **Figure 101** can be seen that the change in the ultimate point of the characteristics of the materials has no relevance in the plastic and elastic part of the curve, even the yield point in the response is the same coordinates, and the peak load does not have significant changes in this structure. The substantial changes in the curves come in the collapse zone where using less rupture point and ultimate strain the response falls drastically and does not have a ductile behavior after the peak displacement.

While the axial load is increased the response of the structure allow and more lateral load in the Pushover analysis and gives fewer lateral displacements, flatting the curves as seen in the figure. Therefore, as regarded the axial load on the piers is directly proportional to lateral load capacity and inversely proportional to the capacity of the displacements allowed in the structure.

Figure 102 shows the behavior of the peak load of the pre-models versus the peak displacements, also, as in the previous figure the size of the points is proportional to the axial load. The behavior of the points has a linear tendency. While the peak lateral load and axial load increase the peak allowed displacements decrease. Therefore, the remarkable conclusion of this figure presents critical information, if the axial load is big the acceptance of more significant lateral loads will occur but will decrease the peak displacements of the response. These changes make that the flexibility of the response is inversely proportional to the loads induced to the structure, this information is an important parameter to consider in the design of Models.

Figure 103 present the detailed information of the pre-models of Model 1. It was made some pre-models that had some steel plated on the top, to recreate the restrains in the top of the structure shown in the original blueprints. As the

SEISMIC PERFORMANCE OF SMA-REINFORCED ECC PIER SYSTEM OF THE SALITRAL BRIDGE

element of importance is the RC column, the steel plate was designed using infinite rigid characteristics thus the main reason for the plates is to distribute the applied load to the structure. It was made models using a plate with dimensions of 110 cm x 110 cm, 180 cm x 180 cm and without steel plate. As seen the steel plate called 110x110 does not change the response of the structure significantly, meanwhile using the 180x180 plate it has only the change in the peak displacement, increasing it around one meter. It can be said that for the response in the structure using the Software Vector2 the steel plates on the top does not have significant differences to consider.

Figure 103 is evident the decreasing in the lateral displacement once the axial load is increased, also how to increase the acceptance of lateral loads with the more axial load. There was made some models using "Tension only reinforcement" but it does not converge to a specific result, this is the reason why is not presented in the details of the responses of the pre-models.

Moreover, the last change was made changing the constitutive model of the analysis in Vector2 of the reinforcement. All the previous Models was using the hysteretic response of "Bauschinger effect (Seckin)", this change applies the hysteretic response of Seckin with local accumulation to consider the cracks opening as a part of the decrease in the structural performance and the strains taken by the longitudinal reinforcement. As seen, no matter the changes in the model the elastic response of the structure is the same; the yellow vertical line on **Figure 104** represents the change between the elastic and inelastic zone. The main differences are presented in the inelastic response. Using a value of 50 milli-strain in the ultimate strain produces a sudden fall in the response after the peak load is achieved, the change of the hysteretic response does not present any significant changes in the response of the structure compared to the base model. Then without using smeared reinforcement out of the plane reduce significantly the peak displacements compared to previous models around the half of the previous peak displacements, but not significant changes in the lateral load applied in the Pushover, the absence of the the complete shear reinforcement in that axis cuts at the half the dsiplacements response of the structure in the Model 1.

Then it was made the models comparing different parameters. The trends of the responses are closer to each other. Using as a base the mentioned Model of 0% in smeared reinforcement out of the plane, the change in the ultimate rupture point changes how drastically is the fall of the capacity after the peak load without great relevance. Then, using the "Local accumulation" model in the reinforcement and the ultimate rupture point, the response behaves almost the same as the base model, changing a little after the peak load. As the last part using just the local accumulation model, the response considers better the slips taken by the reinforcement due to the cracks in the elements and decreased the allowance in lateral displacements. Therefore, this last model will be used as the RC model and will be called MOD1-P-RC, where MOD1 refers to Model 1, the first letter after the hyphen is the P of Pushover analysis, and RC represents the materials used, in this case, is reinforced concrete.

In **Figure 105** are presented the performance of three different pre-models due its high lateral displacements obtained. All these new changes were made under the review of the literature. The use of the ultimate strain of the smeared and longitudinal reinforcement with a value of 50 milli-strain that is the allowance in the design permitted referenced with a value of 0,05, therefore was used in the model to identify its performance. The use of the 0% reinforcement in the direction out of the plane in the software (361° in FormWorks) was made because the compressive strength in the models was achieving values higher than 28,0 MPa up to 42 MPa. There were thought it could be modified in the response because of the confinement of the enduring of the shear reinforcement in the top of the pier with a separation of 10,0 cm, therefore was used the Model 1 of RC with consider the shear reinforcement out of the plane, at 0° it was recognized.

Figure 106 represents of the main problem that the structure present, as shown in the response the crack pattern due to the Pushover applied to the Model is creating two simultaneous plastic hinges in the structure. This creates a problem, generating more rotation and Moment, allowing more lateral displacements to the structures. It is necessary to search for a solution to this central problem before adding smart materials as the SMA and ECC.

Additionally, **Figure 107** shows the width of the cracks in the structure, here is also evident the creation of the two simultaneous plastic hinges created with widths around 6 mm to 11 mm, considerable damage provoked by the lateral load.

Then, the main problem of the two simultaneous plastic hinges created still exist under reversed cyclic loading. Therefore, it was thought-out that this anomaly was made by the separation of the shear reinforcement in the piers, due to occurs in the same point of transition. This transition is three times bigger than the separation in the bottom; it goes from stirrups at 10 cm to stirrups at 30 cm each. Therefore, the shear force in the structure cannot be contained and creates a failure zone. Therefore it was created three different models as an alternative solution to the main problem unpredicted. It was made a model giving continuity to the distance of separation between the stirrups in the bottom but as seen in **Figure 108**, the creation of simultaneous plastic hinges still occurring, consequently was created another two models varying just the longitudinal reinforcement and the longitudinal reinforcement with the separation of stirrups. As seen these two last changes are the same without considerable changes, just a little change in the deep of the cracks but not significant. Both changes eliminate the second plastic hinge on top. Therefore, the problem was in the transition of the longitudinal bars passing from #11 to #10 in the edges and from #10 to #9 in the centers, this transition of reinforcement has more significant considerations on the response of the structure. Moreover, represent a improve in the design considering the response in the Model.

Figure 108 shows the response of the models, just mentioned. As seen the models varying the longitudinal bars present very close behavior but changing just the longitudinal reinforcement and not the shear reinforcement is cheaper compared to the other model. Also, the Model just changing the smeared reinforcement presents a more ductile behavior due to the two plastic hinges created in the same structure leading to higher lateral displacements. And **Figure 109** shows the response of the models using changes on the longitudinal and shear reinforcement

Figure 110 shows the resolution response of the non-linear static analysis made to the model 1. This definitive response of the structure occurs using a 15% of nominal axial load and increments of 1,0 mm in each step to the right. The yield point occurs around 70% of the peak lateral load, as seen the response of the models present a very ductile element. The ductility of the structure is very efficient even without considering new materials, thanks to the shear reinforcement applied.

The response of the non-linear static loading discussed before, the exact values of the response are shown in **Table 6** where the yield displacement is almost half of the peak point displacement. The yield load is at 572,10 kN and the peak load 663,80 kN, what gives a ductility of 2,27, taking it as the ratio between the peak load and the yielding load. Then, the residual load-capacity presents that the ductile response can achieve extra load when the peak load passed giving an ultimate displacement of 2113 mm and a drift of 0,05. These results are the parameter to compare the improvement materials adds of SMA and ECC.

Once, the pre-models are finished can be used the Pushover analysis to calculate the yield displacement to make the Reverse cyclic analysis. As shown in **Figure 111** the response of this analysis where the steps of the load pattern were based on its drift, starting in 0,5%, then 1%, 2%, 3% until achieving 10%, with two repetitions per stage. As it is seen was achieved lateral displacements around 3500 mm and lateral loads around 600 kN. The failure occurred in the 11th reverse cycle with displacement at the top of 10%, and it was used in total 680 load stages to achieve the failure. As seen the hysteretic response was acutely pointed at the beginning, but while the load stages increased the behavior start to become wider, this represents a very ductile behavior of the response of the structure.

Figure 111 shows the reverse cyclic response of the model one using the reinforced concrete as the constructed bridge. This response shows that the hysteretic curve presents a ductile behavior and a good level of recovery by the low dissipation of energy compare to other hysteretic responses in other researches. These could be due to the dense shear reinforcement in the bottom of the piers and gives extra ductility to the system. **Figure 112** shows the same analysis of the bridge but making the comparison of using different axial load applied to the piers. In it can be appreciated, as previously discussed, that using 15% of axial load (higher axial loads) the lateral loads increase directly compared to using just the dead load of the superstructure. However, the mode of failure is

more drastically and less ductile, as seen in the Pushover analysis.

In the part of the elastic analysis of the frame was made using the software SAP2000. Therefore the analysis can be made tridimensional. **Figure 114** shows an initial parameter of the state of the structural elements of the frame system, this a checking of the dimensions and reinforcement of the structural elements compared to external loads. The exercise show that the most critical zones of the structure are the beams and the bottom of the piers (confirming the previous analysis made in the software Vector2 in two-dimensions), if the structure had a premature failure, these elements will be the optimum elements to re-dimension or increase the reinforcement area to increase the structural capacity, as seen by the primary studies. However, it is necessary seismic analysis to figure if the external loads can be as high to damage the structure significantly.

Figure 115 shows the shear diagram of the frame system, using the lateral external load in the Y-axis previous defined. This diagram confirms the analogy made to use the frame system in two-dimensions on Vector2. The shear is constant, and the highest during all the column and the coupling beams does not receive significant internal forces or gives extra bracing in this axis. Therefore, the two-dimensional model of Model 1 can be represented as a single pier system and analyze in this way. **Figure 116** presents the shear diagram of the system applying the external lateral load in the X-axis (parallel to the beams). As seen the base shear is not the highest shear of the system, the maximum shear is given in the coupling beams. This results also confirm the results of the Pushover and reverse cyclic loading of Model 2, where the failure occurs in the beams and is the most cracked zone. The shear in all the system is constant during the length of the structural elements.

The shear and flexural moment diagram do not differ in the static or dynamic analysis made, both are the same in shape, but does change in the magnitude of the internal forces and stresses of the system. **Table 7** present the maximum shear of the elements in the modal analysis made. The modal response is the more used analysis and represents better the real behavior of the structure adding the principal modes of deflection as an envelope response.

Figure 117 shows the flexural moment diagram in the frame system with the lateral load on the Y-axis, confirming that there are not flexural moment interacting with the piers. The highest moment is at the base of the piers, that is why of the plastic hinge was created in that side and with a classic crack pattern of failure by flexure. Also, the flexural moment diagrams are the same in shape in the static and modal analysis. **Figure 118** shows the flexural moment diagram on the X-axis of the system, where the highest values are in the beams and the base of the piers, as the response of Vector2 said.

In the response of the structure due to the simulation of the highest earthquake recorded in the history of the country is presented in **Figure 119** and **Figure 120**. These figures show the Shear envelope of Limon Earthquake record in Y and X-axis, the ground accelerations were induced to the frame system using the nomenclature of axis previously defined by the Vector2 and also taken this axis of the acceleration. The shear diagrams present the same behavior of modal analysis discussed before. In the Y-axis, as single piers system, the highest base shear was 107,341 kN and in the X-axis of 176,703. This is more than the modal response highest base shear, as expected, due to the seismic code does not expect an event of this magnitude soon. Therefore it is recommended to do this exercise. These results can be compared to the Pushover analysis and compared the level of damage that the bridge will obtain.

Now using SMA as reinforcement bars in the borders of the plastic hinge, on **Table 8** shows the results of the calculations to calculate the length of the plastic hinge. In that table was the results comparing different authors who researched about methods to approximate the length of the plastic hinge in piers of the bridge, including researches made by Dr. Saiidi Saiidi, first developer of the first constructed SMA-ECC pier bridge in the world. The maximum plastic hinge length obtained was 1,79 m, this result was obtained twice. Therefore, the length of the plastic hinge was designated as 1800 mm from the base. This length is the length of the SMA bars in the piers of the Salitral Bridge. The SMA bars will need to be connected to the steel bars with mechanical connectors; these connectors were designated to have 50 mm of length. Therefore the final length of the SMA bars with connectors will be 1825 mm.

In **Figure 121** is presented the location of the SMA bars used in the models just in the plastic hinge lengths. The SMA bars are changed by the longitudinal steel reinforcement bars; these bars are #11 (11/8 inches). The diameter of the SMA bars are of 35,0 mm due to the approximation of #11 bars, and the bars are requested to the suppliers regarding ± 25,0 mm or 50,0 mm depending on the distributors. The rest of bars in the figure (not in red) are #10 steel reinforcement bars. As a test also, was modeled the use of SMA in all the bars of the plastic hinge length (#11 and #10) of this figure. These SMA bars are smooth, therefore need to be considered in the models and will have the necessity of using mechanical connectors as a link between the SMA and steel bars, as studied in the literature review of multiple papers. These connectors are not smooth and are made of high strength steel, and the used length of each one was of 50 mm, similar to the show in **Figure 55**.

With these parameters cleared, the pushover analysis of the pier system using SMA in the plastic hinge was made. **Figure 122** gives the response of the non-linear static response, whereas seen the lateral load required to achieve a unitary displacement decreased. Therefore the SMA pushover response curve is under the RC capacity curve. This is an expected result with the literature reviewed; the SMA present fewer elastic modulus and the steel stress-strain curves are often over the Nitinol SMA bars, but the behavior is more fragile. This is also shown in **Figure 56**, that is also clear that the recovery capacity is decreased on the steel bars. The peak and average lateral loads decreased around 30% on the SMA pushover analysis compared to the RC response curve.

The detail in **Figure 123** shows the crack pattern in the most critical zone of the piers. Whereas seen the cracks produced by the model was located cracks, and this is validated on the experimental analysis made and showed in **Figure 66**. Here was discussed that the use of SMA as reinforcement on ordinary concrete produce located cracks that can present recovery capacity, but the width of the cracks and separation are highly increased, this was discussed by (X. Li et al., 2015). Therefore, this is an expected result and a validation of the behavior on the models. **Figure 124** shows that there are only three relevant cracks in the response and are the ones that produced the failure. These cracks present width of 20 mm or

less as an average, these with experimental testing is expected that can be recoverable cracks but not completely.

Then, **Table 9** shows the main important points of the capacity curve obtained where the peak displacements is almost 3 times higher than the yield displacement with a value of 1,355 m demonstrating the high ductility of the structure and the ultimate displacement is 1754,98 mm achieving it close to the peak displacement due to the large cracks produced.

Figure 125 is a relation between the displacements of the RC response and the SMA response. Giving a correlation between the curves of the Pushover, similar to the Correlation test of Pearson, and giving a result a confidence correlation of 0,99. Therefore, can be inferred that there are not significant differences between both displacements results.

The reverse cyclic loading of the SMA model 1 was planned as the RC reverse cyclic, using two repetitions and 11 drift stages (starting at 0,5% of drift and finishing at 10%) based on the pushover response as previously discussed. **Figure 126** shows the change of the behavior compared to the RC response is evident and as seen the "mustache shape" gives a visual apparent recovery capacity increment on the frame system but an apparent decrement in the energy dissipation. These will have to be calculated. But when both responses are superposed is not that evident the recovery capacity, **Figure 127** identifies that as the RC curve once unload the fall on the curve is more drastical and the SMA fall in the curve is not that severe but it trends more to zero easily, the intercept point between both curves and zero on the Y-axis is almost the same, therefore the recovery capacity is not that significant and relevant.

Figure 128 shows the crack pattern of the system is similar to the pushover analysis, where are located large cracks in the concrete, due to the incorporation of SMA. The maximum crack width is about 3,73 mm as shown in **Figure 129** at 8% of lateral drift. As seen in **Figure 130** the cracks shape and its widths are almost the same while the drift is increased, but the quantity is increased, the creation of more located large cracks.

These cracks are just located in the plastic hinge length calculated. Therefore, it was asked what would happen if the length of the plastic hinge was modified and therefore the length of the SMA bars. Then, it was made three different models

using a different length of SMA in the plastic hinge, as seen in **Figure 131**, and it was found that there were no changes in the response. The curve and cracks continue the same shape as before, but if it was decreased the cracks in the top part of the SMA was not located.

Then, it was changed all the longitudinal bars of the plastic hinge length by SMA bars; therefore the #11 and #10 steel bars were substituted by the previously discussed shape memory bars. **Figure 132** shows the pushover response, in there, was presented a high ductile behavior of the pier system but was also obtained a high decrement in the lateral load capacity of the system. The peak displacement was achieved in more than two times the initial peak displacement, but the peak load was decreased in the same two times.

Figure 133 and **Figure 134** shows the magnificence response of the use of SMA reinforcement bars in all the plastic hinge length, where the hysteretic response produce almost perfect recovery in each loop while using SMA just in the borders develop high energy dissipation by plastic deformation. Using superelastic SMA bars in all the cross-section make an elastic-like behavior of the piers. However, it is remarkable to advert that the use of these bars also was directly proportional to the quantity of noise produced in the response. However, also, these models present a disadvantage and it is that creates even larger located cracks, that are recovered by itself once unload. **Figure 135** shows the crack pattern of the system, these cracks are almost cutting the whole length of the cross-section, and as shown by **Figure 136** the width is about 103, 72 mm, a considerable and notable width.

Then, a series of remarkable response was compared per each drift stage. **Figure 137** shows the previously discussed decrement on the lateral load capacity using SMA in all the cross-section versus just in the borders; this is important to consider it on the design stage if a new structure will be made and the vulnerability is high. As expected by the shown in **Figure 138** the hysteretic curve the energy dissipation is considered low compared to just using SMA in the borders, due to its elastic-like behavior and cannot dissipate too much energy with plastic deformation. The most remarkable parameter is the recovery capacity where shown in **Figure 139** where the average recovery is almost 100%, and the lowest points are 95%, this result shows that

using full SMA as reinforcement bars makes an exceptional recovery capacity in concrete structures but presenting large recoverable located cracks.

Then, the ECC was introduced in the models using ECC just in the plastic hinge length and ordinary 28 MPa concrete in the rest of the structure. In this, the use of steel bars is used on the whole structure and is as presented on the original blueprints. The software Vector2 does not bring a constitutive model incorporated to simulate the behavior of this bendable concrete. Therefore, it was introduced manually the points of the tensile stress curve studied on the literature and explained on the methodology and curves presented by (V. C. Li, 2003; V. C. Li et al., 2001).

Then, it was used as reinforcement on the concrete "fibers reinforcement" to behave as an ECC like and then the values of compressive and tensile strength, also the weight and maximum aggregate size was based on the HFA-ECC type. Due to the HFA-ECC present the highest compressive, cracking, tensile and ultimate strengths of all the ECCs available. Also, is the second cheapest ECC type and the second greenest. ECC is considered as a green construction material due to its incorporation of PVA and zero aggregate.

Figure 140 shows the pushover response of the ECC-RC model. The peak load and displacement are significantly higher compared to the SMA-RC and RC responses; this is an expected result with the studied on papers, for example in **Figure 64** and validated the model input parameters used. Then, the lateral load capacity is remarkably improved by just using ECC on the plastic hinge length, giving an essential parameter with not a high increment on the cost.

On **Figure 141** is shown the crack pattern of the piers using ECC, in these the cracks are produced just over the plastic hinge length previously calculated, where the use of ordinary concrete begins. **Figure 142** shows that the maximum crack width is 9,40 mm and these are produced on the ordinary RC. While the zone where the use of ECC showed cracks with a width of 0,01 mm to 0,4 mm. These values are expected as on the literature review indicated that the average crack width on ECC is around 50 µm. Also, as seen in **Figure 143** the stress on the concrete start crushing just on the zone where ordinary concrete was used, on the zone with ECC did not experience significant damage.

Figure 144 is shown the hysteretic response of the reverse cyclic analysis, as seen the behavior presents apparent better recovery capacity than the RC response but not as good as the SMA hysteretic response. Therefore, it can be considered that the recovery capacity is directly proportional to the use of ECC but not severely. **Figure 145** and **Figure 146** shows that, as in the pushover analysis, the critical cracks are produced in the zone where ordinary concrete was used and on the zone with ECC was produced micro-cracks. Moreover, **Figure 147** demonstrate that the stress on the steel reinforcement bars occurred in the zone where are ordinary concrete.

The most relevant results occur when the combined use of SMA and ECC is mixed to improve the behavior of the structure. **Figure 148** shows the capacity curves of the four different models combined. As seen the use of ECC produce high ductility on the response and higher lateral loads capacity. Then the use of SMA decreases the lateral load capacity and peak displacement. Therefore, the combined curve was as expected over the RC response but under the ECC response, consequently validating the models. As seen exist a significant difference of using SMA and ECC on the structure, and a remarkable improvement was achieved.

Figure 149 and **Figure 150** show that the crack pattern of the SMA/ECC model is entirely different from the three models before. It is a combination of the ECC response and the SMA. Giving just one large crack on the plastic hinge length with a width of 5,4 mm. This crack is thicker than the produced by SMA and RC but more prominent than the produced by ECC and RC. The strength on the concrete achieved high compressive values of 54 MPa on the plastic hinge length, but the stress on the steel was not that significant, but the critical values on the bars were achieved out of the plastic hinge and on the steel bars, as seen in **Figure 151** and **Figure 152**.

The reverse cyclic analysis response is shown in **Figure 153**; the behavior is more like the SMA response, this presents an apparent high recovery capacity and the shape present higher slopes on its curves. **Figure 154** and **Figure 155** shows the crack pattern of the response, in this, the cracks are practically null, and the crack maximum crack width at 10% is less than 1,0 mm. Therefore, the behavior is like an elastic material the residual deformation is decreased.

Figure 156 is a combined plot of the hysteretic responses of the models. As seen the SMA and SMA/ECC present similar behavior, while the ECC and RC share similarities on the response of the structure. The RC response presents the highest residual strain on its response, second the ECC, third the SMA and ECC/SMA is the one with the lowest residual deformation.

As part of the remarkable comparison between the models **Figure 157** shows the peak lateral load versus the drift in each step based on (Cortés-Puentes et al., 2018). The general trend is an almost like a quadratic increment, except the SMA response decrease a few on the last drift stages. As previously discussed, the use of SMA decrease the lateral load capacity, and therefore the SMA and SMA/ECC are the lowest curves on the plot. Otherwise, the use of ECC increases the lateral load capacity, in which as seen the ECC response is the highest response curve on the comparison.

Figure 158 is one of the most relevant plots on the research due to it measures the recovery capacity on the models. As seen and expected the RC recovery capacity is the lowest on the responses of the models. Therefore it is essential to make improvements with the smart materials. The use of ECC follows the same trend of the RC recovery capacity but with a small improvement of around 10%. Then, the SMA response does not follow completely the same behavior but also decrease the recovery capacity in each drift stage. After 5% on the drift, the recovery capacity is improved compared to its previous recovery-drift results, giving small residual strain while the lateral displacements are increased. However, using SMA/ECC together produce and exceptional recovery capacity producing a 90% of recovery average and at 10% a difference of 55% compared to the RC response. After 6% of drift, the recovery capacity starts increasing on the response.

A direct result of the recovery capacity is the Energy dissipated by the structure under the reverse cyclic analysis. **Figure 159** presents the energy dissipation versus the drift, in this is as expected that the RC response presents the highest values of energy dissipation and the ECC/SMA the lowest. However, here, the difference between the models are not as drastically as on the previous discussion of recovery capacity. The dissipation of energy is

produced by the plastic deformation on the structures, therefore is relevant to present a low value. The ECC model is the second highest response on the energy dissipated. **Figure 160** shows the equivalent viscous damping; this is a ratio between the energy dissipated and the strain energy. The more full hysteretic loops result in higher equivalent viscous damping. The SMA response presented the highest equivalent viscous damping around 27% and the SMA/ECC the lowest of 17,5% at 10% of lateral drift.

As seen, it exists significant differences between using SMA and ECC compared to ordinary RC, but to make an objective analysis and conclusion it was made a statistical analysis to identify if there exist significant statistical differences between the models. The most relevant parameter on the objectives of the research is to identify the properties of self-centering of the piers of bridges under extreme loading using emerging smart materials. Therefore, the recovery capacity is essential to identify this characteristic. **Table 10** is the table of the result of three different statistical tests to identify significant differences. These three tests compared two different variables or populations of data. Thus each model is compared individually to the RC response. The correlation Pearson test present values higher than 0,95 for the SMA and ECC models showing that there are no significant statistical differences on the responses, but 0,82 on the ECC/SMA, therefore, confirms that there are significant differences between the models. The T-student test the SMA and ECC models produced a p-value higher than 0,05, therefore, it cannot be accepted the null hypothesis and means it does not exist significant differences but in the case of the SMA/ECC p-value is equal to 0,0088, therefore, it cannot be rejected the null hypothesis and means there are significant differences between the populations. The Shapiro test makes the comparison, and the results show that the p-values of the three compared models are over the 0,05 not giving significant differences but is remarkable to add that the p-value of the SMA/ECC is very adjusted to the pivot p-value. This remarks that are always important to generate more than one statistical analysis to produce confidence in the results.

On **Figure 161** The ANOVA test makes a statistical analysis between all the models simultaneously, presenting an advantage compared to the previous statistical analysis.

Then, plots a figure with much remarkable information, where use the recovery data as boxplots presenting the frequently and quartiles visually and the means are easily comparable. The relevant result of the test for this research is present by the letters on the op "a" or "b," these letters are shared by the models that do not present significant statistical differences. Therefore, the ECC and SMA model does not present significant differences with the RC model due to the sharing of the letter "a," but neither present significant differences with the ECC/SMA model due to the letter "b" on the three of it. However, it does exist significant differences on the ECC/SMA and the RC model because they do not share any letter. It is confirming the previous statistical analysis made. Also, the mean of the ECC/SMA model is 20% higher than the RC recovery capacity mean.

Now in the second model **Figure 163** shows the comparison between the Model 1 and Model 2 pre-models, under the same primary parameters and changing the percentage of the axial load. As can be seen, the models have remarkable and utterly different responses. It is important to remember that both models are the Model of the Salitral bridge just changing the direction of the analysis. Therefore it can have similar behavior, and this is not the case. Unlike the very ductile behavior of the frame in the Model 1, in the Model 2 accepts fewer lateral displacements, but can receive the highest lateral loads. This represent very different curves depending on the axis of the earthquake, the response of the same structure varies its behavior and performance completely. As seen the Model 2 is not as malleable as the Model 1 but endure much higher lateral loads compare to the Model 1. The frame endures seven times the peak load of the Model 1, but this can achieve 6,5 times more lateral displacements than the peak displacement of the Model 2.

Figure 164 is graph the peak load versus the peak displacements in which are presented the coordinates in these points of the peak values in the pre-models, separating the main models by colors. As it can be seen the peak values of the Model 2 are grouped in the top-left part of the graph, meanwhile the Model 1 peak values are arranged all in the same place, bottom-right of the chart. This makes the entirely different behavior of the pre-models depending on the direction of the extreme loading induced. This is expected thanks

to the bracing beams in the middle of the system, that contributes to the structural capacity of the structure in the X-axis, otherwise in the other axis not having braces in any point and have a pinned restrain in the top adopts a cantilever behavior, therefore the capacity of allow high lateral loads is decreased.

The behavior of the pre-models of Model 2 is the graph in **Figure 165**, as explained in detail there are six different curves presented in the diagram, but there can be only seen four due the pre-models with the restraint in the Y-axis in the top of the piers have the same response of the structure regardless the axial load applied to the Pier, therefore are three response one curve, one over the other. This is an outstanding detail due in the Model 1 the axial load applied to the pier change directly the displacements and lateral applied loads, contradicting if the model is articulate in the top. As shown in the figure if the Model has a Cantilever behavior due to the weight and shape of the superstructure of the Bridge is more alike. The response of the structures allows fewer lateral loads but more ductile behavior after the peak load. The structure ensures more lateral loads depending directly in the axial loads applied like in the case of study of the Model 1.

The axial load of the weight of the bridge in the piers is around 5% of the axial load, the super-structure and the restraints are not enough to restrain the movement in the Y-axis of the frame. Therefore the superstructure will be a trend to rotate when the tops of the frame do it. If the superstructure were big enough to restrain the movement, the analysis would be completely different putting additional rotation and moment to the bottom of the piers, but this is not the case. It was also modeled different pre-models changing the restrains in the top of the Piers but restraining the movement in the X-axis of the Model or the X-axis and Y-axis, undefine the stiffness matrix and destroy the elements of the Mesh and does not run the load stages.

On **Figure 166** is shown the response of the non-linear static analysis where the lateral load capacity presents a remarkable improvement compared to the Y-axis, achieving a peak load around 1800,00 kN, but the lateral peak displacements were decreased. The critical structural elements to preserve the integrity of the structure corresponded to the beams, as seen in **Figure 167**, both beams present vertical cracks at the middle of the elements, these kind of cracks are typical of flexural cracks applied on beams. If the cracks were inclined are usually given to the shear on beams, but this is not the case. Also, the bottom of the piers was affected, on the plastic hinge calculated on Model one, as seen in **Figure 168**. This figure presents just cracked, and the uncracked element of the frame was red is uncracked, on the beams the cracks widths are around 30,0 mm.

The reverse cyclic analysis response is shown in **Figure 169**, as seen the behavior is like the response of the first Model of RC, changing the magnitude of the lateral load displacement. **Figure 170** is the comparison between the lateral load applied on the Y and X-axis (Model 1 and Model 2). In this is more evident the similar shape on both response but on Model 2 the loads are increased. Then, **Figure 171** shows that the cracks have an angle of 90°, vertical cracks on the middle of the beams and a width of 760 mm on the concrete, as seen in **Figure 172**. Giving all the energy dissipation capacity to the steel bars due to concrete is destroyed at the middle at 10% of lateral drift. The displacements and the crack pattern are shown in **Figure 173** are the displacements acquire by the reinforcement bars, as seen the middle is the critical zone of the whole structure.

Figure 174 is the response of the crack pattern and displacement using rigid infinity beams, as seen the critical zone now is the join between the columns and the beams. Confirming that the main problem is on the beams.

Therefore, it was calculated the plastic hinge on beams, as shown in **Table 11**, with this was put the SMA reinforcement bars on the plastic hinge zone and the critical zone. **Figure 175** shows the location of the SMA bars on the beams. As made on the piers the #11 bars of was replaced by 35 mm diameter bars and the #10 steel bars was used without change. **Figure 176** shows the response of the SMA-RC structure under non-linear static loading, as previously discussed the use of SMA decreases the lateral load capacity on the response of the structures. The pushover analysis with the main failure on the beams behaves in the same way.

A similar failure mode occurred on SMA response, compared to the RC response. **Figure 77** shows the main failure on tridimensional view and the detail, where the failure occurred on the mechanical connectors zone and not on the middle as on the RC beams. **Figure 178** present the crack

width of the model. Passing from 6,8 mm to 987 mm. This huge crack is produced on the concrete at 10% of drift, this level of damage will need special retrofit. Therefore the use of ECC will become an essential factor to recover the integrity of the structure and civilians. In this, the highest stress on the reinforcement, as seen in **Figure 179**, is on the middle due to the reverse loading on each stage.

The reverse cyclic response is shown in **Figure 180**, one remarkable characteristic of the response is that on the first stages presented high lateral load capacity achieving the peak loads, then following a different trend as the usual RC response.

A comparison made with the RC response show these unusual first stages, also is seen that the lateral loads decreased due to the use of SMA and the recovery capacity is the same, but the energy dissipation decreased, as shown in **Figure 181**.

As seen in **Figure 182** the main failure of the structure still occurring at the middle of both beams with vertical cracks on the concrete and therefore the critical stresses of the concrete and steel are in this zone. Cracks width, as identified in **Figure 183** are around 137 mm, not as critical as on RC model and the pushover analysis.

The use of ECC with RC was tested on the next model using just ECC on the same zone of Model 1 (on the piers) and the plastic hinge length used on the beams (same as SMA). **Figure 184** shows the response of the frame; it is evident that the critical zone of failure now changed. Due to the use of ECC on the critical zone, the frame system improved compared to regular concrete. Now the critical zone of failure corresponds to the join of the column-beam, in this part the material is regular concrete. **Figure 185** shows that the cracks width is about 570 mm on the side of the beams, and there are not considerable cracks on other parts of the frame system. Also, now the critical stresses of the reinforcement bars are not on the beams but the piers, changing the response completely, by using ECC, as evident in **Figure 186**.

The use of SMA and ECC combined shows the discussed characteristics before; it improved the ductility of the element the lateral load capacity and critical of the failure. **Figure 187** shows that the non-linear static analysis, the use of just SMA decreased the capacity of lateral load but increased the ductility, the use of just ECC gives an improvement on the lateral load capacity

and the SMA/ECC gives the same but not that much as just ECC, but the recovery capacity improved. **Figure 189** showed that the crack pattern of the used of SMA and ECC combined was similar to the use of just ECC on the system, giving large cracks on the side of the beams but none on the middle of these. The stress of the steel was increased in this zone due to the same reason of the large cracks produced. **Figure 190** shows the comparison of the reverse cyclic responses of the models. As seen the use of ECC produce that the lateral load necessary to move the structure is more than times the load using RC. But this increment on the stiffness of the structure produce a fragile structure compared to the other models and the lateral drift achieved just 2-3% meanwhile the models using regular concrete was able to achieve 10% of lateral drift.

The response of the reverse cyclic analysis is shown in **Figure 190**, as shown the models that used ECC on the plastic hinge length was not as ductile as the use of RC. Due to its present a premature failure at 1% and 2% of lateral drift. Therefore, it cannot be compared the recovery capacity, energy dissipation or equivalent viscous damping. The response of the models using ECC produced noisy curves due to the large premature curves on the side of the beams. However, the first drift stages produced high lateral load capacity compared to the RC and SMA-RC responses, achieving values 2 and almost three times higher compared to the 1, 2 and 3% of drift on models without ECC.

Figure 191 and **Table 12** shows that the cost of using just SMA increased the project on 4,5% and using just ECC on 0,5% but as discussed using just one smart material does not produce significant differences on the recovery capacity. However, using SMA and ECC combined makes a significant improvement on the behavior of the piers under extreme loading, and the extra cost is just 5,3%, is not a high cost compared to the cost of using just RC. Which indicates that it is entirely feasible to construct the Salitral bridge piers using SMA and ECC seen giving more security to the structure and the civilians that transit it.

On the seismic performance, the seismic analysis made showed that the most critical condition of the simulated models was the Time-history response of the Limon Earthquake occurred in 1991. Using this as a critical natural condition, **Figure 192** and **Figure 193** shows that the base shear of this event does not present

critical conditions to the Salitral Bridge. Even the plot was made using a particular scale, and the comparison was viewed clearly. Therefore, the Bridge is not in danger on the critical condition of a high seismic event, even with RC the response was on the elastic zone of the curve.

Conclusions

These are part of the conclusions to show the improvement made to the structures using smart materials like bendable concrete (ECC) and SMA as reinforcement bars on the plastic hinge of the structures. The results presented and analyzed are based on FEM and not experimental tests.

1. The Salitral Bridge was chosen due to its level of importance. It is essential on the economy, tourism, cost of construction and is essential to the free-transit of emergency vehicles to hospitals, airports and maritime ports and present a critical condition.

2. It was used a nominal axial load of 15% based on the literature review of modeling of piers.

3. It was determined that the plastic hinge length of the piers is 1800 mm, based on the literature review and SMA-ECC piers and the plastic hinge length of the beams was used on 1000 mm on the middle of these, based on the literature review. This length was used as the SMA required.

4. The seismic analysis showed that the time-history analysis presented higher base shear than the modal analysis. Therefore, the critical time-history of the Limon earthquake presented the base shear of 176,703 kN on the X-axis and 107,341 kN on the Y-axis.

5. It was used the Nitinol alloy (Nickel and Titanium) due to the price, feasibility on the market and multiple types of research made.

6. The use of SMA decrease the lateral load capacity but increase the recovery capacity of the structure and produced larger located cracks on the concrete.

7. Using SMA on all the reinforcement bars of the plastic hinge length produced remarkable recovery capacity with an average of 95%. However, decreased the lateral load capacity drastically.

8. The ECC used was the HFA-ECC due to is the second greenest and cheapest and present the highest compressive, crack and tensile strength. Also, use PVA fibers that are usually easy to find.

9. The use of ECC produces micro-cracks on the concrete with a width of 50 μm. Due to the size of these, it can be recovered.

10. The hysteretic response of the piers using ECC does not present significant recovery capacity.

11. The use of ECC on the structure modified the response completely, now producing the critical cracks over the plastic hinge calculated on the piers and the sides of the beams (join column-beam) where is located the RC.

12. The recovery capacity was improved using SMA and ECC together and separately. However, together produced an improvement of 55% of recovery capacity compared to RC.

13. It was seemed that the use of SMA and ECC decrease the energy dissipation compared to the RC model significantly.

14. The cost of using SMA on the structure is 4% more than using RC, 0,5% using just ECC and 5,3% using SMA and ECC together.

15. The seismic performance showed that the level of damage due to base shear from the Limon earthquake (critical seismic event) does not produce significant damage to the structure according to the non-linear static analysis made.

16. The statistical analysis showed that there are no significant differences using just SMA or ECC separately. However, it does exist significant differences using SMA and ECC together on the structure.

Recommendations

As a part of these recommendations will be included suggestions for future works or researches, or considerations to include in empirical and FEM models.

1. It is recommended if the Software Vector2 will be used to analyze the crack pattern of ECC structures to model the smallest structural elements, due to the limited number of numbers in the FEM and the micro-cracks produced.
2. It is recommended to make an experimental test on the piers of bridges using just SMA, ECC and both together to validate the results and measure the time of recovery of the elements.
3. When large elements are modeled like the Salitral Bridge piers, is recommended to use another software due to the limit of the maximum elements of the FEM.
4. It is recommended to use HFA or PPF ECC due to its green characteristics, and cheap cost compared to other bendable concretes.
5. It is also recommended to compare to retrofit of structures using ECC/SMA and solutions like CRFP.
6. It is recommended to apply the solution made on this bridge to other structures and decrease the cost of production of the structure.
7. If experimental and/or construction structures will be made using SMA is recommended to investigate with different sellers due to the price vary significantly depending on it.
8. Also, it is recommended to buy large and accumulate a bank of material due to most of the materials are brought from China and the cost can be decreased.
9. It is recommended to inform the Costa Rican Government this thesis and show that there are completely feasible solutions to the infrastructure of Costa Rica and gives great benefits on the maintenance. On countries like the U.S.A. is already a constructed pier of Bridge using ECC and SMA.
10. It is recommended to make a statistical analysis of the results to identify if there exist significant differences between the models and give objectivity to the conclusions. Also, to make more than one statistical analysis to give more confidence in the analysis
11. It is recommended to calculate the cost of the researches or projects to clarify the feasibility of the results.

Appendix

In this Appendix is shown the calculations to have some essential parameters of the bridge. In Appendix 1 is the calculations to calculate some critical parameters of the bridge and use it as input to introduce as variables of the FEM made.

The second appendix represents the models made in FormWorks, due to the length of the models there is no proper appreciation of the details because of the mesh made of the FEM, therefore will also be shown the crucial information of the models in this part.

The third appendix shows the results of the curves generated by the points exported from the Software Augustus, from the models made in FormWorks. In Appendix 4 will be shown the results of the FEM from the Software Augustus and curves produced by the same software for different models. Appendix five presents the script used in RStudio in the language "R" to create plots, data-frames, and statistical analysis.

- **Appendix 1.** Parameters to be used as input in the FEMs and the costs.
- **Appendix 2.** Models and responses of the FEM
- **Appendix 3.** The script of R.

Appendix 1

Table 13. Calculation of the weight of the structure.

Element	Material	Density (kg/m³)	Thickness (m)	Width (m)	Area (m²)	Length (m)	Quantity (units)	Volume (m³)	Weight (kg)
Surface	Concrete	2400	0,2	10,98	2,196	156	1	342,576	822182,4
Pier San José	Concrete	2400	-	-	2,24	35,865	2	80,3376	385620,48
Pier Orortina	Concrete	2400	-	-	2,24	38,197	2	85,56128	410694,144
Beam in the support	Concrete	2400	0,75	1,5	1,125	10,74	2	12,0825	57996
Beam in the pier	Concrete	2400	1,5	1,5	2,25	9,5	2	21,375	102600
Main Beam	Steel	7850	-	-	0,0331	156	2	5,1636	81068,52
2 MC 7x22.7	Steel	7850	-	-	0,00623	5,1	8	0,031773	1995,3444
2L 152x89x7.9	Steel	7850	-	-	0,00368	5,1	17	0,018768	2504,5896
W 27x84	Steel	7850	-	-	0,01554	7,74	21	0,1202796	19828,09206
W 10X33	Steel	7850	-	-	0,00613	7,74	17	0,0474462	6331,69539
W 36X194	Steel	7850	-	-	0,03641	7,74	4	0,2818134	8848,94076
W 10X39 (Central)	Steel	7850	-	-	0,00726	5,35	32	0,038841	9756,8592
W 10X39 (Borders)	Steel	7850	-	-	0,00726	5,57	48	0,0404382	15237,11376
W 24X68	Steel	7850	-	-	0,013	156	2	2,028	31839,6
								Sum	1 956 503,78

Table 14. Tributary weight of the bridge.

Parameter	Magnitude	Units
Weight per Frame	978251,89	kg
Weight per Column	489125,94	kg
Effective Area	22400	cm²
Axial Force	21,84	kg/cm²
Axial Force	2,1413781	MPa

Table 15. Calculation of reinforcement of the Models.

Type	Region	Mat		diam bar (mm)		Quant	Area Cross Section (mm2)	Location
Reinforcement 1		M1	#	10,6	33,66	10,00	8895,883	Borders
Reinforcement 2		M2	#	10	31,75	4,00	3166,922	Borders
Reinforcement 3		M3	#	11	34,93	4,00	3831,975	center
Reinforcement 4		M1	#	9,6	30,48	10,00	7296,588	Borders
Reinforcement 5		M2	#	9	28,58	4,00	2565,207	center
Reinforcement 6		M3	#	10	31,75	4,00	3166,922	center
Reinforcement 7		M1	#	8,6	27,31	10,00	5855,638	Borders
Reinforcement 8		M2	#	8	25,40	4,00	2026,830	center
Reinforcement 9		M3	#	9	28,58	4,00	2565,207	center
Reinforcement 10		M1	#	8,0	25,40	10,00	5067,075	Borders
Reinforcement 11		M2	#	7,6	24,13	10,00	4573,035	Borders
Reinforcement 12		M1	#	7	22,23	4,00	1551,792	center
Reinforcement 13		B	#	10,4	33,02	5,00	4281,678	center
Reinforcement 14		B	#	10	31,75	2,00	1583,461	center

Table 16. Calculation of the materials of the Models.

Material	Reinforcement	Angle	Bar		As (mm2)	Sep (mm)	b_{trib} (mm)	Quant	ρ (%)
Material 1	Reinforcement 1	0°	#	4	126,68	200	400	2	0,3167
	Reinforcement 2	361°	#	4	126,68	200	1800	10	0,3519
Material 2	Reinforcement 1	0°	#	4	126,68	200	1000	6	0,3800
	Reinforcement 2	361°	#	4	126,68	200	800	4	0,3167
Material 3	Reinforcement 1	0°	#	4	126,68	300	400	2	0,2111
	Reinforcement 2	361°	#	4	126,68	300	1800	10	0,2346
Material 4	Reinforcement 1	0°	#	4	126,68	300	1000	6	0,2534
	Reinforcement 2	361°	#	4	126,68	300	800	4	0,2111
Material 5	Reinforcement 1	0°	#	4	126,68	100	400	2	0,6334
	Reinforcement 2	361°	#	4	126,68	100	1800	10	0,7038
Material 6	Reinforcement 1	0°	#	4	126,68	100	1000	6	0,7601
	Reinforcement 2	361°	#	4	126,68	100	800	4	0,6334
Material 7	Reinforcement 1	0°	#	4	126,68	200	1000	6	0,3800
	Reinforcement 2	361°	#	4	126,68	200	1800	4	0,1408
Material 8	Reinforcement 1	0°	#	4	126,68	100	1000	6	0,7601
	Reinforcement 2	361°	#	4	126,68	100	1800	4	0,2815
Material 9	Reinforcement 1	90°	#	4	126,68	150	650	2	0,2598
	Reinforcement 2	361°	#	4	126,68	150	1500	8	0,4504

Table 17. Calculation of the reinforcement ratio of the piers.

Long reinforcement						Shear Reinforcement			Shear Reinforcement		
Length	Corners	Center				Bar	Separation	units	Bar	Separation	units
9,0 m	# 8	# 7	13 M9	14 M10	15 M9	# 4 @ 20,0 cm Out of the plane (90°)			# 4 @ 20,0 cm Out of the plane (90°)		
						ρ = 0,00317%		M9	ρ = 0,00380%		M10
						Stirrups longit (0°)			Stirrups longit (0°)		
						ρ = 0,01583%		M9	ρ = 0,00253%		M10
9,0 m	# 8	# 8	10 M7	11 M8	12 M7	# 4 @ 30,0 cm Out of the plane (90°)			# 4 @ 30,0 cm Out of the plane (90°)		
						ρ = 0,00211%		M7	ρ = 0,00253%		M8
						Stirrups longit (0°)			Stirrups longit (0°)		
						ρ = 0,01056%		M7	ρ = 0,00169%		M8
12,0 m	# 9	# 8	7 M5	8 M6	9 M5	# 4 @ 20,0 cm Out of the plane (90°)			# 4 @ 20,0 cm Out of the plane (90°)		
						ρ = 0,00317%		M5	ρ = 0,00380%		M6
						Stirrups longit (0°)			Stirrups longit (0°)		
						ρ = 0,01583%		M5	ρ = 0,00253%		M6
6,0 m	# 10	# 9	4 M3	5 M4	6 M3	# 4 @ 30,0 cm Out of the plane (90°)			# 4 @ 30,0 cm Out of the plane (90°)		
						ρ = 0,00211%		M3	ρ = 0,00253%		M4
						Stirrups longit (0°)			Stirrups longit (0°)		
						ρ = 0,01056%		M3	ρ = 0,00169%		M4
12,0 m	# 11	# 10	1 M1	2 M2	3 M1	# 4 @ 10,0 cm Out of the plane (90°)			# 4 @ 10,0 cm Out of the plane (90°)		
						ρ = 0,00633%		M1	ρ = 0,00760%		M2
						Stirrups longit (0°)			Stirrups longit (0°)		
						ρ = 0,03167%		M1	ρ = 0,00507%		M2

Table 18.Cost of the piers using RC.

🚛 Ordinary Concrete and reinforcement as built						
Description	Quantity	Length	Necessary	unit	cost/unit	Total
Concrete 28 MPa						
Column with hollow	4,00	30,85	2,24	m³	₡ 96 000,00	₡ 26 535 936,00
Coupling beam	4,00	5,92	1,05	m³	₡ 96 000,00	₡ 2 386 944,00
Filled column	4,00	5,50	3,24	m³	₡ 96 000,00	₡ 6 842 880,00
Ductile reinforcement						
Stage 1	-2000,00	6000,00				
Bar #11	128,00	12,00	1,00	unit	₡ 49 980,00	₡ 76 769 280,00
Bar #10	128,00	12,00	1,00	unit	₡ 40 480,00	₡ 62 177 280,00
Bar #4	0,10	6,00	9779,20	unit	₡ 3 030,00	₡ 4 938 496,00
Stage 1	0,00	6000,00				
Bar #10	128,00	12,00	0,67	unit	₡ 40 480,00	₡ 41 451 520,00
Bar #9	128,00	12,00	0,67	unit	₡ 31 980,00	₡ 32 747 520,00
Bar #4	0,30	6,00	2444,80	unit	₡ 3 030,00	₡ 1 234 624,00
Stage 3	14500,00	22000,00				
Bar #9	128,00	12,00	1,00	unit	₡ 31 980,00	₡ 49 121 280,00
Bar #8	128,00	12,00	1,00	unit	₡ 25 110,00	₡ 38 568 960,00
Bar #4	0,20	6,00	4584,00	unit	₡ 3 030,00	₡ 2 314 920,00
Stage 4	22000,00	31350,00				
Bar #8	256,00	12,00	0,67	unit	₡ 25 110,00	₡ 51 682 406,40
Bar #4	0,30	6,00	2,36	unit	₡ 3 030,00	₡ 1 193,47
Stage 5	31350,00	36350,00				
Bar #8	128,00	12,00	0,67	unit	₡ 25 110,00	₡ 25 841 203,20
Bar #7	128,00	12,00	0,67	unit	₡ 19 220,00	₡ 19 779 686,40
Bar #4	0,20	6,00	3056,00	unit	₡ 3 030,00	₡ 1 543 280,00
Beams						
Bar #11	32,00	12,00	4,00	unit	₡ 49 980,00	₡ 76 769 280,00
Bar #10	64,00	12,00	4,00	unit	₡ 40 480,00	₡ 124 354 560,00
Bar #4	0,15	6,00	1733,38	unit	₡ 3 030,00	₡ 875 354,88
Total						**₡ 645 936 604,35**
Total international			change =$ 1	USD	₡ 565,00	**$ 1 143 250,63**

Table 19. Cost of the piers using SMA and RC.

🚛 Ordinary Concrete, steel reinforcement and SMA								
Description	Quantity	Length	Necessary	unit		cost/unit		Total
Concrete 28 MPa								
Column with hollow	4,00	30,85	2,24	m³	₡	96 000,00	₡	26 535 936,00
Coupling beam	4,00	5,92	1,05	m³	₡	96 000,00	₡	2 386 944,00
Filled column	4,00	5,50	3,24	m³	₡	96 000,00	₡	6 842 880,00
Reinforcement								
SMA								
SMA truss bars	4,00	73,60	294,40	unit	₡	374 850,00	₡	110 355 840,00
Steel reinforcement	**-2000,00**	**6000,00**						
Bar #10	128,00	12,00	1,00	unit	₡	40 480,00	₡	62 177 280,00
Bar #4	0,10	6,00	9779,20	unit	₡	3 030,00	₡	4 938 496,00
Steel reinforcement	**0,00**	**6000,00**						
Bar #10	128,00	12,00	0,67	unit	₡	40 480,00	₡	41 451 520,00
Bar #9	128,00	12,00	0,67	unit	₡	31 980,00	₡	32 747 520,00
Bar #4	0,30	6,00	2444,80	unit	₡	3 030,00	₡	1 234 624,00
Steel reinforcement	**14500,00**	**22000,00**						
Bar #9	128,00	12,00	1,00	unit	₡	31 980,00	₡	49 121 280,00
Bar #8	128,00	12,00	1,00	unit	₡	25 110,00	₡	38 568 960,00
Bar #4	0,20	6,00	4584,00	unit	₡	3 030,00	₡	2 314 920,00
Steel reinforcement	**22000,00**	**31350,00**						
Bar #8	256,00	12,00	0,67	unit	₡	25 110,00	₡	51 682 406,40
Bar #4	0,30	6,00	2,36	unit	₡	3 030,00	₡	1 193,47
Steel reinforcement	**31350,00**	**36350,00**						
Bar #8	128,00	12,00	0,67	unit	₡	25 110,00	₡	25 841 203,20
Bar #7	128,00	12,00	0,67	unit	₡	19 220,00	₡	19 779 686,40
Bar #4	0,20	6,00	3056,00	unit	₡	3 030,00	₡	1 543 280,00
Steel reinforcement	**beams**							
Bar #11	32,00	12,00	4,00	unit	₡	49 980,00	₡	76 769 280,00
Bar #10	64,00	12,00	4,00	unit	₡	40 480,00	₡	124 354 560,00
Bar #4	0,15	6,00	1733,38	unit	₡	3 030,00	₡	875 354,88
Total							₡	**679 523 164,35**
Total international			change =$ 1	USD	₡	565,00	$	**1 202 695,87**

Table 20. Cost of the piers using steel and ECC

Description	Quantity	Length	Necessary	unit	cost/unit	Total
Steel reinforcement, ordinary concrete and ECC						
Concrete 28 MPa						
Column with hollow	4,00	34,55	2,24	m³	₡ 96 000,00	₡ 29 718 528,00
Coupling beam	4,00	5,92	1,05	m³	₡ 96 000,00	₡ 2 386 944,00
ECC						
Columns and beams	4,00	6,60	1	m³	₡ 242 880,00	₡ 6 409 117,44
Ductile reinforcement						
Stage 1	-2000,00	6000,00				
Bar #11	128,00	12,00	1,00	unit	₡ 49 980,00	₡ 76 769 280,00
Bar #10	128,00	12,00	1,00	unit	₡ 40 480,00	₡ 62 177 280,00
Bar #4	0,10	6,00	9779,20	unit	₡ 3 030,00	₡ 4 938 496,00
Stage 1	0,00	6000,00				
Bar #10	128,00	12,00	0,67	unit	₡ 40 480,00	₡ 41 451 520,00
Bar #9	128,00	12,00	0,67	unit	₡ 31 980,00	₡ 32 747 520,00
Bar #4	0,30	6,00	2444,80	unit	₡ 3 030,00	₡ 1 234 624,00
Stage 3	14500,00	22000,00				
Bar #9	128,00	12,00	1,00	unit	₡ 31 980,00	₡ 49 121 280,00
Bar #8	128,00	12,00	1,00	unit	₡ 25 110,00	₡ 38 568 960,00
Bar #4	0,20	6,00	4584,00	unit	₡ 3 030,00	₡ 2 314 920,00
Stage 4	22000,00	31350,00				
Bar #8	256,00	12,00	0,67	unit	₡ 25 110,00	₡ 51 682 406,40
Bar #4	0,30	6,00	2,36	unit	₡ 3 030,00	₡ 1 193,47
Stage 5	31350,00	36350,00				
Bar #8	128,00	12,00	0,67	unit	₡ 25 110,00	₡ 25 841 203,20
Bar #7	128,00	12,00	0,67	unit	₡ 19 220,00	₡ 19 779 686,40
Bar #4	0,20	6,00	3056,00	unit	₡ 3 030,00	₡ 1 543 280,00
Beams						
Bar #11	32,00	12,00	4,00	unit	₡ 49 980,00	₡ 76 769 280,00
Bar #10	64,00	12,00	4,00	unit	₡ 40 480,00	₡ 124 354 560,00
Bar #4	0,15	6,00	1733,38	unit	₡ 3 030,00	₡ 875 354,88
Total						**₡ 648 685 433,79**
Total international			change =$1	USD ₡	565,00	**$ 1 148 115,81**

Table 21. Cost of the piers using SMA and ECC.

Description	Quantity	Length	Necessary	unit	cost/unit		Total	
SMA, ECC and RC								
Concrete 28 MPa								
Column with hollow	4,00	34,55	2,24	m³	₡	96 000,00	₡	29 718 528,00
Coupling beam	4,00	5,92	1,05	m³	₡	96 000,00	₡	2 386 944,00
ECC								
Columns and beams	4,00	6,60	1	m³	₡	242 880,00	₡	6 409 117,44
SMA								
SMA truss bars	4,00	73,60	294,40	unit	₡	374 850,00	₡	110 355 840,00
Ductile reinforcement								
Stage 1	-2000,00	6000,00						
Bar #10	128,00	12,00	1,00	unit	₡	40 480,00	₡	62 177 280,00
Bar #4	0,10	6,00	9779,20	unit	₡	3 030,00	₡	4 938 496,00
Stage 1	0,00	6000,00						
Bar #10	128,00	12,00	0,67	unit	₡	40 480,00	₡	41 451 520,00
Bar #9	128,00	12,00	0,67	unit	₡	31 980,00	₡	32 747 520,00
Bar #4	0,30	6,00	2444,80	unit	₡	3 030,00	₡	1 234 624,00
Stage 3	14500,00	22000,00						
Bar #9	128,00	12,00	1,00	unit	₡	31 980,00	₡	49 121 280,00
Bar #8	128,00	12,00	1,00	unit	₡	25 110,00	₡	38 568 960,00
Bar #4	0,20	6,00	4584,00	unit	₡	3 030,00	₡	2 314 920,00
Stage 4	22000,00	31350,00						
Bar #8	256,00	12,00	0,67	unit	₡	25 110,00	₡	51 682 406,40
Bar #4	0,30	6,00	2,36	unit	₡	3 030,00	₡	1 193,47
Stage 5	31350,00	36350,00						
Bar #8	128,00	12,00	0,67	unit	₡	25 110,00	₡	25 841 203,20
Bar #7	128,00	12,00	0,67	unit	₡	19 220,00	₡	19 779 686,40
Bar #4	0,20	6,00	3056,00	unit	₡	3 030,00	₡	1 543 280,00
Beams								
Bar #11	32,00	12,00	4,00	unit	₡	49 980,00	₡	76 769 280,00
Bar #10	64,00	12,00	4,00	unit	₡	40 480,00	₡	124 354 560,00
Bar #4	0,15	6,00	1733,38	unit	₡	3 030,00	₡	875 354,88
Total							₡	**682 271 993,79**
Total international			change =$ 1	USD	₡	565,00	$	**1 207 561,05**

Table 22. Cost of the piers using different steel reinforcement bars.

RC WITH CHANGES						
Description	Quantity	Length	Necessary	unit	cost/unit	Total
Concrete 28 MPa						
Column with hollow	4,00	30,85	2,24	m³	₵ 96 000,00	₵ 26 535 936,00
Coupling beam	4,00	5,92	1,05	m³	₵ 96 000,00	₵ 2 386 944,00
Filled column	4,00	5,50	3,24	m³	₵ 96 000,00	₵ 6 842 880,00
Ductile reinforcement						
Stage 1	-2000,00	6000,00				
Bar #11	128,00	12,00	1,00	unit	₵ 49 980,00	₵ 76 769 280,00
Bar #10	128,00	12,00	1,00	unit	₵ 40 480,00	₵ 62 177 280,00
Bar #4	0,10	6,00	9779,20	unit	₵ 3 030,00	₵ 4 938 496,00
Stage 1	0,00	6000,00				
Bar #11	128,00	12,00	0,67	unit	₵ 49 980,00	₵ 51 179 520,00
Bar #10	128,00	12,00	0,67	unit	₵ 40 480,00	₵ 41 451 520,00
Bar #4	0,10	6,00	7334,40	unit	₵ 3 030,00	₵ 3 703 872,00
Stage 3	14500,00	22000,00				
Bar #9	128,00	12,00	1,00	unit	₵ 31 980,00	₵ 49 121 280,00
Bar #8	128,00	12,00	1,00	unit	₵ 25 110,00	₵ 38 568 960,00
Bar #4	0,20	6,00	4584,00	unit	₵ 3 030,00	₵ 2 314 920,00
Stage 4	22000,00	31350,00				
Bar #8	256,00	12,00	0,67	unit	₵ 25 110,00	₵ 51 682 406,40
Bar #4	0,30	6,00	2,36	unit	₵ 3 030,00	₵ 1 193,47
Stage 5	31350,00	36350,00				
Bar #8	128,00	12,00	0,67	unit	₵ 25 110,00	₵ 25 841 203,20
Bar #7	128,00	12,00	0,67	unit	₵ 19 220,00	₵ 19 779 686,40
Bar #4	0,20	6,00	3056,00	unit	₵ 3 030,00	₵ 1 543 280,00
Beams						
Bar #11	32,00	12,00	4,00	unit	₵ 49 980,00	₵ 76 769 280,00
Bar #10	64,00	12,00	4,00	unit	₵ 40 480,00	₵ 124 354 560,00
Bar #4	0,15	6,00	1733,38	unit	₵ 3 030,00	₵ 875 354,88
Total						₵ 666 837 852,35
Total international			change =$ 1	USD ₵	565,00	$ 1 180 243,99

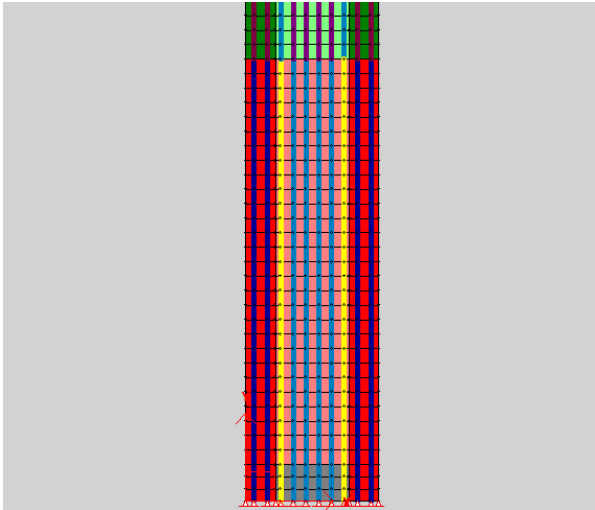# Appendix 2

Figure 194. MOD1 RC with smeared shear reinforcement and truss bars, from 0 mm to 6000 mm.

Figure 195. MOD1 RC with smeared shear reinforcement and truss bars, from 6000 mm to 14500 mm.

Figure 196. MOD1 RC with smeared shear reinforcement and truss bars, from 14500 mm to 22000 mm.
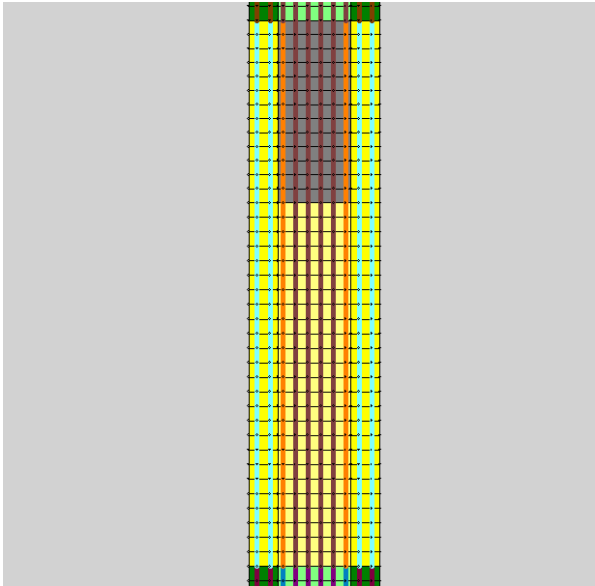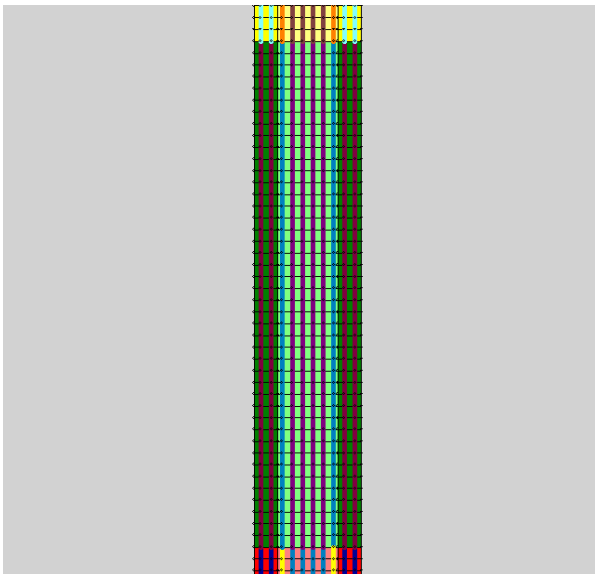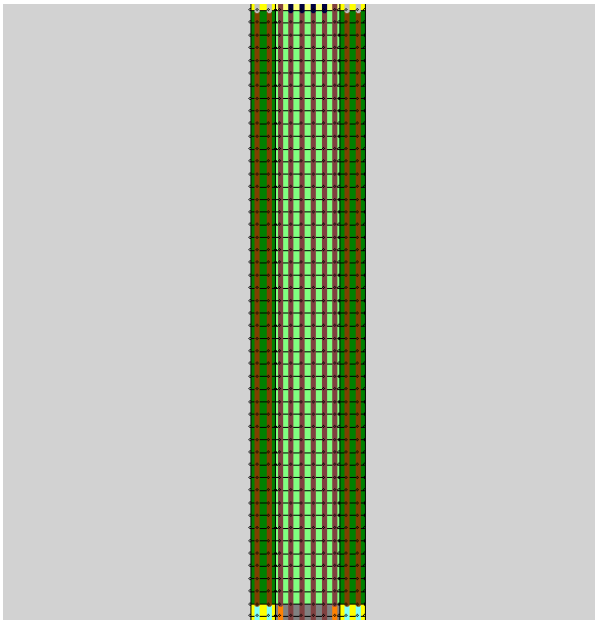

Figure 197. MOD1 RC with smeared shear reinforcement and truss bars, from 22000 mm to 31350 mm.
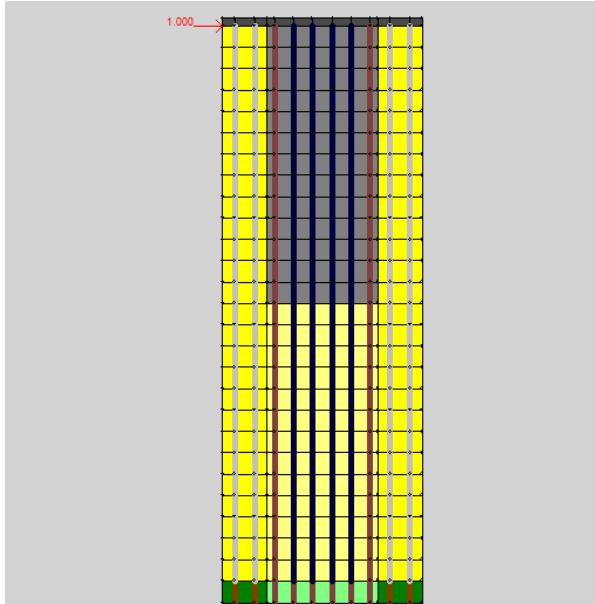
Figure 198. With smeared shear reinforcement and truss bars, from 31350 mm to 36350 mm.
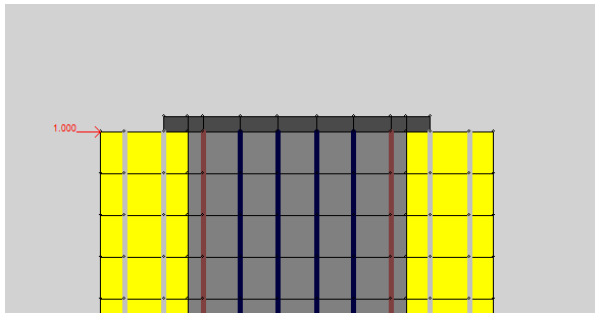

Figure 199. MOD1 using steel plate on top 110x110 cm in Pushover Analysis.

Figure 200. MOD1 using steel plate on top 180x180 cm in Pushover Analysis.
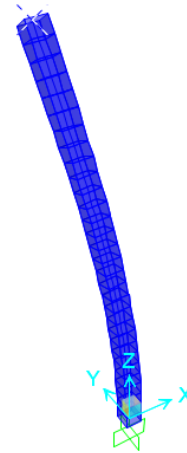
Figure 201. Deformed shape of the single pier.

Appendix 3

```
# Working directory is selected
setwd("~/TEC/2018 II SEM/Graduation Project/RStudio")
# CRAN libraries are loaded
require(MASS)
require(DescTools)
require(Agreement)
require(pastecs)
require(ggplot2)
require(reshape)
require(mgcv)a
require(devtools)
require(gapminder)
# Create a data frame about Seismic events in Costa Rica.
# --------------------------------------------------------------------------------
# Seismic event 1991, Limon, Costa Rica
df_sismo_limon <- read.table("Sismo_Limon.txt", header = TRUE, sep = "\t", quote = "")
class(df_sismo_limon)
# Search fot the class of each column
class(df_sismo_limon$N00E)
class(df_sismo_limon$TIME)
class(df_sismo_limon$N90E)


# Creating the SEISMIC SPECTRUM
fg01 <- ggplot(data = df_sismo_limon) +
        geom_line(aes(x=TIME,y=N00E)) +
        ggtitle("Limon Earthquake, Costa Rica 1991.(EJE X)") +
        ylab("Aceleration (cm/s2)") +
        xlab("Tiempo (s)")

# LIMON'S SEISMIC EVENT IN X.

# A ggplot2 object is requested
fg01

# Spectrum by R
sism_limon_X  <- subset(df_sismo_limon, select = c(TIME,N00E))
spectrum(sism_limon_X)


# LIMON'S SEISMIC EVENT IN Y.

# Creating the SEISMIC SPECTRUM
fg02 <- ggplot(data = df_sismo_limon) +
  geom_line(aes(x=TIME,y=N90E,colour = TIME)) +
  ggtitle("Limon Earthquake, Costa Rica 1991.(EJE Y)") +
  ylab("Aceleration (cm/s2)") +
```

```
  xlab("Tiempo (s)")

# A ggplot2 object is requested
fg02

# Spectrum by R
sism_limon_Y  <- subset(df_sismo_limon, select = c(TIME,N90E))
spectrum(sism_limon_Y)

# -----------------------------------------------------------------------------
#Seismic event at Cichona 2009, Costa Rica
df_sismo_cinchona <- read.table("Sismo_cinchona.txt", header = TRUE, sep = "\t", quote
= "")
class(df_sismo_cinchona)
# Search fot the class of each column
class(df_sismo_cinchona$N00E)
class(df_sismo_cinchona$TIME)
class(df_sismo_cinchona$N90E)

# Creating the SEISMIC SPECTRUM
fg03 <- ggplot(data = df_sismo_cinchona) +
  geom_line(aes(x=TIME,y=N00E)) +
  ggtitle("Cinchona's Earthquake, Costa Rica 2009.(EJE X)") +
  ylab("Aceleration (cm/s2)") +
  xlab("Tiempo (s)")

# CINCHONA'S SEISMIC EVENT IN X.

# A ggplot2 object is requested
fg03

# Spectrum by R
sism_cinchona_X  <- subset(df_sismo_cinchona, select = c(TIME,N00E))
spectrum(sism_cinchona_X)


# CICHONA'S SEISMIC EVENT IN Y.

# Creating the SEISMIC SPECTRUM
fg04 <- ggplot(data = df_sismo_cinchona) +
  geom_line(aes(x=TIME,y=N90E,colour = TIME)) +
  ggtitle("Cinchona's Earthquake, Costa Rica 2009.(EJE Y)") +
  ylab("Aceleration (cm/s2)") +
  xlab("Tiempo (s)")

# A ggplot2 object is requested
fg04

# Spectrum by R
sism_cinchona_Y  <- subset(df_sismo_cinchona, select = c(TIME,N90E))
spectrum(sism_limon_Y)
```

```
# ---------------------------------------------------------------------------------
#Seismic event 1990, Cobano, Costa Rica
df_sismo_cobano <- read.table("Sismo_cobano.txt", header = TRUE, sep = "\t", quote =
"")
class(df_sismo_cobano)
# Search fot the class of each column
class(df_sismo_cobano$N00E)
class(df_sismo_cobano$TIME)
class(df_sismo_cobano$N90E)

# Creating the SEISMIC SPECTRUM
fg05 <- ggplot(data = df_sismo_cobano) +
  geom_line(aes(x=TIME,y=N00E)) +
  ggtitle("Cobano's Earthquake, Costa Rica 1990.(EJE X)") +
  ylab("Aceleration (cm/s2)") +
  xlab("Tiempo (s)")

# COBANO'S SEISMIC EVENT IN X.

# A ggplot2 object is requested
fg05

# Spectrum by R
sism_cobano_X  <- subset(df_sismo_cobano, select = c(TIME,N00E))
spectrum(sism_cobano_X)


# COBANO'S SEISMIC EVENT IN Y.

# Creating the SEISMIC SPECTRUM
fg06 <- ggplot(data = df_sismo_cobano) +
  geom_line(aes(x=TIME,y=N90E,colour = TIME)) +
  ggtitle("Cobano's Earthquake, Costa Rica 1990.(EJE Y)") +
  ylab("Aceleration (cm/s2)") +
  xlab("Tiempo (s)")

# A ggplot2 object is requested
fg06

# Spectrum by R
sism_cobano_Y  <- subset(df_sismo_cobano, select = c(TIME,N90E))
spectrum(sism_cobano_Y)

#---------------------------------------------------------------------------------

df_sismos_CR <- read.table("seismic_events_CR.txt", header = TRUE, sep = "\t", quote =
"")

# Seisimic events toguether en el eje x
fg07 <- ggplot(data = df_sismos_CR) +
        geom_line(aes(x=TIME,y= N00E,colour = EARTHQUAKE)) +
        ggtitle("Earthquakes in Costa Rica.") +
```

```
        ylab("Aceleration (cm/s2)") +
        xlab("Tiempo (s)")
# A ggplot2 object is requested
fg07

# Seisimic events toguether en el eje y
fg08 <- ggplot(data = df_sismos_CR) +
  geom_point(aes(x=TIME,y= N90E,colour = EARTHQUAKE)) +
  ggtitle("Earthquakes in Costa Rica.") +
  ylab("Aceleration (cm/s2)") +
  xlab("Tiempo (s)")
# A ggplot2 object is requested
fg08

# Seisimic events toguether en el eje z
fg09 <- ggplot(data = df_sismos_CR) +
  geom_point(aes(x=TIME,y= UPDO,colour = EARTHQUAKE)) +
  ggtitle("Earthquakes in Costa Rica.") +
  ylab("Aceleration (cm/s2)") +
  xlab("Tiempo (s)")

# A ggplot2 object is requested
fg09

# Density of acelerations
fg10 <- ggplot() +
  geom_density(aes(x = N00E,colour = EARTHQUAKE,group = EARTHQUAKE),data=df_sismos_CR)
# A ggplot2 object is requested
fg10

# Magnitude of the events
fg11 <- ggplot() +
  geom_bar(aes(y = EVENT_MAGNITUDE,x = EARTHQUAKE,colour =
EARTHQUAKE),data=seismic_events_CR)
# A ggplot2 object is requested
fg11


#/////////////////////////////////////////////////////////////////////////////
#Data from the SMA-ECC Model
#Lassonde School of Engineering
#Ignacio Matthews - Student ID:216809121
#/////////////////////////////////////////////////////////////////////////////

#Data of the models. From Vector2, FormoWorks & Augustus.
df_models <- read.table("data_models.txt", header = TRUE, sep = "\t", quote = "")

#Comparison of the Models ("X" vs. "Y").
fg21 <- ggplot(data = df_models) +
  geom_line(aes(x=X,y= Y,colour = MODEL)) +
  ylab("Aceleration (cm/s2)") +
  xlab("Tiempo (s)") +
```

```
  transition(gear)

#-------------------------------------------------------------------------------
#           STATISTICAL ANALYSIS
#-------------------------------------------------------------------------------

#Graphs of the Model 1 responses versus drift (Reverse Cycli)
df_graphg <- read.table("ULTIMOS GRAFICOS MOD1.txt", header = TRUE, sep = "\t", quote =
"")

#par(mar=c(5,4,6,2))
#tuk <- glht(fit, linfct=mcp(trt="Tukey"))
#plot(cld(tuk, level=.05),col="lightgrey")

# Tests for group differences (ANOVA) --
# The ANOVA F test for treatment (trt) is significant (p < .0001),
# providing evidence that the five treatments aren't all equally effective
fit <- aov(RECOVERY ~ NAME, data = df_graphg)

# A summary is requested
summary(fit)

# Plots group means and confidence intervals --
# A plot of the treatment means, with 95% confidence limits
# allows you to clearly see these treatment differences
plotmeans(df_graphg$RECOVERY ~ df_graphg$NAME,
          xlab="Material",
          ylab="Recovery",
          main="Mean Plot\nwith 95% CI")

# Multiple comparisons --
# The ANOVA F test for treatment tells you that the five drug regimens aren't equally
# effective, but it doesn't tell you which treatments differ from one another.
# For example, the mean cholesterol reductions for 1time and 2times aren't
significantly different from each other (p = 0.138), whereas the difference between
1time
# and 4times is significantly different (p < .001).
TukeyHSD(fit)

par(mar=c(5,4,6,2))
tuk <- glht(fit, linfct=mcp(NAME="Tukey"))
plot(cld(tuk, level=.05),col="lightgrey")

par(mar=c(5,4,6,2))
tuk <- glht(fit, linfct=mcp(NAME="Tukey"))
plot(cld(tuk, level=.05, colour=NAME),col="lightgrey", xlab="Model",ylab="Recovery
(%)")

#/////////////////////////////////////////////////////////////////////////////////////
#T-STUDENT
```

```
df_ttest <- read.table("T Test MOD1 RECOVERY.txt", header = TRUE, sep = "\t", quote =
"")

# a two-sample t-test allow us to test whether the MEANS of two independent groups
#H0 (null hypothesis): The true probability of succes is not equal to what was proposed
#H1 (alternative hypothesis): The true probability of success is not equal to what was
proposed
#if (p-value > 0.05) the null hypothesis cannot be rejected.

t.test(df_ttest$REC_SMA.ECC,df_ttest$REC_RC)
t.test(df_ttest$REC_SMA,df_ttest$REC_RC)
t.test(df_ttest$REC_ECC,df_ttest$REC_RC)

# S H A P I R O   T E S T

df_ttest$SDSE <- (df_ttest$REC_SMA.ECC - df_ttest$REC_RC)
df_ttest$SDS <- (df_ttest$REC_SMA - df_ttest$REC_RC)
df_ttest$SDE <- (df_ttest$REC_ECC - df_ttest$REC_RC)

shapiro.test(df_ttest$SDSE)
shapiro.test(df_ttest$SDS)
shapiro.test(df_ttest$SDE)

# C O R   R E L A T I O N   P E A R S O N

cor.test(df_ttest$REC_SMA.ECC,df_ttest$REC_RC)
cor.test(df_ttest$REC_ECC,df_ttest$REC_RC)
cor.test(df_ttest$REC_SMA,df_ttest$REC_RC)
```
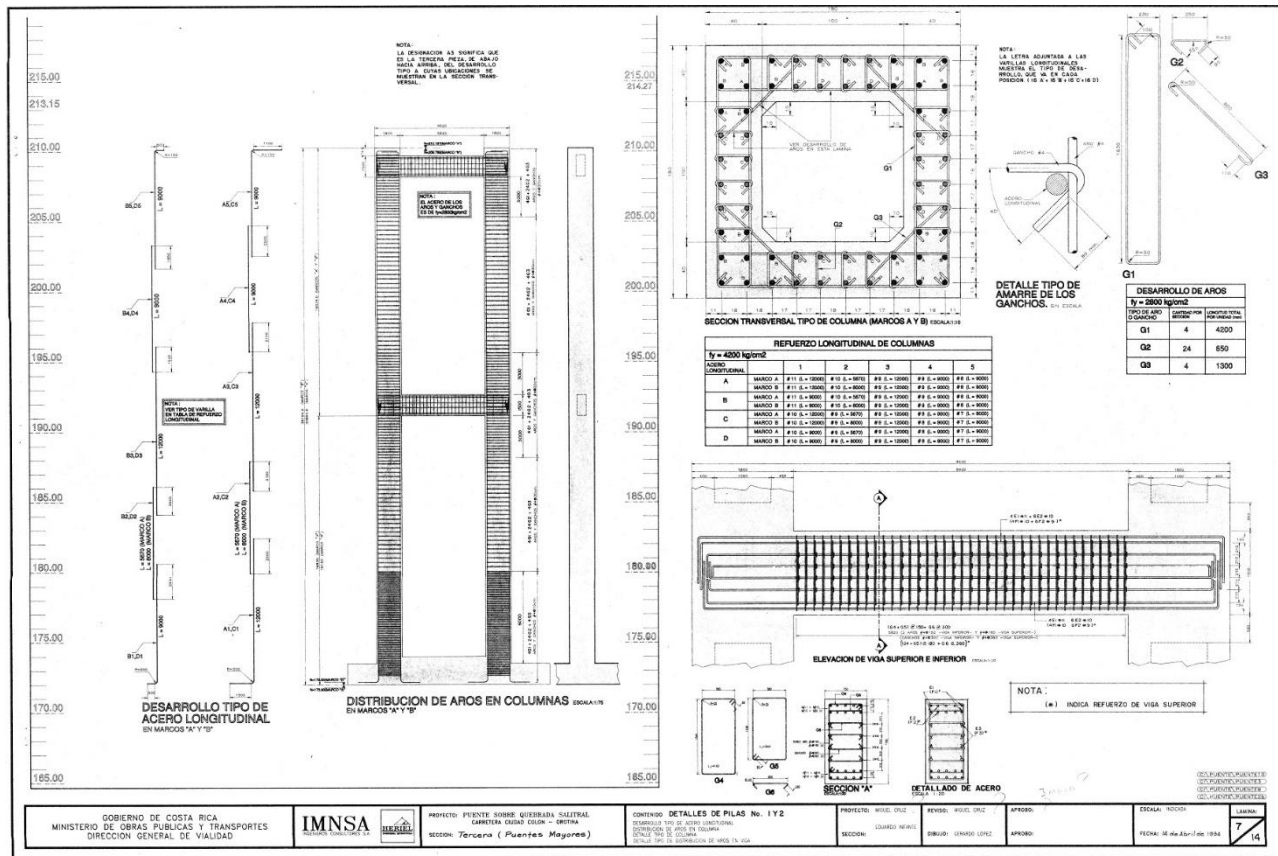
Annexes

The annex 1 shows the original blueprint of the Salitral Bridge given by the eBridge program. This was produced by hand on 1994 and presented low resolution. The second annex is the statistical analysis made with the software R.

Annex 1

SEISMIC PERFORMANCE OF SMA-REINFORCED ECC PIER SYSTEM OF THE SALITRAL BRIDGE

References

Abdulridha, A. (2013). *Performance of Superelastic Shape Memory Alloy Reinforced Concrete Elements Subjected to Monotonic and Cyclic Loading*. University of Ottawa.

Abdulridha, A., Palermo, D., Foo, S., & Vecchio, F. J. (2013). Behavior and modeling of superelastic shape memory alloy reinforced concrete beams. *Engineering Structures*, *49*, 893–904. https://doi.org/10.1016/j.engstruct.2012.12.041

Alvarado, G., Barquero, R., Boschini, I., Climent, A., Laurent, J., Allan, L., … Alberto, V. (2009). *El terremoto de Cinchona del 8 de enero de 2009*. San Jose.

Anwar, A. M., Hattori, K., Ogala, H., Ashraf, M., & Mandula. (2009). Engineered Cementitious Composites for repair of iniatially Cracked Concrete Beams. *Asian Journal of Applied Sciences, 2*(3), 223–231.

Asadi, H., Bodaghi, M., Shakeri, M., & Aghdam, M. M. (2014). Nonlinear dynamics of SMA-fiber-reinforced composite beams subjected to a primary/secondary-resonance excitation. *Acta Mechanica*, *226*(2), 437–455. https://doi.org/10.1007/s00707-014-1191-4

Billah, A. H. M. M., & Shahria Alam, M. (2016). Plastic hinge length of shape memory alloy (SMA) reinforced concrete bridge pier. *Engineering Structures*, *117*, 321–331. https://doi.org/10.1016/j.engstruct.2016.02.050

Blanco, P. (2012). RSN presentó informe sobre terremoto de Sámara. Retrieved from https://www.ucr.ac.cr/noticias/2012/11/08/rsn-presento-informe-sobre-terremoto-de-samara.html

Blogger. (2013). Habituating FEA. Retrieved from http://habituatingfea.blogspot.com/2012/11/types-of-elements-in-fea.html

Brenes, A. (2010). *Gestión de Riesgo, decimosexto informe Estado de la Nación en Desarrollo Humano sostenible*. San Jose.

Buddy Rhodes. (2019). Buddy Rhodes - Concrete Products. Retrieved January 5, 2019, from http://www.buddyrhodes.com/pva-fiber-recs-15/

Chaverri, A. (2016). Axial y Flexión. Cartago: Estructuras de Concreto, Escuela de Ingeniería en Construcción.

Clines, K. (2017). WSDOT building world's first flexible bridge. Retrieved from https://www.equipmentworld.com/video-wsdot-building-worlds-first-flexible-bridge/

Clough, R. W., & Penzien, J. (2010). *Dynamic of Structures*. (L. Vinet & A. Zhedanov, Eds.), *Computer Methods in Applied Mechanics and Engineering* (Third Edit, Vol. 98). Berkley CA: McGraw Hill. https://doi.org/10.1088/1751-8113/44/8/085201

Colegio Federado de Ingenieros y Arquitectos de Costa Rica. (2012). *Lineamientos para el Diseño Sismorresistente de Puentes. Diseño Sismorresistente* (Vol. 1). San Jose. Retrieved from http://civilgeeks.com/2013/09/23/lineamientos-para-el-diseno-sismorresistente-de-puentes/

Cortés-Puentes, L., Zaidi, M., Palermo, D., & Dragomirescu, E. (2018). Cyclic loading testing of repaired SMA and steel reinforced concrete shear walls. *Engineering Structures*, *168*(October 2017), 128–141. https://doi.org/10.1016/j.engstruct.2018.04.044

Cruz Noguez, C. a., & Saiidi, M. S. (2013). Performance of Advanced Materials during Earthquake Loading Tests of a Bridge System. *Journal of Structural Engineering*, *139*(1), 144–154. https://doi.org/10.1061/(ASCE)ST.1943-541X.0000611.

Delgado-Pitti, I., Corrales-Poveda, F., Rojas-Morales, N., & Naranjo-Castillo, V. (2018). *Infraestructura resiliente al cambio climático: Caso de estudio*. San Jose, Costa Rica.

Retrieved from https://www.youtube.com/watch?v=tthjgteYPD0&index=2&list=LLymHJRvJwz71HNZTZ_E6h0w&t=328s

Díaz, R. (2015). Ovsicori reporta un enjambre sísmico en Cinchona. Retrieved from https://www.nacion.com/sucesos/desastres/ovsicori-reporta-un-enjambre-sismico-en-cinchona/M7ZKVESQSZH7HNJD5RN4VTUZXA/story/

eBridge. (2018). *Salitral Bridge report.* Cartago, Costa Rica: Instituto Teconlogico de Costa Rica.

Fedak, L. K. (2012). *Evaluation of Plastic Hinge Models and Inelastic analysis tools for Performance-Based Seismic design of RC Bridge Columns.* Michigan State University.

FEMA 356. (2000). Prestandard and Commentary for the Seismic Rehabilitation of Buildings. *Rehabilitation Requirements*, (1), 1–518.

FIP, I. (2016). *Anti-seismic devices. BSI, London, UK.* (S00 ed.). Selvazzano, Italy.

Hidalgo-Ramirez, M. (2018). *Análisis de la estabilidad de la ladera San Miguel con SVSLOPE , para el Instituto Costarricense de Electricidad.* Instituto Tecnológico de Costa Rica.

Horikoshi T, Ogawa A, Saito T, H. H. (2006). *Properties of Polyvinylalcohol Fiber As Reinforcing Materials for Cementitious Composites* (Vol. 2). Ltd, Japan. Retrieved from http://demo.webdefy.com/rilem-new/wp-content/uploads/2016/10/pro049-016.pdf

Hosseini, F., & Gencturk, B. (2015). Evaluation of Reinforced Concrete and Reinforced Engineered Cementitious Composite (ECC) Members and Structures Using Small-Scale Testing. *Canadian Journal of Civil Engineering*, *42*, 164–177.

Jo, L. S., & Min, P. J. (2017). An Experimental Study on the Structural Behaviors of HIRC Beams Using Nickel-Titanium SMA Wires. *Key Engineering Materials*, *730*, 423–428. https://doi.org/10.4028/www.scientific.net/KEM.730.423

Kabacoff, R. (2015). *R in action, Data Analysis and graphics with R.* Unite States of America.

Kalny, O., & Napier, J. (2014). Response-Spectrum Analysis. Retrieved January 14, 2019, from https://wiki.csiamerica.com/display/kb/Response-spectrum+analysis

Kewalramani, M. A., Mohamed, O. A., & Syed, Z. I. (2017). Engineered Cementitious Composites for Modern Civil Engineering Structures in Hot Arid Coastal Climatic Conditions. *Procedia Engineering*, *180*, 767–774. https://doi.org/10.1016/j.proeng.2017.04.237

Khosravi, H., Ghaderi, M., Atashi, A., & Mousavi, S. S. (2017). *Study on seismic behavior of a concrete elevated tank with frame shaped base using SMA damper.* Neyshabur, Iran.

Li, V. C. (2003). *On Engineered Cementitious Composites (ECC) A Review of the Material and Its Applications. Journal of Advanced Concrete Technology* (Vol. 1). Takayama, Japan.

Li, V. C., Wang, S., & Wu, C. (2001). Tensile strain-hardening behavior or polyvinyl alcohol engineered cementitious composite (PVA-ECC). *ACI Materials Journal.* https://doi.org/10.14359/10851

Li, X., Li, M., & Song, G. (2015). Energy-dissipating and self-repairing SMA-ECC composite material system. *Smart Materials and Structures*, *16*. https://doi.org/10.1088/0964-1726/24/2/025024

Li, Y., Mo, T., Li, S., Liang, Q., Li, J., & Qin, R. (2018). Nonlinear Analysis for the Crack Control of SMA Smart Concrete Beam Based on a Bidirectional B-Spline QR Method. *Hindawi*, *2018*, 16.

López López, A. T., Tomás Espín, A., & Sánchez Olivares, G. (2017). Influencia del tipo de rótula plástica en el análisis no lineal de estructuras de hormigón armado. *Hormigón y Acero*, *68*(282), 107–119. https://doi.org/10.1016/J.HYA.2017.04.006

Mihálcz, I. (2001). Fundamental characteristics and design method for nickel-titanium shape memory alloy. *Periodica Polytechnica Mechanical Engineering*, *45*(1), 75–86. https://doi.org/n/a

Millones, R., Barreno, E., Vasquez, F., & Castillo, C. (n.d.). *Estadística aplicada a la ingeniería y los negocios* (Fondo Edit). Lima, Perú: Universidad de Lima.

Monge-Ruiz, B. F. (2017). *Comparación entre un diseño realizado mediante un análisis estático y uno dinámico de historia en el tiempo para una estructura de mezanine sometida a vibraciones. Tecnologico de Costa Rica.* Instituto Tecnologico de Costa Rica.

Moon, D. Y., Roh, H., & Cimellaro, G. P. (2015). Seismic Performance of Segmental Rocking Columns Connected with NiTi Martensitic SMA Bars. *Advances in Structural Engineering*, *18*(4), 571–584. https://doi.org/10.1260/1369-4332.18.4.571

Muñoz-Barrantes, J. (2017). *Inspección de emergencia de puentes luego del paso de la tormenta tropical NATE: daños observados y otras enseñanzas*. Programa de Ingeniería Estructural. San José, Costa Rica.

Nakashoji, B., & Saiidi, M. S. (2014). *Seismic Performance of Square Nickel-Titanium Reinforced ECC columns with Headed Couplers*. Reno, Nevada.

O'Brien, M., Saiid, S., & Sadrossadat-Zdeh, M. (2007). *A Study of Concrete Bridge columns using innovative materials subjected to cyclic loading. Center for Civil Engineering Earthquake Research* (Vol. 30). Reno, Nevada.

Palermo, D., & Abdulridha, A. (2017). Behavior and modelling of hybrid SMA-steel reinforced concrete slender shear wall. *Engineering Structures*, *147*, 77–89.

Panagiotakos, T. B., & Fardis, M. N. (2001). Deformations of Reinforced Concrete Members at Yielding and Ultimate. *ACI Structural Journal*, *98*(2), 135–148. https://doi.org/10.14359/10181

Pantazopoulou, V. (2018a). *Basic elements of Earthquake Engineering. Dynamic of Structures and Earthquake Engineering*. North York, Ontario.

Pantazopoulou, V. (2018b). *Single Degree of Freedom System. Dynamic of Structures and Earthquake Engineering* (Civil Engineering No. 1). North York, Ontario.

RStudio Team. (2018). RStudio: Integrated Development for R. Boston, MA: RStudio. Retrieved from http://www.rstudio.com/

Singh, G. (2009). *Short Introduction to Finite Element Method. Idi.Ntnu.No*. Norway. Retrieved from http://www.idi.ntnu.no/~elster/tdt24/tdt24-f09/gagan-fem.pdf

Soto-Rojas, M. (2016). *Modelaje No Lineal de Metodología de Reparación y Rehabilitación de la Pila N ° 3 del Puente Sobre el Río Grande de Tárcoles en la Ruta N ° 34 Mediante FRP*. Instituto Tecnologico de Costa Rica.

Soto-Rojas, M., & Palermo, D. (2018). *Assessment of Rehabilitation Methodologies for Damaged Concrete Bridge Pier*. North York, Ontario.

Stoeckel, D. (2011). *Shape Memory and Superelasticity: From Scientific Curiosity to Life Saving Technology. Nitinol Devices and Components, Inc*. New Hampshire, Unite States of America.

Telenoticias. (2018). Ovsicori advierte de potencial terremoto en la Zona Sur debido a la acumulación de energía. Retrieved from https://www.teletica.com/203337_ovsicori-advierte-de-potencial-terremoto-en-la-zona-sur-debido-a-la-acumulacion-de-energia?fbclid=IwAR1QB6-sM4wfsbBs8_a8Y6nwb7nwOvWogfngS7q4R1qB9kTw6b5PPvb7WTU

Umaña-Venegas, J. (2018). Estado de puentes del país genera preocupación a especialistas. Retrieved from https://www.tec.ac.cr/hoyeneltec/2018/10/19/estado-puentes-pais-genera-preocupacion-especialistas

Universidad de Costa Rica. (2018). Laboratorio de Ingeniería Sísmica. Retrieved from http://www.lis.ucr.ac.cr/

Universidad de Costa Rica, Rica, & Instituto Costarricense de Electricidad. (2018). Red Sismológica Nacional. Retrieved from https://rsn.ucr.ac.cr/

Uttamraj, S., Ashwanth, K., & Rafeeq, M. (2016). An comparative study on Conventional concrete and Engineered Cementitious Composites (ECC-PVA)-REVIEW. *IOSR Journal of Mechanical and Civil Engineering*, 19–25. https://doi.org/10.9790/1684-16053011925

Vargas-Alas, L. G., Villalobos-Vega, E., Gooden-Morales, O. A., & Castillo-Barahona, R. (2017). *Evaluación de la Condición del puente sobre la quebrada Salitral Ruta Nacional No.27*. San Jose, Costa Rica.

Vecchio, F. J., Wong, P., & Trommels, H. (2013). Vector2 & Formworks User's Manual. *Second Edition*. Toronto, Canada. https://doi.org/10.1007/s007690000247

Villalobos, D. (2018). *SAP Módulo II*. San Jose, Costa Rica.

Yu-Chen, O., & Nguyen, D. (2014). Plastic hinge length of corroded reinforced concrete beams. *ACI Structural Journal*, *111*(5), 1049–1057.

Zhao, X., Wu, Y. F., Leung, A. Y., & Lam, H. F. (2011). Plastic hinge length in reinforced

concrete flexural members. *Procedia Engineering*, *14*, 1266–1274. https://doi.org/10.1016/j.tcs.2015.08.020

Zhuang, P., & Wang, W. (2016). Performance of Seismic Restrainer with SMA Springs for Sliding Isolation of Single-Layer Spherical Lattice Shells. *Shock and Vibration*, *2016*. https://doi.org/10.1155/2016/9218317

SEISMIC PERFORMANCE OF SMA-REINFORCED ECC BRIDGE STRUCTURES